

MaNEP
SWITZERLAND

Materials with **N**ovel **E**lectronic **P**roperties

NATIONAL CENTRE OF COMPETENCE IN RESEARCH

PROGRESS REPORT

Year 10

April 1st 2010 – March 31st 2011

FNSNF

FONDS NATIONAL SUISSE
SCHWEIZERISCHER NATIONALFONDS
FONDO NAZIONALE SVIZZERO
SWISS NATIONAL SCIENCE FOUNDATION

Die Nationalen Forschungsschwerpunkte (NFS) sind ein Förderinstrument des Schweizerischen Nationalfonds.
Les Pôles de recherche nationaux (PRN) sont un instrument d'encouragement du Fonds national suisse.
The National Centres of Competence in Research (NCCR) are a research instrument of the Swiss National Science Foundation.

NCCR: 10th Progress Report - Cover Sheet

Title of the NCCR	Materials with Novel Electronic Properties (MaNEP)
NCCR Director	
Name, first name	Prof. Øystein Fischer
Institution address	UNIVERSITE DE GENEVE, Faculté des Sciences Département de Physique de la Matière Condensée 24 quai Ernest-Ansermet, CH-1211 Genève 4
Office phone number	022 379 62 70
E-mail	Oystein.Fischer@unige.ch

1. Executive summary [1]
2. Research
 - 2.1 Structure of the NCCR and status of integration [2]
 - 2.2 Results since the last progress report [3]
3. Knowledge and technology transfer [4]
4. Education/training and advancement of women [5]
5. Communication [6]
6. Structural aspects [7]
7. Management
 - 7.1 Activities [8]
 - 7.2 Experiences, recommendations to the SNSF
8. Reaction to the recommendations of the review panel
9. Lists
 - 9.1 Overview of personnel and functions [9]
 - 9.2 Education and training [9]
 - 9.3 Publications [9]
 - 9.4 Lectures at congresses etc. [9]
 - 9.5 Services, patents, licences, start-up companies etc. [9]
 - 9.6 Cooperation with third parties [9]
10. Statistical output data [9]
11. Finance
 - 11.1 Finance NCCR Overview [10]
 - 11.2 Funding sources [10]
 - 11.3 Allocation to projects [10]
 - 11.4 Expenditures [10]
 - 11.5 Comments on finances [11]

Contents

1	Executive summary	3
2	Research	5
2.1	Structure of the NCCR and status of integration	5
2.2	Results since the last progress report	9
	Project 1	9
	Project 2	23
	Project 3	39
	Project 4	59
	Project 5	78
	Project 6	88
	Project 7	99
	Project 8	106
	Techniques and know-how	114
3	Knowledge and technology transfer	123
4	Education, training and advancement of women	129
5	Communication	135
6	Structural aspects	141
7	Management	143
7.1	Activities	143
7.2	Experiences, recommendations to the SNSF	145
8	Reaction to the recommendations of the review panel	147
9	Lists	149
9.3	Publications	149
11	Finance	179
11.1	Finance NCCR Overview	180
11.2	Funding sources	182
11.3	Allocation to projects	183
11.4	Expenditures	186
11.5	Comments on finances	189
12	Appendix: milestones of the MaNEP projects	191

1 Executive summary

MaNEP is now well into the third phase and the scientific activities in the new scientific structure with 8 broad projects are well under way with many new results. Whereas the research and other activities are advancing full speed, the MaNEP management is increasingly focusing on preparing the continuation of MaNEP after June 30, 2013. The present efforts to stabilize MaNEP Geneva in the leading house are advancing very well and we have engaged an effort to find a solution to the continuation of the network. Below we summarize the main results of this year's research and other activities in MaNEP.

Research

Project 1. In this project the physics at oxide and organic interfaces is studied. Cuprate/ferromagnetic systems, interfaces between organic compounds, high- T_c heterostructures have been studied. A large effort in the project concerns the interface between LaAlO_3 and SrTiO_3 . Our recent experiments address the question of the origin of the electron gas found between these two-band insulators. The results point to the presence of an electric field in thin (thickness below 4 unit cells) LaAlO_3 layers suggesting that the polar catastrophe scenario is at work. Domain walls in ferroelectric materials is another exciting interface system studied here theoretically and experimentally. It is found in $\text{Pb}(\text{Zr}_{0.2}\text{Ti}_{0.8})\text{O}_3$ thin films that domain walls are conducting as observed in BiFeO_3 .

Project 2. The goal of the project is to develop nanostructured devices and nanoscale probes for the investigation of the electronic properties of new materials. The current focus is on oxide interfaces and carbon-based systems, and the investigation of topological insulators has emerged as an additional new line of research. The development of higher quality material systems and the use of a broad range of experimental techniques has led to several important results. These include the observation of quantum oscillations in $\text{LaAlO}_3/\text{SrTiO}_3$ interfaces, a quantum Hall effect in graphene, charge density wave in intercalated graphite, band-like transport in n -type organic transistors, and the successful realization of 3D topological insulator devices. Theoretical work represents an important component of the research, crucial for the interpretation and planning of experi-

ments.

Project 3. This project covers a broad selection of applied research involving this year collaborations with 7 industries and covering 5 different topics. We can report important progress in our efforts to improve the overall superconducting critical current of MgB_2 conductors. Furthermore we have been able to make important progress towards using the metal insulator transition in transition metal hydrides to build a hydrogen sensor. Four SNF-supported *economic stimulus package* projects have reinforced strongly our research in collaboration with industry.

Project 4. One of the most important goals of superconductivity research is to create materials with improved superconducting properties, including higher T_c 's, higher critical fields, and higher critical current densities. In this spirit a strong and successful push has been made in this year by the MaNEP collaboration, resulting in the discovery of several novel superconducting materials, some of them having exceptionally high critical temperature. Experimental and theoretical efforts provided increasing indication that, notwithstanding unavoidable effects of electron-phonon coupling which are also observed, the main magnetic and superconducting phenomena in high- T_c materials have strong electron correlation as their common origin.

Project 5. This project reports on important progress in the field of heavy fermion superconductivity, concerning the nature of the Q -phase of CeCoIn_5 , which displays simultaneously superconductivity and magnetism, and

intriguing transport properties in CeCu_2Si_2 , shedding new light on the valence fluctuation mechanism for unconventional superconductivity. Progress has been made in the crystal growth of the non-centrosymmetric superconductor $\text{CeCoGe}_{3-x}\text{Si}_x$ and alloys in the class of Fe- and Mn-monosilicide. Developments of new simulation algorithms for correlated fermions allowed to study some thermodynamic aspects of the 3D Hubbard model down to the Néel temperature.

Project 6. In year 10, we applied a vast arsenal of experimental methods (neutrons, nuclear magnetic resonance, resonant X-rays, etc.), as well as theoretical approaches, to study novel quantum phases and excitations in magnetic materials. The emphasis is on low-dimensional, frustrated and disordered systems. Through internal and external collaborations, we now cover all stages of the research process: sample preparation, characterization, laboratory and large-scale facility measurements, data analysis, modeling and simulation.

Project 7. The subjects of the project are low-dimensional conductors in which various ground states compete with each other. From this competition, new, emergent phenomena may arise. The tuning of the interactions between different ground states, besides temperature, is achieved by chemical means (doping) or/and by applying external pressure.

Project 8. This project is looking at cold atoms with the perspective of both using them as quantum simulators for complicated problems in condensed matter, and also to create and understand novel systems and situations. On the first part, a conjunction of experiments, analytical, and numerical simulations has allowed to make considerable progress on that point. The validation of quantum simulators was considered as one of the breakthrough of the year 2010 by *Science*. Several novel realizations, such as multicomponent systems and out-of-equilibrium situations, were obtained, and analyzed allowing to develop new concepts and methods, both analytical and numerical.

Knowledge and technology transfer

MaNEP has by now developed a close contacts with a number of industries. In addition to the research carried out in Project 3, presently with six different companies, we have during the year continued collaborations with the company Sécheron on electric contacts. As another example, the renowned Swiss manufacturer Caran d'Ache SA is interested in new coatings and we are elaborating a project with them. In order to be able to handle the increased number of applied projects we have obtained supplementary space to install the MaNEP Development Lab. The Geneva Creativity Center is now into an operational mode and the ministry for education and the ministry for economy in Geneva have announced that they will fund this operation. An official inauguration will take place later in 2011.

Education, training and advancement of women

The MaNEP doctoral school is in its 3rd year and is largely composed by international students, and we are glad to announce that 32% of these students are women, a remarkable evolution as compared to earlier years. From January 1, 2011 this program joined forces with the Swiss CUSO doctoral program in physics. The MaNEP winter school 2011 was held at Saas-Fee and was as earlier a great success. In 2010 MaNEP was present actively at the Swiss Physical Society meeting with 138 scientists, of which 59 PhD students presenting 22 oral talks and 100 posters. Physiscope continues its success and is increasingly becoming both an education and a communication tool.

Communication

This year, a large effort has been spent to prepare the centennial of superconductivity, a celebration MaNEP is using in its communication to schoolchildren and the general public. A first event shall take place in April starting with a common press conference between MaNEP and CERN. MaNEP is also collaborating with the Swiss Physical Society in this celebration and other Swiss institutions. The main part of these manifestations shall take place in the fall of 2011.

2.1 Structure of the NCCR and status of integration

2.1.1 Structure of the NCCR

This section provides an up-to-date summary of the organization of MaNEP, the Swiss National Centre of Competence in Research (NCCR) on Materials with Novel Electronic Properties.

Academic institutions members of MaNEP

- University of Geneva (UniGE), home institution
- University of Fribourg (UniFR)
- University of Berne (UniBE)
- University of Zurich (UniZH)
- Federal Institute of Technology, Lausanne (EPFL)
- Federal Institute of Technology, Zurich (ETHZ)
- Paul Scherrer Institute (PSI)
- Materials Science and Technology Research Institute (Empa)
- Haute école de paysage, d'ingénierie et d'architecture, Genève (Hepia)

Industrial Partners

- ABB, Baden
- AgieCharmilles, Meyrin
- Asulab (a member of Swatch Group), Marin
- Bruker BioSpin, Fällanden
- Phasis, Geneva
- Sécheron, Meyrin
- SwissNeutronics, Klingnau
- Vacheron Constantin, Geneva

Scientific Committee

- Leonardo Degiorgi, ETHZ
- Øystein Fischer, UniGE, director
- László Forró, EPFL
- Thierry Giamarchi, UniGE
- Dirk van der Marel, UniGE, deputy director

- Frédéric Mila, EPFL
- Alberto Morpurgo, UniGE
- Christoph Renner, UniGE, deputy director
- Manfred Sigrist, ETHZ
- Jean-Marc Triscone, UniGE
- Urs Staub, PSI
- Andrey Zheludev, ETHZ

MaNEP Forum

Full members:

- Markus Abplanalp, ABB
- Philipp Aebi, UniFR
- Dionys Baeriswyl, UniFR
- Bertram Batlogg, ETHZ
- Christian Bernhard, UniFR
- Gianni Blatter, ETHZ
- Markus Büttiker, UniGE
- Michel Decroux, UniGE
- Leonardo Degiorgi, ETHZ
- Daniel Eckert, Bruker BioSpin
- Tilman Esslinger, ETHZ
- Øystein Fischer, UniGE
- René Flükiger, UniGE
- László Forró, EPFL
- Thierry Giamarchi, UniGE
- Enrico Giannini, UniGE
- Marco Gioni, EPFL
- Didier Jaccard, UniGE
- Janusz Karpinski, ETHZ
- Hugo Keller, UniZH
- Michel Kenzelmann, PSI
- Dirk van der Marel, UniGE
- Joël Mesot, PSI and ETHZ
- Frédéric Mila, EPFL
- Elvezio Morenzoni, PSI

- Alberto Morpurgo, UniGE
- Christof Niedermayer, PSI
- Hans-Rudolf Ott, ETHZ
- Patrycja Paruch, UniGE
- Greta Patzke, UniZH
- Christoph Renner, UniGE
- T. Maurice Rice, ETHZ
- Nico de Rooij, EPFL
- Henrik M. Rønnow, EPFL
- Manfred Sigrist, ETHZ
- Urs Staub, PSI
- Gilles Triscone, Hepia
- Jean-Marc Triscone, UniGE
- Matthias Troyer, ETHZ
- Anke Weidenkaff, Empa and UniBE
- Philip Willmott, PSI
- Klaus Yvon, UniGE
- Andrey Zheludev, ETHZ

Associate members:

- Christophe Berthod, UniGE
- Harald Brune, EPFL
- Kazimierz Conder, PSI
- Jorge Cors, UniGE and Phasis
- Bernard Delley, PSI
- Bertrand Dutoit, EPFL
- Vladimir Gritsev, UniFR
- Hans-Joseph Hug, Empa
- Jürg Hulliger, UniBE
- Ivan Maggio-Aprile, UniGE
- Reinhard Nesper, ETHZ
- Frithjof Nolting, PSI
- Davor Pavuna, EPFL
- Andreas Schilling, UniZH
- Louis Schlapbach
- Philipp Werner, ETHZ
- Oksana Zaharko, PSI

Advisory Board

- Dave Blank, University of Twente, Netherlands
- Robert J. Cava, Princeton University, USA
- Antoine Georges, Collège de France, Paris, France
- Denis Jérôme, University Paris Sud, Orsay, France
- Andrew Millis, Columbia University, USA
- George Sawatzky, University of British Columbia, Canada

Management (UniGE)

- Øystein Fischer, director
- Dirk van der Marel, deputy director
- Christoph Renner, deputy director
- Marie Bagnoud, administrative manager
- Christophe Berthod, education
- Adriana Bonito Aleman, communication and, *ad interim*, knowledge and technology transfer
- Pascal Cugni, administrative assistant
- Michel Decroux, scientific manager, education and training, advancement of women
- Lidia Favre-Quattropani, scientific manager
- Elizabeth Gueniat, executive assistant
- Ivan Maggio-Aprile, computer and internet resources
- Greg Manfrini, technical organization
- David Parietti, communication coordinator
- Christophe Schwarz, secretary

Collaborative projects

1. Novel phenomena at interfaces and in superlattices

Project leader:

- J.-M. Triscone (UniGE)

Members:

- Ph. Aebi (UniFR)
- C. Bernhard (UniFR)
- T. Giamarchi (UniGE)
- E. Morenzoni (PSI)
- A. Morpurgo (UniGE)
- C. Niedermayer (PSI)
- P. Paruch (UniGE)
- J.-M. Triscone (UniGE)
- Ph. Willmott (PSI)

2. Materials for future electronics

Project leader:

- A. Morpurgo (UniGE)

Members:

- M. Büttiker (UniGE)
- L. Forró (EPFL)
- T. Giamarchi (UniGE)
- E. Giannini (UniGE)
- D. van der Marel (UniGE)
- A. Morpurgo (UniGE)
- P. Paruch (UniGE)
- C. Renner (UniGE)
- M. Sigrist (ETHZ)
- J.-M. Triscone (UniGE)

3. Electronic materials for energy systems and other applications

Project leader:

- Ø. Fischer (UniGE)

Members:

- M. Abplanalp (ABB)
- Ph. Aebi (UniFR)
- J. Cors (UniGE and Phasis)
- M. Decroux (UniGE)
- D. Eckert (Bruker Biospin)
- Ø. Fischer (UniGE)
- R. Flükiger/C. Senatore (UniGE)
- J. Hulliger (UniBE)
- M. Kenzelmann (PSI)
- G. Patzke (UniZH)
- C. Renner (UniGE)
- N. de Rooij (EPFL)
- G. Triscone (Hepia)
- J.-M. Triscone (UniGE)
- A. Weidenkaff (Empa and UniBE)
- K. Yvon (UniGE)
- This project is carried out with six participating industries

4. Electronic properties of oxide superconductors and related materials

Project leader:

- D. van der Marel (UniGE)

Members:

- D. Baeriswyl (UniFR)
- B. Batlogg (ETHZ)
- L. Degiorgi (ETHZ)
- Ø. Fischer (UniGE)
- T. Giamarchi (UniGE)
- E. Giannini (UniGE)
- J. Karpinski (ETHZ)
- H. Keller (UniZH)
- M. Kenzelmann (PSI)
- D. van der Marel (UniGE)
- C. Niedermayer (PSI)
- T. M. Rice (ETHZ)
- M. Sgrist (ETHZ)

5. Novel electronic phases in strongly correlated electron systems

Project leader:

- M. Sgrist (ETHZ)

Members:

- D. Baeriswyl (UniFR)
- G. Blatter (ETHZ)
- E. Giannini (UniGE)
- D. Jaccard (UniGE)
- M. Kenzelmann (PSI)
- D. van der Marel (UniGE)
- M. Sgrist (ETHZ)
- M. Troyer (ETHZ)

6. Magnetism and competing interactions in bulk materials

Project leaders:

- F. Mila (EPFL)
- A. Zheludev (ETHZ)

Members:

- T. Giamarchi (UniGE)
- J. Mesot (PSI and ETHZ)
- F. Mila (EPFL)
- H.-R. Ott (ETHZ)
- H. M. Rønnow (EPFL)
- U. Staub (PSI)
- M. Troyer (ETHZ)
- A. Zheludev (ETHZ)

7. Electronic materials with reduced dimensionality

Project leader:

- L. Forró (EPFL)

Members:

- Ph. Aebi (UniFR)
- L. Degiorgi (ETHZ)
- L. Forró (EPFL)
- T. Giamarchi (UniGE)
- M. Grioni (EPFL)

8. Cold atomic gases as novel quantum simulators for condensed matter

Project leader:

- T. Giamarchi (UniGE)

Members:

- G. Blatter (ETHZ)
- T. Esslinger (ETHZ)
- T. Giamarchi (UniGE)
- V. Gritsev (UniFR)
- F. Mila (EPFL)
- M. Troyer (ETHZ)

2.1.2 Status of integration

As described also in chapter 6, structural aspects, the integration in MaNEP follows two lines: the integration of MaNEP Geneva into the University of Geneva, on the one hand, and the continued effort to stimulate collaborations and synergies between the different groups in MaNEP, on the other hand.

Concerning the integration into the University of Geneva, our work in this direction has taken a fast track during this year with the decision to elaborate a detailed project of a new building to unite Mathematics, Astronomy and Physics. It is the stabilization of MaNEP that is the nucleus in this project, and when this project is realized it must be seen as a direct structural result of MaNEP. This project will also give a strong stability to the continuation of MaNEP in Geneva at a high level.

We continue our efforts to establish collaborations inside MaNEP. The internal workshops, held this year in Neuchâtel between January 17 and 21, 2011, are the occasion to have intense and detailed discussions between the group leaders. They turn out to be very fruitful and stimulating. This is the opportunity to mutually inform about the progress in each group participating in a project and to adjust research goals according to the latest results from our research. Thus this event is each year improving contacts and synergies between groups. The milestones are systematically discussed at these meetings as well, and this is a very useful tool to boost integration.

A meeting of the MaNEP Forum was held in connection of these workshops, and for the Forum meetings we always plan to have enough time for the members to discuss on an informal basis. On these occasions it is clear that MaNEP represents major network in Switzerland. This is also demonstrated by the large MaNEP participation at the meetings of the Swiss Physical Society (SPS), where MaNEP is present with its own program every second year. Since the last report, MaNEP was present with a large number of participants at the meeting of the SPS in Basel, which was held on June 21 and 22, 2010. These meetings, which ten years ago attracted only a small number of participants, have gained considerably since the three NCCR in Physics decided to participate. As we have explained in earlier reports, MaNEP in particular played a stimulating and decisive role in this process. There is therefore no doubt that MaNEP has become a major force in the Swiss scientific landscape.

Last year we established eight collaborative projects that continue to motivate collaborations.

The discussions we are presently conducting in order to find a way to keep the network after 2013 clearly shows the need for it. It is also clear that such a network needs a certain amount of financial support from a national funding agency to be as efficient as MaNEP is now in this respect. The proposal NEXT, described in chapter 6, contains a detailed argumentation.

2.2 Results since the last progress report

This section reports on the research performed in the eight MaNEP projects for the period from April 1st 2010 to March 31st 2011.

Project 1 Novel phenomena at interfaces and in superlattices

Project leader: J.-M. Triscone (UniGE)

Participating members: Ph. Aebi (UniFR), C. Bernhard (UniFR), T. Giamarchi (UniGE), E. Morenzoni (PSI), A. Morpurgo (UniGE), C. Niedermayer (PSI), P. Paruch (UniGE), J.-M. Triscone (UniGE), Ph. Willmott (PSI)

Introduction: Interface physics in novel materials is developing very rapidly worldwide with the vision that such interfaces may allow properties to be designed and possibly novel phenomena to be discovered. These new physical phenomena include, for instance, novel spin, charge, or orbital orders, as well as possible new phases. It is the aim of this program to study exciting interface systems to try discovering new properties.

Summary and highlights

We list here some of the achievements obtained last year which are more detailed later in the present report.

- In multilayers from cuprate high-temperature superconductors and ferromagnetic manganites, we studied using polarized neutron reflectometry how the magnetization reversal during a magnetic hysteresis loop evolves.
- On organic-metallic spin-valve structures, we showed that the sign of the spin polarization of current-injected charge carriers can be reversed by implementing a polar layer.
- In the normal state of an underdoped (UD) $\text{La}_{1.94}\text{Sr}_{0.06}\text{CuO}_4$ layer ($T'_c \leq 5$ K) sandwiched between two nearly optimally doped (OP) $\text{La}_{1.84}\text{Sr}_{0.16}\text{CuO}_4$ layers ($T_c \cong 32$ K), we have probed the local diamagnetic response. We show that the entire barrier layer of thickness much larger than typical c -axis coherence lengths of cuprates exhibits Meissner effect for temperatures well above T'_c but below T_c . We show that superfluidity with long-range phase coherence is induced in the underdoped layer by the proximity to optimally doped layers.
- The atomic structure of LaAlO_3 (LAO) grown on SrTiO_3 (STO) has been studied in detail as a function of the number of LAO monolayers (ML). Synchrotron-based surface X-ray diffraction (SXR) revealed the presence of an internal electric field in the LAO layer, that disappears after 4 ML LAO. The electric field induces a partial depolarizing buckling of the cations relative to the oxygen anions, which collapses after 4 ML.
- At the LAO/STO interface, the evolution of the lattice parameter with thickness has been studied and reveals a complete screening of the LAO electric field for LAO layers thicker than 6 ML.
- At oxide interfaces, oxygen exchange between a thin film and its substrate has been studied using oxygen isotope exchange.
- On thin oxide films of LaNiO_3 with two different thicknesses of 4 and 10 unit cells (uc), we have performed photoemission experiments. Comparing the measured spectra of the valence band with previous measurements carried out on powders, we conclude that, while the metallic phase found for the thicker film looks similar to the one observed in powder samples, the insulating phase displayed by the thinnest film looks different.
- We have developed organic Schottky-gated heterostructures based on single-crystals of rubrene and PDIF-CN₂, which are gate-tunable and exhibit band-like transport over a wide range of tempera-

tures.

- In ferroelectric-paraelectric superlattices, the coupling of the ferroelectric polarization across the paraelectric layers has been studied.
- BiFeO₃/LaFeO₃ superlattices have been fabricated and characterized.
- In epitaxial Pb(Zr_{0.2}Ti_{0.8})O₃, the conductivity at 180° domain walls has been studied.

1 Magnetization reversal in YBa₂Cu₃O₇/ La_{2/3}Ca_{1/3}MnO₃ multilayers and spin injection in metal-organic spin-valves (C. Bernhard)

1.1 Magnetization reversal in YBa₂Cu₃O₇/ La_{2/3}Ca_{1/3}MnO₃ multilayers

With polarized neutron reflectometry (PNR), we have investigated how the magnetization reversal in a [YBa₂Cu₃O₇ (10 nm)/ La_{2/3}Ca_{1/3}MnO₃ (10 nm)] × 10 multilayer on a SrTiO₃ substrate evolves during a hysteresis loop [1]. We found that the switching process of the magnetization involves surprisingly large, micrometer-sized domains that are furthermore strongly coupled along the vertical direction, i.e. across the YBa₂Cu₃O₇ layers. This unusual behavior apparently is induced by the SrTiO₃ substrate which at low temperature develops micrometer-sized surface facets that are tilted with respect to each other by up to 0.5 degree [2]. These facets are transmitted through the superlattice [3] and give rise to strain fields that act as templates for the ferromagnetic domains in La_{2/3}Ca_{1/3}MnO₃ (10 nm) whose magnetic properties are known to be very strain-sensitive.

1.2 Spin injection in metal-organic spin-valves

Using the low-energy muon-spin rotation (LE-μSR) technique, we have previously shown that depth-resolved measurements of the spin polarization of current-induced charge carriers can be performed in real spin-valve structures that are comprised of metallic ferromagnetic layers and organic, non-magnetic, spacer layers [4]. Recently, we have used this technique to show that the direction of the spin polarization can be reversed by inserting an additional, thin, LiF layer which acts as an electrical dipole [5]. We have shown that the corresponding “built-in” electric field gives rise to a vacuum level shift between the Fermi level of the ferromagnetic layer and the highest occupied molecular orbital (HOMO) level of the organic material into which the hole-like charge carriers are injected (Fig. 1). Our experiment

- We have studied the effects of temperature on the roughness of an interface. For its static properties we have determined the lengthscales separating the various regimes of roughness. For the dynamics we have determined the dynamical phase diagram and the various lengthscales associated with the motion in a random medium.

demonstrated that this results in a change of the polarization of the current-injected charge carriers. This proof of principle experiment

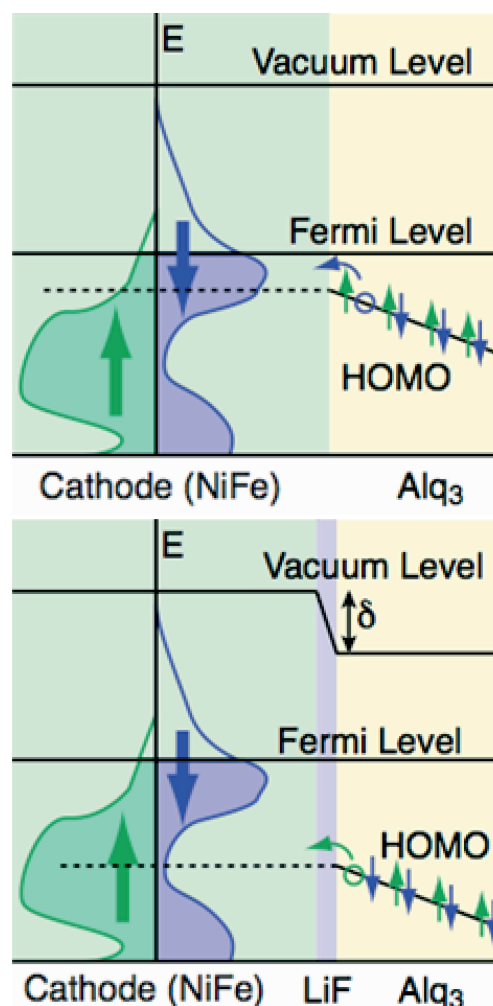


Figure 1: Schematics showing how the vacuum level shift due to the insertion of a polar LiF layer in a metal-organic spin-valve structure gives rise to a change in the polarization of the charge carriers that are injected from the conduction band of ferromagnetic NiFe into the highest occupied molecular orbital (HOMO) of the organic semiconductor Alq₃.

demonstrates the possibility that the spin polarization of current-injected charge carriers in metal-organic spin-valves can be modified with electric fields in addition to magnetic fields. This opens up new possibilities for the design of novel device principles where the processing and storage of information may be combined on a single device.

2 The Meissner effect in a strongly underdoped cuprate well above its critical temperature (E. Morenzoni)

2.1 Introduction

In cuprates that show high-temperature superconductivity (HTS), their “normal” (metallic) state above the critical temperature T_c is quite anomalous, featuring linear temperature dependence of resistivity, a pseudogap in the density of states, absorption throughout the infrared region, signatures of local superconducting correlations, etc. [24]. One unusual feature is the so-called giant proximity effect (GPE), reported by several groups [25, 26]. Such SC1-SC2-SC1 junctions were shown to transmit supercurrents even at temperature $T > T'_c$ and for barriers much thicker (up to 20 nm) than what one would expect from the standard theory of the proximity effect. The problem is that Josephson tunneling experiments are delicate. Even though great effort was spent to rule out filamentary superconductivity, the evidence for this was only circumstantial [26]; one would prefer a direct measurement that can differentiate between “filamentary” and “bulk” superconductivity. The local probe technique we have chosen for this study (low-energy muon-spin rotation, LE- μ SR) in fact fulfills all these requirements. By directly mapping the magnetic field profile in the heterostructure, we can show that the entire underdoped barrier layer displays superconductivity with an effective critical temperature lower but similar to that of the optimally doped top and bottom layers.

2.2 Results

For the present study, we fabricated a number of heterostructures as well as single-phase films for control experiments. The results are presented for heterostructures consisting of three layers, each 46 nm thick; optimally doped $\text{La}_{1.84}\text{Sr}_{0.16}\text{CuO}_4$ was used for the top and the bottom “electrodes”, while underdoped (UD) $\text{La}_{1.94}\text{Sr}_{0.06}\text{CuO}_4$ served as the “barrier”. To directly map the magnetic field profile in the heterostructure as a function of position along

the crystal c -axis, we cool the samples in zero field (ZF) from above T_c to ~ 4.3 K, apply a magnetic field of 9.5 mT parallel to the ab -planes and collect μ SR spectra as a function of the muon implantation energy at increasing temperatures. We observe that the entire heterostructure excludes the magnetic flux like a superconductor: it is the Meissner effect with the UD layer active in the screening. The measured profile can only be observed if shielding supercurrents flow across (i.e. along the c -axis) as well as in the ab -planes of the UD barrier, which taken as an isolated layer would be in the normal state at $T > T'_c$.

2.3 Discussion

We model the field profile by a solution of the London equations in each layer with appropriate boundary conditions and by taking into account the muon stopping profile and obtain the magnetic penetration depths in the electrodes λ and in the barrier λ' . In our inhomogeneous heterostructure, these quantities are the effective length scales indicative of the superfluid densities in the different layers. For example, at $T = 10$ K, we get $\lambda = 334 \pm 6$ nm and $\lambda' = 287 \pm 60$ nm, values comparable to the magnetic penetration depth in optimally doped single-crystals [27]. However, above this temperature, λ' has a much more pronounced temperature dependence than λ (Fig. 2), indicating that the proximity-induced

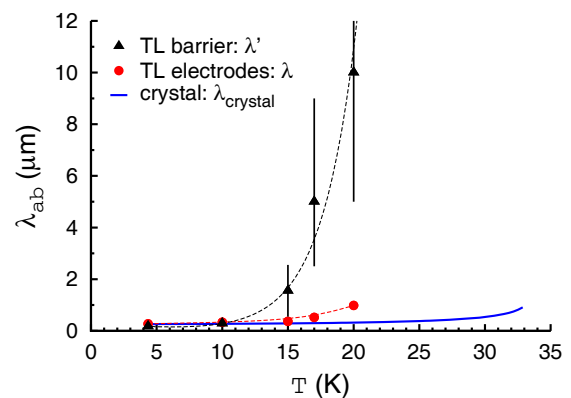


Figure 2: Temperature dependence of the magnetic penetration depths. The values in the barrier (λ') and in the electrode layer (λ) are compared with typical behavior in optimally doped crystals. The dashed lines are guides to the eyes. The divergent behavior of λ' close to 22 K indicates the disappearance of the long range phase coherence in the barrier at that temperature. The temperature dependence indicates that the induced superfluid density in the barrier layer is more sensitive to thermal excitation than in a bulk superconductor.

superfluid can be more easily suppressed by thermal excitations than the superfluid in intrinsically superconducting electrodes. To provide an enhanced length scale of the proximity effect, several models have been proposed. One class of models postulates inhomogeneous barriers that contain superconducting islands embedded in a metallic matrix and forming a percolative network that can transmit supercurrent via Josephson coupling between the islands and between the CuO_2 layers [28, 29, 30]. Another interesting theoretical proposal is the possibility of a new type of proximity effect between superconducting layers separated by an unconventional normal metal, such as a superconductor that has lost its phase rigidity due to phase fluctuations. In this case, the well-defined homogeneous phase field of the S electrodes may quench the superconducting fluctuations present in the S' barrier material, thus increasing the effective critical temperature of the barrier to some temperature T_{eff} smaller than T_c but well above T'_c [29, 30]. To conclude, by performing local magnetic measurements in heterostructures digitally grown by molecular beam epitaxy (MBE), we observe a Meissner effect in a thick UD barrier layer well above its intrinsic critical temperature, T'_c . The induced superfluid density disappears at T_{eff} where $T'_c \ll T_{eff} < T_c$. This result is not expected within the conventional proximity effect theory and constrains the theory of HTS and our understanding of the pseudogap.

3 Surface diffraction studies of oxide interfaces (Ph. Willmott)

3.1 The evolution of the structure of LaAlO_3 on SrTiO_3

Four samples of 2, 3, 4, and 5 ML LaAlO_3 (LAO) grown on SrTiO_3 (STO) were investigated with synchrotron-based surface X-ray diffraction (SXR). Analysis of the data using phase-retrieval methods [6, 7] reveals that the La- and Al-ions shift towards the surface relative to the oxygen anions in an effort to neutralize the internal electric field generated by the nonpolar-polar interface [31], as previously predicted [32]. Because this buckling costs elastic energy, it only *reduces* the field strength and cannot fully compensate for it. At 4 ML, the top of the valence band of the LAO becomes higher than the Fermi energy, and electrons are injected across the interface, agreeing perfectly with the beginning of conductivity only after 4 ML growth, first reported in 2006 [33]. The electric field subsequently collapses, and the buckling is suppressed. The results are sum-

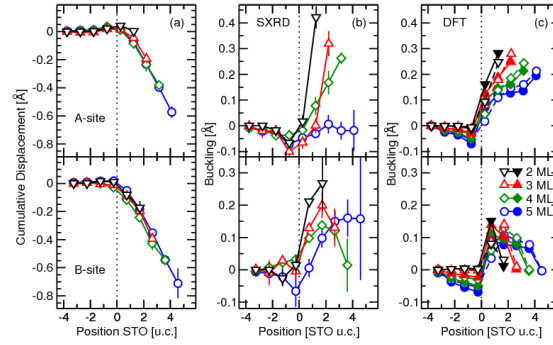


Figure 3: (a) Cumulative displacement out-of-plane of the atomic positions relative to a reference grid defined by bulk STO. For reasons of clarity, only the average of the A-site (upper panels) and B-site (lower panels) atomic layer positions are shown. (b) and (c) show the buckling of the A-site and B-site atomic planes from the refined structure and the DFT calculations, respectively, shown on the same scale. Positive values indicate movements of the cation relative to the oxygen ions towards the surface. In (c) the filled and open circles mark the abrupt and intermixed DFT models, respectively. The dotted lines represent the nominal interface.

marized in Fig. 3 [8]. They agree qualitatively with DFT calculations, which also show only marginal differences between models with an abrupt interface and with a monolayer of 50:50 intermixed LAO:STO. This would imply that intermixing plays a secondary role in this system.

3.2 The performance of the direct-methods algorithm DCAF

The efficacy of the phase-retrieval direct method “DCAF” [6] was tested on the complex system of 4 ML $\text{YBa}_2\text{Cu}_3\text{O}_{7-\delta}$ (YBCO) grown on STO [7]. Using no prior knowledge or input model, the DCAF output electron density map mimicked bulklike YBCO to within approximately 5 pm, while the occupancy of the heavy cations could be determined to within ± 0.05 , although that of the much lighter oxygen ions could only be reliably determined to within about 20% [7].

4 Electrostriction at the $\text{LaAlO}_3/\text{SrTiO}_3$ interface (J.-M. Triscone)

One of the open questions on the LAO/STO conducting interface [31] concerns the origin of the doping. In this regard, the LAO thickness was shown to be a crucial parameter. Indeed, a metallic conduction is observed only when more than 3 unit cells (uc) of LAO are deposited on top of a TiO_2 -terminated (001) STO substrate [33][9]. This result suggests that an

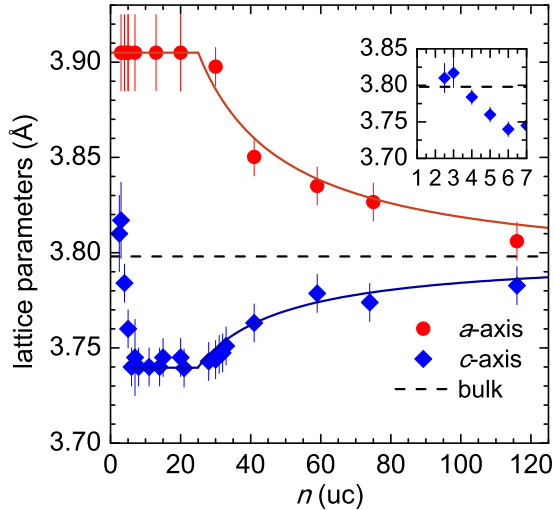


Figure 4: *a* and *c*-axis LAO lattice parameters plotted as a function of the LAO thickness.

electronic reconstruction is responsible for the mobile charges at the interface [34, 35]. LAO, although centrosymmetric, has an intrinsic polar nature [36]. At the interface with STO a polar discontinuity occurs which, in the absence of screening, leads to a huge built-in electric field of ~ 6 V/Å in the LAO layer. The large dipole field inside the layer can be accommodated by polarizing the material through a large polar distortion of the La and O ions [32] and, hence, induces an electrostrictive effect. Above a critical thickness, *Zener* breakdown occurs and charges are transferred to the interface. This doping scenario has been challenged by other experimental studies on oxygen vacancies [37, 38] and cation intermixing [10]. By using X-ray diffraction, we measured the lattice parameters of LAO thin films for different thicknesses in order to quantify the electrostrictive effect. The structural measurements were performed at the surface X-ray diffraction beamline of the Swiss Light Source, in collaboration with Ph. Willmott and S. Pauli. The measurements shown in Fig. 4 reveal, between 6 and 20 uc of LAO, a constant *c*-axis parameter of 3.74 Å, the value predicted for a fully compensated electric field taking into account the elastic strain. Above 20 uc the epitaxial strain is progressively released with both in-plane and out-of-plane lattice parameters relaxing to the bulk value. Analyses of the X-ray rocking curves confirm this change in structure. The experimental data thus reveal a complete screening of the LAO dipole field between 6 and 20 uc of LaAlO₃ in agreement with Ref. [8].

Below 6 uc, a *c*-axis expansion is measured and the lattice value reaches 3.82 Å,

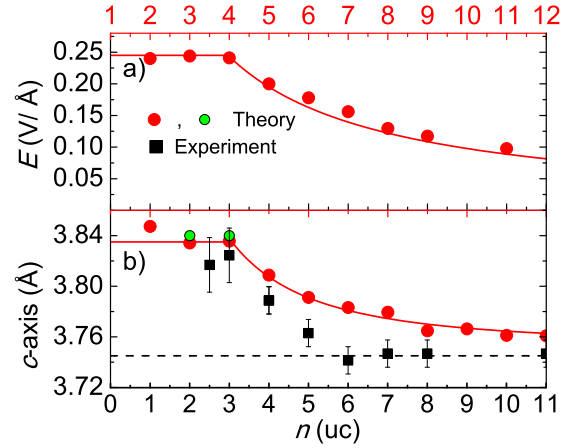


Figure 5: Evolution of (a) the electric field inside the LAO layer and (b) of the LAO *c*-axis with the LAO layer thickness, according to *ab initio* calculations. The green points represent a calculation including 50% intermixing of La-Sr and Al-Ti of the first layer across the interface. Two *x* scales are reported (in red for theory and black for experiment) to normalize at the same critical thickness (4 uc for the experiment and 5 uc for the theory).

at about 2.5 uc. *Ab initio* calculations aimed at simulating the effect of the internal electric field on the LAO layer were performed by P. Ghosez, D. Fontaine and M. Stengel (Liège and Barcelona). In the absence of any compensating charge, the electric field (0.24 V/Å) produces a sizable *c*-axis expansion of 1.7 %, in agreement with the experimental data. Adding carriers to the LAO surfaces reduces the dipole field and the *c*-axis expansion. The evolution of the *c*-axis strain, η , with the field is almost perfectly quadratic: $\eta = \alpha E^2$ with $\alpha = 0.4$ Å²V⁻². The amplitude of the *c*-parameter of LAO is linked to the internal electric field: $c = c_0 + \beta E^2$ with $\beta = 1.5$ Å³V⁻² and $c_0 = 3.7534$ Å (Fig. 5b). In Fig. 5a, the evolution of the electric field inside LAO is plotted for different thicknesses. The agreement between the experimental measurements and the theoretical predictions seems to suggest that the *c*-axis expansion observed in LAO layers thinner than 4 uc can be accounted for by intermixing and partly by an electrostrictive effect. For layers thicker than 6 uc the screening seems to be complete. This work shows that in polar materials a large electrostrictive effect is expected and can be experimentally measured by X-ray diffraction.

5 The origin of oxygen in oxide thin films: role of the substrate (C. Niedermayer)

Based on the work done in the project period 2009 on ¹⁸O exchanged SrTiO₃ single-crystals, we started to grow LaAlO₃ and SrTiO₃

thin films by pulsed laser deposition (PLD) at different growth temperatures on ^{18}O exchanged (100) oriented SrTiO_3 and LaAlO_3 single-crystalline substrates to investigate a potential oxygen diffusion from the substrate into the as-grown film during the growth process. The as-grown films were subsequently characterized by X-ray diffraction and secondary ion mass spectroscopy depth profiling (SIMS). Usually, the oxygen from the target and/or the background gas is taken as the main source for the oxygen supplied to the oxygen content of an oxide thin film. A substrate contribution effect has not been considered as a potential source so far during growth and can have a serious influence on thin film properties. For these diffusion experiments, the average isotope exchange ratio for the substrates was approximately 90%.

Four sets of film-substrate combinations have been investigated: SrTiO_3 on SrTiO_3 , LaAlO_3 on LaAlO_3 , SrTiO_3 on LaAlO_3 and LaAlO_3 on SrTiO_3 . These films have been grown at a background pressure p of $1.5 \cdot 10^{-5}$ mbar, a fluence F of 4 J/cm^2 and a substrate temperature T_s of 750°C , 650°C , and nominal room temperature. SIMS spectra were recorded using a quadrupole mass spectrometer (Hiden analytical EQS) operated with a 2.5 keV Ar ion beam focused to $150 \mu\text{m}$ diameter rastering over a square of $1 \times 1 \text{ mm}^2$ with an effective sampling area of $500 \times 500 \mu\text{m}^2$. The etched area is subsequently measured with a Dektak 8 profilometer to convert etching time into depth. In addition a kinetic energy selection scheme is used to separate species with the same mass. The ^{18}O diffusion from $\text{SrTi}^{18}\text{O}_3$ into SrTiO_3 shows a pronounced dependence on the deposition temperature (Fig. 6a). Whereas for a room temperature deposition, no traceable ^{18}O diffusion into the film has been measured, the situation changes dramatically for elevated deposition temperatures. At 650°C , there is considerable ^{18}O diffusion from the substrate into the film, while at $T_s = 750^\circ\text{C}$ there is no significant difference with respect to the amount of ^{18}O measured in the film and substrate. Measuring Sr and Ti species from the substrate and film simultaneously with ^{16}O and ^{18}O , the elemental composition of film and substrate are very similar. This implies that oxygen in the SrTiO_3 thin film is supplied by the substrate and the oxygen provided by the target seems to play a minor role for this system. The ^{18}O diffusion into LaAlO_3 from $\text{LaAl}^{18}\text{O}_3$ differs significantly compared to SrTiO_3 on $\text{SrTi}^{18}\text{O}_3$. No considerable oxygen diffusion from the substrate into the film is detected, in particular at

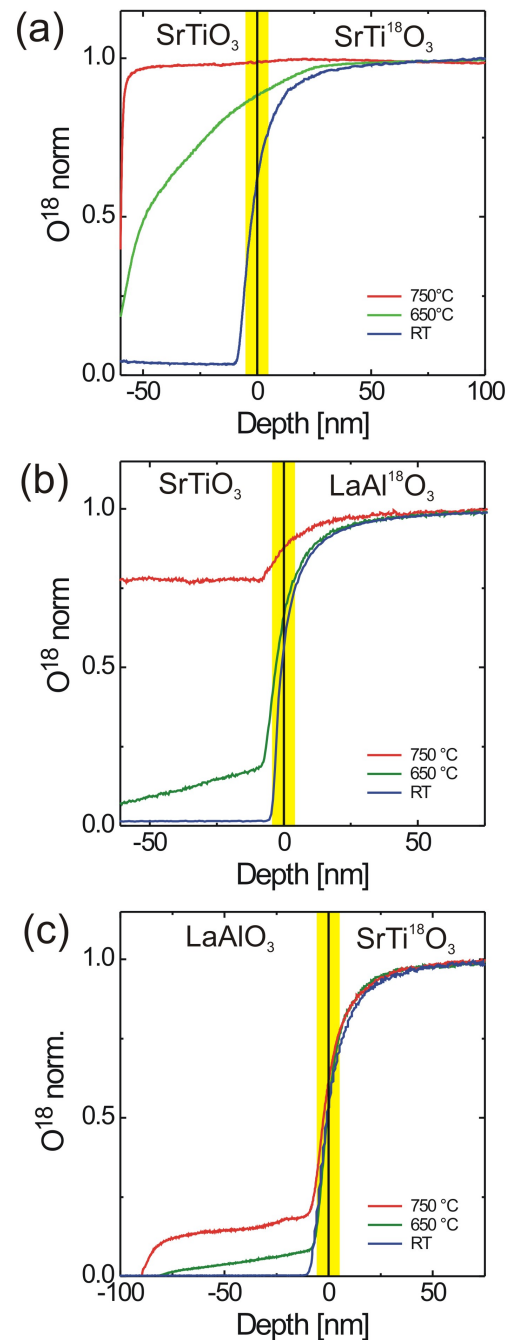


Figure 6: (a) ^{18}O SIMS depth profile of SrTiO_3 on $\text{SrTi}^{18}\text{O}_3$ grown at $T_s = 750^\circ\text{C}$, 650°C and room temperature. The sharp drop of the ^{18}O signal near the SrTiO_3 surface for the film grown at $T_s = 750^\circ\text{C}$ could be related to a back-exchange of ^{16}O at room temperature. (b) ^{18}O SIMS depth profile of SrTiO_3 on $\text{LaAl}^{18}\text{O}_3$ grown at $T_s = 750^\circ\text{C}$, 650°C and room temperature. (c) ^{18}O SIMS depth profile of LaAlO_3 on $\text{SrTi}^{18}\text{O}_3$ grown at $T_s = 750^\circ\text{C}$, 650°C and room temperature. These samples have been grown at a base pressure of 1.5×10^{-5} mbar and a fluence of $\sim 4 \text{ Jcm}^{-2}$. The yellow area visualizes approximately the depth over which the information of the interface region is collected.

the interface region, irrespective of the studied deposition temperature (not shown). In the case of SrTiO₃ grown on LaAl¹⁸O₃ a significant and homogeneous oxygen contribution in the SrTiO₃ is measured for the film prepared at $T_s = 750^\circ\text{C}$ (Fig. 6b). Even at 650°C, there is still a significant ¹⁸O intake which can be detected up to the film surface. It is interesting to note the comparatively large difference in oxygen diffusion properties of the SrTiO₃ thin film considering a modest difference in T_s of 100°C. This is probably due to the activation energy of oxygen diffusion in SrTiO₃ and that a film is inherently defect rich which allows oxygen to diffuse more easily at elevated temperatures compared to a single-crystal ($D_{crystal} = 10^{-15} \text{ cm}^2\text{s}^{-1}$; $D_{defects} = 10^{-11} \text{ cm}^2\text{s}^{-1}$). The large ¹⁸O concentration in SrTiO₃ thin films is unexpected if compared to LaAlO₃ on LaAl¹⁸O₃. This suggests that SrTiO₃ is a material which can either take or give oxygen during film growth, whereas LaAlO₃ is more likely to keep oxygen during the deposition. Oxygen diffusion into LaAlO₃ is more difficult to achieve than into SrTiO₃. This becomes evident when depositing LaAlO₃ onto SrTi¹⁸O₃ (Fig. 6c). The ¹⁸O concentration in the $\approx 100 \text{ nm}$ thin LaAlO₃ films deposited at different temperatures is smaller than in SrTiO₃, still there is a significant amount of ¹⁸O at the film substrate interface for the film grown at $T_s = 750^\circ\text{C}$.

In conclusion, the SIMS experiments indicate that the initially formed film is oxygen deficient and a chemical gradient is established in favor of supplying oxygen to the growing film via the substrate. The results have been published in reference [11]. Next steps will be to investigate the oxygen diffusion properties of oxide thin films prepared by deposition techniques other than PLD to establish a more general picture for the role of substrate with respect to the oxygen content in a film.

6 Photoemission on oxide surfaces: LaNiO₃ (Ph. Aebi)

6.1 Introduction

The perovskite nickelate family RNiO₃, where R is a rare earth element, has been widely studied in the last two decades since it shows very interesting properties. The properties include metal-insulator transitions, charge ordering and unusual magnetic ordering. Moreover, this family has recently been proposed to be multiferroic [39].

Numerous studies carried out with different techniques can be found in the literature (see

reviews from Medarde [40] or Catalan [41] for instance), but the absence of single-crystals caused that the majority of these studies were carried out on powder samples. In the recent years, the emergence of thin film research renewed the interest on this type of materials.

Recently Scherwitzl *et al.* [12] showed that epitaxial LaNiO₃ thin films grown coherently on (001) SrTiO₃ exhibit a metal-insulator (MI) transition as the film thickness is reduced below 8 unit cells. A study on the nature of the gap opening for this transition appears as a compelling thing to do.

6.2 First Results

The thin films of LaNiO₃ with thicknesses of 4 and 10 unit cells were grown following the procedure explained in Ref. [12]. The samples were characterized using X-ray diffraction and resistivity measurements.

Since those experiments were performed *ex situ*, the surface of the thin films was treated with O₂ plasma in order to remove the contamination layer on the surface of the sample arising from its exposure to air. The cleanliness of the surfaces was monitored by X-ray photoemission spectroscopy (XPS). All spectra were collected at room temperature (RT).

Fig. 7a shows the comparison between UPS spectra measured in LaNiO₃ 4 uc and LaNiO₃ 10 uc collected using He I excitation energy in the vicinity of the Fermi level. The change in the density of states (DOS) between the two samples indicates a gap opening for the 4 uc sample, that can be clearly seen in the inset. Comparing these measurements with the ones performed by S. R. Barman *et al.* on polycrystalline samples of NdNiO₃ and LaNiO₃ [42], we can appreciate similarities with the metallic thin film LaNiO₃ (10 uc). We can identify 4 different features appearing close to E_F . These features have been labeled as A, B, C and D. According to their measurements and their calculated density of states, Barman *et al.* concluded that features A and B are primarily due to Ni 3d emission, while the features C and D have more significant O 2p character. In the spectra corresponding to the LaNiO₃ 4 uc sample, those features cannot be precisely identified, reflecting differences in the electronic structure between the insulating and the metallic thin films.

Fig. 7b shows the He II valence band spectrum of samples LaNiO₃ 4 uc, LaNiO₃ 10 uc and from the substrate SrTiO₃. In these spectra it can be observed that more defined features appear for the insulating sample, while

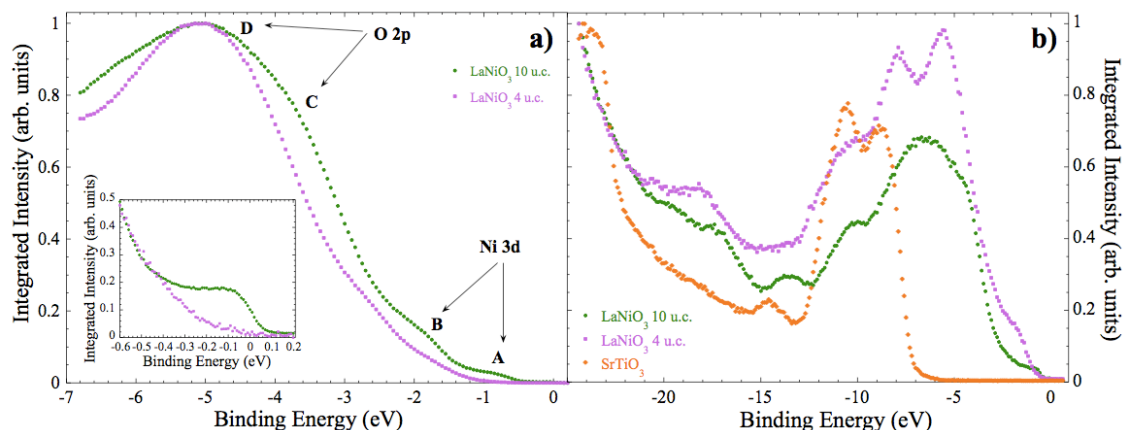


Figure 7: Photoemission spectra in the vicinity of the Fermi level measured at RT on LaNiO₃ thin films of 4 and 10 unit cells and on the SrTiO₃ substrate.

the spectrum of the metallic sample shows a broad band between 8 eV and 1 eV binding energies in analogy to what was observed in polycrystalline PrNiO₃ [43]. This broad band has principally O 2p character and its general appearance is a familiar feature of photoemission spectra from transition metal oxides.

Measurements at grazing incidence indicate that the distinct three features appearing in the insulating sample between 8 eV and 1 eV arise solely from the thin film and do not correspond to photoemitted electrons from the substrate.

However a comparison of this data with the He II valence band of SrTiO₃ shows that similar features appear also in the valence band of the substrate, but at different energies than in the LaNiO₃ 4 uc thin film. A possible explanation to this phenomena could be that the strain from the substrate modifies the LaNiO₃ thin film structure, particularly the octahedral tilts, creating a crystallographic environment for the Ni ions similar to the one of the Ti ions in the substrate. It is known that the B-O-B tilt angle between corner-shared octahedra affects electron hopping matrix elements and hence the transport properties [44, 45, 46]. The deformations of oxygen octahedra driven by collective Jahn-Teller distortions control both metal-insulator transitions and magnetic properties [47].

Also recently a theoretical model showed how the symmetry mismatch imposes an interfacial layer with distortion modes that do not exist in either bulk material, creating new interface properties driven by symmetry alone [48]. According to these authors, depending on the resistance of the octahedra to deformation, the interface layer can be as small as one unit cell or extend deep into the thin film.

This could explain the different electronic properties of these thin films as function of thickness. Above a certain thickness the strain

imposed by the substrate would be released and the electronic properties of the thin film would be more similar to those of the bulk material.

7 Organic Schottky-gated heterostructures (A. Morpurgo)

The electronic properties of interfaces between different organic molecular semiconductors are crucial for the operation of most devices in the field of plastic electronics. In the devices considered so far, such as organic light emitting diodes and solar cells, transport across the interface is the relevant process. However, by analogy with conventional semiconductors in which two-dimensional electron gases are formed, transport *in the plane* of organic interfaces is also expected to be of great interest. Nevertheless, in-plane transport in organic heterostructures has so far received limited attention. Recently, we have demonstrated that organic heterostructures can host new physical phenomena, by showing that at interfaces of TTF and TCNQ crystals — two large gap molecular semiconductors that are essentially insulators — metallic conductivity can be established due to charge transfer from one material to the other. Here, we are focusing on heterostructures made of organic materials in which a small energy gap is present between the highest occupied molecular orbital (HOMO) of one molecule and the lowest unoccupied molecular orbital (LUMO) of the other. In a first study based on TMTSF-TCNQ interfaces, we have shown that the amount of charge transferred across the interface can be understood in terms of a simple band diagram picture [13]. The current goal is to control charge transfer electrostatically, for which we use new heterostructures based on PDIF-

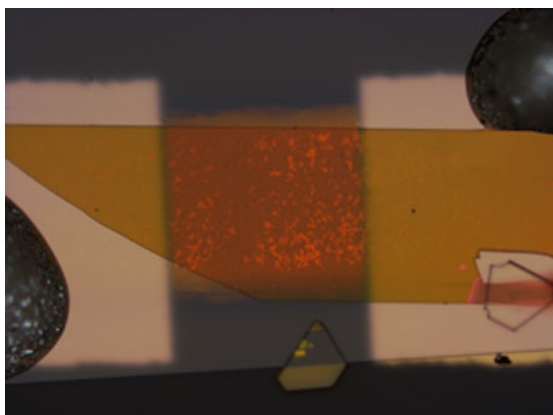


Figure 8: Optical microscope image of a gated rubrene-PDIF-CN₂ heterostructure. The PDIF-CN₂ crystal is the topmost layer. The bright areas on the right and left sides are gold electrodes contacted with silver epoxy. The rubrene crystal appears grey in the background, and under it a chrome strip — corresponding to the gate electrode — is visible. The entire structure is fabricated on a PDMS support.

CN₂ and rubrene, equipped with a Schottky gate electrode (Fig 8). The measurements indicate that the presence of the Schottky gate by itself — that is even when no voltage is applied — has a large influence on the carrier density at the interface. The effect is due to the band-bending associated to the alignment of the Fermi level in the gate and in the organic crystals, which, in the configuration chosen, causes a significant enhancement in the interfacial electron density and in a depletion of the hole density. The carrier density can be further tuned by applying a positive gate voltage, demonstrating the correct operation of the devices. Interestingly, we observe an electron conductivity that increases with lowering temperature down to $\simeq 100$ K. This represents the broadest temperature range in which band-like transport in organic semiconducting transistors has been observed so far (at lower temperatures, the conductivity is suppressed exponentially with a small activation energy ($\approx 5 - 10$ meV, depending on the gate voltage)). Ongoing work aims at gaining a quantitative understanding of the band structure of these gate heterointerfaces and at performing Hall effect measurements, to estimate directly the density of carriers and their mobility. The ultimate goal is to use these interfaces to reach high value of carrier mobility at even lower temperature (≈ 4.2 K).

8 Ferroelectric domains in artificially layered ferroelectric superlattices (J.-M. Triscone)

The continuing drive for device miniaturization poses fundamental questions about the possible existence of a critical thickness for ferroelectricity and the behavior of ferroelectrics in the ultrathin limit. As the thickness of a ferroelectric is reduced to nanometer dimensions, large and energetically costly depolarizing fields develop due to the incomplete screening of the spontaneous polarization. How the material responds to these internal fields determines its structural and electrical properties. One way of reducing the depolarising field is to adopt a structure consisting of alternating domains of opposite polarization leading to overall charge neutrality at the surfaces. In ferroelectrics that are only a few unit cells thick, such domains are extremely tiny (a few nanometers in size) and are extremely difficult to probe [49]. We have found that superlattices composed of ferroelectric PbTiO₃ (PTO) and paraelectric SrTiO₃ (STO) possess very regular and periodic nanodomains giving unprecedented access to the physics of domains in ultrathin films. In particular, we have been able to apply large uniform electric fields and simultaneously study the evolution of the domain structure using X-ray diffraction [14]. The domain structure was found to be very stable. Under applied bias, the domain periodicity remained unchanged, and only the relative sizes of up and down domains were modified. The original domain structure was restored upon removal of the bias. The reversible motion of the domain walls leads to a large enhancement of the dielectric response with little loss. Moreover, the large effective dielectric constant is rather temperature independent, decreasing only at cryogenic temperatures where the domain wall motion is frozen out.

Ferroelectric nanodomains in superlattices have already received significant attention from the theoretical community [50, 51, 52], whereas experimentally they remain largely unexplored. One interesting feature of superlattices is the possibility of electrostatic interaction between the separate ferroelectric layers. For short period superlattices the ferroelectric layers are expected to couple by polarizing the paraelectric component between them. This leads to a uniform polarization throughout the thickness, minimizing depolarizing fields associated with polarization discontinuities. For larger thicknesses of the paraelectric layers, however, it becomes progres-

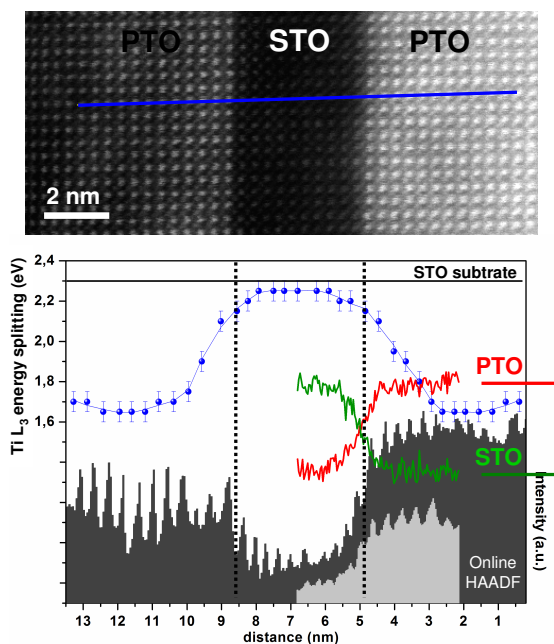


Figure 9: Top: TEM image of a superlattice composed of 18 unit cells of PTO and 10 unit cells of STO showing coherent growth and chemically sharp interfaces. Bottom: depth profile of the Ti L_3 energy splitting (blue points) along the blue line in the TEM image above together with the chemical profiles (green and red curves) determined from the OK edge positions.

sively more costly to maintain a polarization in the paraelectric component and the ferroelectric layers are expected to decouple, confining the polarization to the nominally ferroelectric component only. We have studied the degree of this interlayer coupling using X-ray diffraction, electrical measurements and transmission electron microscopy (TEM) combined with electron energy loss near edge spectroscopy (ELNES). Using the latter technique we have been able to image the structural distortions associated with the ferroelectric domain structures with unprecedented unit cell resolution.

The crystal field splitting of the e_g and t_{2g} energy levels of the transition metal atom (in this case Ti) depends sensitively on the structural distortion, being highest for the most symmetric (cubic) phase. By measuring this energy splitting we can therefore map the structural distortion in each unit cell of the superlattice. Fig. 9 shows that although the interfaces are atomically sharp from the chemical point of view, the structural distortion varies over 5 unit cells within the PTO layer, due to the depolarizing field at the interface. Surprisingly, little variation is observed in the STO layer, indicating a decoupling of the ferroelec-

tric layers.

9 Interfaces, domain walls and disorder: pathways to multifunctionality and complex behavior (P. Paruch)

Interfaces in epitaxial oxide heterostructures can provide pathways to new functional properties via symmetry breaking [53], strain [54], or the coupling between different instabilities in the materials [15], allowing a new “oxide interface engineering” of desirable properties such as ferroelectric behavior and dielectric response. An alternative route towards new functionalities is through ferroic domain walls, where the above effects, as well as extrinsic mechanisms such a local concentration of defects, can play an important role [16][55]. In addition, ferroic domain walls provide a useful model system in which the fundamental static and dynamic behavior of a disordered elastic manifold [17] can be readily accessed. Our research effort focuses on these three subjects, using different atomic force microscopy (AFM) techniques to directly probe individual domain walls in $\text{Pb}(\text{Zr}_{0.2}\text{Ti}_{0.8})\text{O}_3$ and BiFeO_3 , and X-ray scattering complemented by electrical measurements for structural and functional analysis of superlattices of BiFeO_3 - LaFeO_3 .

9.1 $\text{BiFeO}_3/\text{LaFeO}_3$ superlattices

$\text{BiFeO}_3/\text{LaFeO}_3$ superlattices were grown using rf off-axis sputtering on both (100) SrTiO_3 and (110) DyScO_3 substrates with and without a SrRuO_3 bottom electrode. For the superlattices on SrTiO_3 , X-ray diffraction (XRD) experiments show that the out-of-plane lattice parameter decreases almost linearly down to an overall BiFeO_3 content of 50%. When the superlattices are grown on DyScO_3 substrates, with a slightly larger in-plane lattice parameter, there is a sharp drop in the out-of-plane lattice parameter at an overall BiFeO_3 content of about 80% (Fig. 10), which may indicate a change in the magnitude or direction of the ferroelectric polarization, as for a typical ferroelectric the unit cell is elongated along the polarization direction.

Direct measurements of the ferroelectric polarization are in good agreement with the XRD results for the superlattices on DyScO_3 . Superlattices with little LaFeO_3 have similar ferroelectric behavior to pure BiFeO_3 , showing square hysteresis loops with a slightly reduced polarization, but also reduced leakage when compared to pure BiFeO_3 . Superlattices with more LaFeO_3 show very slanted hysteresis loops. In the region close to the abrupt change in the

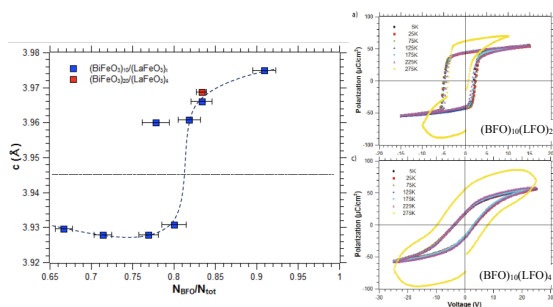


Figure 10: Left: evolution of the out-of-plane lattice parameter in $\text{BiFeO}_3/\text{LaFeO}_3$ superlattices on DyScO_3 . Upper right: polarization-voltage hysteresis for BiFeO_3 rich superlattices. Lower right: polarization voltage hysteresis for LaFeO_3 rich superlattices.

out-of-plane lattice parameter, these slanted loops can be irreversibly changed into normal square loops by applying a sufficiently large voltage. Despite the only gradual change in out-of-plane lattice parameter, the superlattices grown on SrTiO_3 show similar polarization loops as those on DyScO_3 , although we have not observed the irreversible change in the hysteresis response in these superlattices.

We are currently investigating the exact nature of the ferroelectric phase for LaFeO_3 -rich superlattices, which may be due to the presence of pinned domain walls or an in-plane polarization perpendicular to the applied field, and to characterize the magnetic ordering of the $\text{BiFeO}_3/\text{LaFeO}_3$ system.

9.2 New functionalities at ferroelectric domain walls in $\text{Pb}(\text{Zr}_{0.2}\text{Ti}_{0.8})\text{O}_3$

A number of microscopic scenarios have been proposed to explain the domain- and domain-wall-specific conductivity in normally insulating ferroelectric materials, including a reduction of the band gap and a potential step across the domain wall in BiFeO_3 [55], Fowler-Nordheim tunneling/tunneling electroresistance in thin ferroelectric films [56, 57, 58], the possibility of domain wall bending in sub-switching electric fields, and extrinsic mechanisms such as the accumulation of charged defects at domain walls. To better understand the roles played by these different mechanisms, we have investigated 180° domain walls in epitaxial thin films of the relatively simple, tetragonal ferroelectric $\text{Pb}(\text{Zr}_{0.2}\text{Ti}_{0.8})\text{O}_3$, grown by rf magnetron sputtering on SrTiO_3 substrates with 50 nm SrRuO_3 bottom electrodes. As shown in Fig. 11, in ultrahigh vacuum conductive-AFM (C-AFM) measurements of a 71.5 nm thick film, we observe a domain-wall-specific 1000-fold

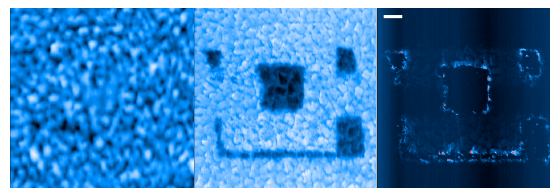


Figure 11: left: uniform topography of measured area after several domain writing steps, showing that the observed signal is not related to metal deposition from the AFM tip. Center: piezoresponse force microscopy (PFM) phase signal showing up- (light) and down- (dark) polarized domains. right: C-AFM taken with 2 V ac, showing strong conduction enhancement localized at domain walls, with a faint conduction increase in the side of the down-polarized domains. The scale bar is 250 nm.

increase in conductivity, and a Schottky-like current-voltage behavior, similar to what has been observed in BiFeO_3 , in spite of the absence in $\text{Pb}(\text{Zr}_{0.2}\text{Ti}_{0.8})\text{O}_3$ of a band gap reduction or a potential step at the 180° domain walls. No conduction increase is measured inside the up-polarized domains, and only a very faint conduction is observed in the down-polarized domains.

We are also continuing our studies of a domain-wall specific lateral piezoresponse in these films [18, 19], collaborating with the group of Salia Cherifi at IPCM Strasbourg, whose second harmonic generation measurements show an unexpected domain-wall-specific in-plane response, and should allow a complete mapping of the local ferroelectric/piezoelectric tensor.

9.3 Thermal effects on ferroelectric domain wall dynamics

To study the growth of nanoscale ferroelectric domains in thin films, domain arrays were written by applying voltage pulses for different time lengths with the AFM tip [20, 21]. From the piezoresponse force microscopy (PFM) measurements, estimates of the domain wall velocity as a function of the writing time and applied electric field during growth were extracted. All domain writing and reading was carried out *in situ* under different pressure, temperature and atmosphere conditions in a variable temperature, ultrahigh vacuum AFM system. Room temperature results for air and N_2 atmospheres at ambient pressure did not show any differences beyond experimental uncertainty. However, a significant difference in domain size was observed between measurements at ambient pressure and $p \sim 10^{-10}$ mbar at room temperature, indicating the influence

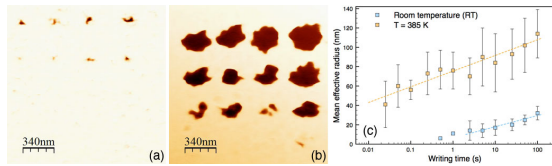


Figure 12: PFM measurements of ferroelectric domains written in ultrahigh vacuum with writing times ranging from 0.1 to 100 s, at room temperature (a) and $T = 385$ K (b). (c) Effective domain radius as a function of writing time for room temperature and $T = 385$ K, with averaging over five and eight measurements, respectively.

of a water meniscus around the tip and the possible role of screening charges from the atmosphere. Moreover, a significant anisotropy in domain shapes was observed in vacuum, compared to more regular, circular domains at ambient pressure. Finally, measurements at $T = 385$ K in vacuum showed an enhanced domain growth, reflected by larger domain sizes with respect to room temperature (Fig. 12). At present, we are working on confirming and comparing these results with domain growth dynamics in different thickness films subjected to different heating regimes.

10 Roughness crossovers of interfaces (T. Giamarchi)

We addressed different open questions in the field of classical disordered elastic systems (DES), i.e. the study of elastic interfaces or periodic systems embedded into a disordered medium. This class of models aims at describing, e.g., ferromagnetic or ferroelectric domain walls in thin films, or vortex lattices in type II superconductors, which can be seen as elastic structures whose underlying medium is necessarily subject to some inhomogeneities. The resulting competition between elasticity and disorder, blurred by thermal fluctuations at finite temperature, gives rise to metastability and glassy properties.

10.1 Thermal effects on the roughness of an interface

We addressed on one hand the question of the geometrical fluctuations of an interface, which can be quantitatively characterized by its roughness as a function of the lengthscale from which it is considered and on the other hand the velocity-force characteristics $v(f)$ of the steady state of a DES in the presence of an external driving force, in particular in the quasi-static creep regime at very small driving force.

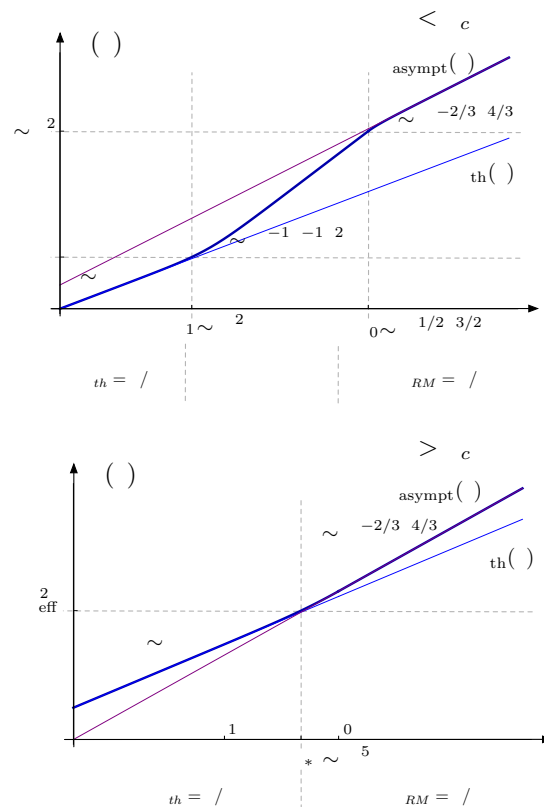


Figure 13: Roughness of an interface of thickness ξ as a function of the distance along the interface. The combination of the thickness and the finite temperature leads to two crossover scales separating regimes of very different roughness.

In the generic DES approach, the bulk properties of the materials are actually reduced to the following parameters: T the temperature, D the strength of disorder (e.g. the variance of a δ -correlated random potential or force), c the elastic constant or stiffness of the interface, ξ the typical width of the interface or alternatively the correlation length of disorder. We focused on the role of a non-zero ξ , as it is always the case in experimental systems, in the particular case of a one-dimensional interface in a random-bond disorder, and identified the characteristic crossover lengthscales in the roughness below and above a typical temperature $T_c \sim (\xi c D)^{1/3}$. Those lengths are of special importance to understand the onset of avalanches occurring in the creep dynamics, and may actually crucially depend on ξ at sufficiently low temperature. We computed the roughness via a Gaussian Variational Method (GVM) both on a 1D DES and on an effective “toy model” [22] (selected as an “editor’s suggestion”). The results are shown in Fig. 13.

10.2 Thermal effects on the roughness of an interface

We studied numerically the depinning transition of driven elastic interfaces in a random-periodic medium with localized periodic-correlation peaks in the direction of motion [23]. Taking into account the finite size along the direction of motion is mandatory to get a reliable analysis of the numerical results. We obtained the dynamical roughness diagram. At small length scales, we find the critical and fast-flow regimes typical of a random-manifold (or domain wall) depinning, and, at large length scales, the critical and fast-flow regimes typical of a random-periodic (or charge density wave) depinning, which corresponds to a quite different universality class. From the study of the equilibrium geometry we are also able to infer the roughness diagram in the creep regime, extending the depinning roughness diagram below threshold. Our results are relevant for understanding the geometry at depinning of arrays of elastically coupled thin manifolds in a disordered medium such as driven particle chains or vortex-line planar arrays. They also allow us to properly control the effect of transverse periodic boundary conditions in large-scale simulations of driven disordered interfaces.

11 Collaborative efforts

YBCO/LCMO studies involve efforts from UniFR and PSI. The LAO/STO studies are pursued at UniFR, PSI and UniGE. Photoemission on nickelates is performed at UniFR with films prepared at UniGE. The behavior of domain walls is studied with an experimental and theoretical collaboration at UniGE.

MaNEP-related publications

- ▶ [1] J. Hoppler, H. Fritzsche, V. K. Malik, J. Stahn, G. Cristiani, H. U. Habermeier, M. Rössle, J. Honolka, A. Enders, and C. Bernhard, *Physical Review B* **82**, 174439 (2010).
- [2] J. Hoppler, J. Stahn, C. Niedermayer, V. K. Malik, H. Bouyanfif, A. J. Drew, M. Rössle, A. Buzdin, G. Cristiani, H.-U. Habermeier, B. Keimer, and C. Bernhard, *Nature Materials* **8**, 315 (2009).
- [3] J. Hoppler, J. Stahn, H. Bouyanfif, V. K. Malik, B. D. Patterson, P. R. Willmott, G. Cristiani, H. U. Habermeier, and C. Bernhard, *Physical Review B* **78**, 134111 (2008).
- [4] A. J. Drew, C. Niedermayer, P. J. Baker, F. L. Pratt, S. J. Blundell, T. Lancaster, R. H. Liu, G. Wu, X. H. Chen, I. Watanabe, V. K. Malik, A. Dubroka, M. Rössle, K. W. Kim, C. Baines, and C. Bernhard, *Nature Materials* **8**, 310 (2009).
- ▶ [5] L. Schulz, L. Nuccio, M. Willis, P. Desai, P. Shakya, T. Kreouzis, V. K. Malik, C. Bernhard, F. L. Pratt, N. A.

- Morley, A. Suter, G. J. Nieuwenhuys, T. Prokscha, E. Morenzoni, W. P. Gillin, and A. J. Drew, *Nature Materials* **10**, 39 (2011).
 - [6] M. Björck, C. M. Schlepütz, S. A. Pauli, D. Martoccia, R. Herger, and P. R. Willmott, *Journal of Physics: Condensed Matter* **20**, 445006 (2008).
 - ▶ [7] C. M. Schlepütz, M. Björck, E. Koller, S. A. Pauli, D. Martoccia, Ø. Fischer, and P. R. Willmott, *Physical Review B* **81**, 174520 (2010).
 - ▶ [8] S. A. Pauli, S. J. Leake, B. Delley, M. Björck, C. W. Schneider, C. M. Schlepütz, D. Martoccia, S. Paetel, J. Mannhart, and P. R. Willmott, *Physical Review Letters* **106**, 036101 (2011).
 - [9] C. Cancellieri, N. Reyren, S. Gariglio, A. D. Caviglia, A. Fête, and J.-M. Triscone, *Europhysics Letters* **91**, 17004 (2010).
 - [10] P. R. Willmott, S. A. Pauli, R. Herger, C. M. Schlepütz, D. Martoccia, B. D. Patterson, B. Delley, R. Clarke, D. Kumah, C. Cionca, and Y. Yacoby, *Physical Review Letters* **99**, 155502 (2007).
 - ▶ [11] C. W. Schneider, M. Esposito, I. Marozau, K. Conder, M. Doebeli, Y. Hu, M. Mallepell, A. Wokaun, and T. Lippert, *Applied Physics Letters* **97**, 192107 (2010).
 - [12] R. Scherwitzl, P. Zubko, C. Lichtensteiger, and J.-M. Triscone, *Applied Physics Letters* **95**, 222114 (2009).
 - ▶ [13] M. Nakano, H. Alves, A. S. Molinari, S. Ono, N. Minder, and A. F. Morpurgo, *Applied Physics Letters* **96**, 232102 (2010).
 - ▶ [14] P. Zubko, N. Stucki, C. Lichtensteiger, and J.-M. Triscone, *Physical Review Letters* **104**, 187601 (2010).
 - [15] E. Bousquet, M. Dawber, N. Stucki, C. Lichtensteiger, P. Hermet, S. Gariglio, J.-M. Triscone, and P. Ghosez, *Nature* **452**, 732 (2008).
 - [16] H. Béa and P. Paruch, *Nature Materials* **8**, 168 (2009).
 - [17] T. Giamarchi, A. B. Kolton, and A. Rosso, in *Jamming, Yielding and Irreversible Deformation in Condensed Matter*, M. C. Miguel and J. M. Rubi, eds. (Springer-Verlag, Berlin, 2006), vol. 688 of *Lecture Notes in Physics*, p. 91.
 - [18] J. Guyonnet, H. Béa, F. Guy, S. Gariglio, S. Fusil, K. Bouzehouane, J.-M. Triscone, and P. Paruch, *Applied Physics Letters* **95**, 132902 (2009).
 - ▶ [19] J. Guyonnet, H. Béa, and P. Paruch, *Journal of Applied Physics* **108**, 042002 (2010).
 - [20] T. Tybell, P. Paruch, T. Giamarchi, and J.-M. Triscone, *Physical Review Letters* **89**, 097601 (2002).
 - [21] P. Paruch, T. Giamarchi, and J.-M. Triscone, *Physical Review Letters* **94**, 197601 (2005).
 - ▶ [22] E. Agoritsas, V. Lecomte, and T. Giamarchi, *Physical Review B* **82**, 184207 (2010).
 - ▶ [23] S. Bustingorry, A. B. Kolton, and T. Giamarchi, *Physical Review B* **82**, 094202 (2010).
- ### Other references
- [24] M. R. Norman, D. Pines, and C. Kallin, *Advances In Physics* **54**, 715 (2005).
 - [25] R. S. Decca, H. D. Drew, E. Osquiguil, B. Maiorov, and J. Guimpel, *Physical Review Letters* **85**, 3708 (2000).
 - [26] I. Bozovic, G. Logvenov, M. A. J. Verhoeven, P. Caputo, E. Goldobin, and M. R. Beasley, *Physical Review Letters* **93**, 157002 (2004).
 - [27] H. Takagi, T. Ido, S. Ishibashi, M. Uota, S. Uchida, and Y. Tokura, *Physical Review B* **40**, 2254 (1989).

- [28] V. Kresin, Y. Ovchinnikov, and S. Wolf, *Applied Physics Letters* **83**, 722 (2003).
- [29] G. Alvarez, M. Mayr, A. Moreo, and E. Dagotto, *Physical Review B* **71**, 014514 (2005).
- [30] D. Marchand, L. Covaci, M. Berciu, and M. Franz, *Physical Review Letters* **101**, 097004 (2008).
- [31] A. Ohtomo and H. Y. Hwang, *Nature* **427**, 423 (2004).
- [32] R. Pentcheva and W. E. Pickett, *Physical Review Letters* **102**, 107602 (2009).
- [33] S. Thiel, G. Hammerl, A. Schmehl, C. W. Schneider, and J. Mannhart, *Science* **313**, 1942 (2006).
- [34] N. Nakagawa, H. Y. Hwang, and D. A. Muller, *Nature Materials* **5**, 204 (2004).
- [35] H. Chen, A. M. Kolpak, and S. Ismail-Beigi, *Physical Review B* **79**, 161402(R) (2009).
- [36] M. Stengel and D. Vanderbilt, *Physical Review B* **80**, 241103(R) (2009).
- [37] A. Kalabukhov, R. Gunnarsson, J. Börjesson, E. Olsson, T. Claeson, and D. Winkler, *Physical Review B* **75**, 121404(R) (2007).
- [38] W. Siemons, G. Koster, H. Yamamoto, W. A. Harrison, G. Lucovsky, T. H. Geballe, D. H. A. Blank, and M. R. Beasley, *Physical Review Letters* **98**, 196802 (2007).
- [39] G. Giovannetti, S. Kumar, D. Khomskii, S. Picozzi, and J. van den Brink, *Physical Review Letters* **103**, 156401 (2009).
- [40] M. L. Medarde, *Journal of Physics: Condensed Matter* **9**, 1679 (1997).
- [41] G. Catalan, *Phase Transitions* **81**, 729 (2008).
- [42] S. R. Barman, A. Chainani, and D. D. Sarma, *Physical Review B* **49**, 8475 (1994).
- [43] M. Medarde, D. Purdie, M. Grioni, M. Hengsberger, Y. Baer, and P. Lacorre, *Europhysics Letters* **37**, 483 (1997).
- [44] I. I. Mazin and D. J. Singh, *Physical Review Letters* **79**, 733 (1997).
- [45] J. F. Mitchell, D. N. Argyriou, C. D. Potter, D. G. Hinks, J. D. Jorgensen, and S. D. Bader, *Physical Review B* **54**, 6172 (1996).
- [46] A. T. Zayak, X. Huang, J. B. Neaton, and K. M. Rabe, *Physical Review B* **77**, 214410 (2008).
- [47] E. Dagotto, *Nanoscale Phase Separation and Colossal Magnetoresistance* (Springer, 2003).
- [48] J. He, A. Borisevich, S. V. Kalinin, S. J. Pennycook, and S. T. Pantelides, *Physical Review Letters* **105**, 227203 (2010).
- [49] S. K. Streiffer, J. A. Eastman, D. D. Fong, C. Thompson, A. Munkholm, M. V. Ramana Murty, O. Auciello, G. R. Bai, and G. B. Stephenson, *Physical Review Letters* **89**, 067601 (2002).
- [50] V. A. Stephanovich, I. A. Luk'yanchuk, and M. G. Karkut, *Physical Review Letters* **94**, 047601 (2005).
- [51] Y. L. Li, S. Y. Hu, D. Tenne, A. Soukiassian, D. G. Schlom, X. X. Xi, K. J. Choi, C. B. Eom, A. Saxena, T. Lookman, Q. X. Jia, and L. Q. Chen, *Applied Physics Letters* **91**, 112914 (2007).
- [52] S. Lisenkov, I. Ponomareva, and L. Bellaiche, *Physical Review B* **79**, 024101 (2009).
- [53] H. N. Lee, H. M. Christen, M. F. Chisholm, C. M. Rouleau, and D. H. Lowndes, *Nature* **433**, 395 (2005).
- [54] J. H. Haeni, P. Irvin, W. Chang, R. Uecker, P. Reiche, Y. L. Li, S. Choudhury, W. Tian, M. E. Hawley, B. Craigo, A. K. Tagantsev, X. Q. Pan, S. K. Streiffer, L. Q. Chen, S. W. Kirchoefer, J. Levy, and D. G. Schlom, *Nature* **430**, 758 (2004).
- [55] J. Seidel, L. W. Martin, Q. He, Q. Zhan, Y.-H. Chu, A. Rother, M. E. Hawkrige, P. Maksymovych, P. Yu, M. Gajek, N. Balke, S. V. Kalinin, S. Gemming, F. Want, G. Catalan, J. F. Scott, N. A. Spaldin, J. Orenstein, and R. Ramesh, *Nature Materials* **8**, 229 (2009).
- [56] V. Garcia, S. Fusil, K. Bouzehouane, S. Enouz-Vedrenne, N. D. Mathur, S. Barthélémy, and M. Bibes, *Nature* **460**, 81 (2009).
- [57] A. Gruverman, D. Wu, H. Lu, Y. Wang, H. W. Jang, C. M. Folkman, M. Y. Zhuravlev, D. Felker, M. Rzechowski, C.-B. Eom, and E. Y. Tsybal, *Nano Letters* **9**, 3539 (2009).
- [58] P. Maksymovych, S. Jesse, P. Yu, R. Ramesh, A. P. Bad-dorf, and S. V. Kalinin, *Science* **324**, 1421 (2009).

Project 2

Materials for future electronics

Project leader: A. Morpurgo (UniGE)

Participating members: M. Büttiker (UniGE), L. Forró (EPFL), T. Giamarchi (UniGE), E. Giannini (UniGE), D. van der Marel (UniGE), A. Morpurgo (UniGE), P. Paruch (UniGE), C. Renner (UniGE), M. Sgrist (ETHZ), J.-M. Triscone (UniGE)

Introduction: The development of novel materials with sufficiently well-controlled properties opens the possibility to fabricate electronic devices that are useful for fundamental physics and have potential for future applications. According to a strategy typical of mesoscopic physics, these devices enable focused experiments to probe specific microscopic electronic processes not accessible in bulk systems. In this project we focus on classes of novel materials that are sufficiently under control to enable the realization of new nanostructures. The materials investigated include oxide heterostructures and thin films, carbon-based materials such as graphene and organic molecular crystals, and their combinations. In the spirit of mesoscopic physics, the experimental program proceeds in conjunction with a theoretical effort, that is needed to provide assistance in designing specific devices and experiments, as well as in the interpretation of the experimental results.

Summary and highlights

Several important results have been obtained in the three main themes of this project (oxide interfaces, carbon electronics, and theory), as well as in the study of topological insulators, a new research line that has started more recently. The observation of quantum conductance oscillations at $\text{LaAlO}_3/\text{SrTiO}_3$ interfaces represents a key finding in the area of oxide nanoelectronics, as it demonstrates the two-dimensional character of the electron gas in this system. Research in carbon electronics has continued in different directions. On graphene and related systems, next to advances in transport experiments (i.e. in nanoribbons and with graphene on SrTiO_3 substrates), the observation of a giant Faraday effect in graphene monolayers, and the discovery of the formation of a charge density wave accompanying superconductivity in intercalated graphite

are important highlights. The observation of band-like transport in n -type organic single-crystal field-effect transistors is a long awaited achievement in the field of organic electronics. The theoretical activity has witnessed a surge of interest in the investigation of the topological electronic properties of different systems, such as unconventional superconductors and graphene. For the latter, the relation between gapped bilayers and topological insulators has been understood in quite some detail, including the experimental relevance of edge effects in real bilayer devices where edges are very disordered. Finally, first experiments on three-dimensional topological insulators (Bi_2Se_3) have demonstrated the possibility to observe and control surface Dirac fermions in these systems, by means of quantum transport measurements on nanostructured devices.

1 Devices based on oxide materials

Research in this area has mainly focused on devices based on $\text{LaAlO}_3/\text{SrTiO}_3$ interfaces and carbon nanotubes combined with ferroelectric films. Next to the scientific results — discussed in detail below — it is worth stressing that considerable technological progress has taken place (e.g. substantial increase in the carrier mobility achieved in $\text{LaAlO}_3/\text{SrTiO}_3$ interfaces).

1.1 Two-dimensional quantum oscillations of the conductance at $\text{LaAlO}_3/\text{SrTiO}_3$ interfaces (J.-M. Triscone and A. Morpurgo)

One of the main unresolved issues concerning the $\text{LaAlO}_3/\text{SrTiO}_3$ interface pertains to the dimensionality of the conducting layer. While it is now clear that, using appropriate growth and annealing conditions, a confined metallic and superconducting electron gas can be formed at such interfaces, no conclusive demonstration of two-dimensional char-

acter in the normal state has been obtained so far. With this in mind, we performed a magneto-transport study on $\text{LaAlO}_3/\text{SrTiO}_3$ interfaces in which the mobility has been boosted by an optimization of the growth conditions, reaching values of the order of several thousands cm^2/Vs . In samples characterized by these mobilities, quantum conductance oscillations become visible at temperatures of the order of 1 K and in magnetic fields of the order of a few Tesla, conditions that are accessible in our laboratories. This work was carried out in the Triscone group in collaboration with the group of Morpurgo in order to explore this phenomenon in magnetic fields up to 15 T and temperatures down to 250 mK. The Fermi surface of two-dimensional electronic states generates clear experimental signatures in the Shubnikov-de Haas (SdH) effect: for a two-dimensional electron gas (2DEG) the quantum oscillations depend only on the perpendicular component of the magnetic field.

Fig. 1a shows the variation of sheet resistance $\Delta R = R(B) - R(0)$ in response to the application of a magnetic field oriented perpendicular to the interface, recorded at different temperatures. The resistance measurements have been performed using a 4 point ac technique, with a current between 10 and 100 nA, in a standard Hall bar defined by photolithography, with a channel width of $500 \mu\text{m}$ and with voltage probes 1 mm apart. Below $T = 7 \text{ K}$, oscillations superimposed on a positive background are observed for fields larger than 3 T. The numerical derivative of the resistance with respect to magnetic field, presented in Fig. 1b, reveals that the oscillations are periodic in $1/B$.

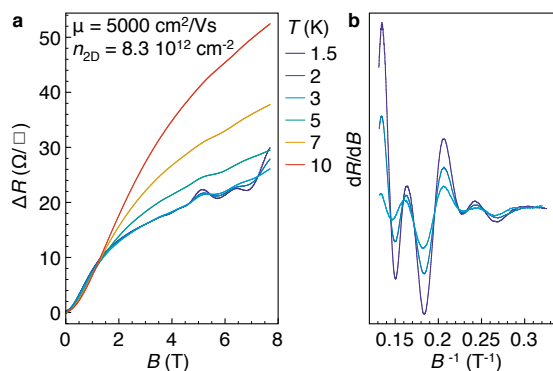


Figure 1: Shubnikov-de Haas oscillations at the $\text{LaAlO}_3/\text{SrTiO}_3$ interface. (a) Variation of the sheet resistance $\Delta R = R(B) - R(0)$ in response to the application of a magnetic field B oriented perpendicular to the $\text{LaAlO}_3/\text{SrTiO}_3$ interface, recorded at different temperatures T . (b) Numerical derivative dR/dB as a function of the inverse of the magnetic field.

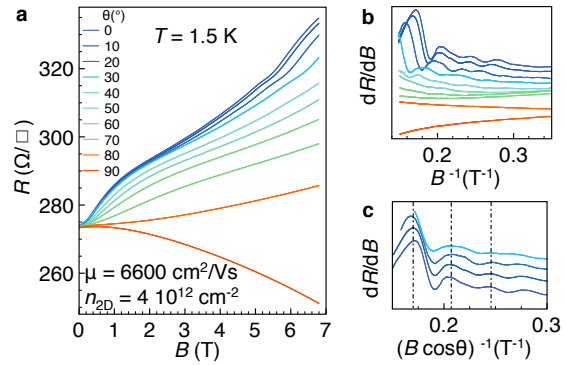


Figure 2: Angular dependence of the quantum oscillations. (a) Sheet resistance R as a function of magnetic field B recorded at different orientations (measured by the angle θ) with respect to the direction normal to the substrate. (b) Numerical derivative dR/dB as a function of the inverse of the magnetic field recorded at different orientations. (c) Numerical derivative dR/dB as a function of the inverse of the component of the magnetic field perpendicular to the plane of the interface. An offset has been introduced in each curve for clarity. The lines are a guide to the eye.

The dimensionality of the electronic states can be assessed by examining the angular dependence of the quantum oscillations. Fig. 2a displays $R(B)$ measured at $T = 1.5 \text{ K}$ on a different sample, for different angles θ . The angle θ measures the inclination of the magnetic field with respect to the normal to the interface at a fixed azimuthal angle. At $\theta = 0^\circ$ the magnetic field is applied perpendicular to the interface, while for $\theta = 90^\circ$ the magnetic field vector lies in the plane of the interface, parallel to the current. At $\theta = 90^\circ$ we observe a fairly large negative magneto-resistance. Figs. 2b and c show the derivative of the data as a function of B^{-1} and $(B \cos \theta)^{-1}$ respectively. It is apparent that the oscillation depends only on the perpendicular component of the magnetic field. This observation directly indicates that the oscillations arise from closed orbits in momentum space along a two-dimensional Fermi surface.

1.2 Nanodevices combining ferroelectric thin films and carbon nanotubes (P. Paruch)

Combining the exceptional electronic and structural properties of carbon nanotubes (CNT) with the non-volatile and reversible polarization of ferroelectric thin films presents a novel route towards multifunctional devices. A key aspect is the possibility to use the polarization to modulate the charge carrier density of the CNT, and the CNT to generate local electric field to control and probe ferroelectric domain structures with nanoscale res-

olution. Previous studies have demonstrated polarization switching of large domains using CNT [1], possible signatures of ferroelectric field effect modulation in devices containing multiple CNT [18], and a clear ferroelectric field effect in nanodevices with nanopatterned ferroelectric structures deposited on CNT [19]. Our current studies have focused on understanding the exact nature of domain switching and growth in the local electric fields of the CNT, as well as ferroelectric field effect modulation of individual single-walled CNT dispersed over the epitaxial ferroelectric thin films.

CNT-ferroelectric devices were realized by dispersion of single-walled CNT from suspension in aqueous solution onto $\text{PbZr}_{0.2}\text{Ti}_{0.8}\text{O}_3$ (PZT) thin films patterned with source and drain electrodes. The films are epitaxially grown on (001) oriented SrTiO_3 , with SrRuO_3 as a back gate electrode. Transconductance measurements on the devices containing semiconducting CNT showed an ON state with positive bias voltage applied to the gate electrode, confirming the *p*-type nature of the CNT-ferroelectric devices noted in previous studies [1]. A clockwise hysteresis in current vs gate voltage was observed, as expected for ferroelectric field effect. At low temperatures, sharp and repeatable fluctuations in the source-drain current — rather than a hysteretic behavior — are observed, with a magnitude comparable to what would be expected for universal conductance fluctuations. To further investigate the low-temperature behavior, as well as the exact correlation between ferroelectric hysteresis and hysteresis in the transconductance, measurements on devices with a range of different thickness ferroelectric films are in progress.

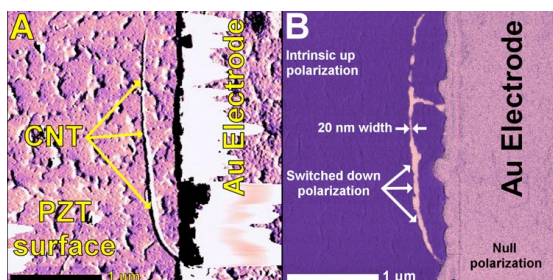


Figure 3: Left: AFM tapping mode topographic image of a 2.5 μm long CNT lying on a PZT thin film, laterally touching a Au electrode. Right: piezoresponse force microscopy (PFM) image of the same area after a 10 μs long +10 V pulse was applied between the top electrode (connected to the CNT) and the gate electrode (SrRuO_3) below the ferroelectric layer. The minimal lateral size of the switched ferroelectric domain is 20 nm.

In the CNT-ferroelectric devices we have also investigated domain switching and stability using the CNT as a local electric field source, to apply voltage pulses of different duration and magnitude across the ferroelectric thin film. With 10 μs voltage pulses, domains 20 nm wide were obtained (Fig. 3). For short writing times, CNT-written domains are generally smaller than those obtained with either standard AFM tips or macroscopic electrodes used to apply the electric field, although the final domain size is much more sensitive to local inhomogeneities in the sample. We are currently investigating polarization switching under CNT using more uniform films, with much smaller source and drain electrodes to minimize leakage.

2 Carbon-based electronics

The investigation of graphene and related materials has progressed through the use of a broad range of different experimental techniques. These include transport through nanodevices, optical spectroscopy to measure Faraday effect and ac Hall effect, electron-spin resonance through solvent-dispersed graphene layers, and scanning tunneling imaging and spectroscopy on superconducting intercalated graphite. On organic semiconductors, our research has focused on transistors based on high-quality single-crystals of *n*-type materials. The development of new nanoscale scanning probes based on carbon nanotubes has also progressed.

2.1 Magneto-transport through graphene nanoribbons (A. Morpurgo)

One of the key difficulties in using graphene for the realization of field-effect transistors is the absence of a gap separating valence and conduction bands, which prevents the use of gate electrodes to completely switch off transport. It has been observed early on that in graphene nanoribbons — i.e. narrow graphene constrictions created by etching larger flakes — the conductance can be suppressed completely at low temperature in a rather broad range of voltages around the charge neutrality point. To explain the phenomenon, size quantization effects were initially invoked, following theoretical predictions. In such a scenario, however, the predicted energy gap is smaller than the magnitude of the disorder normally present in graphene due, for instance, to random charges present on the underlying substrate. This type of disorder is even larger in narrow constrictions, due to the larger influence of the strongly

disordered edges. The presence of strong disorder casts serious doubts about the initially proposed origin of the transport gap. Subsequent theoretical work has suggested that the transport gap may instead originate from strong localization together with charging effects. In simple terms, disorder localizes charge carriers when the Fermi energy is small, leading to the formation of “islands” that make nanoribbons behave as a collection of quantum dots connected in series.

Until recently, no definite experiment capable of discriminating between these two possible explanations was identified. In the course of last year, we have performed a careful study of magneto-transport and shown that magneto-resistance measurements do provide a clear-cut answer [2]. If the opening of a band-gap was the mechanism responsible for the insulating state, the application of a magnetic field B corresponding to a magnetic length significantly smaller than the ribbon width should — via the formation of the zero-energy Landau level characteristic of graphene — suppress the transport gap completely. As a result, the conductance should increase from the small value measured at $B = 0$ ($G \approx 10^{-3} - 10^{-4} e^2/h$ for ribbons having a width of about 70 nm) to a value of $G \approx e^2/h$. On the contrary, if localization is the dominant mechanism, the transport gap should decrease in size by approximately a factor 2 (i.e. no complete suppression). In fact, the magnetic field causes breaking of time reversal symmetry, leading to a doubling of the localization length, thereby effectively increasing the size of the “islands” formed in the ribbons. Since these islands behave as quantum dots, their larger size implies a smaller charging energy and, hence, a smaller trans-

port gap. The magneto-transport measurements as a function of gate voltage and temperature show that indeed this is what happens: the energy scales (in bias voltage and temperature) associated to the transport gap are seen to decrease, but not to disappear (Fig. 4) [2]. In other independent experiments (in collaboration with Prof. Hakonen at the University of Helsinki), we have found additional support for the role of localization in graphene nanoribbons, through measurements of shot noise [3].

2.2 Transport through graphene on SrTiO₃ substrates (A. Morpurgo)

The transport properties of graphene are strongly influenced by the underlying substrate. In suspended graphene — where the substrate is removed — mobility values larger than 200 000 cm²/Vs can be achieved. These values are much larger than those observed on SiO₂ ($\approx 10\,000$ cm²), which is the substrate material normally used. To understand what are the key parameters determining the transport characteristics of graphene, it is interesting to perform studies using different substrates materials, characterized by well-defined, specific physical properties. To this end, we have started studying transport through graphene on SrTiO₃ single-crystals. What makes SrTiO₃ an interesting substrate is the very large relative dielectric constant ($\epsilon \simeq 300$ for T ranging from 300 to 70 K), which increases to even larger values when lowering the temperature from 70 K to 4 K (at 4.2 K $\epsilon \simeq 3000 - 10000$). Analyzing the transport properties in the temperature range where ϵ changes allows us to determine whether or not long range Coulomb potentials, which are strongly influenced by the increase in ϵ , determine the transport properties of graphene.

We performed transport measurements as a function of carrier density n , temperature T and magnetic field B , both in large Hall bar devices and in nanoribbons. We found that in Hall bar devices at $B = 0$ the density dependence of the conductance $G(n)$ does not change at all when the temperature is varied between 60 K and 240 mK (Fig. 5). This observation does not only provide information about scattering mechanism, but also about the low-density regime (where the conductance does not depend on n). Finding that the width (in carrier density) of the region where G is constant remains unchanged while ϵ increases by a factor of approximately 30 – 50, indicates that transport in the low-density regime is not determined by the so-called “puddles”, contrary

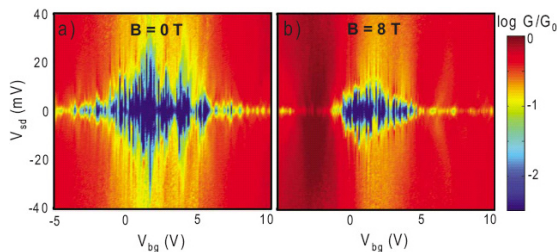


Figure 4: Conductance of a 70 nm wide graphene nanoribbon measured at $B = 0$ (a) and $B = 8$ T (b) as a function of gate and bias voltage. At low bias, the conductance is strongly suppressed in both cases, but in the presence of a magnetic field, the bias voltage needed to increase the conductance is approximately half of that needed at zero field. This is expected if the transport gap is due to strong localization in conjunction with charging effect.

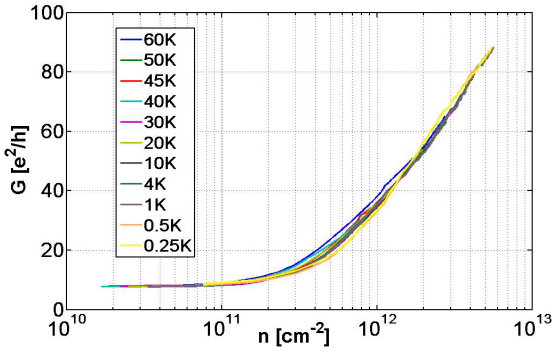


Figure 5: Density dependence of the conductance measured on graphene single-layer Hall bar on SrTiO_3 , at different temperatures in the range between 60 K and 240 mK. In this range the dielectric constant of the substrate changes by approximately a factor of 20 – 30. Nevertheless, the density dependence of the conductance remains entirely unchanged.

to what has been usually assumed in the past (“puddles” are regions in graphene where local accumulation of electrons and holes is determined by the local shift of the Dirac point, caused by random potential fluctuations). Despite the absence of any effect at zero magnetic field, the influence of the dielectric constant becomes apparent at large magnetic field, and in nanoribbons. In particular, we find that at 15 T the resistance at the charge neutrality point — when the Fermi level is in the middle of the $N = 0$ Landau level — decreases with lowering temperature, whereas on SiO_2 under the same conditions, the resistance increases with lowering T and becomes unmeasurably large. As the behavior observed on SiO_2 originates from electron-electron interaction, the phenomenon is a striking manifestation of screening due to the substrate. Similarly, the magnitude of the transport gap in nanoribbons that originates from the charging energies of disorder-induced “islands” is found to be suppressed by one order of magnitude as compared to SiO_2 , due to substrate screening. A quantitative analysis of the observation is ongoing.

2.3 Cyclotron resonance and Faraday rotation in epitaxial graphene (*D. van der Marel, A. Kuzmenko*)

Epitaxial growth of graphene by annealing of silicon carbide [20] is considered as an economically viable method of producing graphene for applications. The properties of graphene on Si- and C-faces of SiC are entirely different [21]. Graphene on the Si-side is Bernal-stacked, and has usually 1 – 2 atomic layers, including a so-called buffer layer covalently bonded to the

substrate. In contrast, graphene produced on the C-side has typically many layers with a random rotational stacking and a layer-dependent doping level, which results in the presence of several types of charge carriers.

We measured magneto-optical spectra on both types of epitaxial graphene. The optical absorption and Faraday rotation spectra (Fig. 6a) were combined to provide the diagonal and the Hall optical conductivities [4], thus producing the complete magneto-optical conductivity tensor. The measurements were performed in the far-infrared region, where the resonances due to Landau level transitions are present. The Faraday rotation of single-layer graphene on the Si-side (Fig. 6b) is found to be as large as several degrees (0.1 radian). This is a very large value given that the rotation, usually proportional to the thickness of the sample, comes from a single-atomic layer. We show that the rotation is strongly enhanced due to the cyclotron resonance, whose energy corresponds to the position of maximum slope.

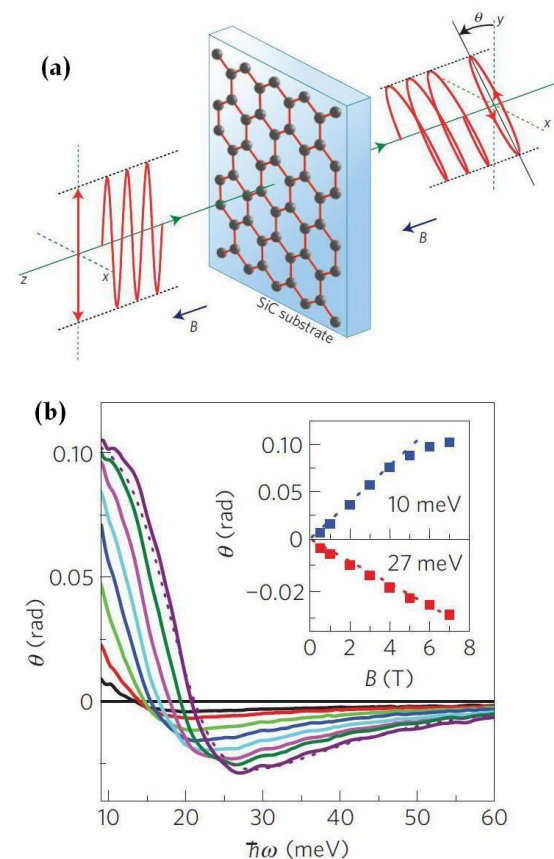


Figure 6: (a) Faraday effect experiment (b) measured on single-layer graphene grown on the Si-face of SiC at 5 K, at different magnetic fields (color code for the magnetic field values are given on Fig. 7). The inset shows the magnetic field dependence at 2 selected photon energies.

The sign of the carriers involved (holes in this case) is given by the sign of the slope, which means that this experiment allows distinguishing electrons and holes without making electrical contacts to the sample. Such a large optical rotation opens pathways to the use of graphene in magneto-optical applications.

The cyclotron frequency is found to depend linearly on the magnetic field. This quasi-classical behavior, different from the square-root field dependence of the Landau level energies of massless Dirac quasi-particles in monolayer graphene, is due to a high doping (about 10^{13} cm^{-2}) induced by the substrate.

The Faraday rotation spectra on multilayer graphene grown on the C-face of SiC are very different (Fig. 7). Here we observe different cyclotron-resonance features: those originating from the highly doped bottom layers, closest to the substrate, and those due to the individual low-index Landau level transitions, coming from the weakly doped top layers (pointed

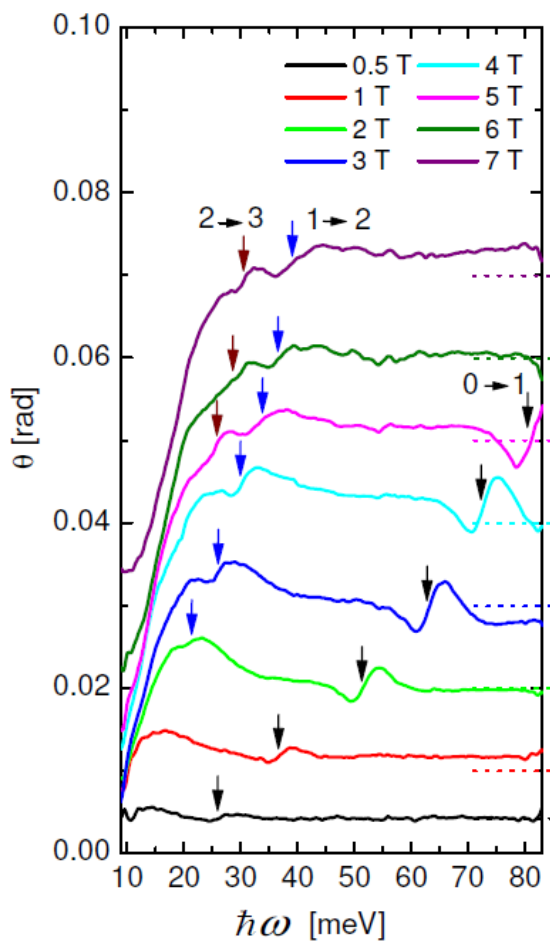


Figure 7: Faraday rotation measured on multilayer graphene grown on the C-face of SiC at 5 K. The arrows show transitions between individual Landau levels.

to by arrows). The cyclotron rotation now originates from electron-like carriers, as evidenced by a different sign of the slope of the Faraday angle as compared to the data on the monolayer graphene. From the slope of Faraday rotation at the transition energies of the inter Landau-level transitions, we derive the sign of the charge carriers involved, which in this case is also of electron type. The energies of the Landau level transitions show clearly a square-root dependence on magnetic field, while the cyclotron energy shows a linear field dependence. This is the behavior expected for the quantum and the classical regimes, respectively.

2.4 Reducing graphene oxide in polar solvent — an ESR study (L. Forró)

An important step towards the application of graphene is elaborating a method for its large scale production which could give a high-quality material. One of the most promising methods is the so-called graphene oxide (GO) route. There are several variants of making of GO [22] with a common expectation to recover the pristine properties of graphene simply by reducing formerly oxidized graphite. However, the optimization of the oxidation/reduction parameters is still in progress. Our previous ESR study [Circic *et al.*, submitted] on hydrazine and hydrogen plasma reduced graphene oxide (RGO) has shown a relatively large amount of defects which may hinder the advantageous properties of graphene.

Recently, the Nesper group has elaborated a reduction method of GO flakes by thermal treatment in a polar solvent without using hydrazine or hydrogen plasma. Both the precursor (GO) flakes (average size $\sim 1 \mu\text{m}^2$) and the final material (RGO) were studied and characterized by ESR in a broad temperature range (4 – 295 K). ESR is able to separate the contributions of localized and conduction electrons from the overall magnetic response and to detect magnetic correlations. For the structural characterization and the size distribution of the flakes, atomic force microscopy (AFM), scanning electron microscopy (SEM), and high-resolution transmission electron microscopy (HRTEM) were used.

Depending on the solvent boiling point, the reduction was done at the following temperatures: 100, 120, and 140°C. The results of thermal treatment in polar solvents are shown in Fig. 8 in the form of χ^*T versus T . They are compared to the behavior of the magnetic

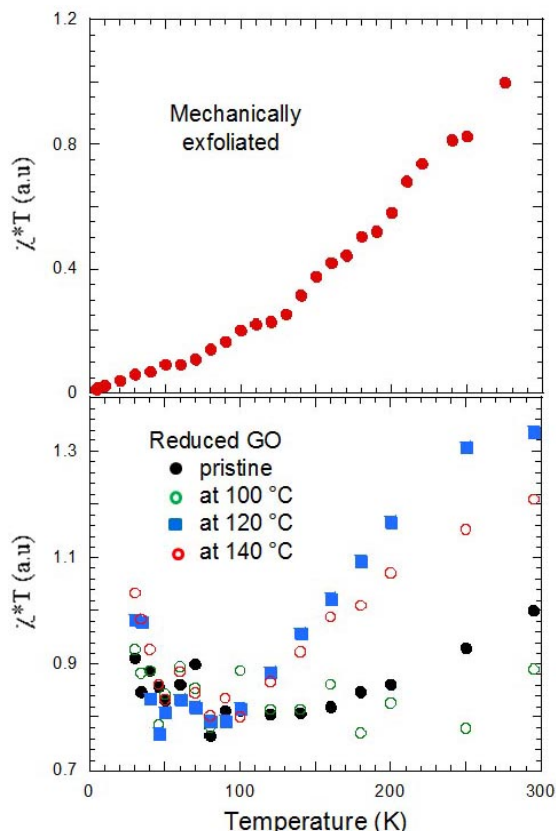


Figure 8: Temperature dependence of the T^* spin susceptibility of GO reduced at different temperatures in a polar solvent (lower panel). The χ^*T plot illustrates how the Pauli component develops as a function of the reduction temperature. It is compared to the sample obtained by mechanical exfoliation (upper panel).

susceptibility of the mechanically exfoliated graphene sample (Fig. 8, upper panel) [5].

In the overall susceptibility, the increasing weight of χ with reduction is noticed in the χ^*T product (Fig. 8). One can clearly distinguish the Curie-term ($\sim T$ independent value) and the Pauli contribution (T dependent term) to the overall susceptibility. With the increasing temperature of the heat treatment one can follow a clear development of a Pauli component to the spin susceptibility in the χ^*T plots. By comparing the slopes of the χ^*T plots for various reduction temperatures one can conclude that the reduction is starting to be efficient above 120°C. This is a highly encouraging result concerning future applications because it shows that the restoration of the metallicity of graphene is feasible with a mild reduction step [6].

However, there is plenty of room for improvement. The choice of the polar solvent, the temperature of the heat treatment, and the size of the starting material's flake should be op-

timized in the near future. The goal is to obtain graphene samples which show properties close to the ones prepared by mechanical exfoliation [5].

2.5 Graphite intercalated compounds (C. Renner)

The goal of this project is to study superconductivity in CaC_6 — the graphite intercalated compound (GIC) with the highest T_c to date [23] — both in single-crystals, as well as in *in situ* intercalated bilayer graphene specimen. Here we focus on intercalated crystals. The superconducting phase of CaC_6 has been investigated previously in great detail using scanning tunneling microscopy (STM) and spectroscopy (STS) by Bergeal *et al.* [24], including the vortex state. They found spectroscopic characteristics in excellent agreement with weak coupling BCS superconductivity. In our work, we achieved first atomic resolution imaging to find that this superconductor also displays a charge density wave (CDW) above the superconducting transition [7].

Stage I calcium intercalated graphite (CaC_6 , Fig. 9) single-crystals were cleaved under ultra-high vacuum conditions and studied by STM at 78 K, above the superconducting transition. Atomic resolution micrographs of the same surface region reveal two distinct atomic scale textures (Fig. 10). The first one (Fig. 10a) is in perfect agreement with a stage I intercalated structure (Fig. 9b). The Fourier transform (Fig. 10b) shows that calcium atoms form a $\sqrt{3}a_0$ lattice, rotated 30° with respect to the carbon lattice a_0 . The second one is a static modulation of the structure and electronic density of states with a period three times that of the Ca superlattice (Figs. 10c, d). An interesting finding is that the surface is much rougher in the absence of stripes than when stripes are

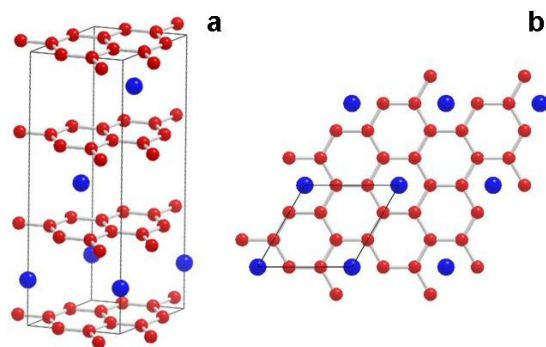


Figure 9: (a) Atomic structure of stage I Ca intercalated graphite. (b) Plane view expected to be seen by STM. Ca atoms are in blue and C atoms are in red.

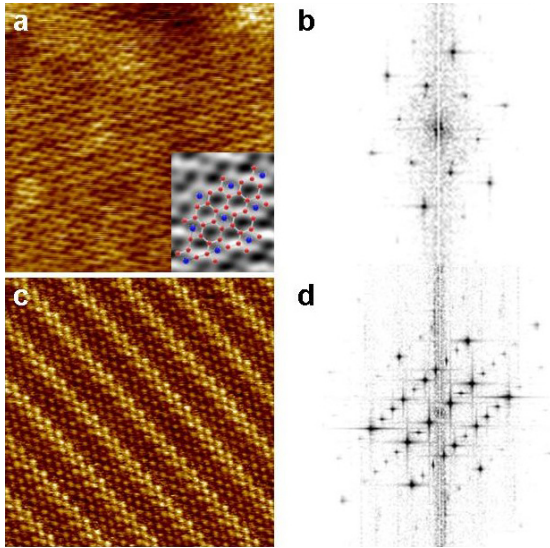


Figure 10: STM micrographs of CaC_6 at 78 K. (a) Atomic scale contrast revealing both the C and Ca lattices. Inset: magnification showing the perfect match to the stage I intercalation model. (b) Fourier transform of the micrograph in (a) showing the hexagonal C and Ca lattices. (c) Charge density wave modulation superposed on the C and Ca lattices and (d) corresponding Fourier transform.

present.

All experimental evidence points to a CDW to explain the static modulation seen in Fig. 10c. CDWs have been suggested as a possible origin for a variety of anomalous long-range superlattices seen in GICs and graphite, by means of electron diffraction and STM. However, in the absence of electronic structure measurements, these experiments were unable to rule out other effects, including Moiré patterns often observed by STM on graphite, electron standing waves, and surface reconstruction or Ca lattice depletion. Fig. 10 demonstrates that the stripes coexist with the expected C and Ca lattices. This precludes the possibility that the stripe phase is a surface reconstruction, i.e. that it results from a depletion or rearrangement of the Ca intercalants or C lattice. Secondly, STS of striped areas reveals a gap of about 475 meV at the Fermi level in the local density of states, which cannot be explained by a Moiré pattern. Finally, we find that the stripe periodicity does not change with tunneling bias, thus ruling out electron standing waves and Friedel oscillations, which are dispersing effects.

We propose the following mechanism for the CDW formation [7]: as the material is cooled, the negative thermal expansion of the graphene sheets flattens the planes, making an in-plane distortion of the Ca lattices between the graphene sheets (as observed in our

STM data) energetically favorable. The distortion is transverse and triggers charge motion on the graphene sheet immediately adjacent to the perturbed Ca atoms, leading to the stripe phase. This scenario is consistent with the observed coincidence of the displaced Ca atoms with the stripe peak in positive bias and the stripe trough in negative bias STM micrographs. Such a mechanism is also consistent with the observation that the stripes do eventually decay during STM imaging, and the hysteretic behavior seen in bulk magnetization. Both findings indicate that the stringent flat, high-purity sample conditions required to maintain the CDW cannot be recovered if the sample transforms out of the CDW phase (where STM shows the surface roughness to increase) or is otherwise affected, so as to destroy the CDW state. These requirements also explain why below the CDW transition the sample behaves as a better metal than when it is in its normal high-temperature state, as it is observed in temperature dependent resistance measurements.

The microscopic process driving the CDW formation is not clear at this time, although Fermi surface (FS) nesting would be a natural candidate. There are several reported FS, determined both experimentally and theoretically. Even though these all exhibit the potential for nesting, we find no nesting vectors matching the q -vector of the stripes observed in our STM data. However, given various discrepancies between the candidate FS, such as missing or extra bands and differing values of charge transfer, together with the difficulties assigning the correct nesting vector for similar systems (e.g. NbSe_2), we cannot discard this possibility. Another interesting open question is the interplay between the CDW and superconducting phases. Both questions are the subject of ongoing investigations.

2.6 Carbon nanotube functionalized atomic force microscopy tips (*P. Paruch*)

The small diameter, high aspect ratio, mechanical robustness, and chemical inertness, in conjunction with their high electrical conductivity, make carbon nanotubes an ideal system to realize new probes for atomic force microscopy. Carbon nanotube functionalized probes have been used previously for nanolithography [25, 26], and ferroelectric switching [8]. In combination with a SiO_2 coating to increase their rigidity, they have also been used for piezoresponse force microscopy, to image ferroelectric domains [27]. The aim of our work is to de-

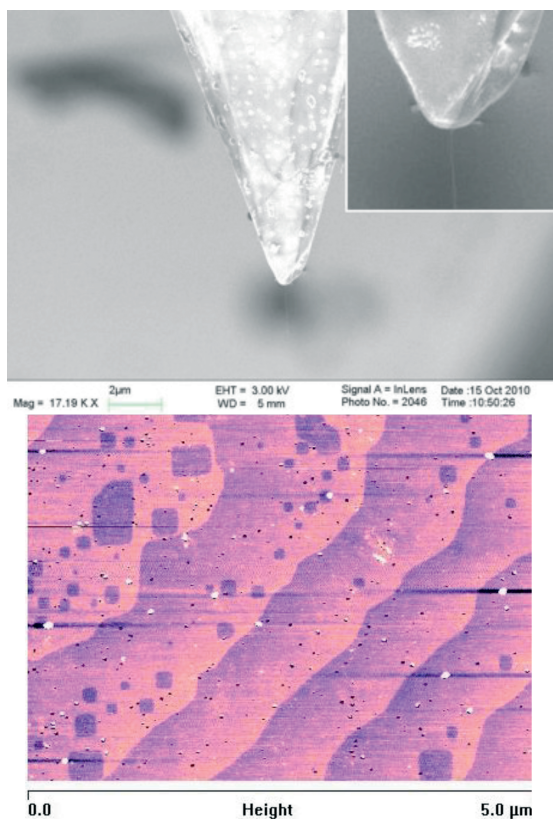


Figure 11: Top: SEM image of a carbon nanotube grown on the apex of a Si MicroMasch tip. Bottom: topography image of an etched SrTiO₃ surface acquired with a CNT-functionalized AFM tip.

velop a polyvalent CNT-AFM tip allowing a broad spectrum of electric and magnetic measurements, enabling nanoscale studies of ferroelectric and multiferroic thin films.

We used chemical vapor deposition (CVD) to directly grow single-walled CNT on commercial Si-based AFM tips. We have optimized all key aspects of the process, including the catalyst preparation (Fe hydroxy polymer) and deposition (electrophoresis was chosen as the most reliable technique to control the catalyst density to desired levels), the reduction and growth temperatures, and the feeder gas mixture. With this process, long (1 – 2 μm), well-aligned CNT grow reliably along the surface of the AFM tip and protrude from its apex (Fig. 11 top). After determining the CNT length by means of either scanning electron microscopy (SEM) or force-distance measurements in tapping mode AFM, the long CNT are shortened using electrical etching to ~ 200 – 400 nm. Topographic AFM imaging using the shortened CNT-functionalized tips shows high resolution, as indicated by a sharper determination of step features, as compared to what is possible with standard AFM tips (Fig. 11 bottom). To allow magnetic as well

as electric AFM measurements, the CNT have to be coated by a magnetic metal prior to SiO₂ rigidification. We are currently optimizing the metal deposition process to allow a uniform and even coating of the CNT.

2.7 Band-like transport in *n*-type organic transistors (A. Morpurgo)

Organic field-effect transistors (FETs) are normally classified as being either *n*- or *p*-type, depending on whether conduction occurs upon accumulation of electrons or holes. In principle, organic semiconductors should support both electron and hole conduction (i.e. ambipolar transport). However, it is well known that electron transport is harder to achieve, as its occurrence is often prevented from a number of extrinsic factors. For instance, for most organic materials, different types of impurities (e.g. oxygen and water) act as efficient electron traps, while not affecting much hole transport. As a consequence, whereas high-quality single-crystal *p*-type FETs could be realized to investigate the intrinsic transport properties of molecular semiconductors, for *n*-type organic semiconductors this has not been possible so far.

We recently discovered that PDIF-CN₂ single-crystals FETs can lead to record high electron mobility values, systematically larger than of 1 cm²/Vs. In this project we have succeeded in using these devices to achieve the first observation of band-like transport in *n*-type organic semiconductors. Specifically, we fabricated PDIF-CN₂ FETs in which a single-crystal is suspended on top of the gate electrode, with air — or vacuum — as gate dielectric, and measured the temperature dependence of the electron mobility. At room temperature, mobility values of ~ 5 cm²/Vs can be reproducibly realized. The mobility increases upon lowering temperature, reaching values of ~ 7 cm²/Vs at about 150 – 200 K (and as large as 11 cm²/Vs in the best devices), before decreasing slowly at lower temperature (Fig. 12). In some devices, we also succeeded in measuring the Hall effect. The increase in mobility with lowering temperature and the observation of Hall effect represent the first demonstration of band-like transport of electrons in organic FETs. In addition, we have also performed measurements with ionic liquid gates (by simply inserting the ionic liquid in the “air gap” of the suspended devices) and found that the presence of ionic liquid does not suppress the carrier mobility significantly in the majority of the devices studied [9]. From the technological point

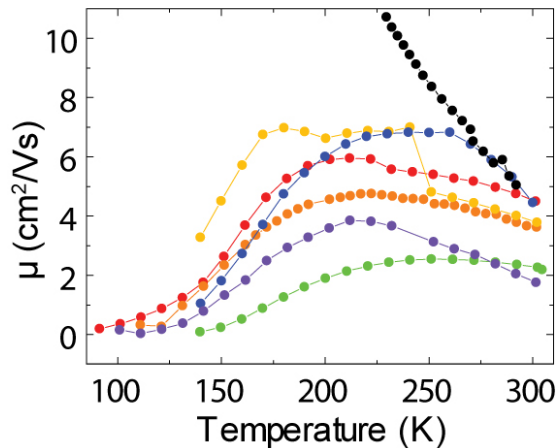


Figure 12: Mobility of PDIF-CN₂ single-crystal transistors measured (in a four terminal configuration) as a function of temperature. Upon lowering temperature from 300 K to 150 – 200 K, the mobility increases. The black dots correspond to the best device, in which a record high — for *n*-type FETs — mobility of 11 cm²/Vs has been reached (the device broke at approximately 220 K).

of view, this is an important result, because the use of ionic liquid gates enables a substantial lowering of the voltage that needs to be applied to the gate, to switch on the device: ionic-liquid gated PDIF-CN₂ FETs work properly with 1 – 3 V applied to the gate electrode.

3 Theory

Next to activities in the originally planned directions — e.g. the investigation of superconductivity in quasi-one-dimensional systems — considerable work has been devoted to the study of the topological electronic properties of different material systems. Last year work in this area has mainly been motivated by the analysis of specific materials that had been subject of previous investigation within MaNEP (e.g. graphene devices and Sr₂RuO₄). At the same time, new systems are also starting to be considered (e.g. three-dimensional topological insulators), which in some cases are also being studied experimentally.

3.1 Gapped bilayer graphene as a marginal topological insulator (M. Büttiker and A. Morpurgo)

Two-dimensional topological insulators are materials characterized by the simultaneous presence of an excitation gap in the bulk and gapless states at the edges. They constitute a new class of condensed matter states, which are not only fundamentally interesting, but

also potentially useful in applications ranging from spintronics to quantum computation. Practical examples of 2D topological insulating materials that can be used in experiments, however, are still limited. Therefore, an important task in this emerging field is to search for more candidates, to examine them in topological terms, and to understand their common aspects and differences.

Gapped bilayer graphene (Fig. 13) bears a great similarity to one of the known classes of two-dimensional topological insulators, namely the quantum spin Hall insulators [28, 29]. In ideal conditions, both systems accommodate counter-propagating gapless edge states (with opposite spin-polarization for quantum spin Hall insulators, and opposite valley-polarization for gapped bilayer graphene), originating from similar nontrivial topological properties of the bulk states [10, 11]. Conduction through these edge states can be dominant in electronic transport when the chemical potential lies in the bulk band gap and the temperature is low enough. A practical — and yet crucial — difference, however, is how the edge states act against disorder that is unavoidably present in the devices. While the edge states in the quantum spin Hall insulators benefit from the topological protection against perturbations that preserve time reversal invariance — a theoretical prediction that has been confirmed in a series of beautiful experiments [30, 31] — the fate and experimental relevance of the edge states in gapped bilayer graphene (where topological protection is missing) have not been analyzed theoretically. Our investigations [10, 11] have addressed and clarified this issue in a two-fold way. Having in mind actual devices, we have analyzed the robustness of the edge states in gapped bilayer graphene against strong edge disorder.

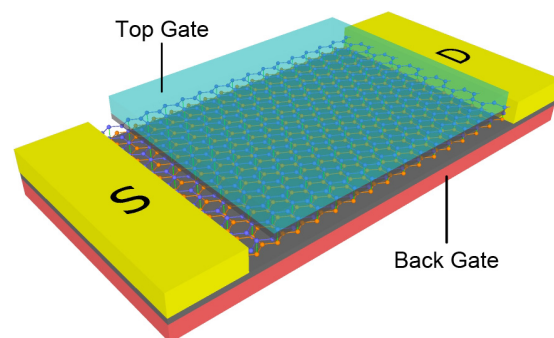


Figure 13: Experimental setup for gapped bilayer graphene. The bulk energy gap can be opened and tuned by applying a perpendicular electric field to the bilayer graphene sample [10].

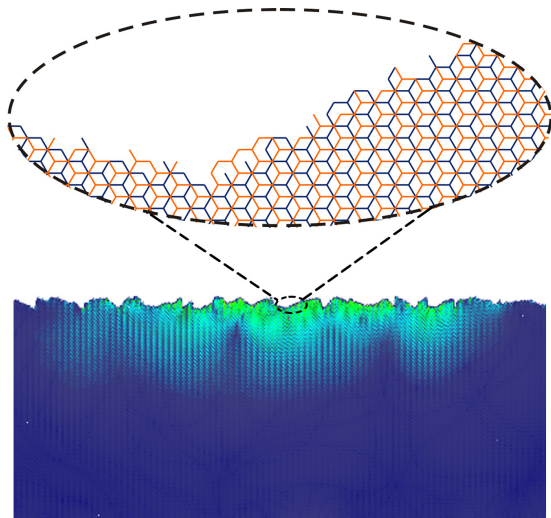


Figure 14: Edge state in a gapped bilayer graphene ribbon. Lower panel: light colors indicate a high electron density. Upper panel: disordered edge [10].

der [10]; on the conceptual side, we have examined the deep connection between the edge and the bulk states, to reveal that the properties of gapped bilayer graphene are those characteristic of marginal topological insulators [11].

In Ref. [10], we have simulated gapped bilayer graphene with realistic edge disorder, and found a universal limit in the localization of the edge states inside the bulk gap (Fig. 14). In this universal limit, the localization length of the edge states depends only on the magnitude of the bulk gap, and remains sizable, with a range of magnitudes that is experimentally relevant. We have also compared gapped bilayer graphene with a (gapped) square lattice tight-binding model. The square lattice tight-binding is topologically trivial and, indeed, we found that edge states are not present neither with ideal nor with rough edges, thereby confirming the crucial role played by the nontrivial topology of the bulk band structure. Next to their clear theoretical interest, our results have experimental relevance: in fact, we found that the contribution to the subgap conductance due to variable range hopping through the localized edge states provides a dominant transport mechanism in devices with only weak bulk disorder. Experimentally, such devices have already been realized by suspending graphene bilayers, and transport measurements seem indeed to be consistent with our predictions.

In Ref. [11], we have analyzed at the conceptual level the edge states associated to each of the valleys present in gapped bilayers, for disorder-free edges with different structures. Specifically, we have examined the defining

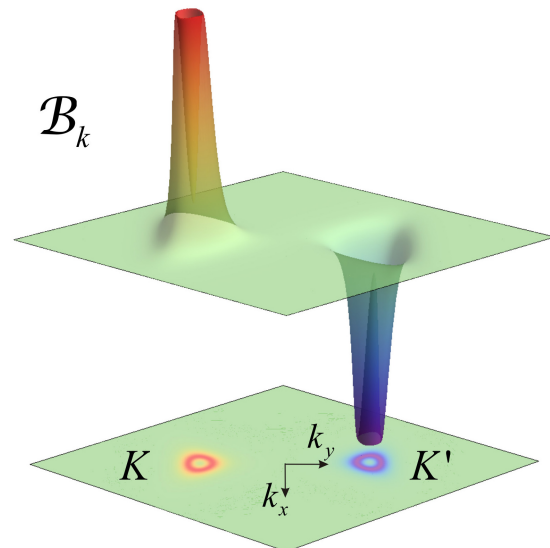


Figure 15: The contribution of the bulk states to the overall topological number, effectively measured by the “magnetic” flux in k -space, is quantized but opposite for the two valleys of gapped bilayer graphene [11].

relation for two-dimensional topological insulators, which states that the number of edge states is determined by the topological number associated to the bulk states, a concept commonly termed bulk-edge correspondence. We found that such a bulk-edge correspondence is absent for individual valleys. In each valley, the actual number of edge states depends on specific boundary conditions (determined by the edge structure), even when the edges do not introduce any intervalley coupling. The absence of a bulk-edge correspondence for individual valleys in gapped bilayer graphene reveals the fundamental difference between this system and quantum spin Hall insulators. The difference is rooted in the fact that the two valleys contribute oppositely to the overall topological number. Therefore, the Brillouin zone as a whole is globally trivial (Fig. 15), despite the fact that individual valleys possess non-trivial topological properties. We have discussed in detail the implications of this finding, and understood them as the defining characteristic of a marginal topological insulator — a concept that had been earlier used in the discussion of abstract theoretical models, but which had not been analyzed in the context of specific material systems. The concept of marginal topological insulator is important, because it is not limited to gapped bilayer graphene, but can be naturally extended to other multi-valley systems.

3.2 Band structure and topological superconductivity (M. Sigrist)

This project is part of the special collaboration program on topological matter. Some projects related to this topic are also reported in Project 4 in connection with chiral p -wave superconductivity in ruthenates.

a) *Band structure and edge spin currents* Aspects of topological unconventional superconductivity in a system whose band structure resembles that of two of the three bands of Sr_2RuO_4 have been investigated by Imai and Sigrist. The $d_{yz}/d_{zx} - t_{2g}$ orbitals are likely the bands subdominant for superconductivity in the material. However, their structure incorporates an intriguing feature. Both orbitals separately generate, through (intraorbital) intersite hopping, two quasi-one-dimensional bands. Interorbital hybridization enters through nearest neighbor hopping and onsite spin-orbit coupling. The resulting two-band structure yields an electron- and a hole-like Fermi surface. It has been recognized several years ago that the configuration of hybridizations leads to the anomalous Hall effect [12][32]. It was also shown that this type of two-band structure yields z -axis polarized spin currents at the surface of the main axis, which could result in corrections to the anomalous Hall effect and spin Hall effect in mesoscopic samples [12].

b) *Topological superconductivity and edge states* There are two unconventional superconducting states with topological properties which are considered in this project, the chiral and the helical p -wave states. The first is most likely realized in Sr_2RuO_4 , similar to the A -phase of ^3He , and has the symmetry $\mathbf{d} = \Delta \hat{z}(k_x \pm ik_y)$. The second one, with $\mathbf{d} = \Delta(\hat{x}k_x + \hat{y}k_y)$, is similar to the B -phase of ^3He . Within a single-band picture, both states have topological character in the sense that a spin-dependent Chern number N_s can be defined, such that for the chiral state $N_\uparrow = N_\downarrow = 1$ and the helical state $N_\uparrow = -N_\downarrow = 1$. The former leads to a quantized edge current in the charge channel, and the latter in the spin channel.

In the two-band situation, both superconducting states receive canceling contributions to the Chern numbers such that they are separately “topological” restricted to the individual Fermi surfaces, but with opposite N_s . Studying a slab (ribbon) geometry, Imai and collaborators show that, nevertheless, edge bound states are generated supporting a net charge or spin current, respectively. These currents are non-universal in magnitude and not topologically protected.

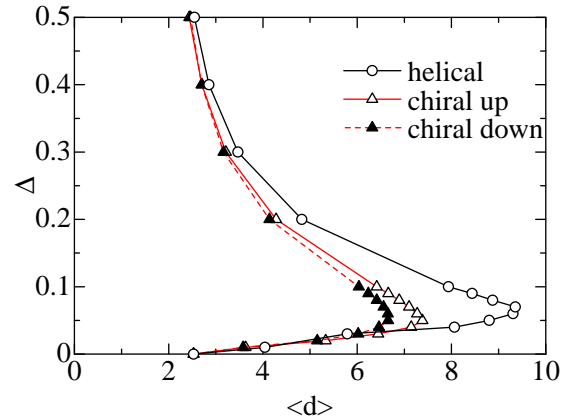


Figure 16: Gap magnitude versus the penetration depth $\langle d \rangle$ (units lattice constant). For the helical state the up and down spin currents are by symmetry equal in absolute magnitude such that only one curve is displayed. For the chiral state the underlying charge current yields different values for up and down spin currents. The overall non-monotonic behavior is in all cases the same. The gap is given in arbitrary units.

In this project, several aspects are studied, such as, for instance, the interplay with the surface spin currents in the two superconducting states. Interestingly, both states maintain a spin current contribution. While this is not surprising for the helical state, which introduces its own spin current together with the one induced by spin-orbit coupling, the chiral state corresponding to an in-plane equal spin pairing states allows for z -axis polarized spin currents. The edge spin current of the metallic normal state is not due to a surface bound state but to interference effects. As soon as superconducting states appear, however, Andreev bound states emerge at the surface co-carrying the spin currents. This can be seen in the penetration of the spin current into the bulk, which for small superconducting gaps increases as compared to the metallic state, as a consequence of the large coherence length (corresponding to the penetration depth of the edge states), and shrinks above a certain gap value because of the decreasing coherence length (Fig. 16).

Further discussions are concerned with the character of the superconducting phase appearing at the surface, as here properties of non-centrosymmetric superconductivity should be present. The experimental implications for the observation of surface currents are being studied. The project is in progress and a first publication is in preparation.

3.3 Quantum wires coupled to a metallic plate (*T. Giamarchi*)

Recently fabricated superconducting wires with diameter $d < \xi_0$ (ξ_0 is the coherence length of the bulk superconductor) have attracted the attention of several theoretical and experimental research groups [33, 34]. Because of their reduced effective dimensionality, interesting phenomena like Luttinger liquid behavior, as well as the existence of quantum phase transitions and quantum critical points, have been predicted to occur [13]. The coupling to the external environment has important consequences on quantum critical systems, and remarkable effects — like the existence of dissipative-driven quantum phase transitions — have been predicted [14][35, 36]. In particular, we showed in a previous work [15] that quasi-particle tunneling between a 1D superconductor and a two-dimensional electron gas (2DEG) led to a quantum phase transition from the Luttinger liquid phase towards a novel phase in which superconductivity is stabilized.

To obtain a more detailed description that includes the effect of Coulomb interactions, we have examined the dissipative effects in a 1D superconductor induced by the local electromagnetic environment (i.e. a diffusive metal placed nearby). Using a path-integral formalism, we have described the dynamics of the plasma mode in a 1D superconductor capacitively coupled to the diffusive modes in the diffusive metal. We have shown that superconductivity in the wire can be drastically modified depending on the screening properties of the metal. In particular, dimensionality plays a major role, yielding a good superconductor with low resistance when the screening metal is two-dimensional, while it would turn the wire into the normal state in the one-dimensional case [16] (this article has been selected as an “Editor’s suggestion”).

4 Collaborative efforts

Among the different activities described above, there are several collaborative efforts that are essential for the success of the research in this project. Examples include collaborations between the groups of Prof. Triscone and Morpurgo on quantum transport through $\text{LaAlO}_3/\text{SrTiO}_3$ interfaces, the groups of Prof. Paruch and Triscone on the investigation of ferroelectrics and multiferroics, the groups of Prof. Morpurgo and Büttiker on the theoretical study of gapped bilayer graphene. Several other collaborations exist on different

projects that are in active stage of development (involving Prof. van der Marel, Renner, and Triscone). Here we describe in more detail a newly started research line that focuses on the investigation of topological properties of electronic materials. This activity originates from a joint proposal of Prof. Morpurgo, Sigrist, and van der Marel, and combines theoretical and experimental research. Part of the theoretical work done in this context is described in sections 3.1 and 3.2. Experiments have focused on the study of Bi_2Se_3 , the most promising representative material among three-dimensional topological insulators, and on HgTe . Bi_2Se_3 crystals were grown in the laboratory of E. Giannini (van der Marel’s group), and have been used to perform both optical spectroscopy experiments and quantum transport measurements on devices. A more exhaustive study and analysis of optical response has been performed on thick HgTe epitaxial films, another material system that is expected to behave as 3D topological insulator.

4.1 Superconductivity in intercalated topological insulators Bi_2Se_3 and Bi_2Te_3 (*E. Giannini*)

Bi_2Se_3 and Bi_2Te_3 , long known as thermoelectric materials, have been only recently found to be topological insulators [37]. Crystals of Bi_2Se_3 and Bi_2Te_3 are commonly reported to grow during slow cooling of the molten binary mixture, in a vacuum sealed quartz holder. We have grown these crystals by using the floating zone technique (FZ). A great care was taken to guarantee the homogeneity of the precursors, by preliminarily melting, crystallizing and re-grinding the precursors three times before the final growth process. Thanks to the peculiarities of the FZ technique, the chemical homogeneity of the produced crystals is improved. Moreover, the strong temperature gradient at the growing front allows a better control of the nucleation and growth process and provides a higher crystalline quality. Large (1 – 5 cm) crystals were grown, from which thin crystalline flakes (down to ~ 10 nm thick, $\sim 5 \mu\text{m}$ wide) have been exfoliated. The direct observation of Dirac fermions in transport measurements, so far hidden by impurity bulk conducting states, have been recently achieved at UniGE by the group of A. Morpurgo [17] on such flakes of Bi_2Se_3 . The addition of a third element in the structure of binary Bichalcogenides can strongly affect the electronic phase. Most excitingly, Cu-atom intercalation in Bi_2Se_3 was reported to result in superconductivity [38]. We have undertaken a system-

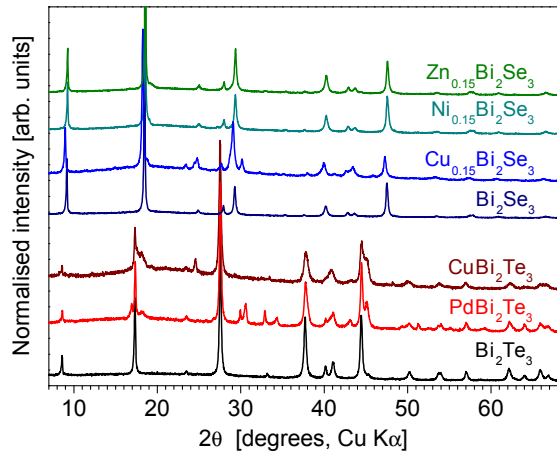


Figure 17: X-ray diffraction patterns of TM-intercalated topological insulators.

atic study of the effect of intercalations in both Bi_2Se_3 and Bi_2Te_3 , by using various transition metals ($TM = \text{Ni}, \text{Cu}, \text{Zn}, \text{Pd}, \text{Ag}, \text{Cd}, \text{Pt}, \text{Au}$). The third atom is expected to intercalate between the two quintuple blocks $Ch1\text{-Bi-}Ch2\text{-Bi-}Ch1$ ($Ch = \text{Se}, \text{Te}$) according to [38]. The intercalated compounds are still found to crystallize in the Bi_2Te_3 -type structure ($R\bar{3}m$ space group) only in the presence of Cu, Ni and Zn in Bi_2Se_3 , and of Pd and Cu in Bi_2Te_3 (Fig. 17).

A transition to a superconducting state was observed in $\text{Cu}_x\text{Bi}_2\text{Se}_3$ ($0 < x \leq 0.3$) and $\text{Pd}_y\text{Bi}_2\text{Te}_3$ ($0.5 \leq y \leq 1$), at T_c of ~ 3.5 K and ~ 5.5 K, respectively (Fig. 18).

4.2 Transport through gated Bi_2Se_3 crystals (A. Morpurgo)

Until recently, band theory of solids has classified all crystalline materials in metals — i.e. systems where the Fermi level is positioned in the middle of a band — and insulators — systems in which the Fermi level is located in the forbidden energy gap between bands. The recent discovery of topological insulators (TIs) has changed the situation. TIs are a new state of matter that occurs in the presence of strong spin-orbit interaction and time-reversal symmetry. In TIs, the Fermi energy is located in an energy gap in the bulk of the material, and inside a band at its surface. The surface states are “topologically protected”: they cannot be driven into an insulating state even in the presence of strong disorder, as long as time-reversal symmetry is present. The nature of the surface states depends on the dimensionality. In 2D TIs, they are helical 1D modes at the edges of the systems, leading to a conductance quantization that has been detected in transport experiments. In 3D TIs, the surface

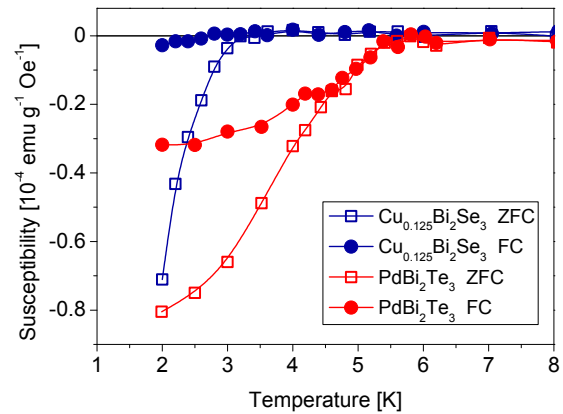


Figure 18: Superconducting transitions of intercalated $\text{Cu}_{0.15}\text{Bi}_2\text{Se}_3$ and PdBi_2Te_3 .

states consist of an individual band of 2D chiral Dirac fermions, in which the spin of an electron is “pinned” by its momentum. These Dirac bands have been observed in spectroscopy experiments (angle resolved photoemission and scanning tunneling spectroscopy) in different materials. However, so far their unambiguous detection in transport measurements has posed problems, owing to the presence of a parasitic parallel conductance due to the material bulk of unknown origin, and to the low mobility of the surface Dirac electrons

To minimize the effect of the parasitic bulk conduction, we have fabricated nanodevices on thin layers of Bi_2Se_3 exfoliated from bulk crystals, employing techniques similar to those used for the fabrication of graphene nanostructures. We performed transport experiments as a function of gate voltage V_g and magnetic field B . At each gate voltage, we observe Shubnikov-de Haas conductance oscillations, whose dependence on V_g gives rise to a fan diagram of Landau levels (Fig. 19). The Landau levels disperse in opposite directions when the gate voltage is swept across the charge neutrality point, providing a direct demonstration of the presence of electrons and holes. The position of the Landau levels can be indexed according to the relation $N = \frac{n\hbar}{e} \frac{1}{N+1/2}$, where n is the density of charge in the surface band of Dirac fermions and N is an integer indexing the Landau levels. The “1/2” term in the denominator — responsible for the so-called “half-integer quantum Hall effect” — is an unambiguous proof of the massless Dirac character of the electrons and holes. The experiments also provide indications regarding other aspects of the electronic properties of Bi_2Se_3 . In particular, they indicate the presence of an impurity band with a rather large density of states in the band gap of Bi_2Se_3 . Finally, since

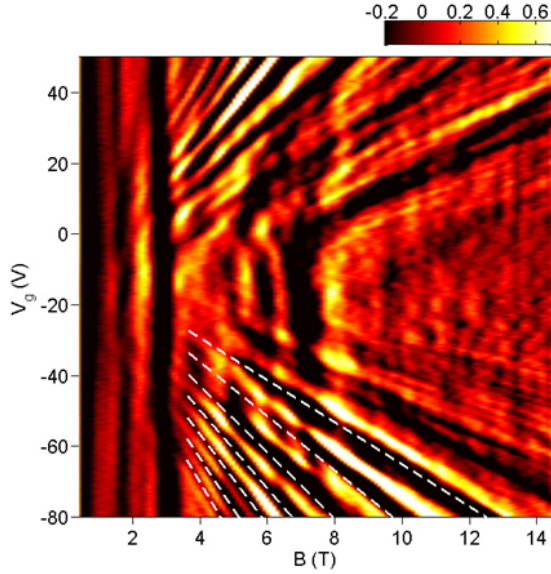


Figure 19: Color plot of $-d^2R/dB^2$ as a function of magnetic field and gate voltage measured at $T = 4.2$ K, in a two-terminal configuration. The dark features fanning out from $V_g \simeq -10$ V, $B = 0$ are minima in the Shubnikov-de Haas oscillations originating from Landau levels of Dirac fermions on the surface close to the gate electrode (the white dashed lines label the Landau levels of the Dirac holes). The V_g -independent “vertical” features are Shubnikov-de Haas oscillations from the far way surface, which is electrostatically screened from the gate electric field.

the electrodes used in our devices consisted of Ti/Al films that become superconducting below $T < 1$ K, we also succeeded in observing a Josephson supercurrent. The critical current of the devices was also found to be gate-voltage dependent, and to exhibit ambipolar behavior (i.e. the critical current becomes larger, as the gate voltage is increased away from the charge neutrality point, irrespectively of its polarity). This finding directly indicates that part of the supercurrent is carried by the Dirac surface fermions.

4.3 Magneto-optical study of HgTe (D. van der Marel)

The observation of the quantum spin Hall effect in CdTe-HgTe-CdTe quantum wells [39, 30] represents a significant advance in the ability to robustly segregate and control currents of opposite spin. The 2D topological edge states at the interface exhibits a quantum phase transition as the HgTe layer is reduced below a critical thickness. Later predictions extend the topological properties to three dimensions [40] when HgTe is strained. This has the effect of opening a bulk gap of the order of 22 meV.

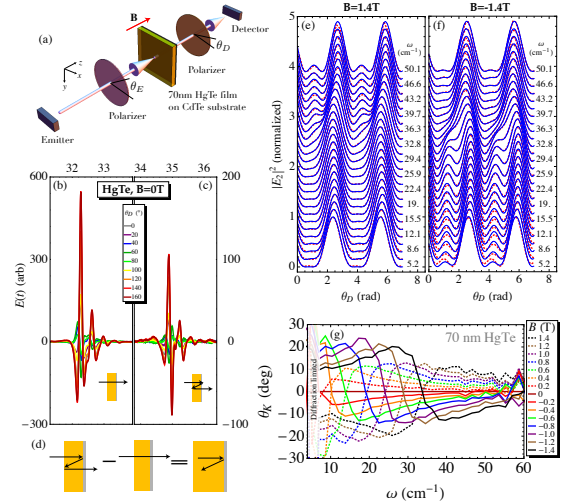


Figure 20: (a) Illustration of the magneto-optical THz apparatus. Example angle-dependent measurements of the 1st (b) and 2nd (c) pulses. (d) Pictorial rational for the expression $\theta_{F,2} - \theta_{F,1} = \theta_K$. Fit quality of the theoretical Faraday angle and ellipticity for (e) +1.4 T and (f) -1.4 T. (g) The Kerr angle determined from the fits for several magnetic fields.

Recently, some of the topological properties of strained HgTe became apparent in the behavior of the quantum Hall effect (QHE), which is attributed to surface states. One of the predicted properties of these materials is the topological magneto-electric effect (TME) [41], implying axion extensions of Maxwellian electrodynamics [42]. These effects have until now remained elusive due to the inexorable background carrier density [42]. Strain applied to bulk zero-gap HgTe, however, opens a band-inversion gap and forms a strong 3D topological insulator [40] with a single Dirac cone and π Berry’s phase.

To probe the topological surface state conduction, we have performed time domain (TD) magneto-optical (MO) measurements using a home-built superconducting magnet in a flow cryostat in a Faraday geometry, illustrated in Fig. 20, where we show also the Kerr angle obtained for fields of ± 1.4 T. The change in shape of the intensity distribution around 35 cm^{-1} is caused by a change in the complex Faraday angle at this frequency, which we attribute to an absorptive transition among surface state Landau-levels.

These data demonstrate that significant hybridization between bulk and surface states renormalizes the Landau levels, leading to a “massive Dirac” spectrum in contrast to the Bi_2X_3 compounds ($X = \text{Se}, \text{Te}$) [43, 44]

MaNEP-related publications

- [1] P. Paruch, A.-B. Posadas, M. Dawber, C. H. Ahn, and P. L. McEuen, *Applied Physics Letters* **93**, 132901 (2008).
- ▶ [2] J. B. Oostinga, B. Sacépé, M. F. Craciun, and A. F. Morpurgo, *Physical Review B* **81**, 193408 (2010).
- ▶ [3] R. Danneau, F. Wu, M. Y. Tomi, J. B. Oostinga, A. F. Morpurgo, and P. J. Hakonen, *Physical Review B* **82**, 161405(R) (2010).
- ▶ [4] I. Crassee, J. Levallois, A. L. Walter, M. Ostler, A. Bostwick, E. Rotenberg, T. Seyller, D. van der Marel, and A. B. Kuzmenko, *Nature Physics* **7**, 48 (2011).
- [5] L. Ćirić, A. Sienkiewicz, B. Náfrádi, M. Mionić, A. Magrez, and L. Forró, *Physica Status Solidi (b)* **246** (2009).
- ▶ [6] L. Ćirić, A. Sienkiewicz, D. M. Djokić, R. Smajda, A. Magrez, T. Kaspar, R. Nesper, and L. Forró, *Physica Status Solidi (b)* **247**, 2958 (2010).
- [7] K. C. Rahnejat, C. A. Howard, N. E. Shuttleworth, S. R. Schofield, K. Iwaya, C. F. Hirjibehedin, C. Renner, G. Aeppli, and M. Ellerby, submitted to *Nature Communications* (2011).
- [8] P. Paruch, T. Tybell, and J.-M. Triscone, *Proceedings of the 10th International Ceramics Congress CIMTEC 2002 D*, 675 (2002).
- ▶ [9] S. Ono, N. Minder, Z. Chen, A. Facchetti, and A. F. Morpurgo, *Applied Physics Letters* **97**, 143307 (2010).
- ▶ [10] J. Li, I. Martin, M. Büttiker, and A. F. Morpurgo, *Nature Physics* **7**, 38 (2011).
- ▶ [11] J. Li, A. F. Morpurgo, M. Büttiker, and I. Martin, *Physical Review B* **82**, 245404 (2010).
- [12] K. Wakabayashi and M. Sigrist, *AIP Conference Proceedings* **893**, 1269 (2007).
- [13] T. Giamarchi, *Quantum Physics in One Dimension* (Oxford University Press, Oxford, 2004).
- [14] H. P. Büchler, V. B. Geshkenbein, and G. Blatter, *Physical Review Letters* **92**, 067007 (2004).
- [15] A. M. Lobos, A. Iucci, M. Müller, and T. Giamarchi, *Physical Review B* **80**, 214515 (2009).
- ▶ [16] A. M. Lobos and T. Giamarchi, *Physical Review B* **82**, 104517 (2010).
- [17] B. Sacépé, J. B. Oostinga, J. Li, A. Ubaldini, N. J. G. Couto, E. Giannini, and A. F. Morpurgo, arXiv:1101.2352 (2011).
- [18] T. Sakurai, T. Yoshimura, S. Akita, N. Fujimura, and Y. Nakayama, *Japanese Journal of Applied Physics* **45**, 1036 (2006).
- [19] W. Y. Fu, Z. Xu, L. Liu, X. D. Bai, and E. G. Wang, *Nanotechnology* **20**, 475305 (2009).
- [20] C. Berger, Z. Song, T. Li, X. Li, A. Y. Ogbazghi, R. Feng, Z. Dai, A. N. Marchenkov, E. H. Conrad, P. N. First, and W. A. de Heer, *The Journal of Physical Chemistry B* **108**, 19912 (2004).
- [21] F. Speck, M. Ostler, J. Röhr, J. Jobst, D. Waldmann, M. Hundhausen, L. Ley, H. B. Weber, and T. Seyller, *Materials Science Forum* **645**, 629 (2010).
- [22] W. S. Hummers and R. E. Offeman, *Journal of the American Chemical Society* **80**, 1339 (1958).
- [23] T. E. Weller, M. Ellerby, S. S. Saxena, R. P. Smith, and N. T. Skipper, *Nature Physics* **1**, 39 (2005).
- [24] N. Bergeal, V. Dubost, Y. Noat, W. Sacks, D. Roditchev, N. Emery, C. Héroul, J. F. Maréché, P. Lagrange, and G. Loupiau, *Physical Review Letters* **97**, 077003 (2006).
- [25] J. H. Hafner, C. L. Cheung, and C. M. Lieber, *Journal of the American Chemical Society* **121**, 9750 (1999).
- [26] H. Dai, N. Franklin, and J. Han, *Applied Physics Letters* **73**, 1508 (1998).
- [27] N. Tayebi, Y. Narui, N. Franklin, C. P. Collier, K. P. Giapis, Y. Nishi, and Y. Zhang, *Applied Physics Letters* **96**, 023103 (2010).
- [28] C. L. Kane and E. J. Mele, *Physical Review Letters* **95**, 226801 (2005).
- [29] B. A. Bernevig, T. L. Hughes, and S. Zhang, *Science* **314**, 1757 (2006).
- [30] M. König, S. Wiedmann, C. Brüne, A. Roth, H. Buhmann, L. W. Molenkamp, X.-L. Qi, and S.-C. Zhang, *Science* **318**, 766 (2007).
- [31] A. Roth, C. Brüne, H. Buhmann, L. W. Molenkamp, J. Maciejko, X.-L. Qi, and S.-C. Zhang, *Science* **325**, 294 (2009).
- [32] H. Kontani, T. Tanaka, and K. Yamada, *Physical Review B* **75**, 184416 (2007).
- [33] K. Y. Arutyunov, D. S. Golubev, and A. D. Zaikin, *Physics Reports* **464**, 1 (2008).
- [34] A. Bezryadin, *Journal of Physics: Condensed Matter* **20**, 043202 (2008).
- [35] M. A. Cazalilla, F. Sols, and F. Guinea, *Physical Review Letters* **97**, 076401 (2006).
- [36] D. Meidan, Y. Oreg, and G. Refael, *Physical Review Letters* **98**, 187001 (2007).
- [37] Y. Xia, D. Qian, D. Hsieh, L. Wray, A. Pal, H. Lin, A. Bansil, D. Grauer, Y. S. Hor, R. J. Cava, and M. Z. Hasan, *Nature Physics* **5**, 398 (2009).
- [38] Y. S. Hor, A. J. Williams, J. G. Checkelsky, P. Roushan, J. Seo, Q. Xu, H. W. Zandbergen, A. Yazdani, N. P. Ong, and R. Cava, *Physical Review Letters* **104**, 057001 (2010).
- [39] B. A. Bernevig, T. L. Hughes, and S.-C. Zhang, *Science* **314**, 1757 (2006).
- [40] X. Dai, T. L. Hughes, X.-L. Qi, Z. Fang, and S.-C. Zhang, *Physical Review B* **77**, 125319 (2008).
- [41] X.-L. Qi, T. L. Hughes, and S.-C. Zhang, *Physical Review B* **78**, 195424 (2008).
- [42] H. Zhang, C.-X. Liu, X.-L. Qi, X. Dai, Z. Fang, and S.-C. Zhang, *Nature Physics* **5**, 438 (2009).
- [43] T. Hanaguri, K. Igarashi, M. Kawamura, H. Takagi, and T. Sasagawa, *Physical Review B* **82**, 081305(R) (2010).
- [44] P. Cheng, C. Song, T. Zhang, Y. Zhang, Y. Wang, J.-F. Jia, J. Wang, Y. Wang, B.-F. Zhu, X. Chen, X. Ma, K. He, L. Wang, X. Dai, Z. Fang, X. Xie, X.-L. Qi, C.-X. Liu, S.-C. Zhang, and Q.-K. Xue, *Physical Review Letters* **105**, 076801 (2010).

Other references

- [18] T. Sakurai, T. Yoshimura, S. Akita, N. Fujimura, and Y. Nakayama, *Japanese Journal of Applied Physics* **45**, 1036 (2006).
- [19] W. Y. Fu, Z. Xu, L. Liu, X. D. Bai, and E. G. Wang, *Nanotechnology* **20**, 475305 (2009).
- [20] C. Berger, Z. Song, T. Li, X. Li, A. Y. Ogbazghi, R. Feng, Z. Dai, A. N. Marchenkov, E. H. Conrad, P. N. First, and W. A. de Heer, *The Journal of Physical Chemistry B* **108**, 19912 (2004).
- [21] F. Speck, M. Ostler, J. Röhr, J. Jobst, D. Waldmann, M. Hundhausen, L. Ley, H. B. Weber, and T. Seyller, *Materials Science Forum* **645**, 629 (2010).

Project 3 Electronic materials for energy systems and other applications

Project leader: Ø. Fischer (UniGE)

Participating members: M. Abplanalp (ABB), Ph. Aebi (UniFR), J. Cors (UniGe and Phasis), M. Decroux (UniGE), D. Eckert (Bruker-BioSpin), Ø. Fischer (UniGE), R. Flükiger/C. Senatore (UniGE), J. Hulliger (UniBE), M. Kenzelmann (PSI), G. Patzke (UniZH), C. Renner (UniGE), N. de Rooij (EPFL), G. Triscone (Hepia), J.-M. Triscone (UniGE), A. Weidenkaff (Empa and UniBE), K. Yvon (UniGE)

Introduction: This project aims at the development of practical applications of research carried out in MaNEP. Most of the subprojects are carried out in direct collaboration with industrial partners.

Summary and highlights

Five areas are covered by this project.

1. Applied superconductivity on superconducting wires in collaboration with Bruker-BioSpin and on superconducting fault current limiters (SFCL) in collaboration with ABB. In the first subproject we have achieved a remarkable improvement of the overall critical current of MgB_2 wires, bringing this technology closer to the market. The research on SFCL has focused on the study and improvement the thermal properties of Coated Conductors (CC) and we report an important step forward by modifying the CC to achieve higher heat propagation velocities, essential for a cost efficient use of SFCL.

2. Oxides for energy harvesting. Here we follow two promising routes for harvesting electric power from either mechanical or thermal energy. Piezoelectric thin films deposited on Si have been characterized and their capacity for mechanical energy harvesting demonstrated. We have continued our search for promising oxide materials for thermoelectric power generation. A new collaborative effort on the compound $Ca_3Co_4O_7$ has been started.

3. Applications of artificial superlattices. We have continued our collaboration with the company SwissNeutronics. This year, we have developed a first prototype of adaptive neutron optics allowing focusing the neutron beam on a small spot and thus providing an enormous gain in neutron intensity.

4. Hydrogen detectors and other sensors. Our collaboration with Asulab in the Swatch group in order to develop a hydrogen sensor based on the metal-insulator transition in $LaMg_2PdH_x$

($x = 0 - 7$) has made important progress. We have demonstrated reproducible thin film production and the response of the film is relatively rapid and reproducible and meets the 0.5% target for detecting hydrogen. In parallel to the study of the transition metal hydrides, we have also made progress in the use of nanoparticles as gas detectors, in particular MoO_3 based nanorods. This research is complemented by the work carried out with Nirva Industries to improve electrochemical oxygen sensors. Finally in our approach to develop a giant piezo-resistance silicon cantilever, we have demonstrated that the expected gain factor is canceled by other effects and that this approach is unfortunately not giving the hoped for result.

5. New surface treatments for microcomponents. In this part of Project 3, we are following two routes: 1) marking technology for watch components together with the watch manufacturer Vacheron Constantin and 2) in an SNF-supported *economic stimulus package* we are developing a new cut-and-coat process by wire-EDM. In the first part we have made important progress towards an automated marking line in order to implement this new technology for systematic marking of different watch components. In the second subproject, we are developing a new method to cut and at the same time coat the surface with a material adapted to a special practical use. This process is developed together with AgieCharmilles and is presently presented to other companies who we expect may be interested to use such materials.

1 Applied superconductivity

1.1 Densification of long lengths of *in situ* MgB₂ wires (R. Flukiger, C. Senatore, D. Eckert; Bruker-BioSpin)

The cold-high-pressure densification technique (CHPD) developed in Geneva in 2008 has led to a considerable improvement of the critical current density J_c of *in situ* MgB₂ wires. After applying CHPD at 1.5 GPa, a record value of J_c has been reached, with $J_c(4.2\text{ K}) = 10^4\text{ A/cm}^2$ at 13.8 T [1] for monofilamentary wires alloyed with malic acid (C₄H₆O₅) reacted at 600°C for 4 hours. This method has now been successfully applied to multifilamentary MgB₂ wires, where the value of J_c has been enhanced by a factor 2.3, 4.5 and 6 at 4.2 K, 20 K and 25 K, respectively, regardless of the applied fields. In view of industrial applications, CHPD was extended to longer wire lengths through the construction of a prototype machine, where densification is achieved by an automatic press/release/advance mechanism. The new machine (Fig. 1) takes into account the experience previously acquired with the laboratory device, but allows a considerably faster change between the various pressing and releasing operations, combined with a forward movement of the wire. Due to the limited amount of available prototype MgB₂ wire with C₄H₆O₅ additive, the first tests were restricted to a length of 1 meter. The results confirm the results on short wire samples, J_c being enhanced by a factor of 2 over the whole field region. This result is very promising in view of an industrial application of MgB₂ wires.

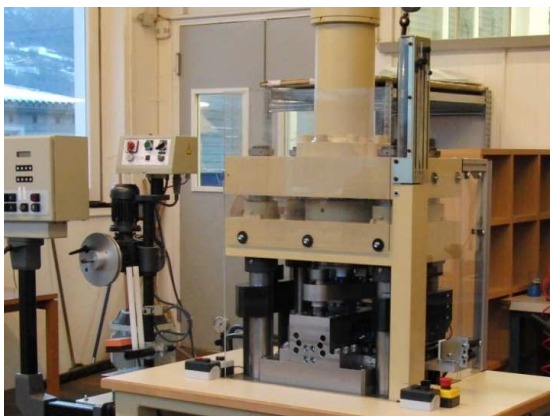


Figure 1: Prototype machine for densification of long lengths of MgB₂ wires.

1.2 Fundamental mechanisms behind the improvement of J_c in densified MgB₂ wires (R. Flukiger, C. Senatore, D. Eckert; Bruker-BioSpin)

High-field resistivity and specific heat measurements were performed on binary and malic acid (C₄H₆O₅) added MgB₂ wires, without and with CHPD, in order to investigate the fundamental physical mechanisms behind the enhancement of the electrical transport properties after densification. In particular, the effects of CHPD on the fundamental superconducting properties, T_c distribution, B_{c2} and B_{irr} , as well as on the parameters influencing the effective cross-sectional area for the current transport, i.e. percolation threshold and grain connectivity, were investigated.

The main results are the following ones [2]:

- a common feature observed in binary and in malic acid doped wires is the reduction of the electric resistivity with densification, reflecting an improvement of connectivity between the MgB₂ grains. The homogeneity of J_c in the superconducting layer is also improved in densified wires;
- in the case of doped MgB₂, the reduction of ρ is accompanied by an enhancement of the upper critical field B_{c2} and a reduction of T_c . This is caused by a slightly increased carbon content in the densified filaments: the reduced reaction path in the precursor powders has an influence on the kinetics;
- combining the analysis of the T_c distribution, as determined from calorimetry, with the results of the $\rho(T)$ measurements, we obtained insights on the influence of CHPD on percolation. In particular, by integrating the T_c distributions between the onset T_c and $T(\rho = 0)$, i.e. the temperature corresponding to $\rho = 0$, we determined for the first time the minimum superconducting volume fraction needed for a full percolation path with zero resistivity (Fig. 2). This volume fraction is strongly reduced in densified wires, from 25% to 12.5%.

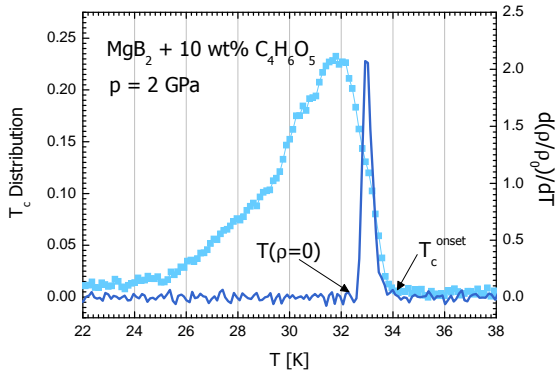


Figure 2: T_c distribution for the malic acid doped wire densified at $p = 2$ GPa (left axis, solid symbols) and derivative of the $\rho(T)$ curve (right axis, solid line).

1.3 Electromechanical behavior of RHQT-Nb₃Al wires (R. Flukiger, C. Senatore, D. Eckert; Bruker-BioSpin)

With respect to Nb₃Sn, the main advantage of Nb₃Al is its considerably lower stress sensitivity of the critical current. There is substantial progress in the development of long length Nb₃Al wires by the rapid-heating, quenching and transformation (RHQT) process. In collaboration with the National Institute for Material Science (NIMS), Tsukuba, Japan, we carried out the first measurements of RHQT-Nb₃Al wires under mechanical loads. Two types of investigations were of interest: first the behavior of the critical current I_c under transverse compressive stress, and second its variation under uniaxial tensile stress. Data regarding I_c versus transverse pressure are rare in scientific literature and are urgently needed. Recently, within a collaboration with CERN, we developed a probe for the study of critical current versus

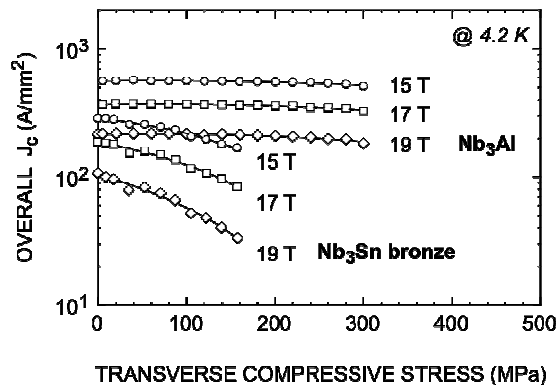


Figure 3: Overall critical current density versus transverse compressive stress at 19 T of a RHQT-Nb₃Al wire and a bronze Nb₃Sn wire with comparable cross sections.

transverse compressive stress up to 300 MPa. At such a high pressure, the I_c of RHQT-Nb₃Al at 19 T is only reduced to 88% of its initial value and recovers upon unloading to 94% [3]. These values are improved at lower magnetic fields. In Fig. 3, the overall critical current density obtained for this RHQT-Nb₃Al wire is compared with that of a bronze Nb₃Sn wire with similar cross section. Note the extraordinary weak stress dependence of RHQT-Nb₃Al. Finally, it should be mentioned that modern high-performance Nb₃Sn wires are even more transverse pressure sensitive than bronze processed wires.

1.4 Superconducting fault current limiter (M. Decroux, M. Abplanalp; ABB)

a) *Introduction* The superconducting fault current limiters (SFCL) are nowadays mainly built with coated conductors (CC). However CC, mostly developed for transport applications, suffer from an important weakness. They can sustain only very low mean electric field due to low propagation velocities of the switched zone — few cm/s compare to more than 20 m/s in films grown onto sapphire wafers [4] — and the poor thermal properties of the structure. Therefore during this year we have characterized the thermal properties of the CC by measuring their thermal conductivities and we have studied a new way to improve the propagation velocities of the switched region in SFCL.

b) *SFCL geometry and thermal link.* To increase the propagation velocities of the normal zone, we propose a special geometry in which the superconducting line is a meander (as presented in Fig. 4). This geometry offers

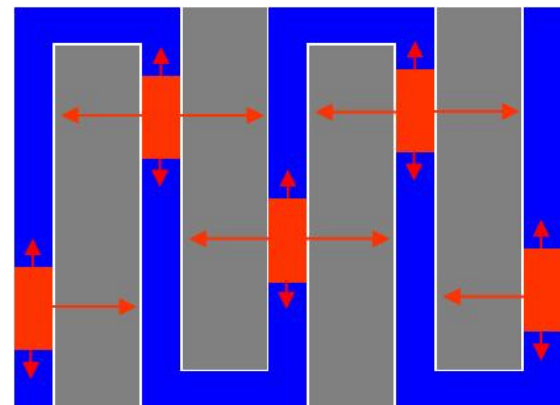


Figure 4: Sketch of the meandered geometry proposed for the SFCL in order to increase of the effective propagation velocity of the normal zone. The thermal links are the grey rectangles.

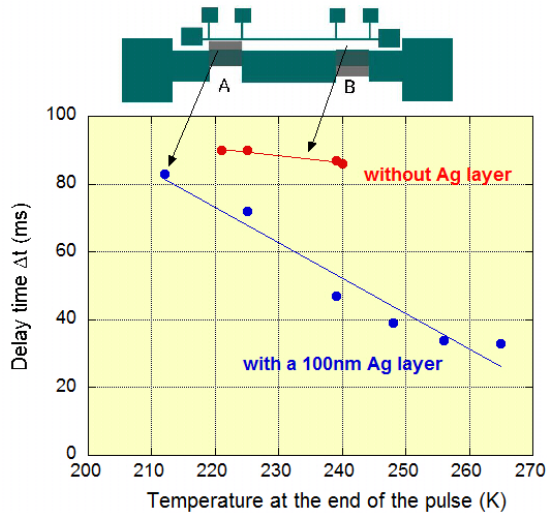


Figure 5: Delay time between the heater and the detector line in region with (A) and without (B) the thermal link as a function of the temperature of the constriction at the end of the current pulse.

the advantage to use the lateral propagation of the heat to increase the effective propagation velocity. Indeed, when a part of a line has switched in the normal state, the heat front generated in this region will propagate laterally and will switch the adjacent lines. However, in between the lines, the heat propagates into the substrate (Hastelloy/MgO bilayer) which has a very low thermal conductivity. This thermal propagation can be improved by adding a thermal link (a film with a high thermal conductivity, e.g. Ag), onto the bilayer and in between the lines (as shown on Fig. 4) [5].

To prove the benefit of the thermal link, we have developed a test structure (Fig. 5), which allows measuring the propagation of the heat in the substrate and in the substrate/Ag bilayer simultaneously. In this design, the heat front is generated by two constrictions which are switched by applying a current pulse ($I > I_c$). We have measured, for different Ag thicknesses, the time taken by the heat to travel the 600 μm from the constrictions to the detector line [5]. Fig. 5 clearly shows the benefit of the thermal link. The delay time decrease from 90 ms, for the propagation into the substrate (region B), to around 35 ms, for the region with the 100 nm thick Ag thermal link (region A). More studies are needed to quantify the effect of the current flowing in the thermal link and of the thermal conductivity of the Ag layer on the delay time. For thicker Ag films (250 and 500 nm) we however observe that this delay time does not decrease anymore as it is expected. We think that this problem is due to the

thermal conductivities of the Ag layer and/or the MgO/Ag interface. Prior to the Ag deposition, the surface is degraded or contaminated during the lift-off process with different chemicals. To check this influence, MgO surfaces were put in contact with different chemicals and Ag layers were grown. We obtained good value of the resistivity of the Ag layer, independently of the MgO surface treatment, indicating that the thermal conductivity is certainly not altered. This suggests that the MgO/Ag interface is responsible for the results we observe for thicker Ag layers. Further studies are needed to confirm this behavior, especially a characterization of the interfaces in CC.

c) *Measurement of the thermal conductivity of coated conductors.* The thermal conductivity of the different layers of the CC's structure plays a crucial role in the propagation velocities of the normal zone. The main contributions to the equivalent thermal conductivity of the CC are coming from the substrate and the Ag layer.

First we have measured, with our recently developed set-up (see last progress report), the thermal conductivity of the substrate (Hastelloy/MgO). Different tests have been performed to optimize the reproducibility of the measurements. We obtain reproducible results, within 10 – 15%, with a value of $k = 10 \text{ W/mK}$ (at 100 K) close to the only value reported in the literature for the Hastelloy (8 W/mK at 100 K). To calculate the thermal conductivity of the Ag layer, we have carefully measured the thermal conductivity of a CC (Hastelloy (100 μm)/buffer layer/YBCO/Ag (2 μm)) with and without the Ag layer (Fig. 6). From these measurements, we can estimate that the

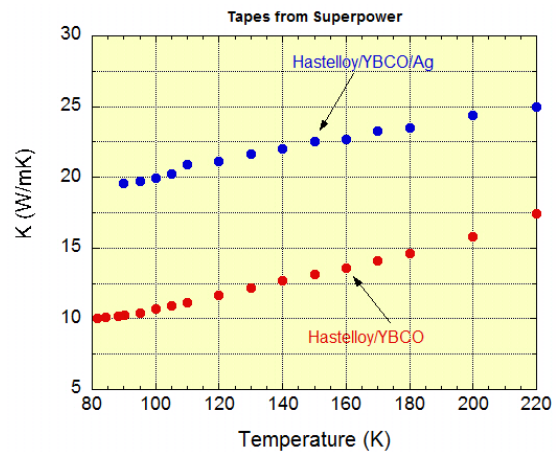


Figure 6: Thermal conductivity of a coated conductors with (blue points) and without (red points) the 2 μm by-pass silver layer.

thermal conductivity of the 2 μm Ag layer is $k_{Ag} = 475 \text{ W/mK}$ at 100 K. This is a value close to the reported values in the literature ($k_{Ag} = 450 - 500 \text{ W/mK}$). This means that even if the Ag layer is grown on a rough YBCO surface, its thermal conductivity is not altered. Then the problem encountered with the thermal link is certainly coming from the MgO/Ag interface.

2 Oxides for energy harvesting

2.1 Epitaxial ferroelectric thin films on silicon for energy harvesting applications (J.-M. Triscone, G. Triscone, N. de Rooij)

The aim of this project is to explore the fully epitaxial integration of ferroelectric thin films onto silicon as a possible way to provide new and/or improved functionalities to microelectromechanical systems (MEMS) devices. Because of the chemical reactivity of the metal-oxygen-silicon system and the mismatch of the lattice parameters and thermal expansion coefficients, the choice of oxides that can be epitaxially grown on silicon is limited. The route we are exploring in this project is the integration of high-quality ferroelectric thin films on silicon through a thin buffer layer of epitaxial SrTiO₃ (STO).

a) *Growth and characterization of epitaxial Pb(Zr,Ti)O₃ thin films on silicon* Typically the heterostructures realized are based on STO (6 nm)-buffered 2" and 3" silicon wafers on top of which we grow a thin layer of metallic SrRuO₃ (30 nm), used as a bottom electrode, and a thin film of ferroelectric Pb(Zr_{0.2}Ti_{0.8})O₃ (PZT) of about 150 nm. X-ray diffraction (XRD) measurements, as well as transmission electron microscopy analyses clearly indicate the epitaxial relationship between the oxide multilayer and the (001) silicon wafer. Polarization-voltage measurements yield a value of remnant polarization of 70 $\mu\text{C}/\text{cm}^2$, while piezoelectric force measurements (PFM) give a value of the piezoelectric coefficient d_{33} of about 50 pm/V. In order to fully characterize the ferroelectric properties, we tried to determine the critical temperature of the PZT epitaxial thin film through XRD measurements of its lattice parameters between 30 and 800°C. The evolution in temperature of the PZT tetragonality exhibits an unexpected behavior, with evidence of a structural change at or above 700°C (Fig. 7).

This result strongly suggests that the ferroelectric-paraelectric transition, associated with the structural transition, occurs at

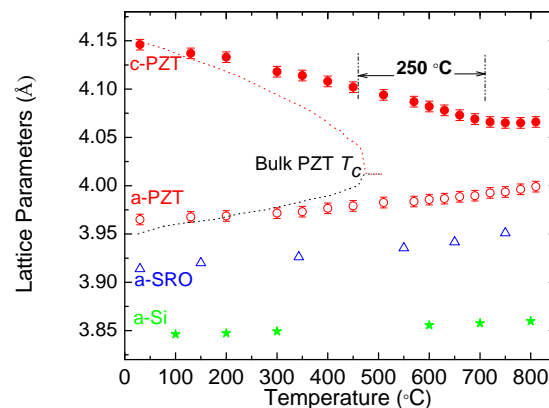


Figure 7: (a) Evolution in temperature of the lattice parameters for the silicon substrate (green \star), SRO a -axis (blue \triangle), PZT a - (red \circ) and c -axes (red \bullet). The dotted lines represent the bulk PZT behavior: c -axis in red and a -axis in black.

a temperature which is 250°C higher with respect to the bulk value. This significant enhancement of the critical temperature can be explained in terms of the two-dimensional clamping of the thin film on the underlying oxide layers [6]. The possibility to obtain high-quality epitaxial PZT films exhibiting bulk-like values of the remanent polarization and piezoelectric coefficient confirms the potential of epitaxial oxides on silicon. Moreover, a transition temperature much higher than the bulk can be an advantage in terms of thermal budget associated with microfabrication or device operation.

b) *Electrical and mechanical characterization of MEMS cantilevers based on epitaxial oxide materials for energy harvesting* Our vibrational energy harvesting devices consist of multilayered epitaxial oxide films deposited on a silicon cantilever beam terminated with a Si proof mass, designed based on our modeling [7]. The harvester (Fig. 8) was fabricated using micro-patterning techniques optimized for the oxide layers deposited on silicon as detailed in [8]. The polarization was used to optimize the necessary process steps. No degradation of the PZT properties were induced by the final processing chosen.

The resonant frequency of the epitaxial PZT cantilever, characterized using a Polytec MVS-400 laser Doppler vibrometer, was found at 2302 Hz with a quality factor of 363. An electromechanical coupling coefficient of 6% was obtained from the difference between the resonant and antiresonant peaks measured on a Hewlett Packard HP 4194A impedance/gain-phase analyzer. A damping ratio of 0.0004 was obtained using the half-power bandwidth

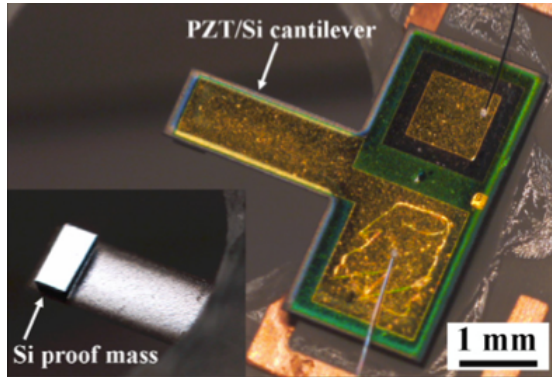


Figure 8: Optical image of an epitaxial PZT harvester ($1000 \mu\text{m} \times 2500 \mu\text{m} \times 10 \mu\text{m}$) with a Si proof mass ($1000 \mu\text{m} \times 500 \mu\text{m} \times 230 \mu\text{m}$). The inset shows the Si mass on the back side of the harvester.

method. The power generation performance of the device was investigated with a shaker (Bruel & Kjaer type 4811), driven by a vibration exciter controller (BK type 1050) and a power amplifier (BK type 2712), by applying an acceleration as a mechanical input. The device was connected to various resistive loads, and the current generated under different acceleration levels was recorded with a multimeter (Agilent 34411A). A maximum output power of $14 \mu\text{W}/\text{g}^2$ with $60 \mu\text{A}/\text{g}$ output current from a single device was obtained for an optimal resistive load of $4.7 \text{ k}\Omega$, and thus resulting in the output voltage of $0.28 \text{ V}/\text{g}$ (Fig. 9). The maximum power density was as high as $105.66 \mu\text{W}/(\text{g}^2\text{mm}^3)$. A good agreement between measurements and theoretical calculations was obtained [7]. A very interesting outcome was that the epitaxial PZT harvester generates high output power and current with usable voltage, and requires low optimal resistive

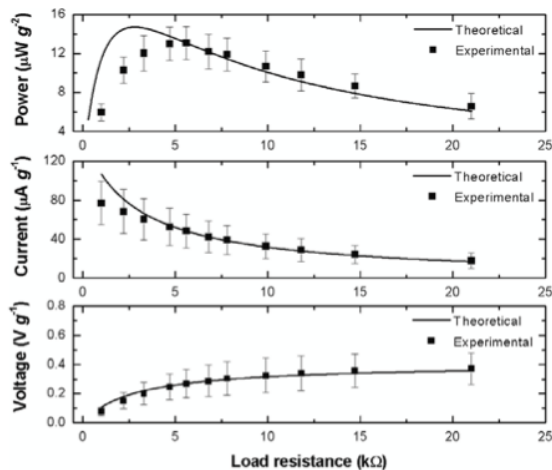


Figure 9: Theoretical and experimental power, current and voltage values versus load resistance.

load.

These results indicate the potential of epitaxial PZT thin films for energy harvesting applications and may lead to an improvement of the overall performance of energy harvesting devices. The next points to be addressed are the lowering of the resonant frequency through an improvement of the structure design based on the use of the silicon-on-insulator technology, and a study of the power management circuits in order to realize fully-functional vibration energy harvesting systems based on this technology.

c) *Growth of $\text{Pb}(\text{Zr}_{0.52}\text{Ti}_{0.48})\text{O}_3$ thin films* The performance of energy harvesters usually depends on their electrical characteristics, such as dielectric constant and piezoelectric coefficients. In case of PZT energy harvesters, the electrical characteristics depend strongly on the Zr/Ti composition. In order to find possible ways to enhance the performance of our piezoelectric devices, we started to explore the PZT solid solution phase diagram. In particular, we started to grow PZT thin films with a stoichiometry of $\text{Pb}(\text{Zr}_{0.52}\text{Ti}_{0.48})\text{O}_3$ by rf magnetron sputtering. Close to the morphotropic phase boundary, i.e. for a $x = 0.52$ Zr content, such compound exhibits an enhanced piezoelectric response, which could be exploited for high-performances energy harvesting devices. $x = 0.52$ films characterization in terms of crystalline structure, morphology, remanent polarization and piezoelectric response is ongoing with the goal to optimize the growth conditions in order to maximize the d_{33} and d_{31} coefficients.

2.2 Development of unconventional thermoelectrics (A. Weidenkaff)

a) *Development of better thermoelectrics* Polycrystalline thermoelectric oxides suffer from a relative low thermoelectric performance at low temperatures compared to tellurium based conventional materials. Thus, materials with improved $ZT = S^2T/\kappa\rho$ have to be developed by understanding the structure-property relations in transition metal oxides. Very high ZT values ($ZT = 1$ and $ZT = 2.4$) were published recently for cobaltate and titanate species, respectively [14, 15]. Nevertheless, we found that these values are hardly reproducible and not all being found in polycrystalline bulk materials. With innovative soft chemistry synthesis procedures we are varying the anionic sublattice, in addition to well known cationic substitution reactions [9].

Complex ternary oxynitrides (Sr(Ti, Nb)O₃:N) [9] and binary (oxy)nitrides (CrN) show interesting transport properties due to the possible variations of the band structure [10] and present a far less studied family of compounds compared to oxides.

CrN compounds exhibit relatively low electrical resistivity associated with large Seebeck coefficients (e.g. in CrN: $S = -135 \mu\text{V K}^{-1}$ at $T = 300 \text{ K}$). Thus CrN can be considered as a promising thermoelectric material [16]. It was shown that the Seebeck coefficient and electrical resistivity of hole doped CrN are enhanced to result in a power factor PF of $3.4 \cdot 10^{-4} \text{ W K}^{-2} \text{ m}^{-1}$ at $T = 400 \text{ K}$. Therefore incorporation of oxygen into CrN, leading to CrO_{0.09(3)}N_{0.90(7)} can result in the creation of a potential new n -type thermoelectric material for thermoelectric modules.

The temperature dependence of the electrical resistivity in the temperature range of $3 \text{ K} < T < 850 \text{ K}$ reveals semiconducting characteristics up to a temperature of $T \sim 600 \text{ K}$ with a minimum value of $\rho \sim 2.8 \text{ m}\Omega\text{cm}$ at $T = 300 \text{ K}$. The hysteresis indicates a first order transition and is in agreement with data reported for CrN [17]. The Seebeck coefficient of the sample is negative and increases in absolute value almost linearly with increasing temperature.

Another potential n -type materials for thermoelectric applications is EuTiO₃ (ETO) which is isostructural with SrTiO₃ (STO). Both STO and ETO have the same lattice parameter of $a = 3.905 \text{ \AA}$ and a cubic $Fm\bar{3}m$ structure. However the heavier Eu²⁺ decreases the thermal conductivity and improves ZT . The temperature dependence of the electrical resistivity in the temperature range of $2 \text{ K} < T < 1200 \text{ K}$ of EuTiO_{3- δ} and EuTi_{0.98}Nb_{0.02}O_{3- δ} , results in a metal-insulator (MI) transition: a decrease of resistivity upon increase of temperature, reaching the minimum of 10^{-3} Ohm m at highest temperature of 1200 K . The Arrhenius plot for reduced ETO shows a change of the activation energy of the electrons from 0.49 eV at high temperatures to 0.195 eV at low temperatures, with a transition temperature of 486 K . By plotting the same resistivity curve in $\ln\rho$ versus $T^{-0.25}$ scale the three-dimensional variable range hopping (VRH) can be examined [18]. Indeed, at low temperature range ($180 \text{ K} < T < 390 \text{ K}$) the conductivity is linear, confirming VRH as a mechanism of electronic transport. At higher than 390 K the $\ln\rho$ versus $T^{-0.25}$ plot is no more linear, which can be an effect of electron-electron interaction not taken into account in VRH model [18]. The Arrhenius

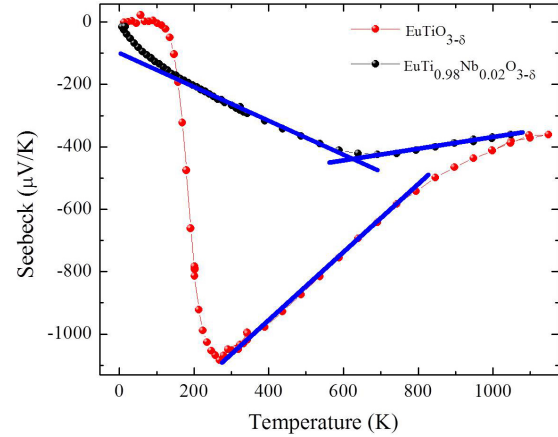


Figure 10: Temperature dependence of the Seebeck coefficient.

plot for reduced and Nb doped ETO shows a change of the activation energy of the electrons from 0.21 eV at high temperatures to 0.048 eV at low temperatures, with a transition temperature of about 200 K . By plotting the same resistivity curve in $\ln\rho$ versus $T^{-0.25}$ scale, only high temperature ($T > 300 \text{ K}$) VRH as a mechanism of electronic transport can be confirmed. The MI transition is also detected by Seebeck measurements (Fig. 10). The corresponding $S(T)$ curves are negative in the whole temperature range confirming n -type (most probably due to Ti $4d^1$) electron conductivity. The thermopower exhibits a maximum at 268 K and 640 K , reaching $-1084 \mu\text{V/K}$ and $-421 \mu\text{V/K}$ for EuTiO_{3- δ} and Nb-substituted EuTiO_{3- δ} , respectively. The thermal band gap due to oxygen vacancies present in materials is believed to affect electronic transport and thus thermopower [19]. The thermal band gap is calculated to be $E_g = 2eS_{max}T_{max}$ and it is nearly the same for both samples (0.62 eV for EuTiO_{3- δ} and 5.9 eV for Nb-doped EuTiO_{3- δ}) which is double as high as the thermal band gap for SrTiO₃ ($E_g = 0.3 \text{ eV}$). Another origin of the peak in $S(T)$ curves can be associated with the phonon drag effect [20]: if the phonon-electron interaction is predominant at T_{max} , the phonons will tend to push the electrons to one end of the material, giving rise to an enhancement of $|S|$ [14].

The total thermal conductivity consists of electronic and lattice contributions. The electronic contribution in a good approximation can be estimated using Wiedemann-Franz law and is proportional to the electronic conductivity. The electronic part of the thermal conductivity reveals a gradual increase with temperature reaching the maximum of $5 \cdot 10^{-2} \text{ W S}^{-1} \text{ K}^{-1}$. In the temperature region $2 < T < 300 \text{ K}$, the

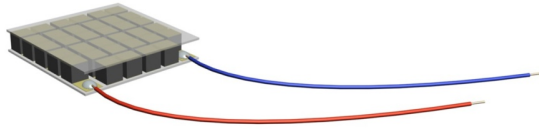


Figure 11: 34-legs thermoelectric oxide module (TOM)

dominating thermal conductivity is of phonon contribution and reaches a maximum value of $2.5 \text{ W S}^{-1} \text{ K}^{-1}$ for $\text{EuTiO}_{3-\delta}$ and $2.87 \text{ W S}^{-1} \text{ K}^{-1}$ for Nb-doped $\text{EuTiO}_{3-\delta}$. The phonon (lattice) contributions are affected by point defects and Umklapp processes, grain boundaries, size of the grains and density of the samples, and the obtained values are reasonably low for thermoelectric modules production. The maximum power factor calculated as S^2/ρ for both samples is one of the highest known for oxides and reaches $10^{-3} \text{ W S}^{-1} \text{ K}^{-2}$ at 1000 K.

b) *Modelling the thermoelectric conversion process* The energy conversion efficiency of thermoelectric modules can be calculated and modeled if the thermoelectric materials characteristics S , ρ , κ and ZT are determined. Thermoelectric oxide modules (TOM), as shown in Fig. 11, where firstly constructed and parameters as, e.g., interior radiation and heat conduction in the module were calculated, based on the thermoelectric properties of the p - and n -type materials and the radiation of absorber plate [11]. A TOM with geometry (cross-section of the leg $4 \times 4 \text{ mm}^2$ and length of 5 mm) shows maximum output power of $P_{max} = 63 \text{ mW}$ at $\Delta T = 500 \text{ K}$.

2.3 $\text{Ca}_3\text{Co}_4\text{O}_9$: synthesis and photoemission characterization (Ph. Aebi, A. Weidenkaff, J. Hulliger)

a) *Introduction* Oxide ceramics are promising candidates for thermoelectric power conversion in the medium and high-temperature region up to 1200 K due to their thermal stability, lack of harmful or scarce elements and possibility for a large scale production. $\text{Ca}_3\text{Co}_4\text{O}_9$ (Ca349) presents a modulated layered crystal structure consisting of distorted cubic $[\text{Ca}_2\text{CoO}_3]$ and distorted hexagonal $[\text{CoO}_2]$ sublayers, jointly forming a layered crystal lattice with a monoclinic unit cell. Single-crystals of Ca349 have attracted special interest as their figure of merit was reported to reach 0.87 at 1000 K [21].

b) *Preparation* Platelet-shaped crystals of Ca349 were grown from $\text{K}_2\text{CO}_3:\text{KCl}$ flux

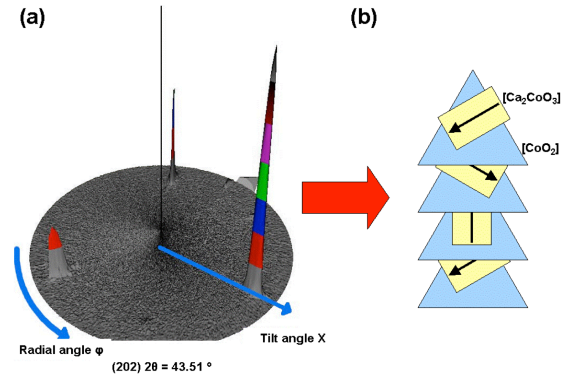


Figure 12: (a) Pole figure of the (202) plane recorded on flux grown $\text{Ca}_3\text{Co}_4\text{O}_9$ crystals. (b) Schematic drawing of the suggested orientational disorder of the $[\text{Ca}_2\text{CoO}_3]$ layers.

following the procedure by [22] with a modified temperature program with cooling from 1163 K to 973 K with a rate of 2 K/h. The Ca349 phase was identified by powder XRD and the crystal morphology and orientation observed by SEM and pole figure measurements.

c) *Characterization* Pole figures measured on a 4-circle diffractometer equipped with an eulerian cradle have revealed 3 reflections spaced equally by 120° (Fig. 12a), which leads us to propose a stacking scheme of the Ca349 compound were the cubic $[\text{Ca}_2\text{CoO}_3]$ randomly accommodates one of three orientations moderated by the hexagonal $[\text{CoO}_2]$ layer (Fig. 12b).

d) *Photoemission results* Due to the high surface sensitivity of the photoemission technique we had to cleave the samples in order to expose a fresh surface to the measurement. The large amount of carbon found on the spectra immediately after cleaving indicates that maybe the samples are not really cleaved but rather exfoliated, namely that the surface thus revealed is not characteristic of the bulk. This is confirmed by SEM images showing a ruptured surface consisting of several torn sheets. However a LEED pattern can be observed, revealing the good crystalline quality of the sample. Our aim was to reproduce previous ARPES measurements taken on $\text{Ca}_3\text{Co}_4\text{O}_9$ [23], especially to observe a band crossing the Fermi step, but our measurements did not exhibit this band, only a broad band around 1.5 eV binding energy, reflecting a mixture of O $2p$ and Co $3d$ states. However this band disperses (Fig. 13, inset).

e) *Plasma treatments* The idea of applying O plasma is twofold: first to get rid of the C, and second to dope the sample with O. The observed effects correspond to what is expected:

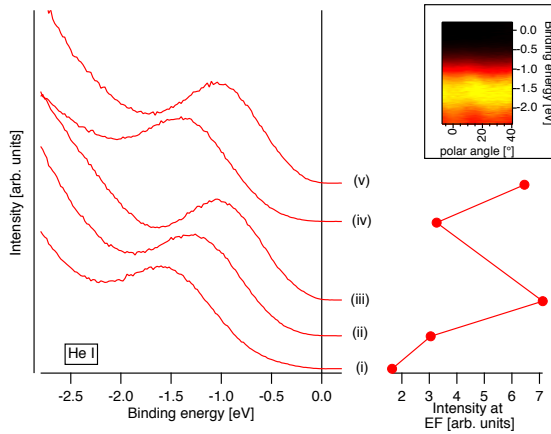


Figure 13: Results for different plasma treatments: (i) cleaved, (ii) 1 min. O plasma, (iii) 5 min. O plasma, (iv) 5 s H plasma, (v) 5 min. O plasma. Left graph: valence band. Right graph: spectral intensity at E_F . Inset: dispersion of valence band

it removes the carbon, and strongly affects the valence band. As can be seen in the left part of Fig. 13, the band is shifting to the right upon application of an O plasma. This is reflected by an increase of the spectral intensity at E_F (right part). Application of an H plasma has an antagonist effect on the valence band: peak shifts to the left and intensity at E_F decreases. A further application of an O plasma shows that these effects are reversible. The differences in intensity at E_F reflect differences in electrical conductivity, which were also observed with transport measurements on samples annealed in various gases.

3 Applications of artificial superlattices

3.1 Adaptive optics for neutrons (M. Kenzelmann; SwissNeutronics)

a) *Concept of bending* From basic mechanics, the relation between the local curvature $C(x)$ and the local applied moment $M(x)$ of a homogeneous beam is given by $C(x) = \frac{M(x)}{E \cdot I(x)}$ where $I(x)$ is the local moment of inertia of the beam and E is the elastic modulus [24]. The local moment of inertia $I(x)$ for a beam can be approximated by $I(x) \approx \frac{w \cdot t^3}{12}$, where w is the width of the beam and t the thickness. The local curvature $C(x)$ of the aimed shape-function can be approximated by its second derivative: $C(x) \approx \frac{d^2}{dx^2} f(x)$. The shape function for a parabola is $y = \sqrt{2xp}$ where p designates the focal parameter of the parabola. For a constant beam width w , the thickness profile of the beam with length

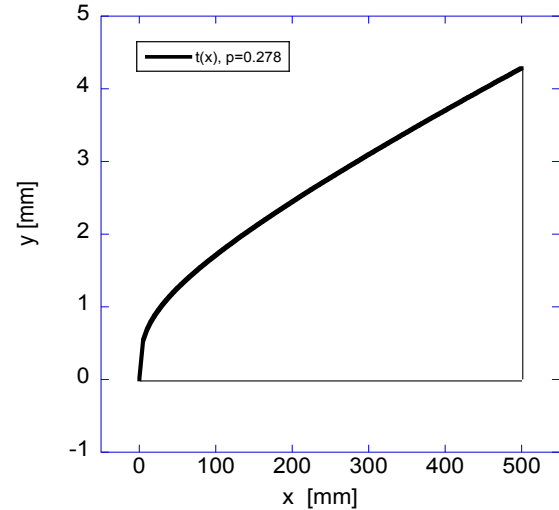


Figure 14: Thickness profile of the glass substrate for $p = 0.278$, $F = 1$ N, $w = 100$ mm.

L can be expressed by the following equation

$$t = \sqrt[3]{\frac{12F \cdot (L - x)}{E \cdot w} \cdot \frac{1}{\frac{d^2}{dx^2} f(x)}} \quad (2.1)$$

The thickness profile of the prototype made from glass is shown in Fig. 14. The design parameters are: length $L = 500$ mm, constant width $w = 100$ mm, applied force $F = 1$ N and focal parameter of the parabola $p = 0.278$. In order to use glass as a substrate for the parabolic bent optic with supermirror coating requires high-precision glass machining capabilities supplied by the company SwissNeutronics. Fig. 15 shows the special substrate installed in a small apparatus with provision to deflect the mirror at one end.

b) *Proof of concept* The bending properties were characterized using a theodolite to probe the evolution of the surface normal along the mirror. Fig. 16 depicts the measured data in comparison to the theoretical values. At the up-stream end the real curvature follows very

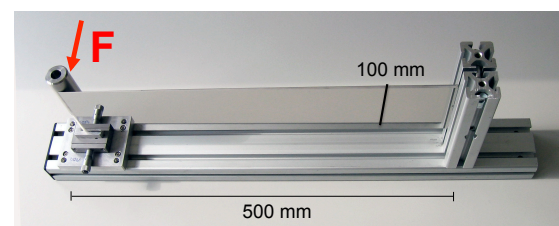


Figure 15: Prototype of the adaptive, parabolic optic with supermirror coating ($m = 3.6$). The thickness of the glass substrate decreases from right to left. The apparatus has manual provision to deflect the substrate (left hand side).

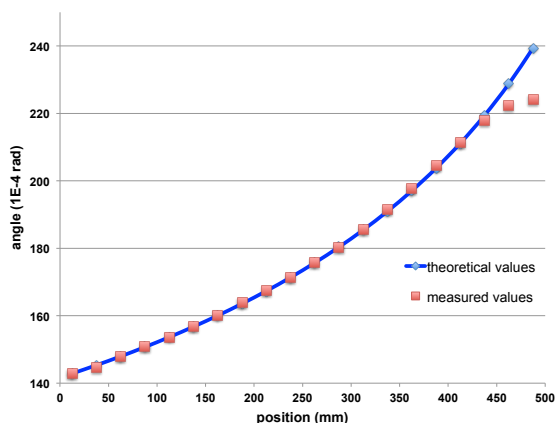


Figure 16: Profile of the surface normal along the bent substrate. The real values are measured using a theodolite. The position zero corresponds to the up-stream end of the mirror.

precisely the theoretical profile. At the downstream, approximately within a region of 50 mm, the real curvature is smaller than the targeted progression. There are two reasons for this figure error: i) influence of stress from the supermirror coating, ii) finite thickness at the end of the mirror. The supermirror coating has some residual compressive stress, which is a constant contribution to the local momentum. Hence it affects the bending properties mostly where the substrate thickness becomes thin. As shown in Fig. 14, the thickness of the substrate is zero at the downstream end. However for reasons of the machining and the stability of the glass substrate, a minimum thickness was decided for the first prototype, which is 0.8 mm for the last 15 mm. Therefore the mechanical properties, thus the bending at the downstream end, are not exactly according the theory.

The performance of the device was tested with neutrons using the beamline Morpheus at PSI. The spatial distribution of the neutron beam deflected from the parabolic optic was mea-

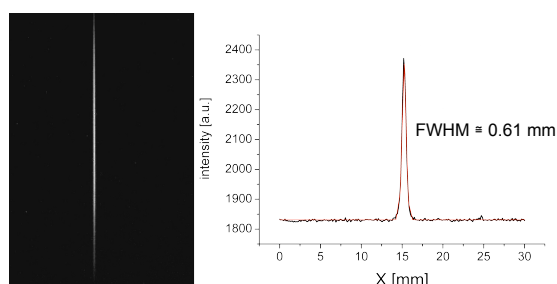


Figure 17: First data from the neutron measurements of the prototype. Left: image of the beam on the 2D position sensitive detector. Right: integrated intensity together with a Gaussian fit of the peak.

sured with a 2D position sensitive detector. Fig. 17, left, shows the image of the neutron beam spot when the detector is placed at the focal spot of the parabola. The integrated plot (Fig. 17 right) illustrates the beam profile. A gaussian fit to this profile results in a FWHM of 0.61 mm. The beam width at the mirror position is approximately 1.7 mm (including divergence). For a perfect geometry of the parabolic optic, the expected FWHM of the beam at the detector position is 0.6 mm due to the divergence of the incident beam. Hence the focusing of the optic complies very well with the theoretical expectations.

c) *Conclusion* A first prototype of an adaptive neutron optic with parabolic shape was fabricated. Its bending properties were characterized optically confirming the concept of the bending. First neutron tests were performed at the very end of the last cycle at SINQ (PSI) providing promising results. However, much more time was needed for the adjustment of the optical device than expected. More extensive studies with neutrons are planned in May 2011. With this adaptive neutron optical device, it is possible to optimize the focal spot on small samples providing enormous gain in the neutron intensity for the experiments. By adapting the applied force, the lateral position of the device and the angle of incidence, the neutrons can be focused to match the individual size of the samples.

4 Hydrogen detectors and other sensors

4.1 Progress towards a resistive thin film hydrogen detector (K. Yvon, J. Cors, Ø. Fischer; Asulab (Swatch group))

a) *Aim of project* Hydrogen fuel cells and electrolyzers play a key role in future energy scenarios. Mass markets such as hydrogen powered vehicles and hydrogen production units for residential areas require hydrogen detectors and sensors on a very large scale. The devices must be cheap, sensitive and selective, and allow to detect hydrogen in various gases (e.g. oxygen) in the entire concentration range (0.5 – 100% H₂). This project aims at developing tailored sensing devices that are cheaper and more selective than those currently available, by using thin films and novel materials undergoing hydrogen-induced metal-insulator transitions. Here we report on first results concerning the deposition of thin films of an active material and their analysis. The work is performed within the framework of a CTI

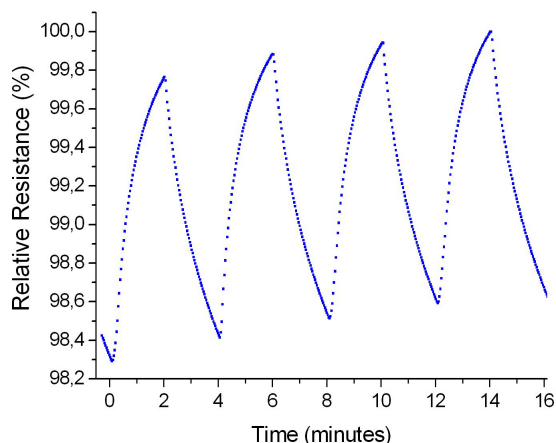


Figure 18: Resistance versus time during cycling between 1 bar of hydrogen and vacuum at 25°C for a thin LaMg_2Pd film (120 nm thickness) precharged with hydrogen.

project and benefits from support by an industrial partner.

b) *Materials available* Among the materials investigated during the last year, the intermetallic compound LaMg_2Pd has been identified as a suitable candidate for that purpose. Measurements on the bulk have shown that a hydrogen induced metal-insulator transition occurs near room temperature and at relatively low hydrogen pressures between a partially charged phase of composition $\text{LaMg}_2\text{PdH}_{\sim 3}$ and a fully charged phase of composition $\text{LaMg}_2\text{PdH}_7$.

c) *Work performed* We have now succeeded in depositing this material in the form of thin films by sputtering. A single-target of LaMg_2Pd was used and the film is deposited on a SrTiO_3 substrate. The method is fully *in situ* and no further annealing was necessary. X-ray diffraction confirmed the presence of the active phase LaMg_2Pd and some impurities like La_2O_3 .

The films were then precharged with hydrogen and subjected to cycling experiments in pure hydrogen at room temperature in a self-made *in situ* chamber. The resistance of the films was monitored by using the 4-wires method while filling the chamber with 1 bar hydrogen during two minutes and subsequent pumping during two minutes. As shown in Fig. 18, the resistance of the film increases by $\sim 1.5\%$ during absorption and decreases by nearly the same amount during desorption.

The response is relatively rapid, the reproducibility of the signal is good, and the drift is relatively small. X-ray patterns taken both before and after hydrogenation confirmed the

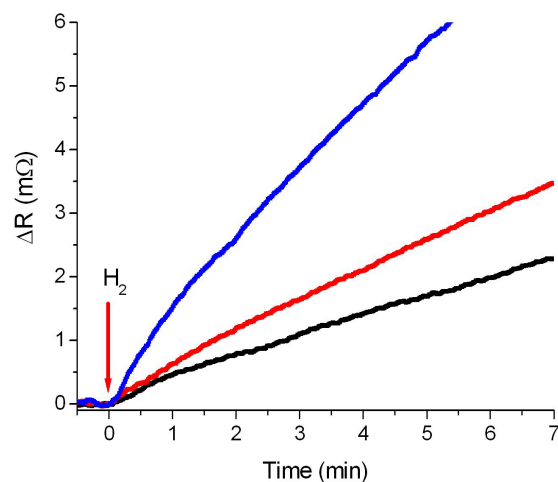


Figure 19: Relative resistance change, ΔR , at 25°C as a function of time for a thin precharged LaMg_2Pd film (120 nm thickness) in a 1 bar atmosphere of argon containing 0.5% (black), 1.5% (red) and 3% (blue) hydrogen. Arrow indicates addition of hydrogen.

presence of the active phase LaMg_2Pd , of the intermediate hydride phase $\text{LaMg}_2\text{PdH}_{\sim 3}$, of the fully charged phase $\text{LaMg}_2\text{PdH}_7$, and of some lanthanum oxide La_2O_3 . Most importantly, the film remained intact during cycling. Next, various concentrations of hydrogen (0.5%, 1.5% and 3%) were added to an argon atmosphere. As shown in Fig. 19, the resistance increases immediately for all hydrogen concentrations. In particular, the lowest hydrogen concentration (0.5%) shows already a useful signal, thus meeting the 0.5% target for detecting hydrogen.

The kinetics are relatively rapid and the changes in resistance scale with partial hydrogen pressure. No significant degradation of the signal occurred during extended cycling experiments (data not shown). Thus the device shows also promise for use as a hydrogen sensor.

d) *Conclusions and perspectives* In conclusion, thin films of intermetallic LaMg_2Pd have been deposited for the first time. The process used is simple, reproducible and fully *in situ*, and thus can be likely upscaled in an industrial environment. The kinetics are good but need to be improved. The film's sensitivity to hydrogen is sufficient for use as a hydrogen detector. Future work will concentrate on patterning and decreasing the film thickness, on investigating the film's properties in hydrogen rich atmospheres, and on finding low-cost substrates and suitable materials to protect the active layer from potentially corrosive gases, such as water vapor, oxygen, etc.

4.2 Novel chemical sensors based on W/Mo-oxide nanomaterials (G. Patzke)

a) *Gas sensing facilities* Over the past months, we have successfully constructed the laboratory facility for quantifying gas sensing properties of oxide nanomaterials (Fig. 20). In addition, the according interdigital electrodes are fabricated in the cleanrooms of FIRST (ETHZ). The substrate is positioned on a thermostable quartz holder. The interdigital finger patterns are created with lift-off techniques and deposition of titanium (10 nm) and gold (100 nm). The distance between the electrode fingers is set as 25 μm . The sample on the electrode is thermally treated by calcination at 400°C over night. Gas sensing properties are measured as follows:

- the heater is located in the chamber and can be operated up to 400°C, controlled by an external temperature regulator. Nominal and actual values are recorded in real time;
- the interdigital electrode is fixed on a glass substrate on the bronze over the heater and the effective operating temperature is measured by an external temperature controller;
- two gold wires are fixed on the electrode for measuring the electrical properties;
- one drop of deionized water with dissolved nanopowders is put in between the electrode fingers on the substrate, followed by drying;
- synthesized air as carrier gas and the target gas are introduced via two flowmeters with constant flowspeed into the chamber.

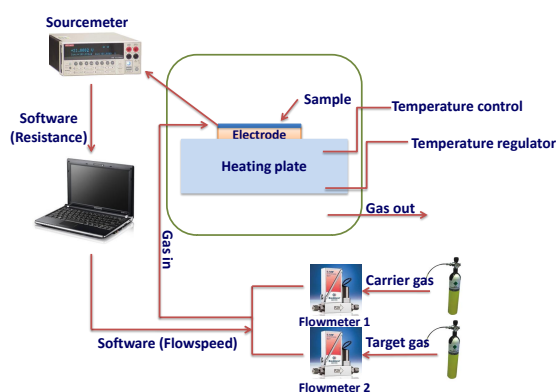


Figure 20: Schematic representation of the laboratory sensor facility.

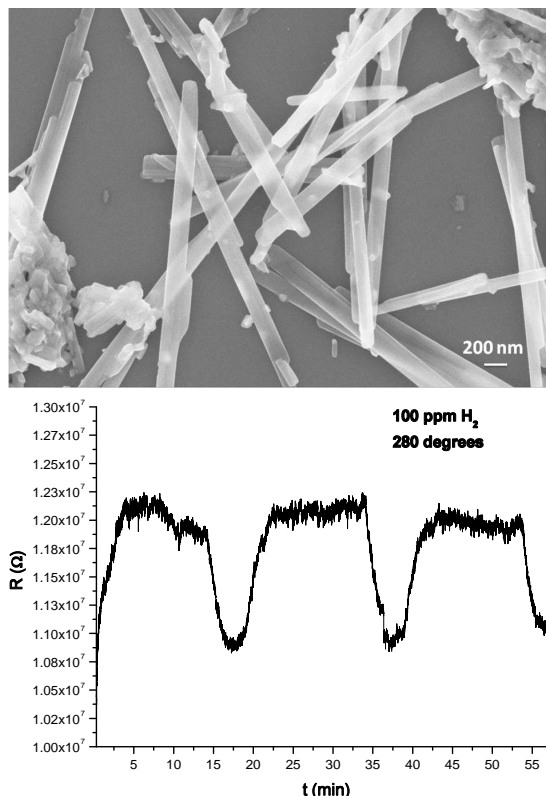


Figure 21: Top: SEM image of MoO_3 nanorods, and bottom: dynamic response towards 100 ppm H_2 at 280°C.

b) *H_2 sensing properties of nanostructured MoO_3* It is well known that molybdenum trioxide (MoO_3) nanowires have been intensively investigated for diverse applications such as selective catalysts and gas sensors for more than a decade. They are reported to display outstanding gas sensing properties due to their flexible redox behavior [25]. The oxygen adsorption/desorption process occurs at temperatures above 200°C on the oxide surface. The charge exchange (electron transfer) between adsorbed species (O_2^- , O^- and O^{2-}) and metal oxide induces a change of sensor signal. When MoO_3 is in contact with a reducing gas, such as H_2 , ethanol, NH_3 , etc., the resistance of the metal oxide decreases.

Our research group has been focusing on the synthesis of α - MoO_3 nanorods (Fig. 21 top) and nanofibers via novel one-step hydrothermal approaches starting from different precursors [12][26]. We now improve their sensitivities by doping the fiber surface with Pt nanoparticles.

The optimal operating temperature was fixed according to the maximal sensitivity, which is defined as $S = R_{\text{air}}/R_{\text{target gas}}$. MoO_3 is a typical n -type semiconductor, which is demonstrated by lower resistance in the presence of

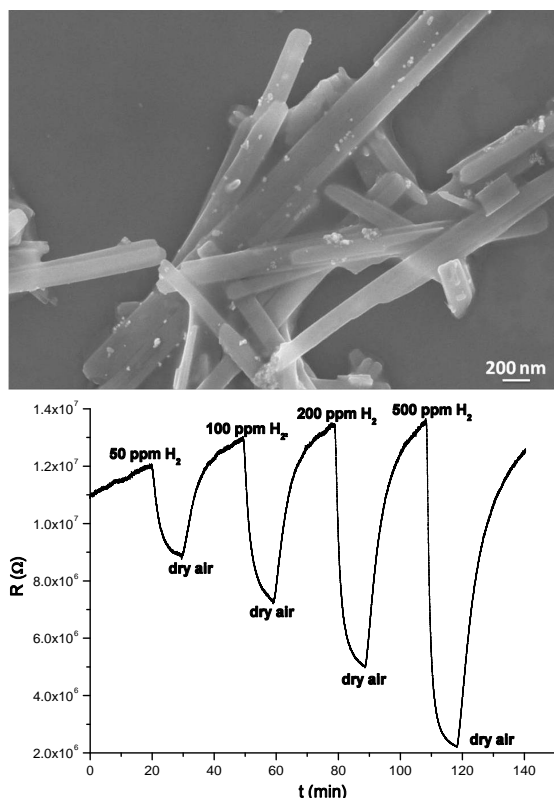


Figure 22: Top: SEM image of $\text{MoO}_3\text{-Pt}$ rods; bottom: dynamic response towards H_2 gas of different concentrations at 175°C .

reducing gases, such as H_2 , ethanol, etc. The operating temperature of MoO_3 was defined as 280°C for 100 ppm H_2 diluted in synthetic air (Fig. 21 bottom).

c) *H_2 sensing properties of nanostructured MoO_3 doped with Pt* Surface doping of nanosize metal oxides by noble metals is a widely used method for enhancing their gas sensing properties. Pt catalyzes the dissociation of hydrogen at relatively low temperatures. The chemical surface reaction between target gas and metal oxide is accelerated on the surface of the Pt nanoparticles. For this work, the previously synthesized MoO_3 nanorods were used as precursor for the one-step synthesis of $\text{MoO}_3\text{-Pt}$ by dissolving MoO_3 in a PtCl_2 solution at room temperature. The sample maintained its structure and morphology after thermal treatment at 400°C in air for 1 h. The Pt nanoparticles were characterized by SEM and EDX (Fig. 22 top).

The operating temperature was set at 175°C , which is considerably lower than the operating temperature of pure MoO_3 (280°C). Moreover, the sensitivity towards 50 ppm H_2 was improved. Increasing concentrations of H_2 (50 – 500 ppm) were stepwise tested under the same conditions. The sensing curves represent reli-

able response and recovery times for low H_2 contents (Fig. 22 bottom).

4.3 Electrochemical sensors with higher resolution (J. Cors, Ø. Fischer)

The technical goal of this project is the development of electrochemical sensors with higher resolution than existing commercial devices. This applied research project started in 2010 as part of the SNF-supported *economic stimulus packages*. The starting industrial partner was the Geneva-based company Nirva Industries (formerly MecSens SA). For non-technical reasons, Nirva Industries has now stopped the production and development of sensing devices, and we are now in the process of incorporating a new industrial partner.

a) *Scope of the project* The main distinctive feature of the electrochemical sensor studied here is the large surface gold cathode of 6.2 mm diameter. A sophisticated mechanical design allows a polymer membrane to cover uniformly the cathode while maintaining a thin, continuous layer of liquid electrolyte (an aqueous solution of KCl and KOH in the case of the oxygen sensor) between the polymer and the gold surface (Fig. 23). The large sensing area makes it possible to generate measurable currents even at trace level concentrations (below 1 ppb of dissolved oxygen).

The research activities in this project follow two main directions: 1) the optimization of the sensing surface, and 2) the development of the appropriated electronics to measure the dc current proportional to the gas concentration (mainly O_2). Different configurations of the sensor (essentially the electrode material, the polarity, and the electrolyte) make also possible the measurement of gases like ozone and hydrogen.

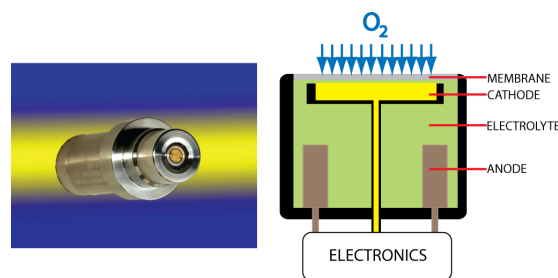


Figure 23: View of the sensor and its schematics: the oxygen molecules permeate through the polymer membrane and are reduced at the cathode generating a dc current proportional to the oxygen concentration.

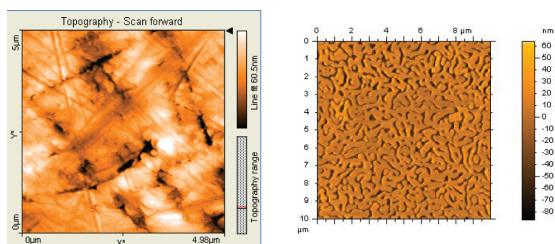


Figure 24: AFM images of gold electrode surfaces: left: machined polished gold with $Ra = 28$ nm (image size $5 \mu\text{m} \times 5 \mu\text{m}$). Right: epitaxial gold Au(111) on mica (image size $10 \mu\text{m} \times 10 \mu\text{m}$).

b) *The cathode sensing surface* At this stage we have focused the project on gold electrodes for the measurement of oxygen. Platinum electrodes (for hydrogen measurement) will be elaborated later on upon requirements of a new industrial partner. We have prepared and studied the electrochemical sensing properties of three different types of gold surfaces, namely:

- machined polished gold cathodes (bulk) (Fig. 24 left);
- cold-coated glass slides (prepared by sputtering);
- epitaxial Au(111) films grown on mica (prepared by sputtering) (Fig. 24 right).

The morphology of the different surfaces was characterized by atomic force microscope (AFM) roughness measurements. This has provided a variety of samples with surface roughnesses ranging from $Ra = 28$ nm to samples showing atomically flat terraces over several microns.

c) *Low-noise, ultra-low-current electronics* At trace levels of dissolved oxygen detection, the current generated by the sensing electrode is in the nA range. There is thus an analogy with scanning tunneling microscopy (STM) amplifier electronics, where ultra-small dc currents have to be amplified and filtered to provide accurate z-feedback. In this project, we have transferred MaNEP STM electronics expertise to design a new amplifier setup for the oxygen sensor. Basically, STM-approved ultra-low leakage-current amplifiers (leakage current of 20 – 200 fA) have been used to design a new measuring circuit that is able to measure sensor currents five times smaller than in the commercial electronics. Still in analogy with STM instrumentation, to minimize noise and wiring effects, the amplifier circuit has been miniaturized to be placed in the head of the sensor, very close to the current generation source

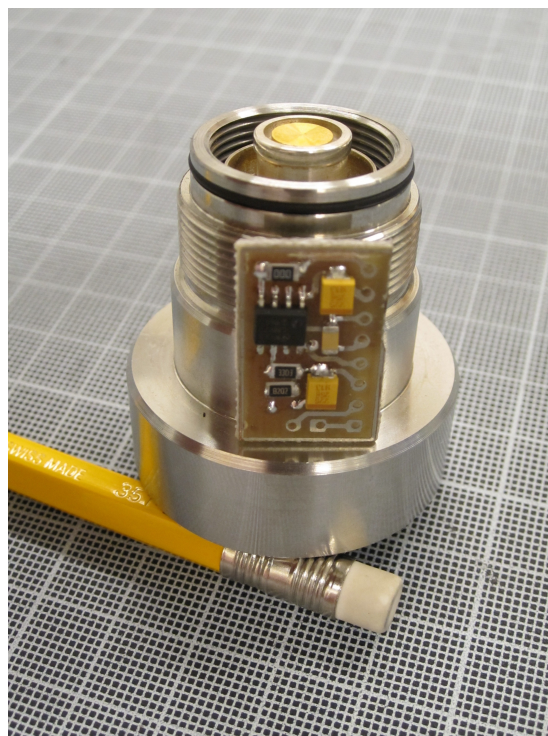


Figure 25: New compact amplifier bloc circuitry (sensor head beside for comparison).

(Fig. 25). Minor mechanical modifications are under way to finish this development.

The electronics setup has been used to characterize the sensing properties of the different electrode surfaces. We have observed that, systematically, smooth gold surfaces are able to generate higher currents at same oxygen concentration. While commercial devices generate an average current of $1 \mu\text{A}/\text{mm}^2$ in air, we have observed that epitaxial gold Au(111) surfaces yield currents in excess of $1.4 \mu\text{A}/\text{mm}^2$ in air. Experiments have been done to verify to what extent this is a geometric effect — the liquid electrolyte wets easily a smooth atomically flat surface — or an intrinsic catalytic effect of an ordered, reconstructed and clean gold surface. We have observed the sensing structures (gold surface/electrolyte layer/membrane) with a very powerful optical microscope. The electrolyte layer thickness could be modified mechanically. By focusing the image first on the electrode, and then on the membrane surface, the thickness of the electrolyte layer could be measured (since the thickness of the membrane is known) from the z-displacement of the optical axis. There is a region, below $5 \mu\text{m}$ of electrolyte thickness, where the current grows exponentially, leading to a very high sensitivity of the sensor (Fig. 26). Only ultra-flat electrodes can maintain a continuous liquid film on

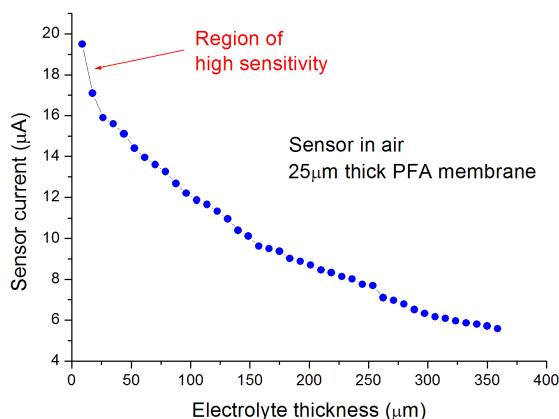


Figure 26: Sensor current as a function of electrolyte thickness.

the whole surface without creating dry spots that might automatically reduce the sensing current.

This result shows that higher sensitivity can be obtained by implementing flat gold surfaces that can keep very good electrolyte “wettability” over the whole cathode surface. To further understand the sensing performance of epitaxial gold films, we have also explored the possibility of “surface activation” that occurs naturally on freshly sputtered films. “Surface activation” is a technical term related to the process of radically cleaning a surface, removing all impurities and restoring the intrinsic surface properties. For example, wetting is a physical process that is strongly dependent on surface activation since impurities modify the surface free energy. This research is presently under way.

4.4 Giant piezoresistance silicon cantilever (C. Renner)

a) *Introduction* The detection of mechanical displacements in the nanometer range is of great industrial interest. Applications include MEMS and NEMS devices, strain and pressure gauges, biomechanical sensors and many more. Current transducer schemes include piezoresistive, optical, capacitive, magnetomotive, and single-electron transistor based detection. Except for piezoresistance, they all become impractical upon scale reduction due to severe loss of signal intensity. Only piezoresistance is broadly scalable, making it highly desirable for detecting nanoscale range displacements of submicron sized devices.

Last year, we reported on a very large resistance increase in thin silicon slabs upon application of a compressive stress. This extraordinarily large piezoresistance, first observed in

silicon nanowires [27], had been explained in terms of a stress-induced modulation of the surface depletion region of width ω [28]. Unfortunately, upon closer inspection, we found this technologically very promising property to be an experimental artefact due to the very act of measuring the piezoresistance. Indeed, the very large piezoresistance is due to surface trapping of charges induced by the voltage (V_{DS}) applied to measure the device conductance (Fig. 27a) [13].

b) *Results* A variety of unreleased and released, n -type and p -type microwires, nanowires, and nanoribbons were fabricated using a top-down approach from silicon-on-insulator wafers of different device layer thicknesses and background doping levels. On wafer, large area strain gauges were also

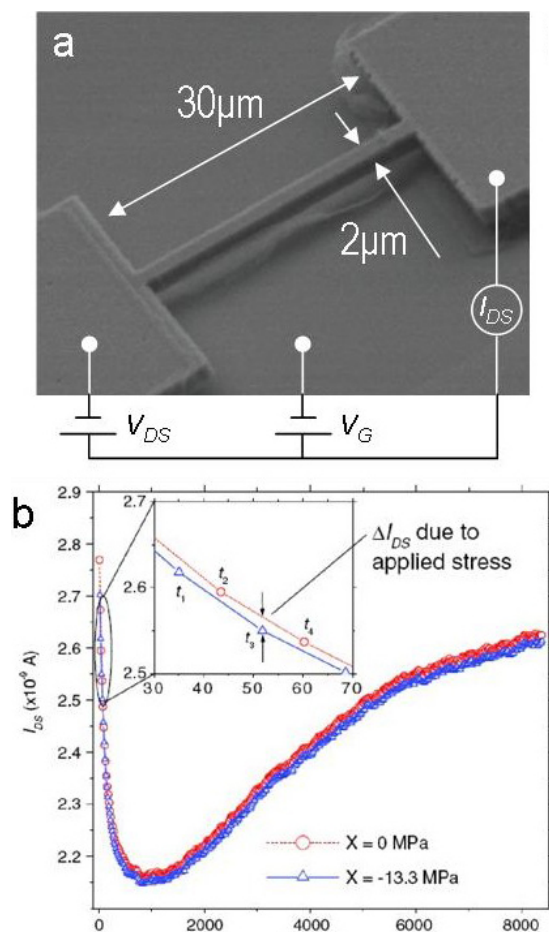


Figure 27: (a) SEM picture of a silicon bridge. (b) Measurement of $I_{DS}(t)$ after applying a source-drain voltage of $V_{DS} = 0.5$ V at $t = 0$ across a $200\text{ nm} \times 2000\text{ nm} \times 30\text{ \AA}$ n -type nanoribbon and alternating the stress between 0 MPa and -13.3 MPa. V_G was held at 0 V for the duration of the measurement. The inset indicates the sequence of measurements used in the stress modulation technique, where the lines are a guide to the eye.

fabricated, thereby allowing the applied stress, X , to be monitored *in situ*. We use a three-point bending setup, with a piezoelectric pusher that permits rapid and repeatable switching between zero and finite stress regimes; this heterodyne detection technique is crucial in differentiating the intrinsic stress related response from other spurious effects. All previously published experiments were obtained in the usual way, where X is ramped or stepped monotonically with time. The device conductance G was measured by monitoring the current I_{DS} induced by an applied voltage V_{DS} while the silicon base was held at a constant back-gate voltage V_G (Fig. 27a).

Figs. 27b and 28 illustrate how nature tricked us into believing in giant piezoresistance in microstructured silicon devices. Changing the applied bias V_{DS} to measure the device resistance alters the configuration of the trapped charges in the device surface. These charges modify the local electrostatic potential and, most detrimental to the piezoresistance measurements, drift with a long time constant, thus contributing a time dependent component to the current, as shown in Fig. 27b. The non-monotonic behavior can be fully explained and modeled in terms of different time constants for trapped electron and hole carriers [13]. If the current is measured while monotonically ramping X , a significant portion of the change in current will have nothing to do with the applied stress, and the apparent piezoresistance will be dominated by the surface charge dynamics. Using our heterodyne detection technique, the zero stress current is measured alternatively with each finite stress measurement (Fig. 27b, inset). This enables us to compensate the conductance drift due to the trapped charges as shown in Fig. 28. Note that, depending on the amount of trapped charge, their dynamics, and the data acquisition rate, very different piezoresistance line shapes can be obtained, especially those reported for silicon nanowires in Fig. 2 of He and

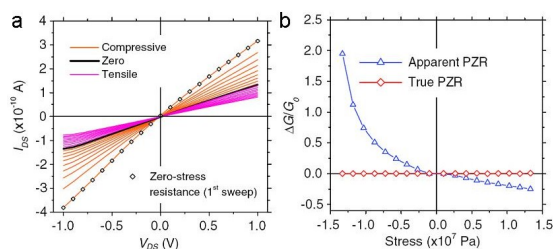


Figure 28: Successive $I_{DS} - V_{DS}$ measurements of a $50 \text{ nm} \times 50 \text{ nm} \times 1 \mu\text{m}$ p -type nanowire with $V_G = 0 \text{ V}$. (b) Apparent and true PZR extracted from the $V_{DS} = 0.5 \text{ V}$ data points in (a).

Yang [27].

Our initial findings of gauge factors $GF = \frac{\Delta R}{R_0} / \frac{\Delta \ell}{\ell_0}$ in excess of 6000, compared to 100 for bulk silicon, triggered the interest of industrial companies. Two patent applications were filed and discussions with two companies interested in MEMS devices and touch sensors were initiated. The negative results reported here led to a high-profile scientific publication [13] and several comments in the specialized literature, but they obviously brought our efforts towards applications to an abrupt halt. We also decided to withdraw all pending patent applications. Despite these setbacks, we are still exploring alternative ways to achieving the very challenging all electrical detection of minute displacements in MEMS-type devices, a highly desirable feature for biomechanical assays, atomic force microscopy and ultimate mass sensing.

5 New surface treatments for microcomponents

5.1 Marking technology for watch components (J. Cors, J.-M. Triscone, Ø. Fischer; Vacheron Constantin, Phasis)

In this project, a STM-inspired device (comprising XYZ micromotors, electronic servo-control, and a programmable spark generator) is used to mark watch components at the microscopic scale. The technology is able to “write” microscopic dots of *in situ* synthesized alloys on the surface of metallic objects. The chemical composition of the dots can be adjusted to play the role of a chemical signature for authentication purposes¹. In previous work², we have demonstrated that the technology can be used on a wide range of technical, commercial alloys. Thus, the span of potential applications ranges from jewelry (anti-counterfeiting marks) to medical implants, and aircraft spare parts (traceability). In a first step, we have focused our efforts on the high-end watch industry. Our partner is the renowned watch manufacturer Vacheron Constantin in Geneva (Fig. 29) and the MaNEP start-up Phasis. The technical goals and quality standards expected by such a partner create the optimum stretch to develop the technology to its highest level of performance. This work is also supported by a new CTI grant³.

a) *Surface-alloy-writing of characters and decorative patterns, automation* The experimental

¹International Patent Application WO 2008/010044 A3

²CTI feasibility project N° 8897.1

³CTI feasibility project N° 10281.2



Figure 29: Vacheron Constantin watch parts blend technical expertise with a refined aesthetics and an exceptional level of finishing.

setup is now able to write alphanumeric characters automatically. Indeed, new developments in the numerical control of the tip movement allow for the reliable, unwatched alloy-writing of chains of characters. Serial numbers, words, phrases can be written on small metal parts. Another new development concerns the elaboration of patterns like logos or artistic drawings. The XY movement of the writing tip can be monitored using a joystick. This gives to the operator the freedom to create patterns of almost any shape. Even multi-alloy decorative structures can be created by switching the nanopowder-based dielectric liquid between selected pattern segments (Fig. 30). Another important development concerns the setup of a prototype part changer for batch processing (Fig. 31). A main objective of the CTI project is indeed the possibility to mark thousands of

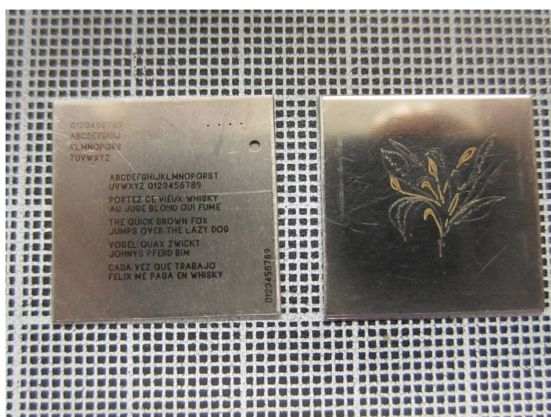


Figure 30: Left: automatic writing of numbers and letters with a TiB_2 alloy. Right: multi-alloy decorative pattern (substrates: steel 316L).

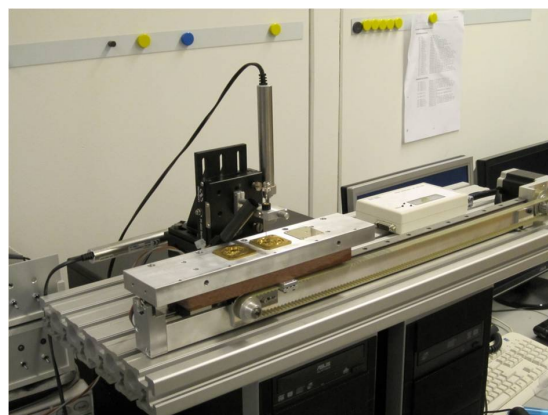


Figure 31: First automated marking line for batch processing of watch parts.

watch components per year with a minimum of scrap parts.

b) *Local-probe metallurgy* The energy of the individual micro-sparks can be precisely controlled by a dedicated, programmable spark generator. Since the marking process results from the interaction of the radiating plasma and the surface of the substrate, fine adjustments of the alloy composition are possible by tuning the spark shape (the current) and power. The spark is assimilated here to a tiny microreactor. This particular feature is illustrated here in the case of a dielectric containing TiN nanopowders. TiN is extensively used in both functional and decorative coatings. It is known that TiN_x stoichiometry and structure have a strong influence on the visual appearance of the coating [29]. By changing the spark shape, marks of different colors have been achieved using the same composite dielectric (Fig. 32).

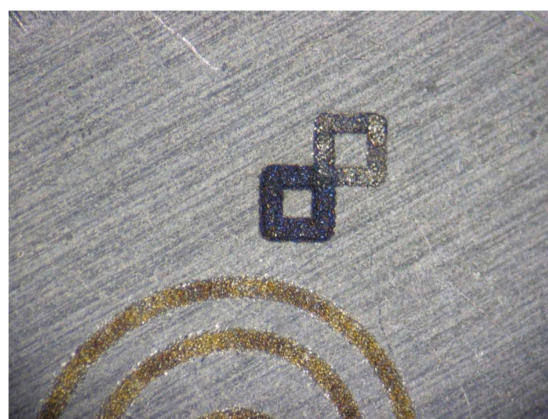


Figure 32: Local fine-tuning of TiN_x composition (substrate: stainless steel).

5.2 Cut-and-coat process by wire-EDM (J. Cors, Ø. Fischer; AgieCharmilles)

This applied research project started also in 2010 as part of the SNF-supported *economic stimulus package*. electrical discharge machining (EDM) is used to shape and cut solid conducting materials, including very hard metals and ceramics (Fig. 33). For traditional machining applications, a computer-driven mechanism seeks to maximize erosion on one of the electrodes, cathode or anode workpiece. At the same time, erosion is minimized on the remaining electrode to preserve machining accuracy and tool costs.

The goal of the present project is to develop a new functionality for wire-EDM technology: the possibility to achieve a controlled transfer of electrode material to the workpiece surface. This would offer to AgieCharmilles (+GF+ group) the opportunity to enter the growing market of coated metal parts.

a) *Development of EDM-coating technologies*
Traditional EDM machines operate in cycles composed of a) an ignition delay b) a pulse time for the current and c) a pause time. While the ignition delay (or breakdown time) cannot be controlled, both the pulse time (or on-time) and the pause time (or off-time) are set by the machine operator. For standard machining, different settings of peak currents, on-times and off-times have been optimized and stored over the years in what is known today as "Machining Technology Tables". These conventional settings achieve maximum machining speed while minimizing electrode wear. From the physics point of view, the workpiece erosion results from a) a polarity effect in the power distribution in the plasma column during on-time, and b) the different thermal properties of the tool and the workpiece [30].

For example, conventional die-sinking EDM uses on-times in excess of 25 μs to optimize ma-

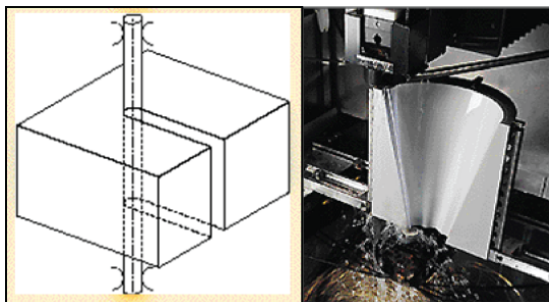


Figure 33: The metal part is shaped by erosive sparks from a wire electrode immersed in a liquid dielectric.

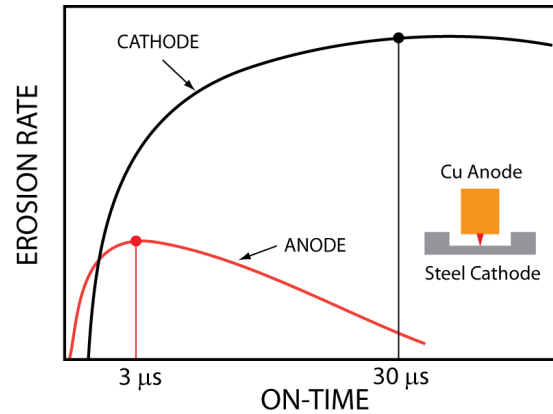


Figure 34: Schematic behavior of anode and cathode erosion rates as a function of spark duration (copper anode, steel cathode).

chining performance (Fig. 34). In the present work we have explored unusual machine settings to elaborate "coating technologies", by modifying the generator settings under conditions where both tool wear and workpiece erosion occur simultaneously. To achieve surface alloying, these new machine settings promote a controlled wear on the electrode, and simultaneously induce local surface melting on the workpiece. During the first year of the project, the main objective was to determine the conditions and parameters to achieve controlled metal transfer from a rod- or rectangle-shaped electrode to the workpiece surface. We have used, in a first step, traditional EDM die-sinking machines with a rotating electrode (Fig. 35). AgieCharmilles has provided the required flexible access to the software and the electronics. The coating tests have been done using cylindrical and rectangular electrodes of different metals and alloys of commercial interest.

The machining parameters (peak current, on-time, off-time, servo-control) have been adjusted to produce homogeneous coatings. The



Figure 35: In a first step, bulk, cylindrical electrodes have been used to explore the coating parameters. The use of simple, rod-shaped electrodes avoids the costly and time-consuming process of dedicated wire fabrication in the research phase.

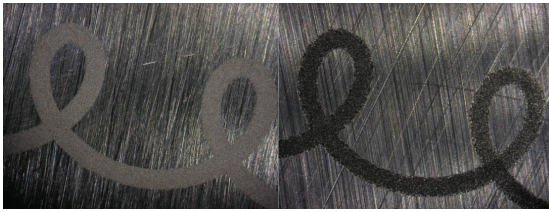


Figure 36: Left: standard machining parameters and copper electrode. Right: tungsten electrode and coating parameters activated. Width of the pattern is 1 mm.

surface chemical composition of the treated workpieces was determined by extensive use of a Roanalytic Compact eco X-ray fluorescence desktop analyzer. This instrument was installed close to the laboratory to provide rapid feedback for the iterative tuning of machine settings. The elaborated coatings/surface alloys (Fig. 36) have a typical thickness of 5 – 10 μm as determined from X-ray analysis and from metallographic cuts.

For this particular project, one important requirement of the SNF was the obtention of multiplier effects in industry. In that perspective, we have elaborated a set of coated parts for demonstration purposes. Some of the elaborated parts are shown in Fig. 37. The goal is to retain the attention from potential users that can apply the technology to their actual products.

To this end, a number of companies from different industrial sectors have been invited to evaluate the technology. The use of concrete application examples optimizes the chances for a faster technology transfer. Within this project, most of the coming developments will be application-oriented taking into account specific technical requirements. We have received very positive words of interest. “Test cuts” are under way for some of these industries.

6 Collaborative efforts

This project is characterized by several close collaborations between researchers of MaNEP and our industry partners. On superconductivity there is a long-standing collaboration between Bruker-BioSpin and Prof. René Flükiger. This collaboration is now taken over by Dr. Carmine Senatore on the MaNEP side. There is in addition a growing collaboration between MaNEP and CERN on the development for new superconducting wires for the future upgrade of LHC. The collaboration between ABB and MaNEP on superconducting thin film fault current limiters has made further progress this year.



Figure 37: Left: abrasive structures in hard coating (for tools like files). Center: a decorative logo in hard surface alloy (polygon size 6 mm). Right: a small cutting die machined by wire-EDM, a tungsten coating was produced using a tungsten wire electrode.

The search for mechanical energy harvesting devices is a close collaboration between three partners: the group of Jean-Marc Triscone (UniGE), the group of Nico de Rooij (EPFL, Neuchatel) and the group of Gilles Triscone (Hepia, Geneva). A new collaboration has been started between Philipp Aebi (UniFR), Jürg Hulliger (UniBE) and Anke Weidenkaff (Empa and UniBE) in order to synthesize and characterize new materials for thermoelectric power. The research on neutron supermirrors is a close collaboration between MaNEP researchers at PSI and the company SwissNeutronics with occasional collaboration with the group of Jean-Marc Triscone (UniGE).

The research on transition metal hydrogen detectors is a collaboration between the groups of Klaus Yvon, Øystein Fischer, Jorge Cors (UniGE) and Asulab (Swatch group). In particular we have combined the competence on hydrides of Klaus Yvon with the thin film synthesis competence in Øystein Fischer’s group as well as Jorge Cors knowledge on the field of gas sensors and Asulab’s experience in sensing devices. In this field a close collaboration has also developed between Greta Patzke (UniZH) and Jorge Cors (UniGE). The projects on surface treatments consists of two close collaborations between the groups of Øystein Fischer and Jorge Cors on the one hand and two companies on the other hand: Vacheron Constantin and AgieCharmilles. In both these projects, we are now building a close collaboration between MaNEP and these companies. The MaNEP start-up Phasis is also part of these projects.

MaNEP-related publications

- ▶ [1] R. Flükiger, M. S. A. Hossain, C. Senatore, F. Buta, and M. Rindfleisch, *to be published in IEEE Transactions on Applied Superconductivity* (2011).
- ▶ [2] C. Senatore, M. S. A. Hossain, and R. Flükiger, *to be published in IEEE Transactions on Applied Superconductivity* (2011).
- ▶ [3] B. Seeber, A. Ferreira, G. Mondonico, F. Buta, C. Senatore, R. Flükiger, and T. Takeuchi, *Superconductor Science & Technology* **24**, 035011 (2011).

- [4] L. Antognazza, M. Therasse, M. Decroux, F. Roy, B. Dutoit, M. Abplanalp, and Ø. Fischer, *IEEE Transactions on Applied Superconductivity* **19**, 1960 (2009).
- [5] L. Antognazza, M. Decroux, M. Therasse, and M. Abplanalp, *IEEE Transactions on Applied Superconductivity* (2011), doi:10.1109/TASC.2010.2100351.
- [6] A. Sambri, S. Gariglio, A. Torres Pardo, J.-M. Triscone, O. Stéphan, J. W. Reiner, and C. H. Ahn, *Applied Physics Letters* **98**, 012903 (2011).
- [7] D. Isarakorn, D. Briand, P. Janphuang, A. Sambri, S. Gariglio, J.-M. Triscone, F. Guy, J. W. Reiner, C. H. Ahn, and N. F. de Rooij, *Smart Materials and Structures* **20**, 025015 (2011).
- [8] D. Isarakorn, A. Sambri, P. Janphuang, D. Briand, S. Gariglio, J.-M. Triscone, F. Guy, J. W. Reiner, C. H. Ahn, and N. F. de Rooij, *Journal of Micromechanics and Microengineering* **20**, 055008 (2010).
- [9] M. H. Aguirre, A. Shkabko, and A. Weidenkaff, *Crystal Growth and Design* **10**, 3562 (2010).
- [10] A. Shkabko, M. H. Aguirre, I. Marozau, M. Doebeli, M. Mallepell, T. Lippert, and A. Weidenkaff, *Materials Chemistry and Physics* **115**, 86 (2009).
- [11] C. Suter, P. Tomš, A. Weidenkaff, and A. Steinfeld, *Materials* **3**, 2735 (2010).
- [12] G. R. Patzke, A. Michailovski, F. Krumeich, R. Nesper, J.-D. Grunwaldt, and A. Baiker, *Chemistry of Materials* **16**, 1126 (2004).
- [13] J. S. Milne, A. C. H. Rowe, S. Arscott, and C. Renner, *Physical Review Letters* **105**, 226802 (2010).
- [14] H. Ohta, S. Kim, Y. Mune, T. Mizoguchi, K. Nomura, S. Ohta, T. Nomura, Y. Nakanishi, Y. Ikuhara, M. Hirano, H. Hosono, and K. Koumoto, *Nature Materials* **6**, 129 (2007).
- [15] S. Li, R. Funahashi, I. Matsubara, K. Ueno, and H. Yamada, *Journal of Materials Chemistry* **9**, 1659 (1999).
- [16] C. X. Quintela, F. Rivadulla, and J. Rivas, *Applied Physics Letters* **94**, 152103 (2009).
- [17] A. Mavromaras, S. Matar, S. B., and G. Demazeau, *Journal of Magnetism and Magnetic Materials* **134**, 34 (1994).
- [18] N. F. Mott, *Metal-insulator transitions. 2nd ed.* (Taylor & Francis, 1990).
- [19] J. Ravichandran, W. Siemons, D.-W. Oh, J. Kardel, A. Chari, H. Heijmerikx, M. Scullin, A. Majumdar, R. Ramesh, and D. Cahill, *Physical Review B* **82**, 165126 (2010).
- [20] D. G. Cantrell and P. N. Butcher, *Journal of Physics C* **20**, 1985 (1987).
- [21] M. Shikano and R. Funahashi, *Applied Physics Letters* **82**, 1851 (2003).
- [22] M. Mikami, S. Ohtsuka, M. Yoshimura, Y. Mori, T. Sasaki, R. Funahashi, and M. Shikano, *Japanese Journal of Applied Physics* **42**, 3549 (2003).
- [23] T. Takeuchi, T. Kondo, T. Kitao, K. Soda, M. Shikano, R. Funahashi, M. Mikami, and U. Mizutani, *Journal of Electron Spectroscopy and Related Phenomena* **144-147**, 849 (2005).
- [24] C. Morawe, P. Pecci, J. C. Peffen, and E. Ziegler, *Review of Scientific Instruments* **70**, 3227 (1999).
- [25] K. Galatsis, Y. X. Li, W. Wlodarski, and K. Kalantar-zadeh, *Sensors and Actuators B: Chemical* **77**, 478 (2001).
- [26] X. K. Hu, Y. T. Qian, Z. T. Song, J. R. Huang, R. Cao, and J. Q. Xiao, *Chemistry of Materials* **20**, 1527 (2008).
- [27] R. He and P. Yang, *Nature Nanotechnology* **1**, 42 (2006).
- [28] A. C. H. Rowe, *Nature Nanotechnology* **3**, 311 (2008).
- [29] P. Roquiny, F. Bodart, and G. Terwagne, *Surface and Coating Technology* **116**, 278 (1999).
- [30] D. D. DiBitonto, P. T. Eubank, M. R. Patel, and M. A. Barruffet, *Journal of Applied Physics* **66**, 4095 (1989).

Other references

Project 4 Electronic properties of oxide superconductors and related materials

Project leader: D. van der Marel (UniGE)

Participating members: D. Baeriswyl (UniFR), B. Batlogg (ETHZ), L. Degiorgi (ETHZ), Ø. Fischer (UniGE), T. Giamarchi (UniGE), E. Giannini (UniGE), J. Karpinski (ETHZ), H. Keller (UniZH), M. Kenzelmann (PSI), D. van der Marel (UniGE), C. Niedermayer (PSI), T. M. Rice (ETHZ), M. Sigrist (ETHZ)

Summary and highlights: The discovery of high- T_c superconductivity in the iron-pnictides has sparked a worldwide goldrush for other high- T_c superconductors. In this project the first synthesis and crystal growth of $\text{Cs}_{0.8}(\text{FeSe}_{0.98})_2$ which becomes superconducting at 27 K is reported. LaRu_2P_2 was found to have a T_c of 4.1 K. In structurally related $\text{InBi}_{1-x}\text{Sb}_x$ and $\text{In}_{1-x}\text{Ga}_x\text{Sb}$ superconductivity up to 8 K was found. Scanning tunneling spectra of $\text{Fe}_{1+x}\text{Te}_{1-y}\text{Se}_y$ show clearly the coherent peaks and the superconducting gap. Single-crystalline samples of $\text{Sm}_{1-x}\text{Th}_x\text{FeAsO}$, $\text{SmFeAs}_{0.5}\text{P}_{0.5}\text{O}_{1-y}$, $\text{SmFe}_{1-x}\text{Co}_x\text{AsO}$, $\text{NdAs}(\text{O},\text{F})$, and $\text{Ba}_{1-x}\text{Rb}_x\text{Fe}_x\text{As}_2$ were prepared and the superconducting properties were studied. Interplay between superconductivity and antiferromagnetism was investigated in the iron-pnictides and chalcogenides with muon-spin resonance and infrared optical spectroscopy. STM showed for the first time unambiguously the Van Hove singularity of $\text{Bi}_2\text{Sr}_2\text{CuO}_6$. Variational studies have been applied to the repulsive Hubbard model and for study of BCS-BEC crossover in the attractive case. Strong interplay between lattice effects and superconductivity is observed by measuring the effect of pressure and isotope substitution on the superconducting properties of the cuprates and the Fe-pnictides and chalcogenides. Very large Faraday rotation was observed in infrared transmission spectra of the perovskite EuTiO_3 . In Mott-insulating Sr_2VO_4 spin- and orbital-moments were found to compensate each other due to spin-orbit interaction.

1 Novel superconducting materials

1.1 Synthesis and crystal growth of $\text{Cs}_{0.8}(\text{FeSe}_{0.98})_2$: a new iron-based superconductor with $T_c = 27$ K (M. Kenzelmann)

The recent discovery of the Fe-based superconductors has triggered a remarkable renewed interest for possible new routes leading to high-temperature superconductivity. As observed in the cuprates, the iron-based superconductors exhibit interplay between magnetism and superconductivity suggesting the possible occurrence of unconventional superconducting states. Other common properties are the layered structure and the low carrier density. Among the iron-based superconductors, FeSe_{1-x} had the simplest (11-type) structure with layers in which Fe cations are tetrahedrally coordinated by Se [1]. It was found, that hydrostatic pressure modifies the electronic phase diagram of FeSe_{1-x} and induces static magnetic order which can coexist with superconductivity [2]. Moreover, the substitution of Te for Se leads to an increase of T_c up to 14 K. We have done systematic investigation of the magnetic and superconducting properties, and their interplay, in $\text{Fe}_y\text{Se}_x\text{Te}_{1-x}$ with different nominal Fe content and different Se:Te ratio [3, 4, 5, 6]. The tentative three-

dimensional phase diagram showing dependence of the transition temperatures T_c and T_N of $\text{Fe}_y\text{Se}_x\text{Te}_{1-x}$ for $0 < x < 0.5$ and $0.9 < y < 1.1$ was built based on our study. Fe_yTe is always antiferromagnetically ordered. Upon substituting Te by Se the order becomes weaker while superconductivity is enhanced and finally the system becomes bulk superconducting. This behavior can be tuned not only by the substitution of Se but also by adjusting the Fe content. The superconductivity is suggested to be of multiband nature, where different doping channels might be involved.

Very recently superconductivity at above 30 K was found in $\text{K}_{0.8}\text{Fe}_2\text{Se}_2$ [31]. This is so far the highest T_c for Fe-chalcogenides, even though the superconducting fraction is low and the transition is broad. It is also reported in [31] that single-crystals of several mm^3 could be grown from the self-flux. Shortly after that, we have reported for the first time on the synthesis and crystal growth of a new analog compound with Cs intercalated between FeSe layers [7].

Single-crystals of cesium intercalated iron selenides of nominal compositions $\text{Cs}_{0.8}(\text{FeSe}_{0.98})_2$ were grown from the melt using the Bridgeman method. The nominal stoichiometry of the starting material that is $\text{FeSe}_{0.98}$ was chosen based on our previous

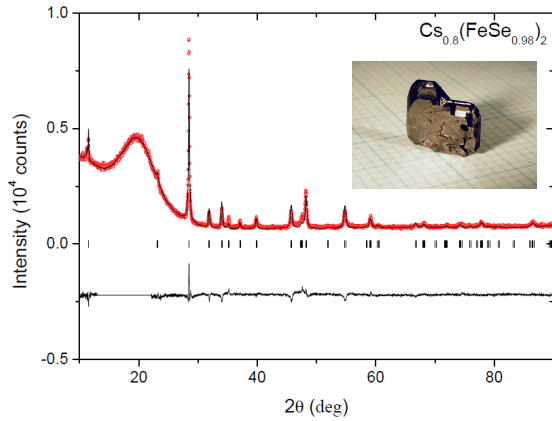


Figure 1: Rietveld refinement pattern (upper-red) and difference plot (lower-black) of the X-ray diffraction data for the crystal with the nominal composition of $\text{Cs}_{0.8}(\text{FeSe}_{0.98})_2$. The rows of ticks show the Bragg peak positions for the $I4/mmm$ phase. The inset shows a picture of a piece of $\text{Cs}_{0.8}(\text{FeSe}_{0.98})_2$ crystal.

studies [1] which demonstrated that for this particular Fe/Se ratio the content of secondary phases is the smallest. The superconducting transition has been detected by ac susceptibility using a conventional susceptometer. The onset of the critical temperature has been determined to $T_{c, \text{onset}} = 27.4$ K.

Room temperature XRD experiments revealed that the crystals do not contain any impurity phases (Fig. 1). The only detected phase is the tetragonal phase of ThCr_2Si_2 type (space group $I4/mmm$). This structure has the same FeSe layers as in (11) FeSe [1], but in the last (space group $P4/nmm$) these layers are identical with respect to the translation along z -direction (this is obvious, because the unit cell contains only one FeSe-layer). In $\text{Cs}_{0.8}(\text{FeSe}_{0.98})_2$ the unit cell is doubled along z -axis. The neighboring along z -direction FeSe layers are shifted by $(1/2, 1/2, 1/2)$, so that upwards SeFe_4 pyramid is faced with the downwards pyramid along z -direction and the intercalated atom is located between more distant Se-atoms along z . The Fe-Fe layer distance in $\text{Cs}_{0.8}(\text{FeSe}_{0.98})_2$ increases to 7.6423 Å in comparison with 5.5234 Å in FeSe. The intercalation of Cs also increases the Fe-Se bond length within the layers. Further investigations of $\text{Cs}_{0.8}(\text{FeSe}_{0.98})_2$ applying bulk methods like neutron scattering and muon-spin rotation both at ambient and high pressures are underway.

1.2 Mass enhancement in the $4d$ analogue LaRu_2P_2 (B. Batlogg)

One of the central questions concerning the new superconductor family, based on Fe-

pnictides and related ones, concerns the origin of the pairing interaction and the role played by the correlation among the Fe-derived electronic states, which are known to be partly hybridized with the pnictogen p -states. The correlation effects, together with the Fermi surface (FS) geometry, are thought to hold the key to the understanding of the essential physics governing the Fe-based superconducting materials.

We have studied LaRu_2P_2 and compare it to the LaFe_2P_2 and SrFe_2P_2 , in which the spatial extent of the d -orbitals is different and thus one would expect different strength of the correlation effects. This difference is expected to be reflected in the enhancement of the quasi-particle mass compared to the calculated band mass. In the Ru compound the superconducting transition temperature is 4.1 K.

We have synthesized LaRu_2P_2 crystals with a small residual resistivity and mounted them on torque cantilevers to measure the magnetization in pulsed fields up to 60 T. These experiments were performed at the National High Magnetic Field Laboratory in Los Alamos, USA, yielding highly consistent data sets on three different crystals.

In Fig. 2, the inset shows the oscillatory part of the magnetic torque at 1.5 K and at 20 K. Repeating these measurements at various temperatures and at various angles with the respect to the Ru-P layers, we extract the essential parameters describing electronic states at the Fermi energy: cross-section of the extremal orbits on the various FS sheets (frequency of the oscillations), and the quasi-particle mass (from the T -dependent oscillation amplitude, Fig. 2, main part). The extremal orbits are in excellent agreement with the local density

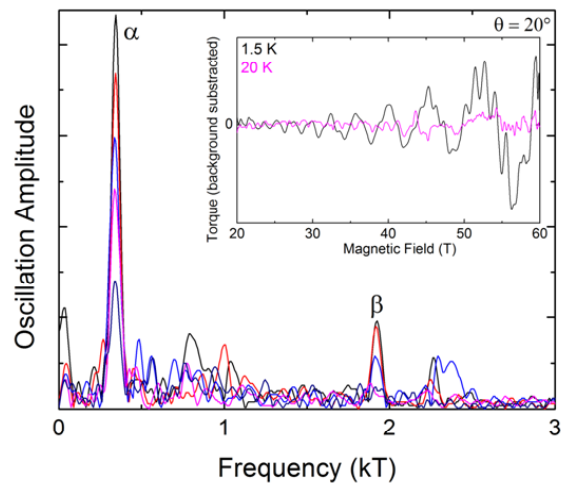


Figure 2: Oscillatory part of the magnetization measured in pulsed magnetic fields up to 60 Tesla.

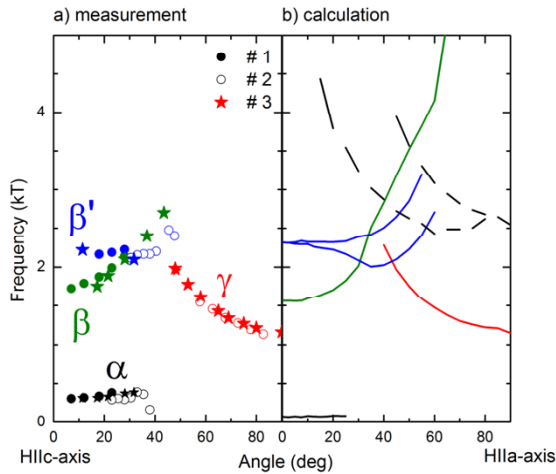


Figure 3: Comparison of measured and calculated frequencies of quantum oscillations. Different colors correspond to different extremal orbits.

approximation (LDA) calculated FS (Figs. 3 and 4).

The effective masses for the two main FS sheets are found to be larger than the calculated band mass. The ratio of the measured to the band mass is 1.4 and 2, respectively. This result is remarkable for two reasons. First, the band mass in the Ru compound is smaller, indeed, than in the Fe analogue. This is in line with expectations due to more extended $4d$ -orbitals. Second, the mass enhancement is found to be as large as in the independently studied SrFe_2P_2 , which is counter to naïve expectations (the FS geometry is essentially the same in both compounds). The larger spread of the $4d$ -wave function in Ru is thus counteracted by a not yet identified effect that enhances correlation. A possibility might be the different degree of hybridization of the d -states with the p -states due to different bare orbital-energies.

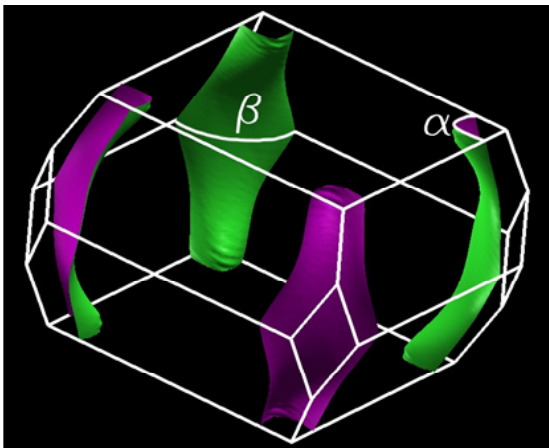


Figure 4: Calculated parts of the Fermi surface with two extremal orbits (α , β) indicated.

Superconductivity in the Fe-based pnictides and chalcogenides, therefore, is neither simply due to a particular Fermi surface geometry nor due to particularly strong correlation. Rather, some additional factor such as bonding geometry and band degeneracy (e.g. orbital-fluctuation effects) might also play a role.

1.3 Superconducting $\text{In}_{1-x}\text{Ga}_x\text{Sb}$ and $\text{Bi}_{1-x}\text{Sb}_x\text{In}$ (E. Giannini)

The search for superconductivity in materials having a crystal structure related to that of Fe-pnictides and Fe-chalcogenides (based on the PbO-type structure $P4/nmm$) has led to the study of the quaternary compound BiOCuS and the binary one BiIn . Doping BiIn with Sb was found to mimic the effect of pressure and induce superconductivity, with a maximum T_c of ~ 8 K ($\text{Bi}_{0.95}\text{Sb}_{0.05}\text{In}$). Increasing the Sb content causes a phase separation between non-miscible BiIn and SbIn . The latter is a narrow-gap semiconductor (with band gap of 0.17 eV at 300 K), and possesses the largest ambient temperature electron mobility ($78000 \text{ cm}^2\text{V}^{-1}\text{s}^{-1}$). Its crystal structure is cubic of the zincblende-type (space group $F\bar{4}3m$) instead of tetragonal ($P4/nmm$). Very interestingly, we have found that substitutions of Ga for In can induce superconductivity in $\text{In}_{1-x}\text{Ga}_x\text{Sb}$ ($0.2 \leq x \leq 0.4$) with a $T_{c,max} = 4.5$ K. This enriches the growing family of semiconductors that become superconducting upon opportune chemical substitutions. However, in this case, as well as in $\text{Bi}_{1-x}\text{Sb}_x\text{In}$, no carriers are doped into the system and conductivity is more likely induced by the lattice compression rather than by the formation of an impurity band, like it is in B-doped SiC .

2 Iron-based chalcogenides

2.1 Fe-chalcogenides, crystal growth and high pressure studies (E. Giannini)

Crystals of $\text{Fe}_{1+x}\text{Te}_{1-y}\text{Se}_y$ ($0 \leq y \leq 0.3$) have been grown for various experimental studies in the frame of a wide collaboration among various MaNEP groups. The electronic structure of these materials is being investigated by ARPES (M. Grioni, EPFL), STM (\emptyset . Fischer, UniGE), and optical spectroscopy (D. van der Marel, UniGE). The influence of spin-fluctuations on charge dynamics in Fe-chalcogenides and Fe-pnictides have been observed by means of infrared spectroscopy [8].

Pressure is found to have a strong effect on magnetism and superconductivity in both Fe-chalcogenides and Fe-pnictides (see [32] for a

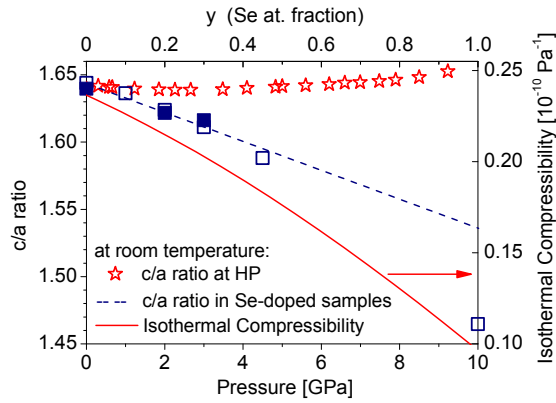


Figure 5: Effect of hydrostatic mechanical pressure (red stars) and internal chemical pressure (blue squares and dashed guide line [9]) on the lattice parameters of $\text{Fe}_{1.087}\text{Te}$. The isothermal compressibility is measured at room temperature and plotted as a function of pressure (red curve).

review), and particularly in FeSe_{1-y} , in which T_c rises from 8 K to 37 K under 9 GPa. However, undoped Fe_{1+x}Te does not exhibit any superconducting signal under pressures up to 19 GPa. In order to elucidate the reason of such difference between FeSe and FeTe , we have performed high-energy X-ray diffraction studies on pulverized crystals of $\text{Fe}_{1.087}\text{Te}$ under hydrostatic pressure up to 12 GPa, and compared the pressure effects to those of Se substitutions. The reduction of the a -lattice parameters is found to be larger than upon Se substitutions, whereas the effect of mechanical and chemical pressure on the c -axis is comparable. A stronger uniaxial pressure is exerted by the Se substitutions, whereas under hydrostatic pressure the unit cell is shrunk more isotropically. This is clearly shown by plotting the c/a ratio as a function of both the pressure and Se content (Fig. 5). From this data the isothermal compressibility of $\text{Fe}_{1.087}\text{Te}$ could be extracted as well, and is found to decrease as a function of pressure from ≈ 0.20 to $\approx 0.10 \cdot 10^{-10} \text{ Pa}^{-1}$ in the range 0 – 10 GPa (Fig. 5). Uniaxial pressure mimicked by the tensile strain is reported to induce superconductivity in strained FeTe thin films [33].

At ambient pressure, $\text{Fe}_{1.087}\text{Te}$ undergoes a structural transition from tetragonal to monoclinic, associated to the magnetic transition to an antiferromagnetic (AF) state, at $T_N = 67$ K. When cooling $\text{Fe}_{1.087}\text{Te}$ under pressures above 0.8 GPa, an intermediate structural modification appears in a limited range of temperatures, between the tetragonal paramagnetic phase at high T , and the monoclinic AF phase at low T (Fig. 6). In the same pressure range anomalies are observed in transport and mag-

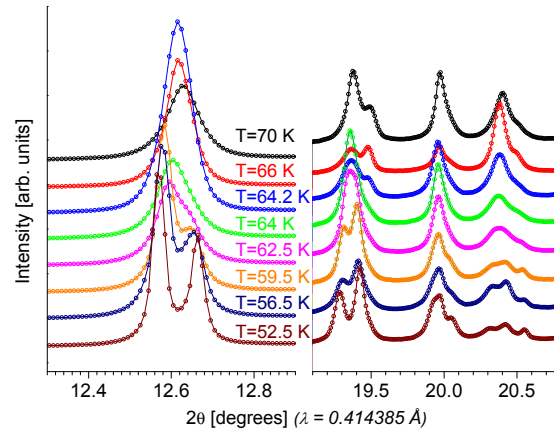


Figure 6: Diffraction patterns of $\text{Fe}_{1.087}\text{Te}$ under $P \approx 1$ GPa. A high-symmetry diffraction pattern is observed at 62 – 64 K.

netic measurements as well. The study of the high-pressure electronic and magnetic behavior is in progress in collaboration with the groups of L. Forró and H. Rønnow at the EPFL.

2.2 Scanning tunneling microscopy studies of the Fe-chalcogenide superconductor $\text{Fe}_{1.013}\text{Se}_{0.7}\text{Te}_{0.3}$ (\emptyset . Fischer)

We have performed scanning tunneling microscopy (STM) experiments on $\text{Fe}_y\text{Se}_x\text{Te}_{1-x}$ single-crystals, which have the simplest crystal structure among the various Fe-based superconductors. The crystals, grown at UniGE using the Bridgman-Stockbarger method, have the composition $\text{Fe}_{1.013}\text{Se}_{0.7}\text{Te}_{0.3}$, with a T_c of 12 K.

In a first set of measurements, the crystals were cleaved *in situ* in ultrahigh vacuum conditions and measured at room temperature. Very flat surfaces are observed by STM, revealing the individual atoms arranged in the square lattice symmetry expected for the Fe-Se/Te layers (Fig. 7a). For a reason which still remains unknown, the surfaces of Fe-based compounds are particularly difficult to probe by tunneling spectroscopy. Our first low-temperature measurements were performed by gluing the sample at the apex of the tip, and tunneling onto a gold thin film. In this geometry, the tunneling current is injected along a direction parallel to the Fe-Se/Te layers, perpendicularly to the crystal c -axis. Tunneling spectra acquired at 1.8 K reveal a clear conductance dip flanked by coherence peaks located at an energy close to 5 meV (Fig. 7b). With increasing temperature this gap progressively fills in, and disappears above 12 K (T_c), underlying its superconductive origin. Other spectral features are also observed at lower energies, possibly related to

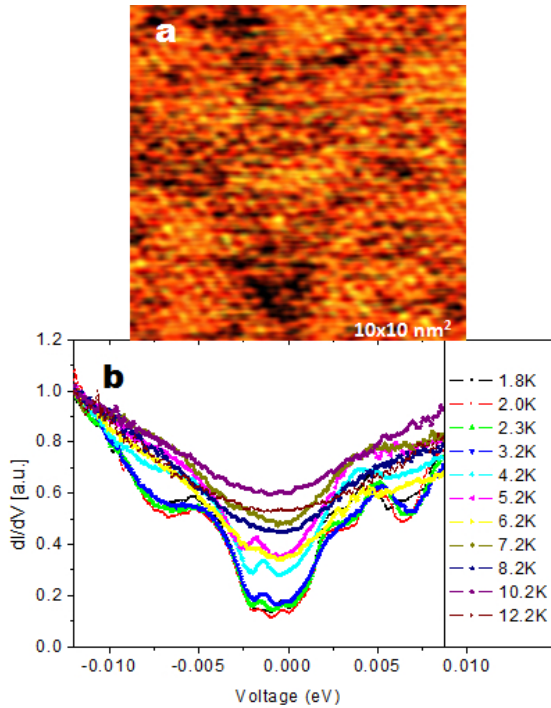


Figure 7: STM on $\text{Fe}_{1.013}\text{Se}_{0.7}\text{Te}_{0.3}$ single-crystals. (a) $10 \times 10 \text{ nm}^2$ STM topography revealing the atomic lattice of the Fe-Se/Te layer. (b) Temperature evolution of the tunneling spectra acquired with the tunneling current injected perpendicular to the c -axis.

the multiband character of the electronic structure in these compounds [34]. Measurements on the (001) surfaces are currently in progress.

3 Iron-pnictide superconductors

3.1 Superconductivity above 50 K in Th-substituted SmFeAsO (*J. Karpinski*)

Superconducting poly- and single-crystalline samples of the $\text{Sm}_{1-x}\text{Th}_x\text{FeAsO}$ with partial substitution of Sm^{3+} by Th^{4+} with a sharp diamagnetic onset at T_c up to $\sim 53 \text{ K}$ were synthesized using high-pressure technique [10]. The unit cell parameters a and c shrink with Th substitution and the fractional atomic coordinate of the As site, z_{As} , remains almost unchanged, while that of Sm/Th, $z_{\text{Sm/Th}}$, increases. The As-Sm/Th distance shortens and the O-Sm/Th distance elongates. Equivalently one may focus on the “layers” of the structure: the Sm/ThO layer expands ($\Delta s_1 = 0.055 \text{ \AA}$), the AsFe layer remains unaffected, and the distance s_3 between the Sm/ThO and the AsFe layers shortens by $\Delta s_3 = -0.048 \text{ \AA}$ (Fig. 8a). Bulk superconducting samples do not undergo a structural phase transition from tetragonal to orthorhombic symmetry at low temperatures. Upon warming from 5 to 295 K the

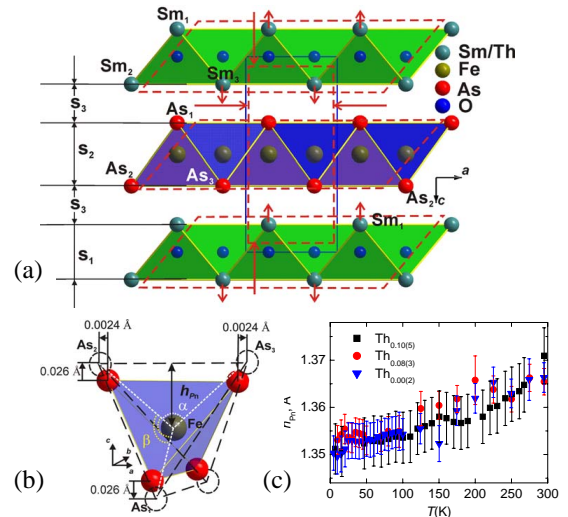


Figure 8: (a) Schematic representation of the projection of $\text{Sm}_{1-x}\text{Th}_x\text{FeAsO}$ lattice fragment on the ac -plane and the changes in its dimensions (red dotted lines) with substitution of Sm by Th. (b) Schematic representation of the thermal expansion of FeAs_4 tetrahedron for $\text{Sm}_{0.90(5)}\text{Th}_{0.10(5)}\text{FeAsO}$ at 15 K (solid lines and circles) and 295 K (dotted lines and circles). (c) Pnictogen height (h_{Pn}) as a function of temperature for the three $\text{Sm}_{1-x}\text{Th}_x\text{FeAsO}$ compositions.

increase in the FeAs layer thickness is dominant (Fig. 8b and c), while the changes in the other structural building blocks are minor, and they compensate each other, since the As-Sm/Th distance contracts by about the same amount as the O-Sm/Th expands. The upper critical field estimated from resistance measurements is anisotropic (Fig. 9) with slopes of $\sim 5.4 \text{ T/K}$ ($H \parallel ab$ -plane) and $\sim 2.7 \text{ T/K}$ ($H \parallel c$ -axis), at temperatures sufficiently far below T_c . The low-temperature upper critical field anisotropy γ_H is in the range of ~ 2 , consistent with the tendency of a decreasing γ_H with decreasing temperature in $\text{SmFeAsO}_{1-x}\text{F}_y$ single-crystals [11]. Magnetization hysteresis loops of single-crystal of $\text{Sm}_{1-x}\text{Th}_x\text{FeAsO}$ measured at various temperatures below T_c in magnetic fields up to 7 T applied parallel to the crystal c -axis are presented in Fig. 10. The wide loops, with a width almost independent of the field, indicate a rather high critical current density, J_c , in the sample. The J_c estimated from the width of the hysteresis loop using Bean’s model is, at 2 K, close to 10^6 A cm^{-2} in the field range investigated (Fig. 10, inset). The slight increase in critical current density for higher magnetic fields may indicate an increase in the effectiveness of pinning centers giving rise to a “peak effect”. A similar behavior was found in F doped SmFeAsO single-crystals [10, 11].

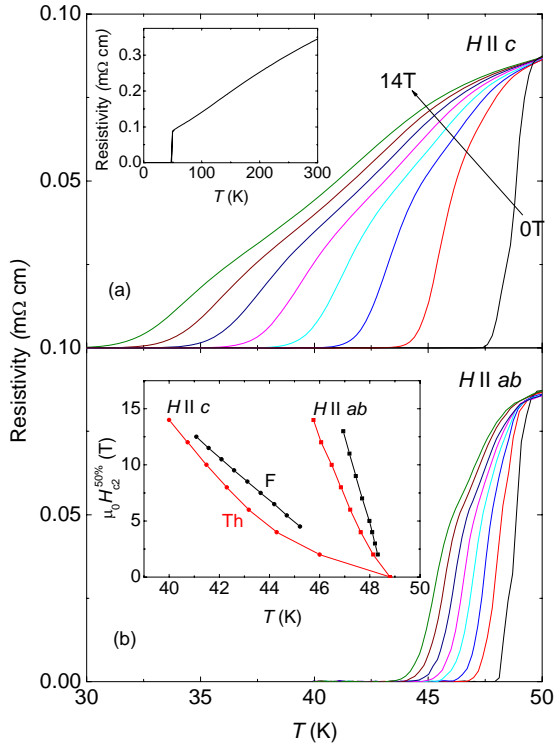


Figure 9: Temperature dependences of the resistivity for a $\text{Sm}_{0.89(2)}\text{Th}_{0.11(2)}\text{FeAsO}$ single-crystal measured with the field $H \parallel ab$ (a) and $H \parallel c$ (b), from 0 to 14 T (0, 2, 4, 6, 8, 10, 12, 14 T). Inset of a) shows the resistivity in the temperature range of 2 – 300 K. Inset of (b) shows temperature dependence of the upper critical field with $H \parallel ab$ and $H \parallel c$ for the $\text{Sm}_{0.89}\text{Th}_{0.11}\text{FeAsO}$ (with 50% ρ_n criterion). For comparison the data for $\text{SmFeAsO}_{0.7}\text{F}_{0.25}$ are shown.

3.2 Structural details and superconductivity with T_c above 50 K in Th-substituted SmFeAsO (B. Batlogg)

Tetravalent Th has been substituted for trivalent Sm at a level of up to 10%, and the influence on the structural and superconducting properties were studied in detail on poly- and single-crystal samples. Remarkably, it is the increase in the Fe_2As_2 -layer thickness that dominates the expansion, while the changes in the other layers are smaller and even compensate each other, since the As-Sm/Th distance appears to contract by about the same amount as the O-Sm/Th distance expands. The superconducting properties are little affected by Th substitution. The upper critical fields and their anisotropy, as well as the penetration lengths and their anisotropy are close to that of the non-substituted related compounds, and are dominated by the multi-gap multi-band superconducting state.

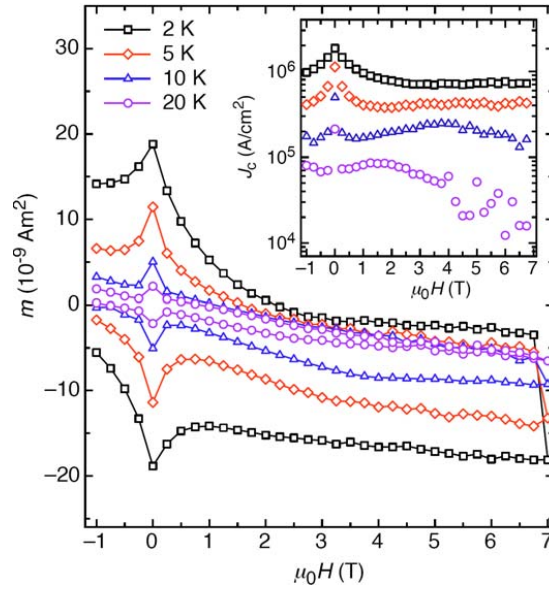


Figure 10: Magnetic hysteresis loops measured on a single-crystal at 2 K, 5 K, 10 K, and 20 K in a field up to 7 T ($H \parallel c$). Inset: critical current density calculated from the width of the hysteresis loops.

3.3 Superconductivity in $\text{SmFe}(\text{As},\text{P})\text{O}$ compound (J. Karpinski)

We have investigated the interplay of composition, structure, magnetism and superconductivity in the $\text{SmFeAs}_{1-x}\text{P}_x\text{O}$ compound through preparation of samples with different synthesis methods and annealing conditions. The samples synthesized at ambient pressure are not superconducting down to 2 K, thus implying that isovalent P substitution leads to pure geometrical lattice effects without charge carrier transfer. The superconductivity with a maximum $T_c \cong 24$ K was observed in poly- and single-crystalline $\text{SmFeAs}_{0.5}\text{P}_{0.5}\text{O}_{1-y}$ samples only after heat treatment under high pressure. Neutron powder diffraction investigations show lower occupation of oxygen site in high-pressure treated samples, which introduced charge carriers in the samples and induced superconductivity. The influence of P substitution and pressure-induced oxygen deficiency on subtle structural intra- and interlayer spacing variation and charge carrier transfer were explored. Muon-spin rotation experiments indicate continuous suppression of both the ordering temperature and the frequency of magnetic order upon P substitution. For superconducting $\text{SmFeAs}_{0.5}\text{P}_{0.5}\text{O}_{1-y}$ samples only dynamic magnetism survived, while the ambient prepared samples with the same amount of P substitution still show a static magnetic moment at temperatures below ~ 60 K. Point-contact Andreev-reflection

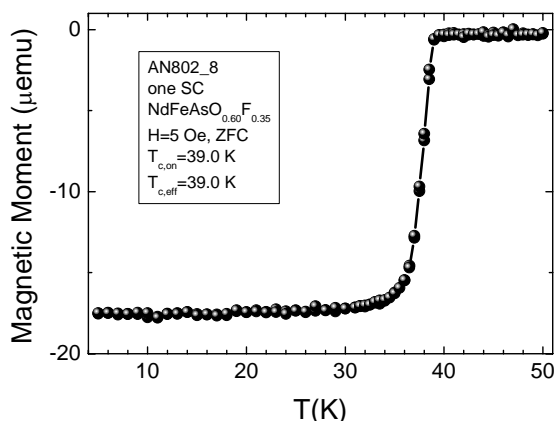


Figure 11: Magnetic moment versus temperature for a NdFeAs(O,F) single-crystal.

spectroscopy indicates the existence of two energy gaps in superconducting samples. Single-crystals were used for electrical transport and magnetic torque studies.

3.4 $\text{SmFe}_{1-x}\text{Co}_x\text{AsO}$ and NdFeAs(O,F) single-crystals from NaAs flux (J. Karpinski)

In order to increase the size and surface quality of LnFeAsO single-crystals, different kind of fluxes were investigated. By using NaAs and KAs fluxes, $\text{Sm(Fe}_{1-x}\text{Co}_x\text{)AsO}$ and NdFeAs(O,F) crystals of a size up to 0.7 mm have been grown. Magnetization measurements of $\text{Sm(Fe}_{1-x}\text{Co}_x\text{)As}$ and NdFeAs(O,F) crystals show relatively sharp superconducting transitions with maximum T_c of 16 and 39 K respectively (Fig. 11). Fig. 12 shows NdFeAs(O,F) crystals.

3.5 Superconductivity in RbFe_2As_2 (B. Batlogg)

The superconducting state of RbFe_2As_2 with a T_c of 2.5 K has been synthesized and studied by transport and muon-spin rotations experiments. The temperature dependence of both the upper critical field and the magnetic penetration depth distinctly deviate from that of a single-band superconductor with a uniform gap. Instead, the upward curvature of H_{c2} and the overall T dependence of the penetration depth are well parametrized by a two-gap model. The gap-to- T_c ratio for the large gap is compared to other superconducting “122” members of the Fe-pnictides and is found to be significantly smaller. Different interband scattering are invoked as possible reasons.

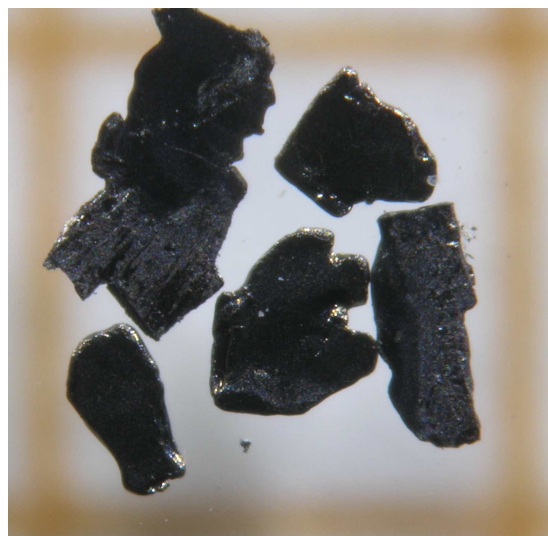


Figure 12: Single-crystals of NdFeAs(O,F) grown from NaAs flux on mm scale.

3.6 Studies of superconducting properties of 122-type Fe-based arsenides (J. Karpinski)

Polycrystalline samples of the $\text{Ba}_{1-x}\text{Rb}_x\text{Fe}_2\text{As}_2$ system were synthesized using quartz ampoule technique for $0 < x < 0.5$ and $x = 1$. X-ray diffraction measurements confirmed the existence of a continuous solid solution. Superconducting properties were studied by magnetization measurements. T_c as a function of Rb content shows a broad plateau with the maximum $T_c = 37$ K (Fig. 13).

Large single-crystals of $\text{EuFe}_{2-x}\text{Co}_x\text{As}_2$ with a size up to few millimeters were grown using the Sn flux method and characterized using X-ray diffraction, WDX analysis, resistivity and magnetization measurements. Co substitution for Fe gradually suppresses the spin-density wave (SDW) ordering and induces superconductivity. We observed diamagnetic re-

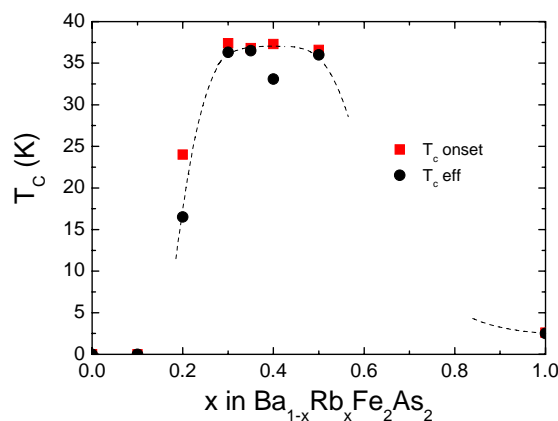


Figure 13: T_c as a function of Rb content in polycrystalline $\text{Ba}_{1-x}\text{Rb}_x\text{Fe}_2\text{As}_2$ solid solution.

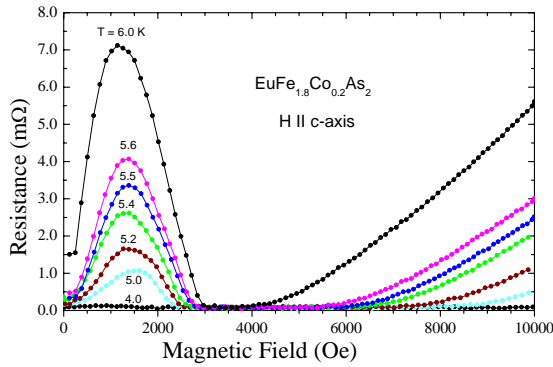


Figure 14: Resistance versus magnetic field for $\text{EuFe}_{1.8}\text{Co}_{0.2}\text{As}_2$ single-crystal measured at various temperatures. $H \parallel c$ -axis, $j \perp c$ -axis.

sponse and zero resistance below 5 K for $x = 0.2$. The resistivity for the $\text{EuFe}_{1.8}\text{Co}_{0.2}\text{As}_2$ single-crystal shows anomalous field dependence (Fig. 14). Below 5 K zero resistance and field induced transition to normal state are observed. In the temperature range 5 – 7 K, with increasing fields, resistance shows a maximum (at ~ 1000 Oe) then drops to zero and finally the transition to normal state is observed. Phenomenologically this behavior is similar to the magnetic field induced superconductivity which Fischer and collaborators [35] observed in $\text{Eu}_x\text{Sn}_{1-x}\text{Mo}_6\text{S}_8-y\text{Se}_y$, in agreement with the exchange compensation effect predicted by Jaccarino and Peter [36].

3.7 Study of the coexistence and competition of antiferromagnetism and superconductivity in $\text{Ba}(\text{Fe}_{1-x}\text{Co}_x)_2\text{As}_2$ (C. Niedermayer)

The discovery of high-temperature superconductivity in iron arsenide pnictides has renewed interest in the relationship between magnetism and superconductivity. Similar to the cuprate high-temperature superconductors, superconductivity emerges in close proximity to an antiferromagnetically ordered state. The suspicion that this proximity is not accidental is supported by the finding that superconductivity and magnetism even coexist in parts of the phase diagram, as shown for Co doped BaFe_2As_2 in Fig. 15 [37]. Our combined neutron scattering, muon-spin rotation, and optical data establish that bulk superconductivity and magnetism coexist on the nanometer scale and that both phenomena compete for the available low-energy states [12]. Systematic neutron and X-ray diffraction studies of the underdoped $\text{Ba}(\text{Fe}_{1-x}\text{Co}_x)_2\text{As}_2$ superconductors have revealed several intriguing results regarding the interactions among structure, magnetism and superconductivity. High-

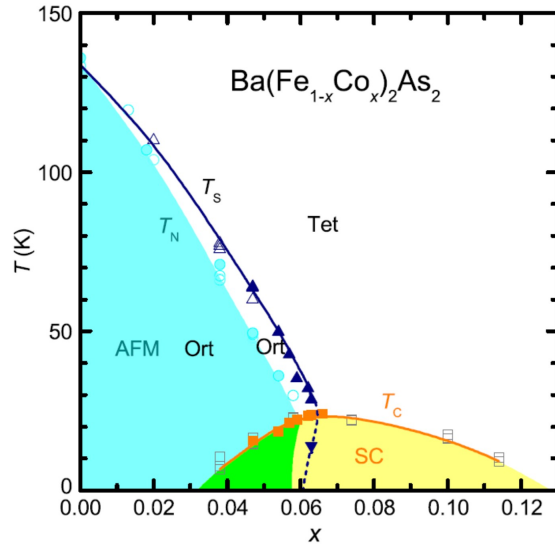


Figure 15: Phase diagram of $\text{Ba}(\text{Fe}_{1-x}\text{Co}_x)_2\text{As}_2$.

resolution X-ray diffraction measurements reveal an unusually strong response of the lattice to superconductivity. The orthorhombic distortion of the lattice is suppressed and, for doping near $x = 0.06$, the orthorhombic structure evolves smoothly back to a tetragonal structure (Fig. 15). It was proposed that the coupling between orthorhombicity and superconductivity is indirect and arises due to the magneto-elastic coupling, in the form of emergent nematic order, and the strong competition between magnetism and superconductivity [37]. The strong coupling between magnetism and superconductivity manifests itself in a dramatic reduction of the magnetic Bragg peak intensity on entering the superconducting state.

Fig. 16 shows data taken on the cold triple axis spectrometer RITA-II at SINQ (PSI) on $\text{Ba}(\text{Fe}_{0.9505}\text{Co}_{0.0495})_2\text{As}_2$. The change in inten-

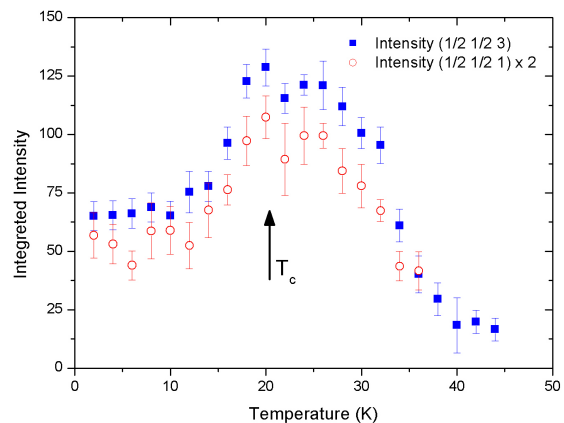


Figure 16: Suppression of the magnetic Bragg peak intensity on entering the superconducting state for $\text{Ba}(\text{Fe}_{0.9505}\text{Co}_{0.0495})_2\text{As}_2$.

sity below $T_c = 20$ K for both the $(1/2\ 1/2\ 1)$ and $(1/2\ 1/2\ 3)$ magnetic Bragg peaks occurs in the same manner so that the effect cannot be explained by a change in magnetic structure or a spin reorientation. Similar data were obtained by other groups, however with a much smaller reduction of the Bragg peak intensity below T_c [38, 39]. A decrease of the magnetic volume fraction can also be ruled out by our muon-spin rotation data on the same sample, which show that the magnetism extends throughout the sample volume both above and below the superconducting transition temperature [12]. The combined muon and neutron data point toward the scenario that the ordered Fe moment is reduced on entering the superconducting state. Along with the observation of a redistribution of the low-energy magnetic excitations, this indicates competition between coexisting superconductivity and magnetic order.

3.8 Charge dynamics of the Co-doped BaFe_2As_2 (L. Degiorgi)

The discovery of superconductivity in several families of closely related iron-pnictides has generated considerable interest, primarily because superconductivity is possible at high-temperature in materials without CuO_2 -planes, and has also induced a frenetic search for possible common mechanisms between them and the superconducting cuprates. Furthermore, these materials provide an interesting arena to study the impact of electronic correlations with respect to the emergence of structural/magnetic and superconducting phase transitions. A recent optical study on LaFePO gave evidence of electronic correlations in the iron-pnictides, indicating that the kinetic energy of the electrons is reduced to half of that predicted by band theory of nearly free electrons, and implying that these systems could be on the verge of a Mott (insulator) transition.

Our strategy consisted in comparing the electrodynamic response of $\text{Ba}(\text{Co}_x\text{Fe}_{1-x})_2\text{As}_2$ for several Co-dopings, which belong to the so-called 122 family and are prominent examples of oxygen-free iron-pnictide superconductors. We presented systematic measurements across the phase diagram, from underdoped non-superconducting ($x = 0$ and 0.025), to underdoped superconducting ($x = 0.051$), to near optimal doping ($x = 0.061$), to overdoped superconducting ($x = 0.11$), and finally to overdoped non-superconducting ($x = 0.18$) compositions. Particular emphasis is devoted to

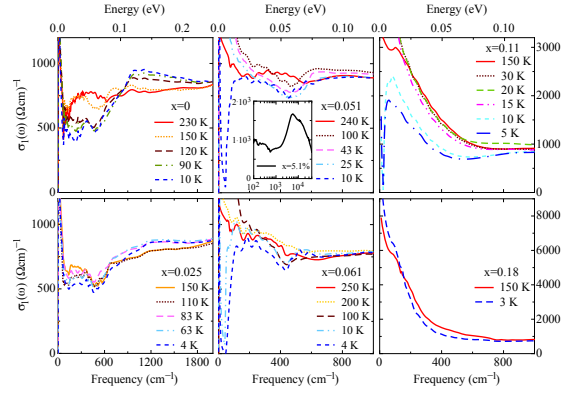


Figure 17: Real part $\sigma_1(\omega)$ of the optical conductivity for $\text{Ba}(\text{Co}_x\text{Fe}_{1-x})_2\text{As}_2$ with x ranging from 0 to 18% in the far and mid-infrared spectral range at selected temperatures above and below the various phase transitions. The inset displays $\sigma_1(\omega)$ at 300 K for $x = 0.051$, emphasizing its representative shape for all compounds at high frequencies up to the ultraviolet.

the impact of the various transitions on the charge dynamics in these Co-doped 122 materials. Our primary goal was to exploit their electrodynamic response in order to establish with spectral weight argument their degree of electronic correlations.

Fig. 17 highlights the temperature dependence of $\sigma_1(\omega)$ for all dopings in the energy ranges pertinent to the SDW and superconducting transition. The excitation spectrum at high frequencies, shown in the inset of Fig. 17, is identical for all Co-dopings and is consistent with previous investigations. There is a strong absorption band peaked at about 5000 cm^{-1} , further characterized by a broad high-frequency tail and generally ascribed to the contribution due to the electronic interband transitions. $\sigma_1(\omega)$ for $x = 0$ suddenly decreases below 800 cm^{-1} at temperatures below T_{SDW} . This leads to a depletion in the range between 200 and 800 cm^{-1} (Fig. 17), inducing a removal of spectral weight. The depletion as well as the peak at about 800 cm^{-1} in $\sigma_1(\omega)$ are indicative for the opening of a pseudogap, which we identify with the SDW single-particle excitation. For $x = 0.025$ Co-doping, the depletion and the (pseudo)gap feature in $\sigma_1(\omega)$ are less evident and pronounced, even though there is a spectral weight redistribution, leading again to its overshoot above 700 cm^{-1} for temperatures below T_{SDW} . The signatures for the SDW pseudogap-like excitation and the related spectral weight redistribution are no longer well distinct for the $x = 0.051$ Co-doping. For this latter compound at and above the optimal Co-doping ($x = 0.061$ and 0.11 , respectively),

the total reflection at $\omega \leq \omega_g$ for $T \ll T_c$ leads instead to the opening of the superconducting gap. The removed spectral weight is shifted into the collective excitation at zero frequency. Finally, the electrodynamic response of the $x = 0.18$ compound merely displays a simple metallic behavior.

We propose a scenario where the conduction band derives from d -states and splits into two parts: a purely itinerant one close to the Fermi level and represented by the two Drude components as well as by a bottom part with states below the mobility edge and thus rather localized (Fig. 18, inset). This latter part gives rise to the mid-infrared-band in $\sigma_1(\omega)$, which turns out to be strongly temperature dependent upon magnetic ordering and affected by the opening of the SDW gap. We calculate the ratio between the integral of $\sigma_1(\omega)$ up to ω_{opt} and the one up to ω_{band} (Fig. 18, inset). This is an estimation, exclusively obtained from the experimental findings, of the ratio between the optical kinetic energy (K_{opt}) extracted from $\sigma_1(\omega)$ and the band kinetic energy (K_{band}) extracted from the band structure within the tight-binding approach. The inverse of K_{opt}/K_{band} , which then defines the degree of electronic correlations, is plotted in Fig. 18 within the phase diagram of the Co-doped 122 iron-pnictides. K_{band}/K_{opt} thus tracks the evolution of the superconducting dome in the phase diagram of $\text{Ba}(\text{Co}_x\text{Fe}_{1-x})_2\text{As}_2$. Interest-

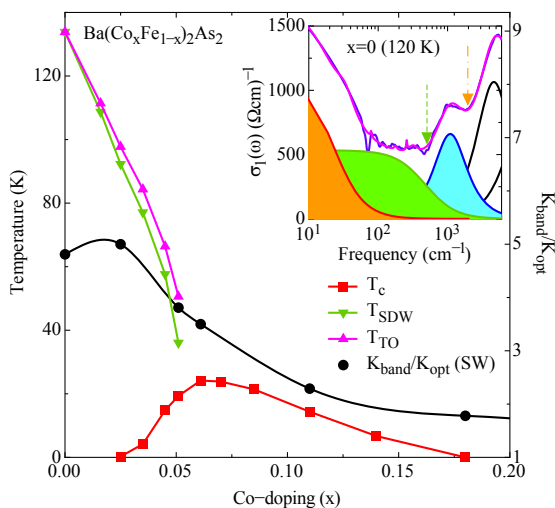


Figure 18: Phase diagram of $\text{Ba}(\text{Co}_x\text{Fe}_{1-x})_2\text{As}_2$ (left y-axis), and the average of the ratio K_{band}/K_{opt} from the spectral weight (SW) analysis with $\omega_{opt} = 500 \text{ cm}^{-1}$ and $\omega_{band} = 2000 \text{ cm}^{-1}$. The inset displays the optical conductivity at 120 K for the parent compound ($x = 0$). Dashed and dashed-dotted arrows mark the cut-off frequencies ω_{opt} and ω_{band} (see text).

ingly enough, electronic correlations seem to be stronger for the parent-compound and for Co-dopings $x \leq 0.061$ than for those in the overdoped range. There is indeed evidence for a crossover from a regime of moderate correlations for $x \leq 0.061$ to a nearly free and non-interacting electron gas system for $x \geq 0.11$.

3.9 Strong coupling to magnetic fluctuations in the charge dynamics of Fe-based superconductors (D. van der Marel)

We have carried out a comprehensive comparison of the infrared response of two systems, characteristic of classes of the 122 pnictide (SrFe_2As_2) and 11 chalcogenide ($\text{Fe}_{1.087}\text{Te}$) Fe-compounds with magnetically-ordered ground states. In the 122 system, the magnetic phase shows a decreased plasma frequency and scattering, and associated appearance of strong mid-infrared features. The 11 system, with a different magnetic ordering pattern, also shows decreased scattering, but an increase in the plasma frequency, while no clear mid-infrared features appear below the ordering temperature (Fig. 19). This marked contrast can be understood in terms of the diverse magnetic ordering patterns of the ground state. While the high-temperature phases of these systems are similar, magnetic order strongly affects the charge dynamical response. Near the magnetic phase boundary, spin-fluctuations provide a dissipation channel which involves an electron traversing a Fermi pocket in a Landau damping process. Below

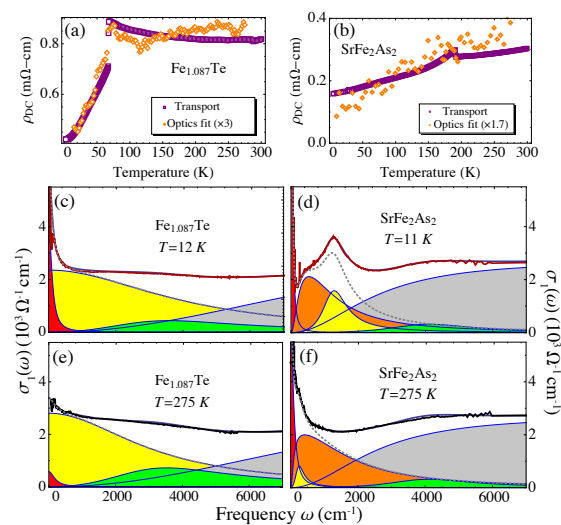


Figure 19: dc resistivity measured by transport (squares) and optically (diamonds) for (a) $\text{Fe}_{1.087}\text{Te}$ and (b) SrFe_2As_2 . Components of fits to the optical conductivity at high and low temperatures for $\text{Fe}_{1.087}\text{Te}$ (c, e) and SrFe_2As_2 (d, f).

the magneto-structural transition temperature T_{ms} , hybridization and splitting of bands open an SDW gap excitation pathway, giving rise to the 550 cm^{-1} excitation. The second excitation is due to a process where a down-spin electron in an occupied state at momentum $-k_F$ undergoes a similar gap-crossing excitation to a state at $+k_F$, while flipping its spin. This is normally disallowed due to the photon momentum and spin selection rules, but can become allowed through the simultaneous emission of a $S = 1$ magnon of momentum $-2k_F$, so that the overall momentum and spin of the process is conserved. Thus, while the average SDW gap excitation appears near 550 cm^{-1} , and is roughly consistent with the BCS expectation $2\Delta \sim 3.5k_B T_{ms} \sim 462 \text{ cm}^{-1}$, magnon-assisted pair breaking absorption occurs higher near $k_c v_s \sim 360 - 900 \text{ cm}^{-1}$, which wholly encompasses the observed splitting between the high- and low-energy features in SrFe_2As_2 . In this scenario, the low-temperature characteristics of the high-energy peak in SrFe_2As_2 are expected to evolve with temperature as a direct consequence of broadened spin-excitations as the temperature is raised, as observed. For $T > T_{ms}$, one expects an overdamped paramagnon response, thus explaining the difficulty in tracking this feature into the high-temperature phase.

The influence of spin-fluctuations on charge dynamics of two systems is closely related to Fe-based superconductors. The spin-charge coupling is most evident at the magneto-structural transitions in these compounds, where transport and charge excitations are sensitive to drastic changes in the spin-susceptibility. These observations are robust and likely extend to the superconducting portions of the global phase diagram for Fe-based superconductors.

3.10 Isotope effect in Fe-based superconductors (H. Keller)

This $^{54}\text{Fe}/^{56}\text{Fe}$ isotope effect (FeIE) was investigated on T_c in the iron-based superconductor FeSe_{1-x} belonging to the 11 family [13]. The substitution of natural Fe (containing $\simeq 92\%$ of ^{56}Fe) by its lighter isotope ^{54}Fe in $\text{FeSe}_{0.975}$ ($T_c \simeq 8.2 \text{ K}$) leads an isotope shift of the transition temperature of $\Delta T_c = 0.22(5) \text{ K}$, corresponding to an FeIE exponent $\alpha_{Fe} = 0.81(15)$ (Fig. 20) [13]. This value is positive and considerably larger than the BCS value $\alpha_{BCS} = 0.5$.

In addition, the lattice parameters of the $^{54}\text{Fe}/^{56}\text{Fe}$ exchanged FeSe_{1-x} samples were investigated carefully by neutron powder

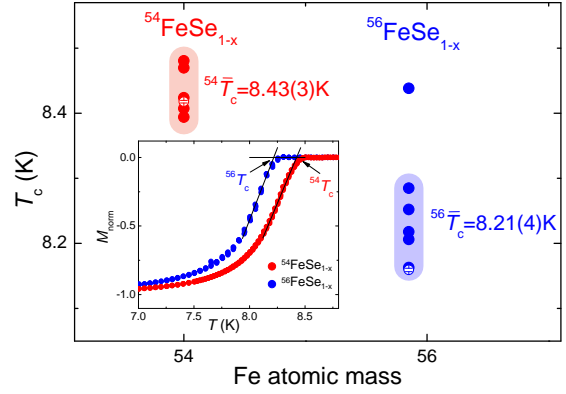


Figure 20: The superconducting transition temperature as a function of Fe atomic mass for FeSe_{1-x} . The open symbols correspond to the samples studied by neutron powder diffraction. The inset shows the normalized magnetization curves for a pair of $^{54}\text{FeSe}_{1-x}$ and $^{56}\text{FeSe}_{1-x}$ samples.

diffraction. It turned out that the a - and b -axes are slightly larger for $^{54}\text{FeSe}_{1-x}$ than those for $^{56}\text{FeSe}_{1-x}$, while the c -axis is marginally smaller for $^{54}\text{FeSe}_{1-x}$ than for $^{56}\text{FeSe}_{1-x}$. However, the volume of the unit cell remains unchanged. These slight differences in the lattice constants in the Fe isotope exchanged samples give rise to a slight change of the shape of the Fe_4Se pyramid and anion height which is known to affect T_c in Fe-based high-temperature superconductors (HTS) [40], and in turn may contribute to the total Fe isotope shift of T_c [13].

The present results of the FeIE on T_c in Fe-based HTS are highly controversial. The values of the FeIE exponent α_{Fe} for various families of Fe-based HTS were found to be as well positive ($\alpha_{Fe} \simeq 0.3 - 0.4$) [41], as negative ($\alpha_{Fe} \simeq -(0.18 - 0.02)$) [42, 43], or even be exceedingly larger than the BCS value $\alpha_{BCS} = 0.5$ as found for FeSe_{1-x} ($\alpha_{Fe} \simeq 0.8$) [13]. Recently, we have shown [14] that the Fe isotope substitution causes small structural modifications which, in turn, affect T_c . Upon correcting the isotope effect exponent for these structural effects, an almost unique value of $\alpha_{Fe} \simeq 0.35 - 0.4$ is found for at least three different families of Fe-based HTS (Fig. 21), in fair agreement with theoretical predictions of a two-band model [15].

4 High- T_c cuprates

4.1 Single-crystal growth of cuprates and related materials (E. Giannini)

The enduring activity on crystal growth of Bi-based superconducting cuprates has focussed on strongly overdoped materials. Crystals of $\text{Bi}_2\text{Sr}_2\text{CuO}_6$ and $\text{Bi}_2\text{Sr}_2\text{CaCu}_2\text{O}_8$ have been

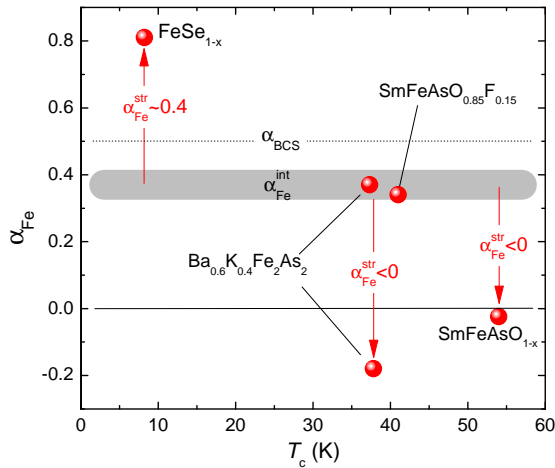


Figure 21: Fe isotope exponent α_{Fe} as a function of the superconducting transition temperature ($FeSe_{1-x}$ [13], $Ba_{0.6}K_{0.4}Fe_2As_2$ and $SmFeAsO_{0.85}F_{0.15}$ [41], $Ba_{0.6}K_{0.4}Fe_2As_2$ [42], and $SmFeAsO_{1-x}$ [43]). The arrows indicate the direction of the shift from the intrinsic FeIE exponent $\alpha_{Fe}^{int} \simeq 0.35 - 0.4$ caused by the structural effects.

grown by the floating zone method and mainly devoted to STM studies. Crystal growth experiments have been conducted on other layered cuprates, of the so-called family of spin-ladder compounds, as well. These materials are described by the general formula $[M_2Cu_2O_3]_m[CuO_2]_n$, where M is generally Sr and/or Ca with $m/n = 5/7, 7/10$ or $9/13$, in which two different kinds of Cu-O layers exists: the CuO_2 chains, and the Cu_2O_3 ladders. Pressure induced superconductivity was discovered in Ca-doped $Sr_{14}Cu_{24}O_{41}$ (at $P = 3 - 5$ GPa, $T_{c,max} = 12$ K) [44]. With the aim to apply chemical pressure and control the carriers doping in this system, we have synthesized and successfully grown crystals of (Bi, Ca)- and (Y, Ca)-co-doped $Sr_{14}Cu_{24}O_{38+\delta}$. These crystals have been grown with the floating zone method in a two-lamp furnace, under oxygen overpressure ($p(O_2) = 3$ bar).

4.2 Analysis of the Van Hove singularity position in the tunneling spectra of $Bi_2Sr_2CuO_{6+\delta}$ (\emptyset . Fischer)

The tunneling spectra measured at low temperature in $Bi_2Sr_2CuO_{6+\delta}$ show unambiguously and for the first time in a cuprate the direct signature of a strong Van Hove singularity (VHS) [16]. It is admitted that the local doping level controls both the opening of the gap and the position of the VHS. The correlation at the local scale between these two parameters is thus of great interest. Starting from a 14×14 nm² map displaying the local gap mag-

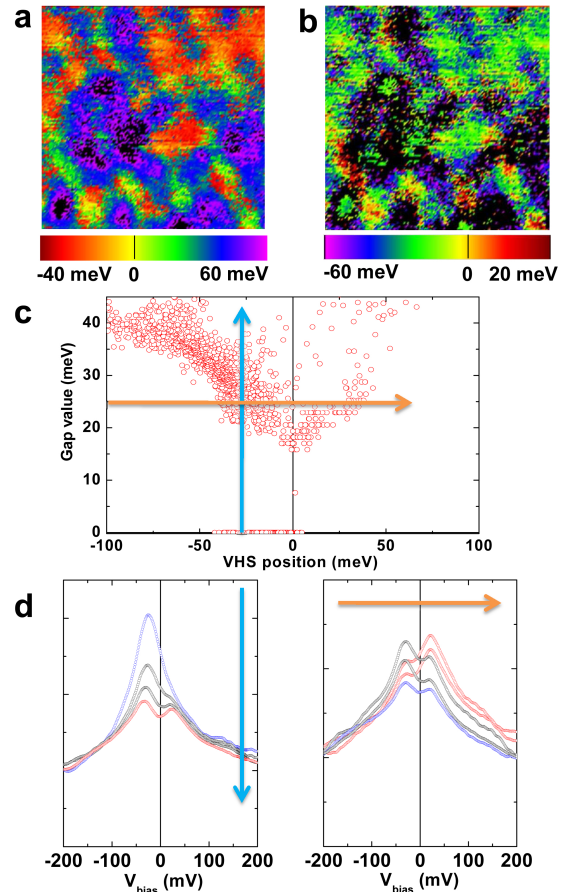


Figure 22: Analysis of STM data acquired in $Bi_2Sr_2CuO_{6+\delta}$ ($T_c = 11$ K). (a) 14×14 nm² map of the gap/VHS (see text). (b) Fitted VHS position map showing a spatial correlation with the map in (a). (c) Fitted VHS position versus gap value. Zero gap values correspond to spectra exhibiting only a single peak. The left side of the panel shows the expected trend that the gap is becoming larger when the VHS shifts towards negative values. For positive VHS positions, the gap becomes larger. (d) left panel (blue arrow on (c)): for a given VHS position (here -30 ± 0.1 meV) one can find spectra with various gap values (ranging from 0 to 37 meV); right panel (orange arrow on (c)): for a given gap value (here 25 ± 0.1 meV) one can find spectra with various VHS positions (ranging from -25 to 15 meV).

nitude (positive values) and the VHS position found in single-peaked spectra (negative values) (Fig. 22a), we have fitted the whole spectra to determine in each pixel the position of the VHS (Fig. 22b). A clear correlation between the two parameters is seen, and reported in Fig. 22c.

In most of the probed area where the VHS is measured at negative energies, we observe that the VHS shifts towards more negative energies when the gap magnitude increases. These trends agree with the picture of a decrease of the local doping level. But in some other re-

gions we contradictorily observe spectra exhibiting large gaps (usually associated with underdoping) and a positive VHS position (overdoping). Moreover the gap versus VHS distribution exhibits a finite width traducing the possibility for some spectra with a unique VHS position to exhibit various gap values, and inversely (Fig. 22d). This shows that local doping variation is not sufficient to explain the evolution of whole the tunneling spectra observed on the surface of Bi-based cuprates.

4.3 Strong-coupling signatures in the tunneling spectra of superconductors (T. Giamarchi)

In superconductors, the interaction of quasiparticles with collective modes leads to signatures in the electron density of states (DOS) [45], which can be detected by tunneling spectroscopy [17]. The precise analysis of these signatures in cuprate superconductors should allow to deduce the energy of the collective modes, and thus determine which excitations are most relevant for superconductivity. It turns out that the line-shape of the signatures in classical superconductors — which are three-dimensional (3D) and have a superconducting gap of s -wave symmetry — is different from the line-shape in two-dimensional (2D) unconventional superconductors with d -wave symmetry [18]. On the one hand, the low dimensionality reinforces the signatures, so that for identical coupling strengths the modification of the DOS is considerably stronger in 2D than in 3D. On the other hand, the spectral line-shape of the signature is determined chiefly by the line-shape of the superconducting coherence peak. Due to the asymmetric shape of the coherence peaks in s -wave superconductors, the strong-coupling signatures are breaks in the DOS, appearing as *peaks* in the second-derivative d^2I/dV^2 spectrum. For d -wave superconductors, however, the coherence peaks are symmetric, and the strong-coupling signatures are minima in the DOS, appearing as *zeros* in the d^2I/dV^2 spectrum, as shown in Fig. 23. Assessing the collective mode energies in high- T_c cuprate superconductors by selecting peaks in the d^2I/dV^2 spectrum, as was done in recent studies [46], is therefore not a reliable procedure. Our results also explain why the signatures of strong electron-phonon coupling are absent in the normal state of conventional superconductors, while the effect of coupling to sharp modes might be observable in 2D materials due to the presence of a Van Hove singularity in the non-interacting DOS.

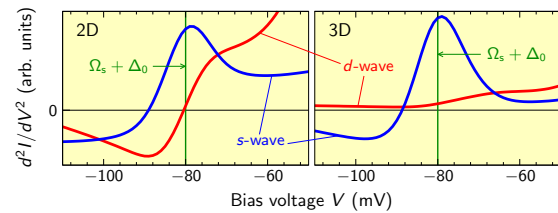


Figure 23: Second derivative d^2I/dV^2 tunneling spectra calculated for two- and three-dimensional superconductors of s - and d -wave symmetries interacting with a collective excitation of energy Ω_s . For s -wave symmetry (blue), the signature of this coupling is a peak in d^2I/dV^2 at the energy $\Omega_s + \Delta_0$, both in 2D and 3D, while for d -wave symmetry (red) the signature is a zero in 2D, and is absent in 3D.

4.4 Cooperon resonance (T. M. Rice and M. Sigrist)

Rice and collaborators derived a low-energy effective model for an array of lightly doped 4-leg Hubbard ladders weakly coupled by interladder tunneling and lightly doped away from half filling [19]. The model has Fermi pockets and a well defined Cooperon resonance formed by a bound pair of holes. Similar features are argued to be the key characteristics of the pseudogap phase of the underdoped cuprates. Superconductivity is generated in the model and in cuprates by an attraction generated on the Fermi surface by virtual scattering into the Cooperon resonance. In underdoped cuprates as the pseudogap opens near the antinodes, the single-particle density of states is reduced, allowing a collective mode in form of a Cooperon resonance to appear.

4.5 Andreev and single-particle tunneling spectroscopies in underdoped cuprates (T. M. Rice and M. Sigrist)

The tunneling spectroscopy between a normal metal and an underdoped cuprate superconductor was calculated by Yang and collaborators [20]. The pseudogap state of the superconductor is modeled by the Yang-Rice-Zhang (YRZ) phenomenological theory. In the low-barrier limit the conductance is strongly enhanced by Andreev scattering only within a voltage region limited by the small superconducting gap on the Fermi pockets. In the high-barrier limit, single-particle tunneling dominates and the large energy pseudogap characterizes the spectra. The theory explains the contrast between the single-gap spectra at overdoping and the two-gap spectra at underdoping.

4.6 Variational results in the repulsive Hubbard model (*D. Baeriswyl*)

The Hubbard Hamiltonian is the paradigmatic model for strongly correlated bosons or fermions. For the case of electrons it assumes the simple form

$$\hat{H} = -t\hat{T} + U\hat{D}, \quad (2.1)$$

where \hat{T} describes single-particle hopping on a lattice and \hat{D} measures the number of doubly occupied sites. Superconductivity is readily obtained for $U < 0$ while for $U > 0$ the question of pairing remains open, although many different methods, from small to large U , indicate that for the square lattice a superconducting ground state with d -wave symmetry is dominant close to half filling [21].

In the recent past, our group has made a rather detailed variational study of the repulsive Hubbard model on a square lattice [22, 23] for U of the order of the band width ($U = 8t$). We have calculated the energy expectation value for the trial state

$$|\Psi\rangle = e^{-h\hat{T}} e^{-g\hat{D}} |\Psi_0\rangle, \quad (2.2)$$

where $|\Psi_0\rangle$ was assumed to be the ground state of a d -wave BCS superconductor. Despite the appealing results of our variational study, which agree nicely both with other theoretical approaches and with the generic experimental phase diagram of the cuprates [24], several questions remain open, such as the limited size of the lattice (typically 8×8) or the bias introduced by starting with a superconducting ground state. Therefore, in the framework of the PhD thesis of Mikheil Menteshashvili, we have started to study the small U limit of the ansatz (2.2), using an expansion in powers of U , similar to earlier calculations for the Gutzwiller ansatz ($h = 0$) [47]. We also address the subtle question of long-range order in the absence of broken symmetry, i.e. using a filled Fermi sea for $|\Psi_0\rangle$ instead of a BCS ansatz. Our preliminary results confirm that the ansatz (2.2) yields an excellent value of the ground state energy for small U (98.7% of the exact correlation energy in one dimension). Moreover, at half filling, the antiferromagnetic correlations are strongly enhanced by correlation effects. However, there are so far no signs of emerging long-range order, which may in fact not be produced by the trial state (2.2) in the absence of (explicit) symmetry breaking.

4.7 Crossover in the attractive Hubbard model (*D. Baeriswyl*)

The BCS-BEC crossover has been successfully explored with ultracold atomic gases obeying Fermi statistics [48]. In the framework of the PhD thesis of Bruno Gut (2009), the ground state fidelity has been advocated for describing the BCS-BEC crossover for the attractive Hubbard model. If only the scattering between (zero-momentum) Cooper pairs is kept in the interaction (reduced BCS Hamiltonian), the so-called fidelity susceptibility can be calculated exactly. The results obtained at half filling for finite-size lattices (up to 20×20) exhibit a pronounced maximum as a function of $|U|/t$ (which we attribute to the BCS-BEC crossover), but strong finite-size effects render the analysis difficult away from half filling. Therefore we have now also studied the mean-field approximation, which yields the exact ground state energy for the reduced BCS model in the thermodynamic limit, but — interestingly — probably not the exact fidelity susceptibility. We find that the maximum, which occurs at a rather low value at half filling ($U \approx 1.2t$), moves to higher values away from half filling. This gives a striking prediction for a crossover as a function of doping for a fixed value of U . Starting at half filling with a value of U in the BEC regime, upon doping at a fixed value of U we may move the system through the crossover line into the BCS regime. The model has a priori nothing to do with cuprates, but it nevertheless can teach us something about the crossover from underdoped to overdoped high-temperature superconductors.

4.8 Pressure effect on superconducting properties of $\text{YBa}_2\text{Cu}_3\text{O}_x$ (*H. Keller*)

Pressure allows one to modify the interatomic distances in a lattice, thus modifying both the phonon spectra and the exchange interaction between Cu spins in cuprates. Therefore, precise knowledge of pressure effects on the superconducting gap Δ_0 , the transition temperature T_c , and the superfluid density $\rho_s \propto 1/\lambda^2$, and their relation to oxygen isotope ($^{16}\text{O}/^{18}\text{O}$) effect (OIE) investigations allows one to disentangle the effects of the lattice from the effects of the exchange interaction between the Cu spins.

We performed muon-spin rotation (μSR) studies of the pressure effect on the magnetic penetration depth λ in $\text{YBa}_2\text{Cu}_3\text{O}_x$ at various oxygen concentrations ($x = 6.45, 6.6, 6.8, \text{ and } 6.98$). It is known that there are two contributions determining the pressure effect on T_c : (i) the

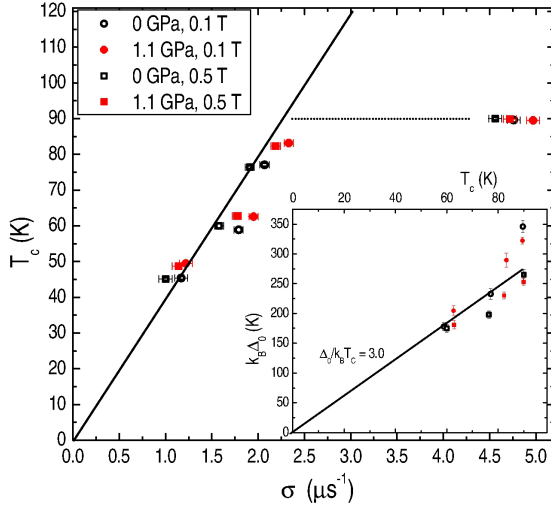


Figure 24: Uemura plot for σ and T_c measured at zero and applied pressure $P = 1.1$ GPa for $\text{YBa}_2\text{Cu}_3\text{O}_x$ at various dopings x . The solid line is the Uemura line while the dotted line is the guide to the eye. The inset shows the relation between Δ_0 and T_c . The solid line corresponds to $\Delta_0/k_B T_c = 3$.

charge transfer from the chain oxygen sites to the CuO_2 -planes and (ii) the pressure effect on the pairing interaction strength [49]. While the first contribution at ambient pressure is well known and follows the Uemura relation [50], the second one, usually determined by the temperature dependence of thermodynamic properties under pressure, is not well studied so far. The μSR technique is a powerful tool to investigate the temperature dependence of the superfluid density $\rho_s \propto \sigma \propto 1/\lambda^2$ at various pressures and fields. From the temperature dependence of the muon depolarization rate σ , the value of $\sigma(T = 0)$ and the gap-to- T_c (Δ_0/T_c) ratio were extracted (Fig. 24).

Both quantities, $\sigma(T = 0)$ and Δ_0/T_c , increase with increasing pressure P , implying that the coupling strength also increases with pressure. The Uemura relation [50] does not hold under pressure, in contrast to previous pressure studies of the organic HTS κ -(BEDT-TTF) $_2\text{Cu}(\text{NCS})_2$ [51]. The slope $\gamma = \partial T_c / \partial \sigma \simeq 20 \text{ K}/\mu\text{s}^{-1}$ is a factor of two smaller than that of the Uemura line $\gamma_U = 40 \text{ K}/\mu\text{s}^{-1}$. Interestingly, the same slope was previously observed for the OIE on the magnetic penetration depth [25]. The parameter γ was found to be independent of the oxygen content for underdoped $\text{YBa}_2\text{Cu}_3\text{O}_x$ with an average value of $\gamma = 20(3) \text{ K}/\mu\text{s}^{-1}$. Taking into account the two above mentioned mechanisms which increase T_c under pressure, the two mechanisms also give rise to an increase of $\sigma = \sigma_U + \sigma_V$. While the first term accounts for the increase

of the carrier concentration in the CuO_2 -plane according to the Uemura relation, the second term is related to the modified pairing interaction V due to pressure.

Assuming $\gamma = 20 \text{ K}/\mu\text{s}^{-1}$ for underdoped $\text{YBa}_2\text{Cu}_3\text{O}_x$ and using the previously reported value $\partial T_c / \partial P = 4 \text{ K}/\text{GPa}$ for underdoped $\text{YBa}_2\text{Cu}_3\text{O}_x$ [52], one can express the pressure effect on σ_V as follows: $\beta_P = \partial \ln \sigma_V / \partial P \equiv (\Delta \sigma_V / \sigma) / \Delta P \simeq 4 / T_c \text{ GPa}^{-1}$. In this form the doping (or T_c) dependence of the pressure effect on σ_V resembles that of the OIE on σ : $\beta_M = \partial \ln \sigma / \partial \ln M$, where $\partial \ln M$ is the relative change of oxygen mass and $\partial P \propto \partial \ln M$. This implies that β_P is finite at optimal doping and increases with decreasing doping (or decreasing T_c). Additional studies are needed to better clarify the relation between β_P and β_M .

This work is part of an extensive program by the Keller group during the past two decades on isotope effects in cuprate HTS [26, 27, 25, 28, 29], in which several novel oxygen isotope ($^{16}\text{O}/^{18}\text{O}$) effects (OIE) on different quantities have been discovered, such as the transition temperature T_c (including site-selective OIE), the in-plane magnetic penetration depth $\lambda_{ab}(0)$ (including site-selective OIE), the anisotropy parameter γ , the pseudogap temperature T^* , the charge-ordering temperature T_{co} , the superconducting energy gap Δ_0 , the Néel temperature T_N , and the spin-glass freezing temperature T_g . Together with the pressure effects reported here, these results indicate strong interplay between lattice effects and the superconductivity in the high- T_c cuprates.

4.9 Spin-phonon coupling in high- T_c cuprates (T. Giamarchi)

The work on spin-phonon coupling in the cuprates has continued [30]. A model for pseudogap formation from coupling to phonons and/or spin-waves in systems with large coupling turns out to have very similar characteristics as for a superconducting gap. It suggests that the pseudogap is a precursor to, and competes with, superconducting pairing. Another gap can appear near E_F because of thermal excitations of phonons or spin-waves in many systems, but it is weaker in terms of total energy and it has no strong T -dependence.

The band structures of pure and hole doped La_2CuO_4 with antiferromagnetic spin-fluctuations were calculated and compared to spectral weights of angle-resolved photoemission spectroscopy (ARPES). It is shown that observations of coexisting Fermi surface (FS) arcs and closed FS pockets are

consistent with modulated spin-fluctuations of varying wave lengths. A connection between results of ARPES, q -dependent spin-excitations seen by neutron scattering, and band results for the modulated spin-wave state suggests that spin-phonon coupling is an important mechanism in the cuprates.

4.10 LMTO band structure calculations of electron- and hole-doped cuprates (*T. Gi-amarchi*)

The studies of electron-doped cuprate systems continue in collaboration with the group at Northeastern University. The effective electron doping to the CuO band from Nd-to-Ce substitution is rather small. Calculations on different rare earth based cuprates show different antiferromagnetic order. It is often believed that the partially occupied f -band in rare earth compounds is a few eV below E_F , even in the ground state, because of strong correlation. First-principle density functional LMTO calculations on Nd_2CuO_4 show that the f -band is partially occupied, but it is tied at the Fermi energy as for itinerant bands. By doing excited state calculations, with an electron removed from different subbands and put into an itinerant state at high energy, it is possible to simulate the photoemission process. The relaxation energy for excitations from the f -state is negative and larger than from itinerant states. The effect is opposite in the inverse process. This shows that the appearance of Hubbard f -bands below and above E_F is a result of relaxation during the excitation process rather than an effect of unusual correlation. This type of calculations is extended to core level excitations, where the relative relaxation energies can be reversed. Another indication is that the spectroscopic image of the CuO band will have another dispersion than the ground state band, which could lead to a new interpretation of effective electron doping.

Results from our calculations on LaCuO and SrCuO with oxygen vacancies within CuO-planes or within apical positions are very different. The latter acts as electron dopants, so that apical O-vacancies in the SrCuO system will approach the situation of strongly hole doped LaCuO.

5 Novel transition metal oxides

5.1 Spin-resonances in EuTiO_3 probed by time-domain GHz ellipsometry (*D. van der Marel*)

Bulk EuTiO_3 has the same perovskite crystal structure as SrTiO_3 , and is magnetic due to the

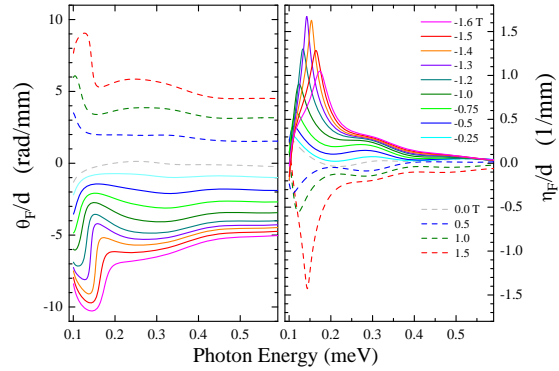


Figure 25: Faraday angle (left) and ellipticity (right) of light transmitted through a thin slab of EuTiO_3 , propagating parallel to an external magnetic field, measured at 4.5 K.

seven parallel spins on the Eu site and has thus $S = 7/2$ and $L = 0$ and Landé factor $g = 2$. The local magnetic moments in EuTiO_3 , because the $4f^7$ states of the Eu^{2+} ions, have only spin- and no orbital-component. The material is on the borderline between antiferromagnetic and ferromagnetic ordering [53, 54] and becomes fully spin-polarized by application of a moderate magnetic field [55], or tensile strain [56]. The interaction of photons with the electron-spin through the magnetic field component is expressed by the dynamic magnetic susceptibility $\mu_{\pm}(\omega)$.

We determined the transmission amplitude and phase for left circular polarized (LCP) (–) and right circular polarized (RCP) (+) light between 0.1 meV and 3.5 meV at magnetic fields H between 0 T and –1.6 T at 4.5 K. The transmission shows a pronounced absorption and a step-like phase increase for RCP light which strongly depend on the applied magnetic field whereas the transmission and phase for LCP light do not show any magnetic field dependence. The observed circular dichroic phenomenon is present on an energy scale which corresponds to an electronic dipole transition inside the Zeeman split $4f$ -multiplet. For a $g = 2$ system the Zeeman energy is about 0.12 meV per Tesla which is a priori as observed. The ellipsometric parameters η_F and θ_F

$$\eta_F(\omega) = \frac{\ln|T_-/T_+|}{2}, \quad \theta_F(\omega) = \frac{\arg(T_+/T_-)}{2}, \quad (2.3)$$

are displayed in Fig. 25. The lower limit of 0.1 meV constitutes the diffraction limit below which no radiation passes through the 8 mm wide aperture. The selective absorption of one particular chirality gives rise to a large Faraday rotation in a broad band of GHz radiation

(Fig. 25, right) of more than $250 \text{ deg mm}^{-1}\text{T}^{-1}$ which peaks up to an unprecedented level of $590 \text{ deg mm}^{-1}\text{T}^{-1}$ at 0.14 meV (34 GHz) at a relatively modest field of 1.6 Tesla . These are very large rotations compared to previously known record bulk materials.

5.2 Mute moment order in Sr_2VO_4 (D. van der Marel)

Sr_2VO_4 has the same crystal structure as the parent compound of the high- T_c superconductors La_2CuO_4 [57, 58]. Both materials are Mott-Hubbard insulators one electron on the V-site in the case of Sr_2VO_4 , and one hole per copper-site for La_2CuO_4 . Based on these similarities, several laboratories have searched for superconductivity in doped Sr_2VO_4 [59, 60, 61]. While superconductivity has been elusive, Sr_2VO_4 passes as a function of temperature through a number of different electronic phases which are not yet fully understood and which have not been observed in the cuprate family. Below 10 K the material is ferromagnetic. Between 10 K and 97 K the system enters a different magnetic and orbital-state, which is not ferromagnetic and the nature of which has not yet been fully understood. Above 127 K the material is paramagnetic. Phase-coexistence is found between 97 and 127 K . The most important difference in electronic structure of La_2CuO_4 and Sr_2VO_4 results from the different ground state degeneracy of open $3d$ -shell in both materials: the hole on the Cu-atom in La_2CuO_4 occupies a $3d_{x^2-y^2}$ -orbital. The single electron on the V ion in Sr_2VO_4 occupies the degenerate set of $3d_{xz}$ and $3d_{yz}$ orbitals. This orbital degree of freedom profoundly affects the physical properties.

We measured and analyzed the optical conductivity of Sr_2VO_4 . In addition to the infrared-active phonons we observed additional excitations at 290 cm^{-1} and 840 cm^{-1} which we identify as electronic transitions of the V^{4+} ions, shown in Fig. 26.

The observed excitation energies allow to estimate the relevant spin-orbit coupling and crystal-field parameters. The V^{4+} ions are in a $j_z = \pm 1/2$ due to the opposition of spin ($s_z = \pm 1/2$) and orbital ($l_z = \pm 1$) angular momentum. Due to the factor of two different gyromagnetic factors for spin and orbital angular momentum, the magnetic moments are muted. At low temperature these “mute moments” are antiferromagnetically ordered.

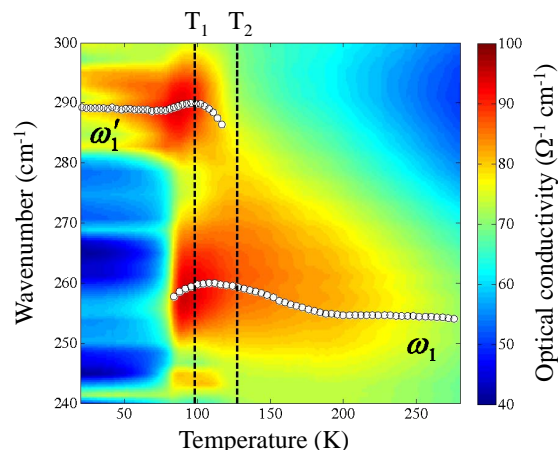


Figure 26: Colormap of the experimental optical conductivity in energy range corresponding to the low-energy set of transitions. The open symbols represent the temperature dependence of the central frequency of the Lorentz oscillator used to fit the reflectivity data. T_1 and T_2 correspond to the maxima of the two pronounced peaks in the specific heat.

6 Collaborative efforts

Most of the projects described here involve collaborations between one or several MaNEP teams. Samples were prepared in the groups of Karpinski and Giannini, and measured in the groups of Fischer, Batlogg, Degiorgi, Keller, van der Marel, and Niedermayer. Experiments at large facilities, such as PSI, were carried out by collaborations of scientists from different groups (Groni together with van der Marel, for example). Theoretical work addressing specific (STM, ARPES) experimental issues was discussed with those experimental groups.

MaNEP-related publications

- [1] E. Pomjakushina, K. Conder, V. Pomjakushin, M. Bendele, and R. Khasanov, *Physical Review B* **80**, 024517 (2009).
- ▶ [2] M. Bendele, A. Amato, K. Conder, M. Elender, H. Keller, H.-H. Klauss, H. Luetkens, E. Pomjakushina, A. Raselli, and R. Khasanov, *Physical Review Letters* **104**, 087003 (2010).
- [3] R. Khasanov, M. Bendele, A. Amato, P. Babkevich, A. T. Boothroyd, A. Cervellino, K. Conder, S. N. Gvasaliya, H. Keller, H.-H. Klauss, H. Luetkens, V. Pomjakushin, E. Pomjakushina, and B. Roessli, *Physical Review B* **80**, 140511(R) (2009).
- ▶ [4] M. Bendele, S. Weyeneth, R. Puzniak, A. Maisuradze, E. Pomjakushina, K. Conder, V. Pomjakushin, H. Luetkens, S. Katrych, A. Wisniewski, R. Khasanov, and H. Keller, *Physical Review B* **81**, 224520 (2010).
- ▶ [5] M. Bendele, P. Babkevich, S. Katrych, S. N. Gvasaliya, E. Pomjakushina, K. Conder, B. Roessli, A. T. Boothroyd, R. Khasanov, and H. Keller, *Physical Review B* **82**, 212504 (2010).
- [6] P. Babkevich, M. Bendele, A. T. Boothroyd, K. Conder, S. N. Gvasaliya, R. Khasanov, E. Pomjakushina, and

- B. Roessli, *Journal of Physics: Condensed Matter* **22**, 142202 (2010).
- ▶ [7] A. Krzton-Maziopa, Z. Shermadini, E. Pomjakushina, V. Pomjakushin, M. Bendele, A. Amato, R. Khasanov, H. Luetkens, and K. Conder, *Journal of Physics: Condensed Matter* **23**, 052203 (2011).
 - ▶ [8] J. N. Hancock, S. I. Mirzaei, J. Gillett, S. E. Sebastian, J. Teyssier, R. Viennois, E. Giannini, and D. van der Marel, *Physical Review B* **82**, 014523 (2010).
 - [9] R. Viennois, E. Giannini, D. van der Marel, and R. Černý, *Journal of Solid State Chemistry* **183**, 769 (2010).
 - ▶ [10] N. D. Zhigadlo, S. Katrych, S. Weyeneth, R. Puzniak, P. J. W. Moll, Z. Bukowski, J. Karpinski, H. Keller, and B. Batlogg, *Physical Review B* **82**, 064517 (2010).
 - ▶ [11] P. J. W. Moll, R. Puzniak, F. Balakirev, K. Rogacki, J. Karpinski, N. D. Zhigadlo, and B. Batlogg, *Nature Materials* **9**, 628 (2010).
 - ▶ [12] P. Marsik, K. W. Kim, A. Dubroka, M. Rössle, V. K. Malik, L. Schulz, C. N. Wang, C. Niedermayer, A. J. Drew, M. Willis, T. Wolf, and C. Bernhard, *Physical Review Letters* **105**, 057001 (2010).
 - ▶ [13] R. Khasanov, M. Bendele, K. Conder, H. Keller, E. Pomjakushina, and V. Pomjakushin, *New Journal of Physics* **12**, 073024 (2010).
 - ▶ [14] R. Khasanov, M. Bendele, A. Bussmann-Holder, and H. Keller, *Physical Review B* **82**, 212505 (2010).
 - ▶ [15] A. Bussmann-Holder, A. Simon, H. Keller, and A. R. Bishop, *Journal of Superconductivity and Novel Magnetism* (2010), doi:10.1007/s10948-010-0864-z.
 - ▶ [16] A. Piriou, N. Jenkins, C. Berthod, I. Maggio-Aprile, and Ø. Fischer, *Nature Communications* **2**, 221 (2011).
 - [17] Ø. Fischer, M. Kugler, I. Maggio-Aprile, C. Berthod, and C. Renner, *Reviews of Modern Physics* **79**, 353 (2007).
 - [18] C. Berthod, *Physical Review B* **82**, 024504 (2010).
 - ▶ [19] R. M. Konik, T. M. Rice, and A. M. Tsvelik, *Physical Review B* **82**, 054501 (2010).
 - ▶ [20] K.-Y. Yang, K. Huang, W.-Q. Chen, T. M. Rice, and F.-C. Zhang, *Physical Review Letters* **105**, 167004 (2010).
 - [21] D. Baeriswyl, *Journal of Superconductivity and Novel Magnetism* **24**, 1157 (2011).
 - [22] D. Eichenberger and D. Baeriswyl, *Physical Review B* **76**, 180504(R) (2007).
 - [23] D. Eichenberger and D. Baeriswyl, *Physical Review B* **79**, 100510(R) (2009).
 - [24] D. Baeriswyl, D. Eichenberger, and M. Menteshashvili, *New Journal of Physics* **11**, 075010 (2009).
 - [25] H. Keller, in *Superconductivity in Complex Systems*, K. A. Müller and A. Bussmann-Holder, eds. (Springer-Verlag, Berlin, Heidelberg, 2005), vol. 114 of *Structure and Bonding*, p. 143.
 - [26] G.-m. Zhao, K. Conder, H. Keller, and K. A. Müller, *Journal of Physics: Condensed Matter* **10**, 9055 (1998).
 - [27] G.-m. Zhao, H. Keller, and K. Conder, *Journal of Physics: Condensed Matter* **13**, R569 (2001).
 - [28] H. Keller, A. Bussmann-Holder, and K. A. Müller, *Materials Today* **11**, 38 (2008).
 - [29] H. Keller and A. Bussmann-Holder, *Advances in Condensed Matter Physics* **2010**, 393526 (2010).
 - ▶ [30] T. Jarlborg, *Solid State Communications* **151**, 639 (2011).
- ### Other references
- [31] J. Guo, S. Jin, G. Wang, S. Wang, K. Zhu, T. Zhou, M. He, and X. Chen, *Physical Review B* **82**, 180520(R) (2010).
 - [32] D. C. Johnston, *Advances In Physics* **59**, 803 (2010).
 - [33] Y. Han, W. Y. Li, L. X. Cao, X. Y. Wang, B. Xu, B. R. Zhao, Y. Q. Guo, and J. L. Yang, *Physical Review Letters* **104**, 017003 (2010).
 - [34] T. Hanaguri, S. Niitaka, K. Kuroki, and H. Takagi, *Science* **328**, 474 (2010).
 - [35] H. W. Meul, C. Rossel, M. Decroux, Ø. Fischer, G. Remenyi, and A. Briggs, *Physical Review Letters* **53**, 497 (1984).
 - [36] V. Jaccarino and M. Peter, *Physical Review Letters* **9**, 290 (1962).
 - [37] S. Nandi, M. G. Kim, A. Kreyssig, R. M. Fernandes, D. K. Pratt, A. Thaler, N. Ni, S. L. Bud'ko, P. C. Canfield, J. Schmalian, R. J. McQueeney, and A. I. Goldman, *Physical Review Letters* **104**, 057006 (2010).
 - [38] D. K. Pratt, W. Tian, A. Kreyssig, J. L. Zarestky, S. Nandi, N. Ni, S. L. Bud'ko, P. C. Canfield, A. I. Goldman, and R. J. McQueeney, *Physical Review Letters* **103**, 087001 (2009).
 - [39] A. D. Christianson, M. D. Lumsden, S. E. Nagler, G. J. MacDougall, M. A. McGuire, A. S. Sefat, R. Jin, B. C. Sales, and D. Mandrus, *Physical Review Letters* **103**, 087002 (2009).
 - [40] Y. Mizuguchi, Y. Hara, K. Deguchi, S. Tsuda, T. Yamaguchi, K. Takeda, H. Kotegawa, H. Tou, and Y. Takano, *Superconductor Science & Technology* **23**, 054013 (2010).
 - [41] R. H. Liu, T. Wu, G. Wu, H. Chen, X. F. Wang, Y. L. Xie, J. J. Ying, Y. J. Yan, Q. J. Li, B. C. Shi, W. S. Chu, Z. Y. Wu, and X. H. Chen, *Nature* **459**, 64 (2009).
 - [42] P. M. Shirage, K. Kihou, K. Miyazawa, C.-H. Lee, H. Kito, H. Eisaki, T. Yanagisawa, Y. Tanaka, and A. Iyo, *Physical Review Letters* **103**, 257003 (2009).
 - [43] P. M. Shirage, K. Miyazawa, K. Kihou, H. Kito, Y. Yoshida, Y. Tanaka, H. Eisaki, and A. Iyo, *Physical Review Letters* **105**, 037004 (2010).
 - [44] M. Uehara, T. Nagata, J. Akimitsu, H. Takahashi, N. Môri, and K. Kinoshita, *Journal of the Physical Society of Japan* **65**, 2764 (1996).
 - [45] J. R. Schrieffer, D. J. Scalapino, and J. W. Wilkins, *Physical Review Letters* **10**, 336 (1963).
 - [46] J. Lee, K. Fujita, K. McElroy, J. A. Slezak, M. Wang, Y. Aiura, H. Bando, M. Ishikado, T. Masui, J. X. Zhu, A. V. Balatsky, H. Eisaki, S. Uchida, and J. C. Davis, *Nature* **442**, 546 (2006).
 - [47] D. Baeriswyl and K. Maki, *Physical Review B* **31**, 6633 (1985).
 - [48] I. Bloch, J. Dalibard, and W. Zwerger, *Reviews of Modern Physics* **80**, 885 (2008).
 - [49] X. J. Chen, H. Q. Lin, and C. D. Gong, *Physical Review Letters* **85**, 2180 (2000).
 - [50] Y. J. Uemura, G. M. Luke, B. J. Sternlieb, J. H. Brewer, J. F. Carolan, W. N. Hardy, R. Kadono, J. R. Kempton, R. F. Kiefl, S. R. Kretzman, P. Mulhern, T. M. Rise-man, D. L. Williams, B. X. Yang, S. Uchida, H. Takagi, J. Gopalakrishnan, A. W. Sleight, M. A. Subramanian, C. L. Chien, M. Z. Cieplak, G. Xiao, V. Y. Lee, B. W. Statt, C. E. Stronach, W. J. Kossler, and X. H. Yu, *Physical Review Letters* **62**, 2317 (1989).
 - [51] M. I. Larkin, A. Kinkhabwala, Y. J. Uemura, Y. Sushko, and G. Saito, *Physical Review B* **64**, 144514 (2001).

- [52] C. C. Almasan, S. H. Han, B. W. Lee, L. M. Paulius, M. B. Maple, B. W. Veal, J. W. Downey, A. P. Paulikas, Z. Fisk, and J. E. Schirber, *Physical Review Letters* **69**, 680 (1992).
- [53] A. C. Komarek, H. Roth, M. Cwik, W.-D. Stein, J. Baier, M. Kriener, F. Bouree, T. Lorenz, and M. Braden, *Physical Review B* **75**, 224402 (2007).
- [54] T. R. McGuire, M. W. Shafer, R. J. Joenk, H. A. Alperin, and S. J. Pickart, *Journal of Applied Physics* **37**, 981 (1966).
- [55] V. V. Shvartsman, P. Borisov, W. Kleemann, S. Kamba, and T. Katsufuji, *Physical Review B* **81**, 064426 (2010).
- [56] J. H. Lee, L. Fang, E. Vlahos, X. Ke, Y. W. Jung, L. F. Kourkoutis, J.-W. Kim, P. J. Ryan, T. Heeg, M. Roeckerath, V. Goian, M. Bernhagen, R. Uecker, P. C. Hammel, K. M. Rabe, S. Kamba, J. Schubert, J. W. Freeland, D. A. Muller, C. J. Fennie, P. Schiffer, V. Gopulan, E. Johnston-Halperin, and D. G. Schlom, *Nature* **466**, 954 (2010).
- [57] M. Cyrot, B. Lambert-Andron, J. Soubeyroux, M. Rey, P. Dehauht, F. Cyrot-Lackmann, G. Fourcaudot, J. Beille, and J. Tholence, *Journal of Solid State Chemistry* **85**, 321 (1990).
- [58] M. J. Rey, P. Dehauht, J. C. Joubert, B. Lambert-Andron, M. Cyrot, and F. Cyrot-Lackmann, *Journal of Solid State Chemistry* **86**, 101 (1990).
- [59] W. E. Pickett, D. Singh, D. A. Papaconstantopoulos, H. Krakauer, M. Cyrot, and F. Cyrot-Lackmann, *Physica C* **162-164**, 1433 (1989).
- [60] D. J. Singh, D. A. Papanconstantopoulos, H. Krakauer, B. M. Klein, and W. E. Pickett, *Physica C* **175**, 329 (1991).
- [61] R. Arita, A. Yamasaki, K. Held, J. Matsuno, and K. Kuroki, *Journal of Physics: Condensed Matter* **19**, 365204 (2007).

Project **5****Novel electronic phases in strongly correlated electron systems**

Project leader: M. Sigrist (ETHZ)

Participating members: D. Baeriswyl (UniFR), G. Blatter (ETHZ), E. Giannini (UniGE), D. Jaccard (UniGE), M. Kenzelmann (PSI), D. van der Marel (UniGE), M. Sigrist (ETHZ), M. Troyer (ETHZ)

Summary and highlights: Several Ce-based heavy fermion superconductors have been investigated. Progress has been made in explaining the nature of the high-magnetic-field low-temperature phase “Q-phase” of CeCoIn₅, in particular, performing neutron scattering experiments for various field directions and in the theoretical analysis based on the scenario of a FFLO state. Simultaneous measurements of transport properties show that CeCu₂Si₂ has a maximum of the Hall and Nernst coefficients at a pressure of 4.5 GPa coinciding with the maximum of the superconducting transition temperature, $T_c \approx 2.4$ K. New crystals of the non-centrosymmetric heavy fermion material CeCoGe_{3-x}Si_x have been grown to investigate magnetic and superconducting properties. Motivated by Sr₂RuO₄, the quasi-particle spectrum of a domain wall in a chiral p -wave superconducting state is under investigation and features of “topological Josephson junctions” are studied. In the context of vortex matter, dynamical aspects of strong pinning are analyzed based on a model of single-pin single-vortex configuration. Turning to magnetic properties, helimagnetic and spin-glass like states have been studied in the non-centrosymmetric B20-alloys (Fe,Rh)Si and (Mn,Rh)Si. Moreover, a phase diagram describing the transition between a paramagnetic insulating and ferromagnetic metallic state in the alloy Fe(Si,Ge) has been discussed theoretically. Various theoretical studies are in progress to elucidate the physics of electrons at interfaces between strongly correlated electron systems. Eventually, we also report on developments of new algorithms for the simulation of fermions in the moderately correlated regime, e.g. the thermodynamics of the 3D Hubbard model down to the Néel temperature.

1 Q-phase of CeCoIn₅ (M. Kenzelmann, M. Sigrist)

The novel phase appearing at high magnetic fields and low temperatures in the heavy fermion superconductor CeCoIn₅ (nowadays known as “Q-phase”) has been early on interpreted as a Fulde-Ferrel-Larkin-Ovchinnikov (FFLO) state, with a spatial modulation of the superconducting order parameter. Recent measurements using neutron scattering [1, 2] and nuclear magnetic resonance (NMR) [25] discovered an incommensurate magnetic order in this phase for magnetic fields in the basal plane of the tetragonal crystal lattice. The neutron scattering results by Kenzelmann and collaborators show that this magnetism is closely connected with the superconducting phase and both orders disappear simultaneously at H_{c2} by a first order transition. Moreover, these studies identify a single type of incommensurate magnetic phase, with presumably two degenerate wave vectors, $\mathbf{Q} = \mathbf{Q}_0 \pm \mathbf{q}_{ic}$, $\mathbf{Q}_0 = (\pi/a, \pi/a, \pi/c)$ and $\mathbf{q}_{ic}^{(1)} = (0.12 \pi/a, 0.12 \pi/a, 0)$ and $\mathbf{q}_{ic}^{(2)} = (0.12 \pi/a, -0.12 \pi/a, 0)$, for both fields along [1 1 0] and [1 0 0] directions. This result led to the conclusion that the magnetic order would

be determined most likely by nesting features in the band structure [2].

1.1 Domains of the Q-phase

With the goal to test the appearance of the two degenerate phases for different field direction, Kenzelmann’s group has recently performed a high-field neutron diffraction experiment for magnetic fields along the crystallographic [1 1 0] direction ($\mathbf{H} \parallel [1 1 0]$). This field direction is particularly interesting as it treats the directions of the wave vectors $\mathbf{q}_{ic}^{(1,2)}$ differently and should lift the degeneracy. Indeed the domain of the spin-density wave with the wave vector perpendicular to the magnetic field is present, while there is no signature of the domain of the spin-density wave with the wave vector along the magnetic field (Fig. 1). As mentioned, this very different population of these two magnetic domains is allowed by symmetry, but cannot be explained on the basis of magnetic anisotropies. These measurements provide evidence for an intricate interplay between the superconductivity and magnetism in CeCoIn₅, and show that the superconducting

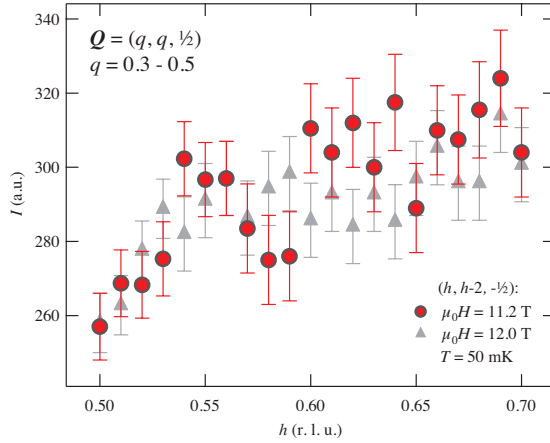


Figure 1: Neutron diffraction intensity for wave vectors $(h, h-2, -0.5)$, showing the absence of magnetic diffraction peaks in the Q -phase.

properties are crucial in the population of magnetic domains.

1.2 High-field Q -phase of CeCoIn_5

Last year Yanase and Sigrist discussed the “ Q -phase” as a secondary state in the background of an FFLO phase whose wave vector Q_{FFLO} lies parallel to the applied field [3, 4]. At the nodes of the modulated FFLO-superconducting order parameter, zero-energy quasi-particle states accumulate and take advantage of Fermi surface nesting to undergo a transition to an incommensurate magnetic phase. In the first study, it was assumed that the magnetic order is strongly localized around the FFLO-nodes and, consequently, would generate satellite peaks in addition to the Bragg peaks of the magnetic order. Such peaks have not been seen in most recent neutron scattering studies by Kenzelmann’s team [2]. Therefore, Yanase and Sigrist extended their study to include the case of a weakly localized and even an extended magnetic phase within the FFLO phase and considered both field directions, $[1\ 1\ 0]$ and $[1\ 0\ 0]$ (Fig. 2) [5]. Comparing with most recent neutron scattering data, the description based on the magnetism only weakly localized in the nodes of the FFLO state is fully compatible so far.

An interesting question appears for the field direction $[1\ 0\ 0]$, where the neutron scattering data suggest the appearance of two degenerate states, with wave vectors $q_{\text{ic}}^{(1,2)}$, forming domains. Actually, the magnetic moment (pointing along the c axis of the crystal) may be represented by a two-component order parameter

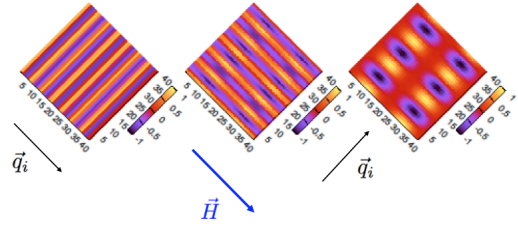


Figure 2: Different scenarios for the appearance of incommensurate magnetic order in the FFLO phase. The magnetic field lies along $[1\ 1\ 0]$ direction and $Q_{\text{FFLO}} \parallel \mathbf{H}$. Left panel: extended magnetic phase yielding $q_{\text{ic}} \parallel \mathbf{H}$ incompatible with neutron scattering; center panel: weakly localized phase leading to $q_{\text{ic}} \perp \mathbf{H}$ consistent with neutron scattering; right panel: strongly localized phase (discussed previously) also with $q_{\text{ic}} \perp \mathbf{H}$, incompatible with new neutron scattering experiments due to missing satellite peaks.

(η_1, η_2) :

$$M(\mathbf{r}) = M_0 e^{i\mathbf{Q}_0 \cdot \mathbf{r}} \left\{ \eta_1 \cos(\mathbf{q}_{\text{ic}}^{(1)} \cdot \mathbf{r}) + \eta_2 \cos(\mathbf{q}_{\text{ic}}^{(2)} \cdot \mathbf{r}) \right\}. \quad (2.1)$$

This should leave a clear signal in the field distribution observable in nuclear magnetic resonance (NMR). States with $\eta_1 = \eta_2$ (double- q state) would yield a single-peak in the field distribution on certain In-sites, while $(\eta_1, \eta_2) \propto (1, 0)$ or $(0, 1)$ (single- q state) would give rise to a double peak structure. The latter situation has been observed in most recent NMR experiments favoring the single- q type of states (Kumagai *et al.*, unpublished; the same NMR measurements give also strong evidence for the FFLO-phase). Yanase and Sigrist examined some consequences of the single- q phase based on a phenomenological theory [5]. For fields parallel to $[1\ 0\ 0]$ the double- q phase may appear near the magnetic transition within the FFLO phase, if $q_{\text{ic}}^{(1)} + q_{\text{ic}}^{(2)}$ are nearly commensurate with Q_{FFLO} . Furthermore, ultrasound can probe the presence of the two-component order parameter by testing the renormalization of the elastic constant C_{66} corresponding to the in-plane polarized transverse mode along the $[1\ 0\ 0]$ direction.

2 CeCu_2Si_2 : valence fluctuation mediated superconductivity? (D. Jaccard)

The aim of this subproject is a better understanding of the physics underlying the double-dome structure of T_c in the (P, T) plane of the first heavy fermion superconductor, CeCu_2Si_2 . In particular, the data are analyzed within the framework of the valence fluctuations the-

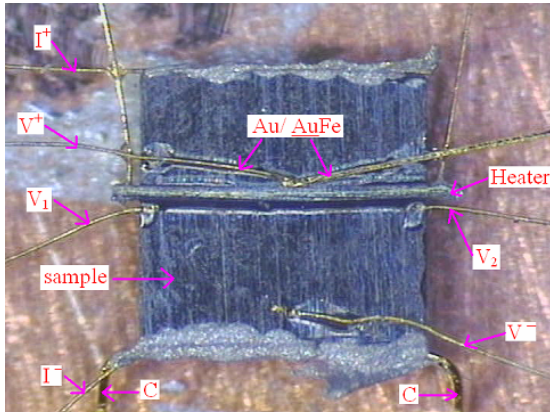


Figure 3: $CeCu_2Si_2$ single-crystal with its different contacting wires (before pressurization); sample dimensions: $600\ \mu m \times 575\ \mu m$, thickness $\sim 25\ \mu m$.

ory ([26] and ref. therein). Although superconductivity in this compound was discovered over 30 years ago, fundamental questions concerning the pairing mechanism(s) still remain open. Since spring 2009, Jaccard’s group has focussed on this project, making important experimental progress. In particular, the planned multiprobe experiment under pressure could be carried out successfully. A tiny, very high-quality $CeCu_2Si_2$ single-crystal of an older, home-made batch [27] was selected, prepared (re-dimensioned to fit into the pressure cell) and contacted with seven very thin Au wires to allow several types of measurements (Fig. 3): resistivity, Hall effect, ac specific heat, thermopower and Nernst effect. First of all, an extensive study at ambient pressure in the dilution refrigerator was performed, down to low temperatures (50 mK) and up to high magnetic fields (8 T).

Subsequently, the sample (still with the same contacts) was transferred into a Bridgman type pressure cell. Due to the recent pressure cell developments in Jaccard’s lab, this type of cell now provides very good hydrostatic conditions up to 7 GPa by the use of a liquid pressure medium (Daphne oil) [6]. Even so, the pressure needs to be changed at room temperature. They performed measurements at 9 different pressures up to 6.8 GPa in the dilution refrigerator. Since then, a separate experiment to calibrate the Au/Au-Fe thermocouple (which was used in the multiprobe experiment) has also been carried out under magnetic field at low temperatures. To our knowledge, this achievement is, up to now, unique. For the first time, Nernst and Hall effect have been measured (under pressure) in $CeCu_2Si_2$, and a complete data set of complementary physical quantities (resistivity, ac specific heat and thermopower)

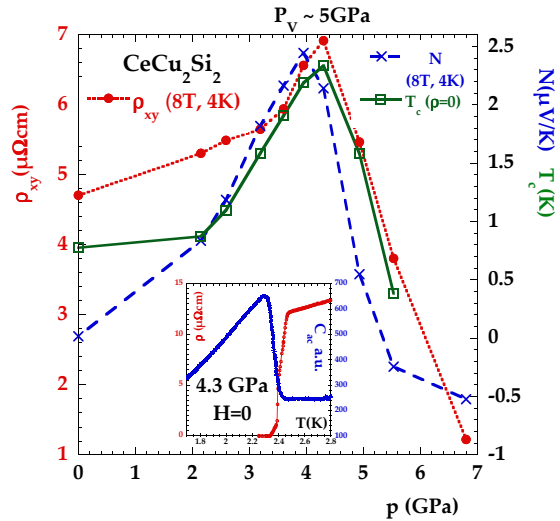


Figure 4: Pressure dependence of Hall (ρ_{xy}) and Nernst (N) signals in $CeCu_2Si_2$ (at 4 K and in a magnetic field of 8 T). Both quantities exhibit a maximum in vicinity of $P_V \approx 5\ GPa$, i.e. in the pressure region with the highest superconducting T_c (also shown). The inset compares the superconducting transition in zero field at 4.3 GPa, as seen in resistivity and ac specific heat: their coincidence and the overall low transition width of $\Delta T/T \approx 6\%$ highlight the good sample and setup quality.

has been obtained simultaneously on the very same $CeCu_2Si_2$ single-crystal. The data quality and consistency is high because (1) previous data are reproduced whenever they exist (resistivity, ac specific heat, thermopower) and (2) the good sample quality gives rise to a unprecedented high superconducting transition temperature, T_c , of roughly 2.4 K around $P_V \approx 5\ GPa$ (seen both in the resistivity and ac specific heat, Fig. 4, inset). Presently, detailed data analysis is still under way, with the theoretical support of Prof. K. Miyake from Osaka University, Japan.

Although the analysis is not yet fully completed, some selected, preliminary results will be mentioned here:

- At ambient pressure, the Nernst effect data indicate that, if any, the vortex contribution — well-known for example from high- T_c superconductors [28]) — is quite small and dominated by a contribution strongly coupled to the antiferromagnetic phase [7]. Under pressure there is also no evidence for a vortex contribution in the superconducting mixed phase.
- The transverse resistivity (ρ_{xy}) data (Hall effect) at low temperature show a clear enhancement around $P_V \approx 5\ GPa$, a feature which is predicted within the frame-

work of the valence fluctuations theory [26]. Hence these Hall data may yield new evidence for valence fluctuation mediated superconductivity in CeCu_2Si_2 under pressure. Whether similar conclusions apply to the origin of the enhanced Nernst signal in the same pressure region still needs to be elucidated, but seems likely (Fig. 4).

- On the same footing, a careful examination of the pressure dependence of the electric resistivity — which has been tracked over the whole available temperature range, i.e. from room temperature down to the superconducting transition — indicates a clear increase of the “residual” resistivity in the vicinity of $P_V \approx 5$ GPa. Such a feature also derives from the valence fluctuation scenario and may therefore be taken as a further strong indicator in its favor. Furthermore, the pressure dependence of resistivity at higher temperature may provide hints that the critical end point of the hypothetical valence transition line in the (P, T) plane of CeCu_2Si_2 is in fact situated at very low or even at negative temperature. Hence only a crossover regime can be observed around P_V , in agreement with theory [26].

3 $\text{CeCoGe}_{3-x}\text{Si}_x$ heavy fermions system (E. Giannini)

CeCoGe_3 is a heavy fermions compound in which either the pressure or Si substitutions for Ge continuously drive the ground state from a magnetic to a non-magnetic phase, and can tune the system to a quantum critical point (QCP). Pressure induced superconductivity without inversion symmetry is found in CeCoGe_3 ($x = 0$). At intermediate Si content ($1 \leq x \leq 1.5$) the system is in a quantum critical regime. In order to investigate the whole phase diagram, polycrystals of the solid solution $\text{CeCoGe}_{3-x}\text{Si}_x$ ($0 \leq x \leq 3$) have been processed by arc melting, followed by a long annealing at 900°C in vacuum closed atmosphere.

Single-crystals of CeCoGe_3 were successfully grown in Bi-flux using the two-crucibles tech-

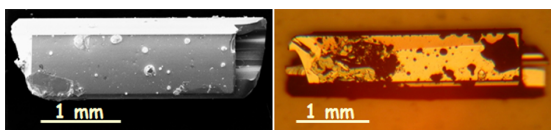


Figure 5: Crystals of CeCoGe_3 grown in Bi-flux.

nique, under vacuum. In the presence of Si substitutions, only small crystals and a weak substitution level were obtained (Fig. 5). The magnetic anisotropy has been investigated in CeCoGe_3 and the P -dependent phase diagram is being studied on compositions close to quantum criticality ($\text{CeCoGe}_{2.1}\text{Si}_{0.9}$), by the group of H. Rønnow at the EPFL.

4 Chiral p -wave pairing in Sr_2RuO_4 (M. Sigrist)

The group of Sigrist continued the studies on chiral p -wave pairing in two directions which are both also connected with the collaborative project “Topomatter” attached to Project 2.

4.1 Domain walls in chiral p -wave superconductors

Previous investigations were devoted to the effect of domain walls on the Josephson current between a chiral p -wave superconductor and a conventional superconductor. Domain walls intersecting the Josephson junction can alter the interference pattern of the critical current in a magnetic field [8], as observed in the experiments by van Harlingen’s group [29]. The basic condition for this effect is the non-trivial structure of the domain wall, in particular the property of the phase involved in the Josephson effect. While this has been well understood within the Ginzburg-Landau formulation used by Bouhon and Sigrist [8] and led to a good overall description of the experiment, the discussion on the level of the electronic spectrum associated with the domain walls is still open. Similar to the well-known chiral edge states also the domain walls develop confined chiral modes. For topological reason, there are twice as many modes in the domain wall than that found at the edge. The coupling among these modes yields a rearrangement of the spectrum such that the zero-energy modes are shifted apart towards the maximal momenta along the domain walls, unlike the case of edge states which cross zero energy at zero momentum. In order to obtain a non-trivial phase structure of the domain wall, it is necessary to analyze the properties of these quasi-particle bound states, when the band structure and the order parameter are varied. This project is still in progress, as it turned out to be more subtle than initially expected.

4.2 Topological Josephson junction in the 3 Kelvin phase

The so-called “3 Kelvin phase” is an inhomogeneous superconducting state in eutectic Sr_2RuO_4 -Ru where superconductivity first nucleates at the interface between Sr_2RuO_4 and μm -sized Ru inclusions. In their previous study, Kaneyasu, Sigrist and collaborators have shown that the evolution of the interface state towards the bulk chiral p -wave phase involves one additional symmetry breaking phase transition at T^* above the bulk transition [9, 10]. Signs consistent with such a phase transition have been experimentally observed at $T^* \sim 2.3$ K recently. The work of the present period focusses on a recent experiment at Kyoto University (unpublished) which considers the Josephson effect from a Pb film through Ru into Sr_2RuO_4 . The temperature dependence of the Josephson critical current of this setup is non-monotoneous, a feature which has most likely its origin in the topological structure of the 3 Kelvin phase. Sigrist and collaborators show that the proximity effect of Pb into the Ru-metal inclusions would push T^* of the additional transition towards the bulk transition temperature $T_c = 1.5$ K of Sr_2RuO_4 . At $T^* \approx T_c$ the topology of the order parameter coupling to the proximity-induced s -wave state within the Ru-inclusion changes, leading to a frustrated Josephson junction, as reported last year [9], and a strongly reduced critical current. First studies show that the critical current in the regime $T < T_c$ is determined by the depinning of a spontaneously created flux pattern [9]. This work is in progress and is in part performed by a student’s internship of MaNEP advancement of women program.

5 Vortex matter (G. Blatter)

A sufficiently strong magnetic field penetrates a type II superconductor in the form of quantized vortices which arrange in a triangular lattice (elastic manifold with moduli c_{11} , c_{44} , c_{66}) [30]) due to their repulsive interaction. External currents drive the vortices through the Lorentz force density F_L , giving rise to vortex motion and dissipation; the vortex motion is counteracted by vortex pinning via a defect-induced irregular potential. These defects influence both the static and dynamic response; the former generates disordered phases (glassy, etc.), whereas creep (at $F_L < F_c$) and resistive flux-flow (at $F_L \gg F_c$) after depinning are examples of the latter (F_c is the critical force density) [30].

5.1 Dynamic aspects of strong pinning

While the static force due to individual weak pins averages out in a direct summation resulting in collective pinning $\propto n_p^2$, with n_p the density of pins [31], sufficiently strong pins deform the vortex lattice plastically and generate a pinning force $\propto n_p$ under direct summation [32, 31]. The crossover between the two regimes is determined by the Labusch criterion [32][11]. In their study, Thomann, Geshkenbein and Blatter are interested in the dynamic aspects of strong pinning and its behavior near the crossover to weak pinning. They focus on a generic isotropic type II superconductor and discuss the force-velocity characteristics of a strongly pinned vortex lattice using three generic pinning models, with linear, quadratic, and cubic force profiles.

The F_L - v relation is found by solving the force balance equation $\eta v - F_L - \langle F_{\text{pin}} \rangle(v) = 0$ (with the mean vortex velocity v and the viscosity η), where the pinning force density is averaged over space, time, and disorder. Within the dilute limit, the focus is on a single-pin single-vortex setting with an effective one-dimensional vortex displacement $u(x)$. A strong pin is conveniently described by a linear force $f(u) = -f_0 u / \sigma$, $|u| < \sigma$, and 0 otherwise ($F \sim n_p f$); such a pin is always strong due to the discontinuous jumps at $u = \pm\sigma$. Unlike previous work [33, 34], they include the full dynamics of the manifold and solve the relevant equations

$$u(x) = \frac{x - \delta x[u](x)}{1 + f_0 / \sigma \bar{C}}, \quad (2.2)$$

$$\delta x[u](x) = -\frac{f_0}{\sigma} \partial_x \int_{-\sigma}^x dx' G^\dagger(x - x') u(x')$$

exactly via Laplace transformation. Here, $x = vt$ and the interpolation $G^\dagger(x) = (2/\pi\bar{C}) \arctan(x_0/x)^{1/2}$ is used (with $\bar{C} \sim c_{66}(\lambda a_0)^{1/2}$ the effective elastic constant and $x_0 \sim \eta v a_0^3 / \lambda c_{66}$). The resulting velocity-dependence of the pinning force density $\langle f_{\text{pin}} \rangle(v)$ is found through combined time and disorder averages (Fig. 6, inset) and provides the desired F_L - v relation shown in Fig. 6 with a characteristic bistability at small velocities (small inset).

Close to the Labusch point, the critical force $f_c = \langle f_{\text{pin}} \rangle(0) \rightarrow 0$ and the decreasing behavior of $|\langle f_{\text{pin}} \rangle(v)|$ cannot persist. In a next-order expansion close to the Labusch point, Blatter and collaborators make use of piecewise cubic and quartic pinning potentials and calculate the resulting force $\langle f_{\text{pin}} \rangle(v)$ perturbatively for

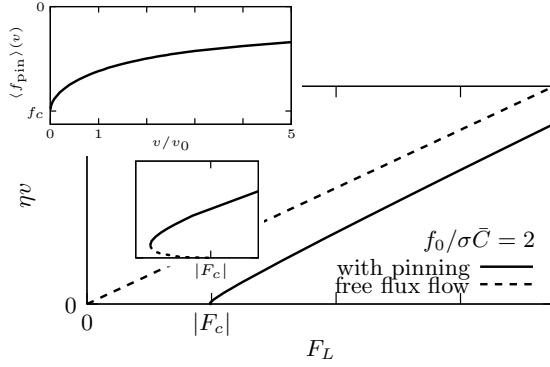


Figure 6: Force-velocity (current-voltage) relation $v(F_L)$ of a vortex lattice pinned by dilute parabolic (linear force) pins of strength f_0 and range σ . The top inset shows the v -dependence of the mean pinning force $\langle f_{\text{pin}} \rangle(v)$ in a single-pin single-vortex setting. The initial $v^{1/2}$ -decrease of $|\langle f_{\text{pin}} \rangle(v)|$ (rooted in the properties of $G^\dagger(x)$) outperforms the linear dependence of the dissipative term ηv at small velocities and results in a bistability in the F_L-v relation, as revealed in the close-up (small inset).

small v using an expansion around the static solution [34]. They find that the v -dependence of $|\langle f_{\text{pin}} \rangle(v)|$ is reverted at a finite velocity v on approaching the Labusch point (Fig. 7).

Furthermore, Blatter and co-workers find that, different from the static situation where f_c vanishes, the dynamic response does not change strongly across the Labusch point and remains qualitatively the same for close-to-weak and critical pins. In a next step, collective effects on the mean pinning force have to be taken into account, as the interaction between pins becomes of importance for $n_p > (\eta v / Ca_0)^{3/2}$.

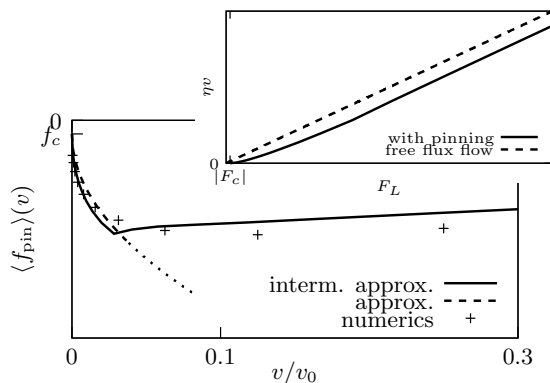


Figure 7: $\langle f_{\text{pin}} \rangle(v)$ for a piecewise cubic pin close to the Labusch point calculated partly perturbatively (solid), perturbatively (dashed), and numerically (crosses). $|\langle f_{\text{pin}} \rangle(v)|$ increases away from the small f_c and crosses over to the standard decreasing behavior at higher velocities. For typical pin densities n_p , this results in the continuous F_L-v relation shown in the inset.

5.2 Random polymer problem

Another work related to vortex matter physics deals with the random polymer problem in $1 + 1$ dimensions (a weak pinning situation), where Blatter and collaborators have concentrated on the short-scale and finite-temperature behavior as described by a short but finite-ranged disorder correlator [12] (behavior in the Larkin domain). Various types of expansions (of the random potential and of the potential correlator) allow for exact solutions and are compared to one another, with the parabolic expansion of the correlator providing the best results. Furthermore, the problematics of non-spectral correlators is discussed.

A new project deals with the pinning problem of geometric barriers in superconductors with complex shape, in particular two adjacent flat strips approximating/mimicking the situation of a layered superconductor in a parallel magnetic field with an interface defined by a pancake-vortex array (experiment in the group of E. Zeldov).

6 Physics of transition metal monosilicides/-germanides

6.1 Magnetic properties of 4d-transition metal monosilicides (E. Giannini)

After having completed the phase diagram of transition metal monosilicides (TMSi) with 3d-TM, and having found a new spin-glass ground state in $\text{Mn}_{1-x}\text{Co}_x\text{Si}$ [13], Giannini's group has extended their study to the transition metals of the 4th period.

A helimagnetic behavior has been found in the solid solution FeSi-RhSi , similar to that already known in FeSi-CoSi , but at higher temperatures (Fig. 8a). Higher transition temperatures are found in the spin-glass $\text{Mn}_{1-x}\text{Rh}_x\text{Si}$ as well, compared to those of $\text{Mn}_{1-x}\text{Co}_x\text{Si}$ (Fig. 8b). This preliminary study indicates that

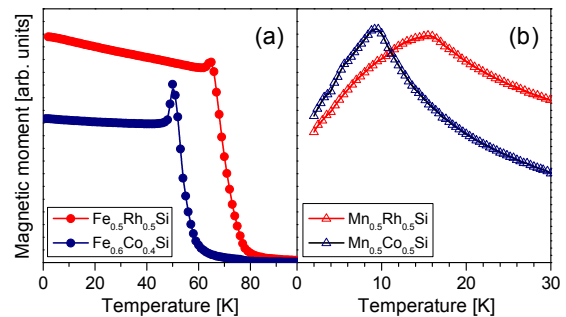


Figure 8: Helimagnetic transition (a) and spin-glass transition (b) in TMSi with 3d and 4d elements.

using transition metals with $4d$ electrons in $TMSi$ enhances the exchange energies.

6.2 FeSi – FeGe: transition between semiconductor and ferromagnetic metal (*T. M. Rice and M. Sgrist*)

The phase diagram of $FeSi_{1-x}Ge_x$ shows a first order phase transition from a paramagnetic insulator (FeSi-limit) to a ferromagnetic metal (FeGe-limit). Already earlier, Rice and collaborators have argued that this transition is correlation-induced based on LDA+U calculations finding that the ordered moment would be $\sim 1\mu_B$ in quantitative accordance with experiments [14]. The behavior proposed here is opposite to the standard Mott transition where correlation induces insulating (magnetic) behavior, going from an insulator to a magnetic metal upon strengthening correlations. To elucidate this property in more detail, Rice and co-workers have analyzed a simplified (one-dimensional) model including both Fe $3d$ - and Si $3p$ -bands which hybridize in a way as to form a narrow-gap semiconductor [15]. The $3d$ -electrons interact onsite via Coulomb repulsion U (intraorbital) and U' (interorbital) and Hund's rule coupling J . This model has been treated by mean field approximation and by density matrix renormalization group (DMRG) method. A first result is the ground state phase diagram, U versus $\alpha = J/U$ (using $U = U' + 2J$), which shows essentially perfect

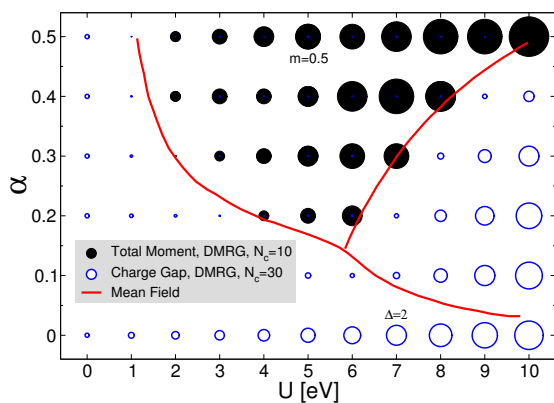


Figure 9: Phase diagram U versus $\alpha = J/U$ obtained from DMRG simulations. The filled circles denote the size of the partially polarized ferromagnetic moment and the empty circles indicate the size of the charge gap. Hereby, two of the circles have been labelled with the value scaling to their diameter ($m = 0.5$ for the black circles and $\Delta = 2$ for empty circles). The solid red lines show the mean field phase boundaries which are extended to higher values of U and include the antiferromagnetic state at $U > 5.9$ eV and $\alpha \sim 0.05 - 0.5$.

agreement between the two methods (Fig. 9). Three phases can be distinguished: (1) the paramagnetic insulating phase for small correlations, (2) the ferromagnetic metallic phase (marked through filled circles) with a magnetic moment approaching $m = 1\mu_B$ and (3) the antiferromagnetic insulating phase. The last phase has been considered only for the sake of completeness. The experimentally relevant phase transition is, however, occurring between (1) and (2). Within the framework of the parameter, it follows the trend of the alloy $FeSi_{1-x}Ge_x$ where Ge-doping increases the lattice constant, reducing the hybridization gap.

The finite-temperature analysis of the mean field results shows also a tricritical point for the phase transition between (1) and (2), which marks the maximum of the magnetic susceptibility in the paramagnetic insulator, a feature seen in FeSi.

7 The nature of the interface between strongly correlated systems (*D. Baeriswyl*)

Interfaces of systems with different electronic properties pose a number of challenging theoretical questions, in particular if one or both materials have strong electronic correlations and/or if different ordering tendencies compete. This can lead to relatively minor effects close to the interface, such as proximity effects where the order of one material penetrates slightly into the other, but in certain cases much more drastic effects are possible, such as electronic [35] or orbital [36] reconstruction. In this context the group of Baeriswyl has discussed the following problems.

7.1 Superconductivity and ferromagnetism

The quasi-classical calculations for a superconducting layer sandwiched between two ferromagnets have been described in the last MaNEP report. One result is worth being mentioned again, namely the tiny effect of the relative orientation of the magnetization on the free energy of the superconducting layer. This means that the quasi-classical theory is not able to account for the strong coupling observed experimentally between superconductivity and ferromagnetism. For this reason these studies were not continued during the last year.

7.2 Interface of magnetic chains

As a warm-up exercise for planned studies of interfaces between one-dimensional systems, the problem of an easy-plane spin-chain (XY model) consisting of two pieces with different

model parameters is currently studied in the framework of a master thesis in Baeriswyl's group. The most simple case is that of a changing sign of the exchange constant J at the interface. In fact, this problem can be reduced to that of a homogeneous chain using simple local transformations of spin-operators. A less trivial case is the XY model in a magnetic field h parallel to the z axis, with different signs of the field in the two segments. The problem is handled using the Jordan-Wigner transformation [37].

7.3 Interface of different one-dimensional electronic systems

The problem of a single-impurity in a Luttinger liquid has been extensively studied since the initial work by Kane and Fisher [38]. The impurity can have dramatic effects on the local electronic structure, especially if the electron-electron interactions are repulsive. The aim is to generalize this problem to that of an interface between two different one-dimensional electronic systems. These may be two Luttinger liquids with different parameters (repulsive/attractive) or a Luttinger liquid on one side and a gapped system (Luther-Emery liquid) on the other side. A related problem is the interface between a Mott insulator (Hubbard chain at half filling) and a band insulator (an electronic chain with a Peierls distortion). Baeriswyl and co-workers want to focus on the possible electronic reconstructions at the interface, for instance the appearance of bound states.

8 Algorithmic developments (M. Troyer)

The main algorithmic development of the past year deals with the diagrammatic quantum Monte Carlo (DiagMC) algorithm for the Hubbard model [16]. This algorithm samples connected Feynman diagrams instead of the partition function and works successfully in the correlated Fermi liquid regime of the Hubbard model. This new algorithm will be used in the future to calculate phase diagrams and equations of state of 2D and 3D Hubbard models in the moderately correlated regime.

Another development are the new tensor-network algorithms for electronic structure calculations [17]. These are higher-dimensional generalizations of the density matrix renormalization group method, representing the first development of such a method for the electronic structure of molecules.

Troyer and collaborators have also written a review article about the recently developed con-

tinuous time quantum Monte Carlo algorithms for dynamical mean field theory which are currently being employed for simulating correlated materials and ultracold atomic gases [18].

8.1 ALPS 2.0

Troyer and collaborators have developed and published a major new version of the ALPS libraries and applications [19]. ALPS 2.0 contains new applications, such as a dynamical mean field theory solvers [18, 20], and a code for time-dependent DMRG simulations. Other major changes in release 2.0 include the use of HDF5 for binary data, evaluation tools in Python, support for the Windows operating system, the use of CMake as build system and binary installation packages for Mac OS X and Windows, and integration with the VisTrails workflow provenance tool.

8.2 Thermodynamics of the Hubbard model

Using a MaNEP-developed continuous time quantum Monte Carlo solver for cluster dynamical mean field theory [21, 18], Troyer and co-workers have simulated the three-dimensional Hubbard models for interactions up to $U \leq 12t$ and temperatures down to the Néel temperature at all fillings [22]. They have calculated all thermodynamic quantities, including energy, free energy, entropy, specific heat, and density, as well as double occupancies and nearest neighbor spin-correlations.

8.3 Topological phases and anyonic models

Troyer and collaborators have developed a new algorithm for the direct simulation of models of non-Abelian anyons [23], and have simulated generalizations of previously studied models of non-Abelian anyons to non-unitary anyonic theories [24]. This may be considered to be more of a mathematical game without physical applications, since they are currently showing that such non-unitary theories are non-physical.

9 Collaborative efforts

Several subjects reported here are benefiting strongly from collaborations within the MaNEP network. An obvious example for Project 5 is the study of the Q -phase of CeCoIn_5 , which is an important topic in Kenzelmann's group on the experimental and in Sigrist's group on the theoretical side. The mutual contact of the two teams have been proven

most important for the reported progress. Further important collaborative topics are not commonly summarized under the title “topological insulators”. Work done in this field is supported by the collaborative project “Topomatter” which was started last year and involves particularly the groups of Morpurgo, van der Marel and Sigrist, but includes an even larger community. Efforts in this field are only partially reported in Project 5 (chiral p -wave superconductivity), but include also work reported in Project 2. Moreover, topologically characterized phases are also discussed from the numerical side by Troyer’s group. The heavy fermion superconductors, including both non-centrosymmetric compounds as well as systems with intriguing valence fluctuation induced features, are part of a collaborating effort mainly through exchange of knowledge. Eventually the field of transition metal silicides and germanides is a subject which is pursued both by experimental (van der Marel, Gianini) and by theoretical teams (Sigrist, Rice). The ALPS project is of importance for MaNEP as several theoretical and experimental groups are using the library for their studies.

MaNEP-related publications

- [1] M. Kenzelmann, T. Strässle, C. Niedermayer, M. Sigrist, B. Padmanabhan, M. Zolliker, A. D. Bianchi, R. Movshovich, E. D. Bauer, J. L. Sarrao, and J. D. Thompson, *Science* **321**, 1652 (2008).
- ▶ [2] M. Kenzelmann, S. Gerber, N. Egetenmeyer, J. L. Gavilano, T. Strässle, A. D. Bianchi, E. Ressouche, R. Movshovich, E. D. Bauer, J. L. Sarrao, and J. D. Thompson, *Physical Review Letters* **104**, 127001 (2010).
- [3] Y. Yanase and M. Sigrist, *Journal of the Physical Society of Japan* **78**, 114715 (2009).
- [4] Y. Yanase and M. Sigrist, *Journal of Physics: Conference Series* **150**, 052287 (2009).
- [5] Y. Yanase and M. Sigrist, *Journal of Physics: Condensed Matter* **23**, 094219 (2011).
- [6] A.-S. Rüetschi and D. Jaccard, *Review of Scientific Instruments* **78**, 123901 (2007).
- ▶ [7] A.-S. Rüetschi, K. Sengupta, G. Seyfarth, and D. Jaccard, *Journal of Physics: Conference Series* **273**, 012052 (2011).
- [8] A. Bouhon and M. Sigrist, *New Journal of Physics* **12**, 043031 (2010).
- [9] H. Kaneyasu and M. Sigrist, *Journal of the Physical Society of Japan* **79**, 053706 (2010).
- ▶ [10] H. Kaneyasu, N. Hayashi, B. Gut, K. Makoshi, and M. Sigrist, *Journal of the Physical Society of Japan* **79**, 104705 (2010).
- [11] G. Blatter, V. B. Geshkenbein, and J. A. G. Koopmann, *Physical Review Letters* **92**, 067009 (2004).
- ▶ [12] V. S. Dotsenko, V. B. Geshkenbein, D. A. Gorokhov, and G. Blatter, *Physical Review B* **82**, 174201 (2010).
- ▶ [13] J. Teyssier, E. Giannini, V. Guritanu, R. Viennois, D. van der Marel, A. Amato, and S. N. Gvasaliya, *Physical Review B* **82**, 064417 (2010).
- [14] V. I. Anisimov, R. Hlubina, M. A. Korotin, V. V. Mazurenko, T. M. Rice, A. O. Shorikov, and M. Sigrist, *Physical Review Letters* **89**, 257203 (2002).
- [15] K.-Y. Yang, Y. Yamashita, A. M. Läuchli, M. Sigrist, and T. M. Rice, arXiv:1102.1190 (2011).
- ▶ [16] E. Kozik, K. Van Houcke, E. Gull, L. Pollet, N. Prokof’ev, B. Svistunov, and M. Troyer, *Europhysics Letters* **90**, 10004 (2010).
- [17] K. H. Marti, B. Bauer, M. Reiher, M. Troyer, and F. Verstraete, *New Journal of Physics* **12**, 103008 (2010).
- ▶ [18] E. Gull, A. J. Millis, A. I. Lichtenstein, A. N. Rubtsov, M. Troyer, and P. Werner, *to be published in Reviews of Modern Physics* (2011).
- ▶ [19] B. Bauer, L. D. Carr, A. Feiguin, J. Freire, S. Fuchs, L. Gamper, J. Gukelberger, E. Gull, S. Guertler, A. Hehn, R. Igarashi, S. V. Isakov, D. Koop, P. N. Ma, P. Mates, H. Matsuo, O. Parcollet, G. Pawłowski, J. D. Picon, L. Pollet, E. Santos, V. W. Scarola, U. Schollwöck, C. Silva, B. Surer, S. Todo, S. Trebst, M. Troyer, M. L. Wall, P. Werner, and S. Wessel, arxiv:1101.2646 (2011).
- [20] E. Gull, P. Werner, S. Fuchs, B. Surer, T. Pruschke, and M. Troyer, *Computer Physics Communications* **182**, 1078 (2011).
- [21] E. Gull, P. Werner, O. Parcollet, and M. Troyer, *Europhysics Letters* **82**, 57003 (2008).
- ▶ [22] S. Fuchs, E. Gull, L. Pollet, E. Burovski, E. Kozik, T. Pruschke, and M. Troyer, *Physical Review Letters* **106**, 030401 (2011).
- [23] R. N. C. Pfeifer, P. Corboz, O. Buerschaper, M. Aguado, M. Troyer, and G. Vidal, *Physical Review B* **82**, 115126 (2010).
- [24] E. Ardonne, J. Gukelberger, A. W. W. Ludwig, S. Trebst, and M. Troyer, *to be published in New Journal of Physics* (2011).

Other references

- [25] B. L. Young, R. R. Urbano, N. J. Curro, J. D. Thompson, J. L. Sarrao, A. B. Vorontsov, and M. J. Graf, *Physical Review Letters* **98**, 036402 (2007).
- [26] S. Watanabe, M. Imada, and K. Miyake, *Journal of the Physical Society of Japan* **75**, 043710 (2006).
- [27] E. Vargoz, D. Jaccard, J.-Y. Genoud, J.-P. Brison, and J. Flouquet, *Solid State Communications* **106**, 631 (1998).
- [28] Z. A. Xu, N. P. Ong, Y. Wang, T. Kakeshita, and S. Uchida, *Nature* **406**, 486 (2000).
- [29] F. Kidwingira, J. D. Strand, D. J. Van Harlingen, and Y. Maeno, *Science* **314**, 1267 (2006).
- [30] G. Blatter, M. V. Feigel’man, V. B. Geshkenbein, A. I. Larkin, and V. M. Vinokur, *Reviews of Modern Physics* **66**, 1125 (1994).
- [31] A. I. Larkin and Y. N. Ovchinnikov, *Journal of Low Temperature Physics* **34**, 409 (1979).
- [32] R. Labusch, *Crystal Lattice Defects* **1**, 1 (1969).
- [33] T. Matsushita, E. Kusayanagi, and K. Yamafuji, *Journal of the Physical Society of Japan* **46**, 1101 (1979).
- [34] A. I. Larkin and Y. N. Ovchinnikov, in *Nonequilibrium Superconductivity*, D. N. Langenberg and A. I. Larkin, eds. (North-Holland, 1986), p. 493.
- [35] S. Okamoto and A. J. Millis, *Nature* **428**, 630 (2004).
- [36] J. Chakhalian, J. W. Freeland, H.-U. Habermeier, G. Cristiani, G. Khaliullin, M. van Veenendaal, and B. Keimer, *Science* **318**, 1114 (2007).

[37] E. Lieb, T. Schultz, and D. Mattis, *Annals of Physics* (N. Y.) **16**, 407 (1961).

[38] C. L. Kane and M. P. A. Fisher, *Physical Review Letters* **68**, 1220 (1992).

Project **6****Magnetism and competing interactions in bulk materials**

Project leaders: F. Mila (EPFL), A. Zheludev (ETHZ)

Participating members: T. Giamarchi (UniGE), J. Mesot (PSI and ETHZ), F. Mila (EPFL), H.-R. Ott (ETHZ), H. Rønnow (EPFL), U. Staub (PSI), M. Troyer (ETHZ), A. Zheludev (ETHZ)

Introduction: This project attacks some of the most intriguing problems in the modern field of quantum magnetism, such as low dimensionality, geometric frustration, quenched disorder and magneto-electric coupling. Such features do not only have a drastic effect on the physical properties, but actually may result in qualitatively new and previously inaccessible quantum magnetic phases. Understanding these phases involves understanding the spatial and temporal spin correlations.

Summary and highlights

Perhaps the main highlight of our activities this year was a very successful application of diverse experimental methods, aimed at measuring spin and charge correlations on different time and length scales. “Classic” techniques such as nuclear magnetic resonance (NMR), and neutron spectroscopy were complemented by resonant X-ray diffraction, the rapidly developing resonant inelastic X-ray scattering, muon-spin relaxation (μ SR) experiments, neutron-spin echo spectroscopy, and extreme high magnetic field measurements. Their successful application was enabled by a sustained effort in the preparation and characterization of material samples, with a particular focus on single-crystals. Multiple techniques were also exploited on the theory side, where analytical developments complementing a variety of numerical methods. Overall, this emphasis on the synergy of different approaches paid off, resulting in several breakthroughs of understanding.

For spin-ladders, we have some exciting new results concerning high-field behavior. t -DMRG numerical studies yielded a spectacular quantitative agreement with neutron scattering data on the strong-rung ladder compound $\text{CuBr}_4(\text{C}_5\text{H}_{12}\text{N})_2$ (BPCB). The synthesis of deuterated single-crystals of the material $(2,3\text{-dimethylpyridinium})_2\text{CuBr}_4$ (DIMPY) will allow a similar comparative study of a strong-leg system. Challenging high-field NMR experiments revealed some very unusual scaling at the quantum phase transition in the spin-ladder BiCu_2PO_6 .

As far as frustrated and incommensurate mag-

netism is concerned, our main result pertains to the Hubbard model in triangular geometry. For the half-filled case, we have shown that the mysterious phase between the metallic and the three-sublattice ordered Mott-insulating state can be described by a pure spin-model, and that it is a spin-liquid with presumably a gapless spectrum and a spinon Fermi surface. Using neutron diffraction in the Dzyaloshinskii-Moriya helimagnet $\text{Ba}_2\text{CuGe}_2\text{O}_7$, we have detected a novel and very peculiar antiferromagnetic-cone phase, which seems to defy a vast body of theoretical work on that compound.

Resonant X-ray diffraction and inelastic scattering have firmly positioned themselves as powerful tools for studying the interplay between charge and spin degrees of freedom. Diffraction experiments yielded a fundamentally important observation of orbital currents in CuO . At the same time, spectroscopic measurements brought insight into the so-called Zhang-Rice states in the quasi-1D cuprate Li_2CuO_2 . A significant step forward was the work on $\text{Sr}_2\text{CuO}_2\text{Cl}_2$ which helped establish a Hubbard model that is globally consistent for known square-lattice cuprates.

A substantial effort this year was aimed at understanding the effect of structural disorder on the quantum ground states in spin-systems. In a groundbreaking NMR study, we found direct evidence of the so-called random-singlet phase of the disordered spin-chain $\text{BaCu}_2\text{SiGeO}_7$. Long and short range ordering in disordered interacting spin-chains was investigated using another local probe, namely μ SR.

1 Excitations in spin-ladders

Antiferromagnetic spin-ladders remain the most important prototypical quantum spin-systems. They serve us to develop and test new numerical methods, to quantitatively validate theoretical concepts, and to address fundamental phenomena such as quantum phase transitions. This year, we continued theoretical and experimental studies of known systems, but also ventured forth to synthesize new ladder materials with specific properties.

1.1 t -DMRG numerical calculations of spin correlations (*T. Giamarchi*)

t -DMRG numerical calculations of spin correlations [1] were performed in the continuity of our investigations of spin- $\frac{1}{2}$ ladders, motivated by the recent measurements on the compound $\text{CuBr}_4(\text{C}_5\text{H}_{12}\text{N})_2$ (BPCB). The correlations reflect the excitations of the system and are directly related to many experimental quantities such as the nuclear magnetic resonance (NMR) relaxation rate or the inelastic neutron scattering (INS) cross section.

We focussed on the evolution of these correlations with the magnetic field and compared their behavior for different couplings. Their characteristic features are interpreted us-

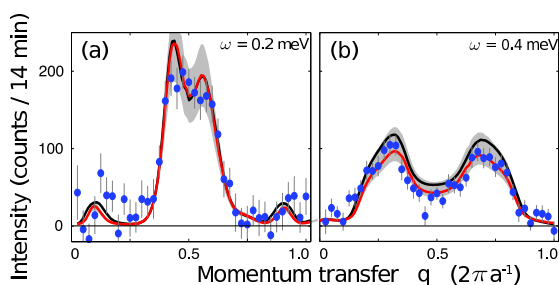


Figure 1: Inelastic neutron scattering intensity measured along \mathbf{a}^* of BPCB with the momentum π in the rung direction ($\mathbf{Q} \cdot \mathbf{d}_i = \pi$) at $h^z = 10.1$ T ($m^z \approx 0.5$) and $T = 250$ mK after subtraction of the zero-field background. In each panel, fixed energy scans are plotted: (a) $\omega = 0.2$ meV, (b) $\omega = 0.4$ meV. The circles correspond to the experimental data. The red (black) solid lines are the $m^z = 0.5$ theoretical data for the ladder (the spin-chain mapping) convolved with the instrumental resolution. The shaded bands indicate the error bar in the experimental determination of a single proportionality constant valid for all fields, energies, and wave vectors. The width of these areas combines the statistics of all our scans with uncertainties in the exact magnetization values at the chosen fields and in the convolution procedure.

ing different analytical approaches such as the mapping onto a spin-chain, a Luttinger liquid (LL) or onto a $t - J$ model. The resolution of the computed correlations is good enough to overlap with the low-energy LL quantitative predictions.

For values of parameters for which INS measurements exist, we compare our results to the experiments on the compound BPCB and find excellent agreement (Fig. 1). We make additional predictions for the high-energy part of the spectrum that are potentially testable in future experiments.

1.2 Tunable spin-ladder $\text{Sr}_{14-x}\text{Ca}_x\text{Cu}_{24}\text{O}_{41}$ (*H. Rønnow*)

The tunable spin-ladder $\text{Sr}_{14-x}\text{Ca}_x\text{Cu}_{24}\text{O}_{41}$ is particularly interesting since it is related to the high-temperature superconducting cuprates and indeed for high Ca-composition ($x > 12$) it becomes superconducting under pressure. In collaboration with the solid state synthesis group of K. Conder (PSI) we have now a series of $\text{Sr}_{14-x}\text{Ca}_x\text{Cu}_{24}\text{O}_{41}$ crystals from $x = 0$ to $x = 13$. Triple axis neutron scattering spectroscopy has been performed at ambient pressure to track the development of the ladder spin gap versus x . Follow up experiments are planned using unpolarized and polarized neutrons for Q1-Q2 2011. A first experiment was performed at 4.5 GPa in the superconducting phase of the $x = 12.2$ compound. Several experimental difficulties related to the pressure setup limited the effective amount of data, and a proposal for additional beamtime is submitted.

1.3 $S = \frac{1}{2}$ Heisenberg antiferromagnet (2,3-dimethylpyridinium) $_2\text{CuBr}_4$ (*A. Zheludev*)

The $S = \frac{1}{2}$ Heisenberg antiferromagnet (2,3-dimethylpyridinium) $_2\text{CuBr}_4$ (DIMPY) is the only known almost perfect 1D spin- $\frac{1}{2}$ strong-leg spin-ladder. Previous neutron studies by other authors were severely limited by a lack of fully deuterated samples [15]. Quick preliminary neutron scattering experiments performed on our new 100% deuterated single-crystals (Fig. 2) revealed previously inaccessible details of the excitation spectrum, including a strong multi-magnon continuum. More detailed measurements, including those at high fields, are planned for the near future.

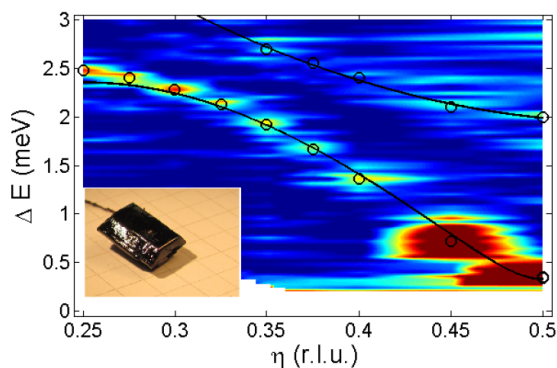


Figure 2: Preliminary inelastic neutron scattering spectrum collected for the strong-leg spin-ladder (2,3-dimethylpyridinium)₂CuBr₄.

2 Quantum criticality and scaling

One of the central themes in modern condensed matter physics is that of quantum phase transitions. A key aspect is the scaling behavior in the vicinity of quantum critical points. This problem has been the subject of numerous theoretical studies. However, on the experimental side, this issue is only now being addressed. In our work we focused on the scaling properties of quantum critical phases in several well-characterized spin-chain and ladder compounds.

2.1 Quantum phase transition in the BiCu₂PO₆ spin-ladder (*H.-R. Ott*)

A quantum phase transition in the BiCu₂PO₆ spin-ladder was studied using high-field NMR. For spin- $\frac{1}{2}$ antiferromagnetic (AF) 2-leg ladders the non-magnetic singlet ground state with massive excitations enters a gapless regime upon application of a magnetic field H_c [16, 17]. The present work intends to extend our previous studies [2] by exploring the field-induced ordered (FIO) phase of the spin- $\frac{1}{2}$ coupled zigzag ladders in BiCu₂PO₆. The unique energy scale of this spin-system, intermediate between cuprates and organic ladders, provides access to the quantum critical regime in a relatively large temperature and field range. Magnetization data on the polycrystalline compound have shown that fields of about 21 T possibly close the spin gap. Single-crystal samples of BiCu₂PO₆ (Fig. 3), recently grown by our group [3], were used to perform NMR studies, the only experimental technique capable of providing information on both the local magnetization and the low-energy dynamics at fields larger than 17 T (at dedicated high-field facilities).

Different ³¹P NMR lines were detected in the



Figure 3: As grown single-crystals of Bi(Cu_{1-x}Zn_x)₂PO₆ ($x = 0\%$, 1% , 5%), together with a rod of BiZn₂PO₆.

investigated field range (16 – 31 T), allowing us to access the FIO phase of BiCu₂PO₆ beyond an extrapolated critical field value of $H_c = 20.94$ T (Fig. 4). The low-energy dynamics was investigated by means of the nuclear spin-lattice relaxation time T_1 . The NMR lineshapes measured with the magnetic field along the crystalline b -axis show clear signatures of a continuous distribution of local magnetic fields, typical of an incommensurate magnetic structure, object of future investigations. Since the second moment represents a measure of the FIO order parameter, detailed data were collected both as a function of temperature (close to H_c and at 23 T) and field (at 1.17 K). Temperature scans at fixed fields allowed us to experimentally determine the phase boundary of the field-induced transition from T_1^{-1} data. The resulting curve in the (H , T) diagram could

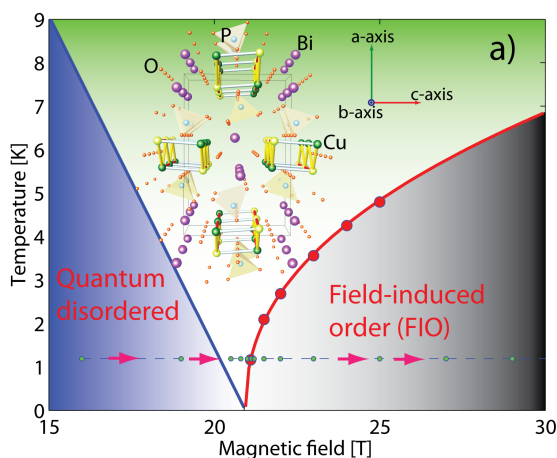


Figure 4: Phase diagram of BiCu₂PO₆, as determined from NMR, showing the critical field $H_c = 20.94$ T. The low-field quantum disordered phase is replaced by a field-induced ordered phase above H_c . The inset shows the material's structure.

be fitted with a power law of the form $T_c \propto a(H - H_c)^{0.43}$, with T_c the critical temperature of the transition. The exponent $\alpha = 0.43$ turned out to differ substantially from the value $\frac{2}{3}$ expected for a magnetic BEC transition.

2.2 Quantum critical scaling in applied fields (A. Zheludev)

Quantum critical scaling in applied fields was studied in the Luttinger spin-liquid phase of the $S = \frac{1}{2}$ Heisenberg spin-chain compound Dioxane-Cu₂Cl₄ [4]. We prepared very large deuterated single-crystal samples of this compound to study the corresponding scaling exponent (the so-called Luttinger parameter K), by measuring the energy dependence of the magnetic dynamic structure factor. In good agreement with theory, K was found to increase from its $K = 0.5$ value in zero field towards unity, reaching $K \sim 0.8$ in the highest experimentally attainable field of 14.5 T.

2.3 Scaling at the field-induced $z = 2$ quantum critical point (A. Zheludev)

Scaling at the field-induced $z = 2$ quantum critical point was studied in the spin-ladder compound IPA-CuCl₃. We have performed inelastic neutron scattering measurements of the corresponding dynamic structure factor at different temperatures at and below the critical field. The data are being analyzed in order to understand the scaling laws and study the lifetimes of higher-energy excitations. A typical raw data set is shown in Fig. 5. Other measurements, using the ultra-high resolution neutron-spin echo technique, were performed away from the quantum critical point (at zero ap-

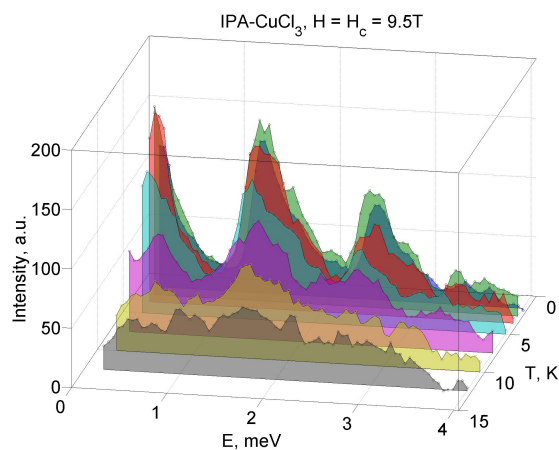


Figure 5: Typical inelastic neutron data collected on the RITA-II spectrometer in IPA-CuCl₃ right at the critical field $H_c = 9.5$ T, at different temperatures.

plied field) and addressed finite-temperature scaling in this system. Significant deviations from the predictions of one-dimensional theories were found and attributed to interladder interactions [5].

3 Frustrated and incommensurate magnetism

Geometrically frustrated systems often possess unique physical properties due to a competition between alternative ground states. While in classical magnetism frustration is often released by forming a multitude of energetically close incommensurate phases, the behavior in the quantum case can be even more complex. On the other hand, incommensurate states are often associated with novel multiferoic properties, due to their coupling to the lattice via Dzyaloshinskii-Moriya interactions or other mechanisms. In this project, we have addressed a broad array of frustrated and incommensurate magnetic systems, both from the theoretical point of view and experimentally.

3.1 Spin-liquid phase of the Hubbard model on a triangular lattice (F. Mila)

Understanding the spin-liquid phase of the Hubbard model on a triangular lattice was the main theoretical result in this area that we have obtained this year. We have shown that this phase can be described by a pure spin-model [6]. The proof is based on a high-order strong coupling expansion (up to order 12) using perturbative continuous unitary transformations. The resulting spin-model is an extended Heisenberg model that contains n -spin interactions with n even. The progressive appearance of high-order terms upon reducing U/t leads to a first-order transition inside the insulating phase from the three-sublattice long-range magnetic order to a spin-liquid phase. Remarkably enough, the double occupancy jumps at the transition although the system remains insulating on both sides of the transition. A comparison with the Gutzwiller projected Fermi sea suggests that the spin-liquid phase has a gapless spectrum and a spinon Fermi surface. Implications for organic systems are under investigation.

3.2 Phase diagram of the fully frustrated transverse-field Ising model on the honeycomb lattice (F. Mila)

Our study of the phase diagram of the fully frustrated transverse-field Ising model on the honeycomb lattice [7] was motivated by the

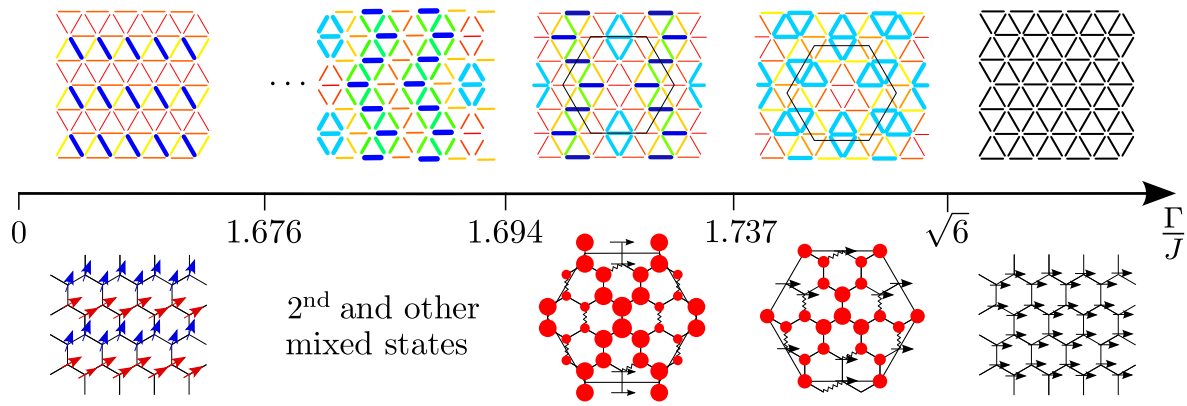


Figure 6: Classical phase diagram in the dimer language (above) and in the spin language (below) of the fully frustrated transverse-field Ising model on the honeycomb lattice. In the dimer representation, the thickness of the bonds is proportional to the dimer density. Thick blue bonds correspond to the highest dimer density. In the spin representation, the radii of the circles are proportional to S_i^z and arrows indicate the orientation of the classical spins.

interest raised by the closely related quantum dimer model on the triangular lattice, which demonstrates a resonating valence bond phase. It turns out that, in addition to the fully polarized phase at a large field, the classical model possesses a multitude of phases that break the translational symmetry which, in the dimer language, corresponds to a plaquette phase and a columnar phase separated by an infinite cascade of mixed phases (Fig. 6). In the mixed phase, stripes of columnar order alternate with stripes reminiscent of the plaquette phase, resulting into an unexpected infinite sequence of phases with increasing commensurability. This opens new perspectives for the crystalline phases of quantum dimer models.

3.3 Ferrimagnetic properties of the multiferroic compound Cu_2OSeO_3 (F. Mila)

Ferrimagnetic properties of the multiferroic compound Cu_2OSeO_3 were studied using ^{77}Se NMR and interpreted in the context of a microscopic model that contains ferro- and antiferromagnetic couplings [8]. We have confirmed that the compound Cu_2OSeO_3 undergoes a ferrimagnetic transition with 3/4 of the Cu^{2+} ions aligned parallel and 1/4 aligned antiparallel to the applied field. The transition to this 3up–1down magnetic state is not accompanied by any splitting of the NMR lines or any abrupt modification in their broadening, proving that there is no reduction in the crystal symmetry from its high- T cubic $P213$ space group, and confirming that this material provides a unique example of a metrically cubic crystal that allows for piezoelectric as well as linear magneto-electric and piezomagnetic coupling.

3.4 Magnetic structure of $\text{Ba}_3\text{NdFe}_3\text{Si}_2\text{O}_{14}$ (U. Staub)

The study of the magnetic structure of $\text{Ba}_3\text{NdFe}_3\text{Si}_2\text{O}_{14}$ was motivated by this material being a candidate for a new mechanism leading to magnetically-induced multiferroicity. This Langanite crystallizes in the chiral $P321$ non-centrosymmetric trigonal space group, lacking inversion symmetry, and orders antiferromagnetically at $T_N = 27$ K. The moments lie in the ab -planes at 120 degree from each other within each triangle. Along the c -axis, the spins rotate to form helices with a periodicity of 7 lattice parameters. We have performed first resonant soft X-ray diffraction experiments at the Fe $L_{2,3}$ edges on this material. We were able to detect $(0, 0, \tau)$, $(0, 0, 2\tau)$, $(0, 0, 3\tau)$ and $(0, 0, 4\tau)$ reflections, with $\tau = 1/7$. The first reflection is of magnetic origin, but expected to be absent from the recent proposed magnetic structure determined by neutron diffraction. It is likely caused by a small deviation of the exact three fold symmetry along the Fe chains or by deviations from a perfect helical structure, with an additional moment component along the c -axis. The origin of the second order reflection, which exhibits a different temperature dependence, is caused by scattering from $\langle M^2 \rangle$. This quantity represents an electric quadrupole (“orbital”) induced by the easy axis of magnetization. It is related to the X-ray magnetic linear dichroism (XMLD) signal observed in collinear antiferromagnets. The exact origin of the two other reflections is presently under discussion and requires measurements of the energy dependence of the reflections with improved signal to noise ratio. Understanding their temper-

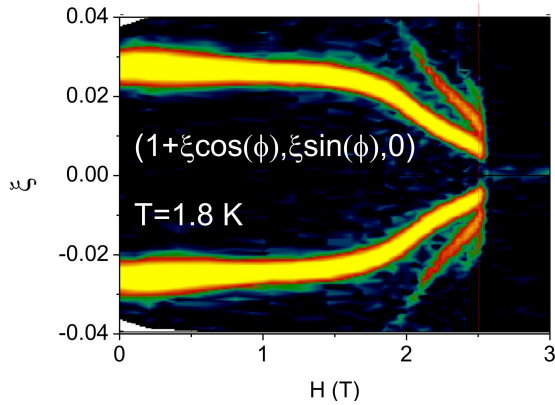


Figure 7: Magnetic elastic scattering in $\text{Ba}_2\text{CuGe}_2\text{O}_7$ as a function of field applied at an angle of 10° relative to the c -axis in the (b,c) -plane. The data were taken on the TASP spectrometer. Below $H = 1$ T the magnetic propagation vector continuously rotates in the tetragonal (a,b) -plane. Higher order satellites appearing near the incommensurate-to-commensurate transition at $H = 2.5$ T signal the formation of a “kink crystal”.

ature and energy dependence will help us to understand the deviation from the established magnet structure and its relation to the mechanism leading to magnetically-induced multi-ferroicity.

3.5 Novel incommensurate phase in $\text{Ba}_2\text{CuGe}_2\text{O}_7$ (A. Zheludev)

A novel incommensurate phase was discovered in $\text{Ba}_2\text{CuGe}_2\text{O}_7$, a tetragonal helimagnet with Dzyaloshinskii-Moriya interactions famous for undergoing interesting transformations in applied fields [18]. We have performed new neutron diffraction experiments paying particular attention to sample alignment, and we have studied the phase behavior in fields applied at an angle with respect to high-symmetry directions. In addition to the previously known commensurate and planar soliton-lattice phases, we have identified a novel antiferromagnetic cone state. Typical diffraction data are shown in Fig. 7.

4 Orbit, charge and spin degrees of freedom in cuprates

Orbital physics plays a profound role for many peculiar phenomena of transition metal oxides. The related material properties thereby originate from correlations and ordering phenomena of the orbital degree of freedom, as well as from the coupling with the spin, lattice and charge degrees of freedom. Cuprates, based on CuO_4 -plaquettes, the building blocks of the

high- T_c superconductors, are ideal model systems to study the interplay of these variables. Resonant X-ray diffraction (RXD) and the recently developed technique of resonant inelastic X-ray scattering (RIXS) provide the necessary experimental tools. This approach was the basis of substantial progress in the understanding of orbital phenomena this year.

4.1 Square-lattice cuprates such as $\text{Sr}_2\text{CuO}_2\text{Cl}_2$ (H. Rønnow)

Experiments on square-lattice cuprates such as $\text{Sr}_2\text{CuO}_2\text{Cl}_2$ enabled us to establish a 1-band Hubbard model that is globally consistent for the parent compounds as well as superconducting species. Measurements on $\text{Sr}_2\text{CuO}_2\text{Cl}_2$ revealed that nearest neighbor (NN) hopping in the 1-band Hubbard model was insufficient to describe the RIXS data (Fig. 8). A model including t , t' and t'' was projected onto a spin Hamiltonian for half-filling and the spin-wave dispersion derived. This model effectively fits $\text{Sr}_2\text{CuO}_2\text{Cl}_2$, La_2CuO_4 , BiSCCO, and YBCO, yielding U and t -values consistent with angle-resolved photoelectron spectroscopy (ARPES) and other electronic measurements. This new consistent effective model will allow quantitative analysis of details of the excitation spectra including multi-particle continua and the zone boundary quantum effect.

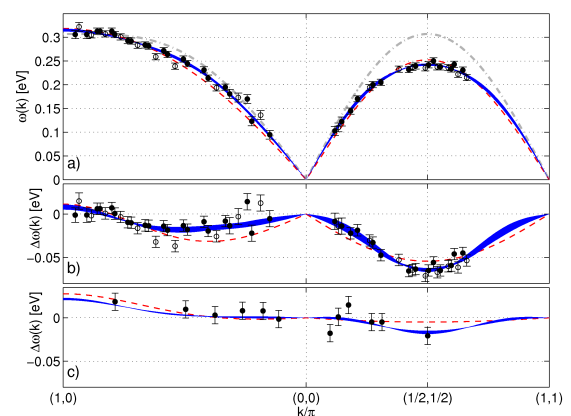


Figure 8: a) Magnon energies extracted from the RIXS data. Open and closed symbols stem from 2 independent measurements on different samples. Dot-dashed line is a nearest neighbor (NN) Heisenberg model with $J = 130$ meV. Red dashed line is a NN Hubbard model fit for $t = 0.261 \pm 0.004$ eV and $U = 1.59 \pm 0.04$ eV. Blue lines are the further neighbor Hubbard fits. b) same as a) with NN Heisenberg dispersion subtracted to better visualize details of the dispersion. The blue band shows the spread in dispersions obtained for fits with 1.9 eV $< U < 4$ eV. c) Fit to the neutron data on La_2CuO_4 .

4.2 The quasi-one-dimensional cuprate Li_2CuO_2 (U. Staub)

The quasi-one-dimensional cuprate Li_2CuO_2 is a prototype edge-sharing chain compound. The Cu^{2+} ions in this strongly correlated material give rise to one spin- $\frac{1}{2}$ per CuO_4 plaquette with a nearest neighbor Cu-O-Cu bond angle close to 90° , implying weak superexchange coupling between Cu spins. As a result, nearest neighbor ferromagnetic and next nearest neighbor antiferromagnetic superexchanges compete within the chains. Below $T_N \sim 9$ K spins order antiferromagnetically between the chains and ferromagnetically in the chains. O K -edge RIXS spectra display a complicated interplay of low-energy excitations from charge, orbital and lattice degrees of freedom. We analyzed in detail non-local charge transfer excitations in terms of Zhang-Rice singlet (ZRS) and triplet (ZRT) excitations, which can be reached in the final state of O K -edge RIXS. The occurrence of these ZRS and ZRT excitations depends on the alignment of the adjacent spins of neighboring plaquettes and allows to directly probe the local magnetic order. Fig. 9a and b displays the O K -RIXS data with orbital, ZRS and ZRT excitations around -2 eV, -3.2 eV and -3.9 eV energy loss, respectively. Temperature dependent measurements depicted in Fig. 9c and d evidence clear opposite temperature behavior for the ZRS and ZRT spectral components, in good agreement with optical conductivity calculations. This establishes RIXS as a sensitive probe of the short range spin order.

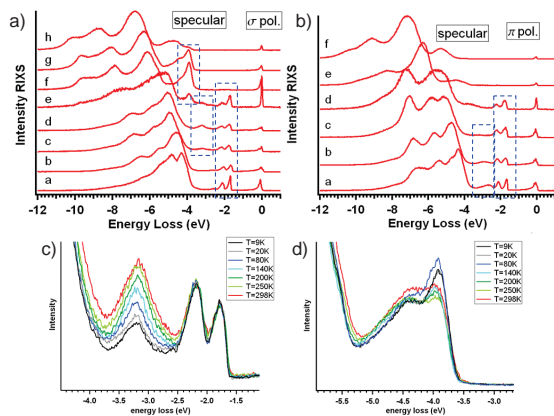


Figure 9: RIXS spectra at O K -edge of Li_2CuO_2 for (a) σ and (b) π polarizations. Temperature dependence of (c) the ZRS and of (d) the ZRT features (with σ polarization).

4.3 Sr_2CuO_3 , a quasi-one-dimensional corner-sharing single-chain compound (U. Staub)

Sr_2CuO_3 is a quasi-one-dimensional corner-sharing single-chain compound possessing the nearly ideal properties of the one-dimensional antiferromagnetic Heisenberg spin- $\frac{1}{2}$ model. The momentum transfer dispersion of the Cu L_3 -RIXS signal in Sr_2CuO_3 along the chain direction reveals that the main spectral weight follows the lower onset of the two-spinon (and higher order) continuum and probes the dynamical spin-structure factor. The line shape is analyzed within the Bethe Ansatz. The modes within the orbital excitation energy range show that the dd excitations in Sr_2CuO_3 are momentum dispersive and may be associated with orbitons, i.e. dispersive orbital excitations mediated by the superexchange interactions. A spin-orbital superexchange model reproduces this orbiton dispersion and explains the large dispersion with decoupling of the orbital and spin degrees of freedom in this one-dimensional system.

4.4 Observation of orbital currents in CuO

Observation of orbital currents in CuO was one of the breakthrough results in our study of orbital phenomena. Recently magneto-electric scattering in GaFeO_3 provided evidence for the occurrence of magneto-electric quadrupole and possibly magnetic charge [9, 10]. Our experiments, here reported, provide the first clear evidence for the existence of orbital currents through the observation of E1-M1 (or E1-E2) XRD at the Cu $L_{2,3}$ -edges in CuO and open the way to test for the existence of orbital currents in cuprates and multiferroics.

Fig. 10A shows the resonance enhancement at the copper $L_{2,3}$ -edges of the superlattice reflection $(1/2, 0, -1/2)$ associated with the antiferromagnetic motif of the copper magnetic moments. Its dependence on the helicity of the X-rays are illustrated in Fig. 10. The diffracted intensity around the L_3 -edge for left and right handed polarization is different for two different azimuthal angles. This dependence *cannot* be described by the collinear antiferromagnetic order determined by neutron experiments alone, because in this case the intensity *does not* depend on the helicity of the X-rays. This dependence is caused by the interference of an additional component with the resonant magnetic signal from the collinear antiferromagnetic order. This component comes via a magnetic dipole transition M1 resulting from the presence, on the microscopic level, of orbital currents.

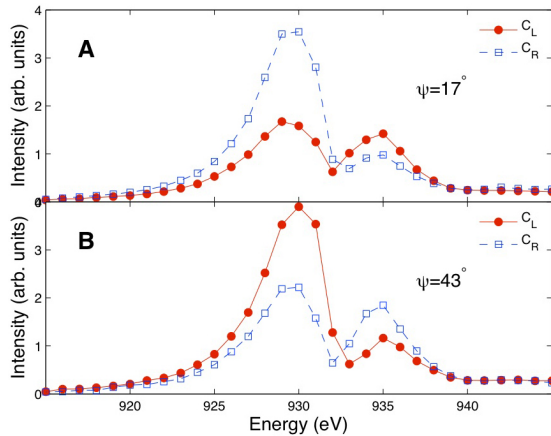


Figure 10: Resonant enhancement of the $(1/2, 0, -1/2)$ superlattice reflection at the Cu $L_{3,2}$ edges as a function of the helicity of the incident X-rays for two chosen azimuthal angles ψ . Panel A corresponds to $\psi = 17^\circ$ and panel B to $\psi = 43^\circ$. Intensities gathered with incident left C_L (right C_R) circularly polarized X-rays are in closed (open) symbols. Data were collected at 100 K.

Our model makes it possible to extract quantitative information about the circulating direction of the orbital currents. For illustrative purpose, it is easier to visualize the direction of the toroidal moments associated with such currents. A toroidal moment Ω associated with an orbital moment L or a spin S is proportional to $\langle \mathbf{R} \times \mathbf{L} \rangle$ or $\langle \mathbf{R} \times \mathbf{S} \rangle$, respectively. Fig. 11A illustrates (in the simplest case) the relation between the orbital currents and the toroidal moment associated with a single

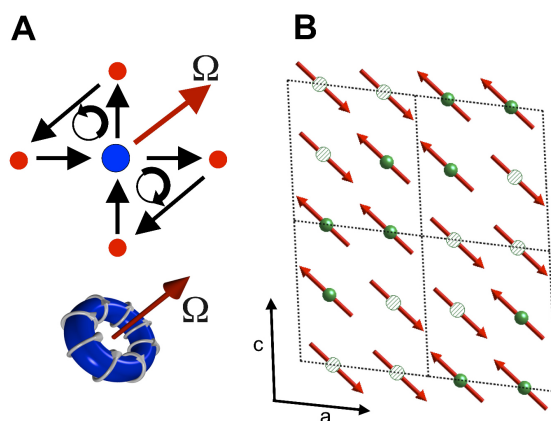


Figure 11: A. Pictorial representation of the relationship between the orbital currents flowing between the copper (blue circle) and oxygen (red circle) atoms and the toroidal moment (red arrow). B. Antiferromagnetic-type ordering of the toroidal moments associated with the orbital currents. The orientation of the toroidal moments follows the value of the irreducible tensors obtained from experimental data.

copper-oxygen plaquette. Fig. 11B shows the ordering pattern of the toroidal moments in the extended magnetic unit cell as determined from our model. They lie in the a, c -plane and they share the same antiferromagnetic pattern of the magnetic moments. The importance of our observations is that it represents the direct evidence of antiferromagnetic ordering of toroidal moments or orbital currents in a material. In this respect, the observation of orbital currents in CuO, the basic building block of cuprate superconductors, provides strong encouragement for models based on orbital current ordering and related phenomena in high- T_c cuprates.

5 Quenched disorder

A strong new thrust in our research this year was aimed at the study of low-dimensional quantum magnetic materials with quenched disorder. Such disorder leads to a localization of quasi-particles and gives rise to quantitatively new thermodynamic phases and behavior. These effects are strongest in low dimensions and in the vicinity of quantum critical points. We have primarily addressed the problem experimentally, in several gapless and gapped $S = \frac{1}{2}$ quantum magnets.

5.1 Local distribution of relaxations in a random Heisenberg chain (*H.-R. Ott*)

A local distribution of relaxations in a random Heisenberg chain was revealed by NMR experiments. Since the original ideas of C. Dasp Gupta and S.-K. Ma in 1979 [19] and the subsequent extension by D. Fisher [20], the real-space renormalization group theory is considered as a general theoretical tool for understanding the low-energy features of *disordered quantum magnets*. Only a few experimental

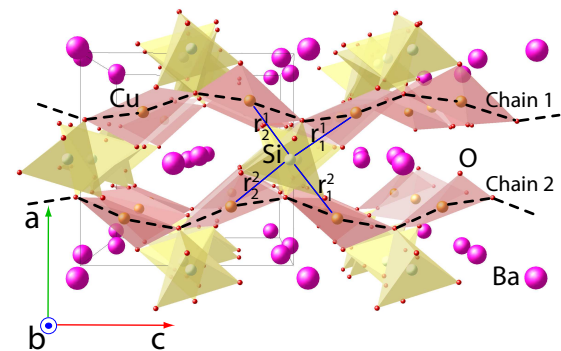


Figure 12: Crystal structure of $BaCu_2Si_2O_7$ emphasizing the copper chains (dashed lines) and the NN configuration of the silicon atoms.

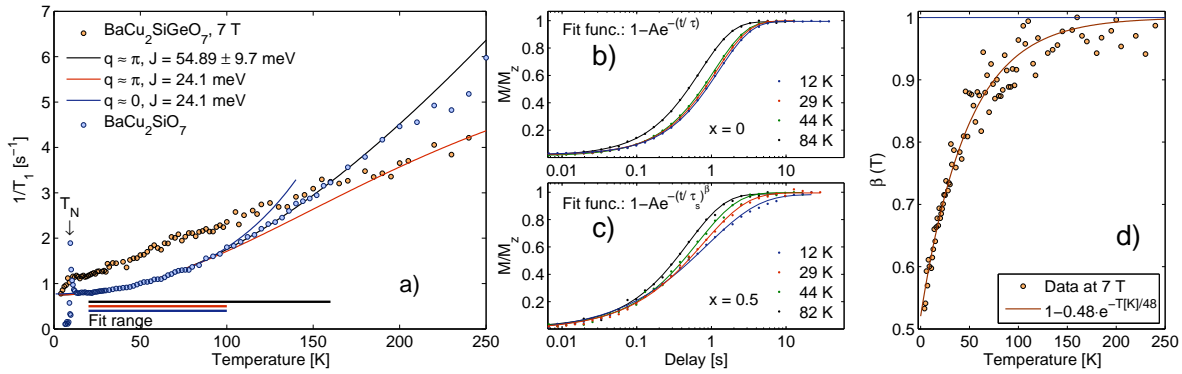


Figure 13: ^{29}Si NMR spin-lattice relaxation data of $\text{BaCu}_2(\text{Si}_{1-x}\text{Ge}_x)_2\text{O}_7$ for $x = 0$ and $x = 0.5$ (no and maximum randomness, respectively). a) Relaxation rates for both cases, b) and c) recovery of magnetization, d) T -dependence of β for $x = 0.5$. The symbols are explained in the panels.

tests of these theories have been reported, especially if studies addressing the low-energy dynamical properties are considered.

In the present work, we have chosen ^{29}Si nuclear magnetic resonance (NMR) and magnetometry measurements to study the compound $\text{BaCu}_2(\text{Si}_{1-x}\text{Ge}_x)_2\text{O}_7$. This system is an excellent realization of a 1D random antiferromagnetic Heisenberg spin-chain (RHC), where random variations of the exchange-coupling constant between spin-sites are a consequence of the different Si and Ge covalent radii. Its structure, shown in Fig. 12, is the same for $0 < x < 1$. NMR probes energy transfers of the order of μeV , providing unique access to the low-energy/long-time scales. In this case, it is a more appropriate technique than standard methods, such as inelastic neutron scattering.

Our main results, summarized in Fig. 13, deal mainly with the spin-lattice relaxation rates T_1^{-1} , which reflect essentially the dynamics of the electron spins as sensed (via the hyperfine coupling) by the nuclei.

The data shown in Fig. 13a for single-crystal samples of pure Si ($x = 0$) and SiGe ($x = 0.5$) compounds, corresponding to no and to full randomness, respectively, indicate clearly and unambiguously the implications of randomness by simple comparison. The pure compound (Fig. 13b) shows a simple exponential relaxation, while the fully random SiGe case (Fig. 13c) displays a *stretched* exponential behavior (most pronounced at low temperatures), indicative of widely distributed relaxation rates T_1^{-1} . It is exactly this *distribution* of relaxation rates which is highly suggestive of the formation of random-singlet states in this class of materials, a cornerstone of the RHC theory. This conclusion is further supported by temperature and field-dependent magneti-

zation measurements [11]. From analyzes of the temperature dependence of the stretched-exponential β factor, shown in Fig. 13d, one can obtain the probability distribution of the NMR relaxation times. The resulting low- T broadening of the relaxations' distribution is a consequence of the low- T inequivalence of spin-sites due to randomness.

The distribution of magnetic relaxation rates vs temperature reported in this work suggests that NMR may successfully be applied to other disordered magnets, thus prompting new theoretical models for interpreting the predicted universal behavior.

5.2 Effect of disorder on weakly coupled $S = \frac{1}{2}$ chains (A. Zheludev)

The effect of disorder on weakly coupled $S = \frac{1}{2}$ chains $\text{Cu}(\text{py})_2(\text{Cl}_{1-x}\text{Br}_x)_2$ was studied with muon-spin relaxation (μSR) spectroscopy. The model compound is a well-known $S = \frac{1}{2}$ spin-chains system with $J = 26$ K. Due to weak interchain interactions, it actually orders at 1.3 K. We have found that the Br version of this material has a similar structure, $J = 46$ K, but orders at a lower temperature of 0.7 K. Having synthesized a series of samples with different Br/Cl ratios, we have employed μSR to probe ordering in disordered chains. From the relaxation curves shown in Fig. 14, one can deduce that, even for $x = 0.01$, the low-temperature phase is highly inhomogeneous, and may in fact be a glassy state. Further systematic studies will cover a wide range of concentrations and employ bulk and neutron scattering measurements.

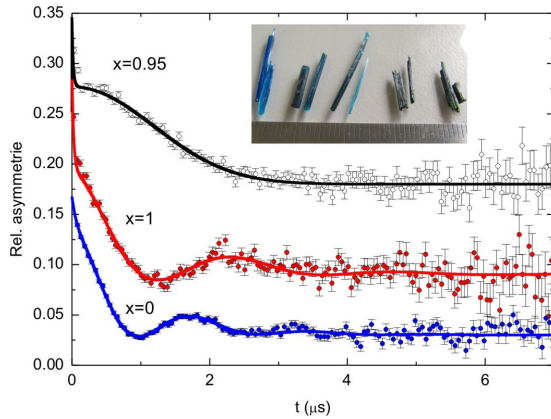


Figure 14: Muon-spin relaxation measured in $\text{Cu}(\text{py})_2(\text{Cl}_{1-x}\text{Br}_x)_2$ for $x = 0, 1$ and 0.95 . Inset: typical samples used in these studies.

5.3 Effect of disorder on a quasi-2D spin-liquid (A. Zheludev)

The effect of disorder on a quasi-2D spin-liquid was studied in $(\text{C}_4\text{H}_{12}\text{N}_2)\text{Cu}_2(\text{Cl}_{1-x}\text{Br}_x)_6$. The parent compound is a well-studied $S = \frac{1}{2}$ quasi-2D quantum spin-liquid [21]. In a magnetic field of $H_c = 7.5$ T, it undergoes 3D ordering via a Bose-Einstein condensation of magnons. Up to $x \sim 0.1$, $(\text{C}_4\text{H}_{12}\text{N}_2)\text{Cu}_2(\text{Cl}_{1-x}\text{Br}_x)_6$ retains the original crystal structure, but the high-field transition becomes considerably broadened (Fig. 15) and field-induced long-range order is suppressed. Disorder also has a profound effect on electron-spin resonance (ESR) spectra, particularly on the intratriplet transition lines. These experiments are currently underway. Large deuterated single-crystals (Fig. 15, inset) are also being readied for neutron experiments.

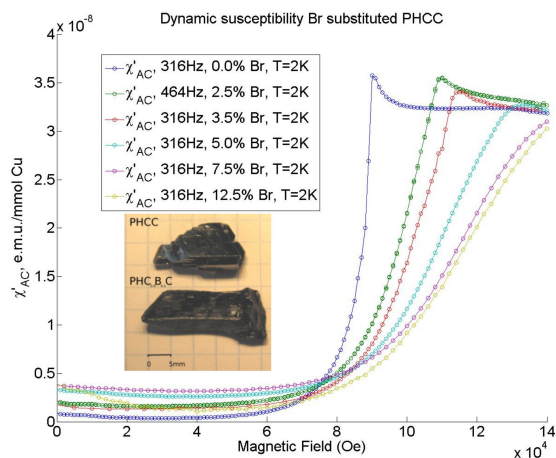


Figure 15: High-field magnetic susceptibility measured in $(\text{C}_4\text{H}_{12}\text{N}_2)\text{Cu}_2\text{Cl}_6$ with different disorder strengths. Inset: deuterated crystals for neutron spectroscopy.

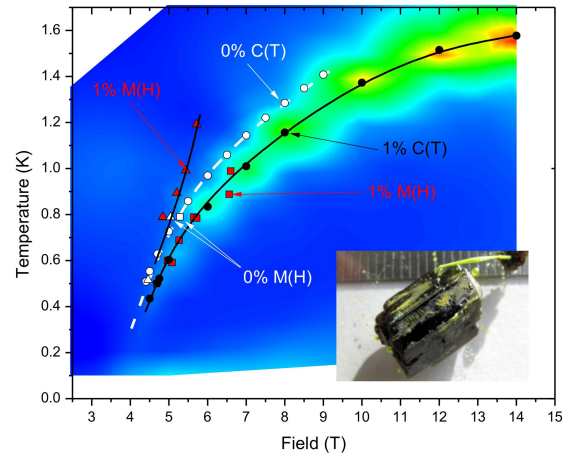


Figure 16: False-color representation of magnetic specific heat measured in $\text{Sul-Cu}_2(\text{Cl}_{1-x}\text{Br}_x)_4$ for $x = 0.01$. Solid black lines indicate the characteristic fields of spin gap closure and onset of static short-range order. The inset shows a 1 g deuterated crystal for neutron studies.

5.4 The frustrated spin-ladder $\text{Sul-Cu}_2(\text{Cl}_{1-x}\text{Br}_x)_4$ (A. Zheludev)

The frustrated spin-ladder $\text{Sul-Cu}_2(\text{Cl}_{1-x}\text{Br}_x)_4$ shows superficially similar behavior, but is considerably more sensitive to even very low concentrations of Br substitutions. The field-induced ordering transition in the pure system produces an incommensurate chiral helimagnetic state [22]. Bulk measurements on the $x = 0.01$ material show that even though gap closure is not much affected, the long-range ordered state is totally suppressed (Fig. 16). In its place one finds a short-range ordered phase, similar to that in the random-field model. It can be explained by the mismatch in the periodicities of short-range helimagnetic spin correlations in individual ladders, a unique feature of this incommensurate system.

6 Algorithmic developments

In parallel to the theoretical investigation of models in the context of specific problems or materials, we have continued to develop numerical tools that can be used in the context of quantum magnetism.

6.1 Tensor network methods (M. Troyer)

We have improved new two-dimensional generalizations of the density matrix renormalization group method, especially the infinite system PEPS (projected entangled-pair states) method [23]. The main achievements of the last year were the implementation of abelian [12]

symmetries in these algorithms, and the development of tensor network algorithms for quantum magnets built from non-Abelian anyons instead of standard SU(2) spins [13].

6.2 ALPS 2.0 (M. Troyer)

We have developed and published a major new version of the ALPS libraries and applications [14]. These developments are described in more details in Project 5, paragraph 8.1.

7 Collaborative efforts

An active collaboration between theorists and experimentalists is a key element of the current project and was highlighted last year. This year, however, was marked by an even tighter collaboration on the experimental side. The key vehicle for this collaboration was an exchange of samples between groups that specialize on different experimental methods. It resulted in a very efficient utilization of infrastructure and expertise, as well as in a fruitful exchange of ideas between groups. Our activities took full advantage of the newly introduced mechanism of so-called collaborative projects within MANEP. Their purpose is to facilitate interactions between groups at different institutions aiming at specific target tasks. Four such projects were initiated this year in the field covered by Project 6: 1. High Pressure Phases in Pure and Doped Quantum Antiferromagnets, 2. Excitations of the Orbital and Spin Degree of Freedom in Quasi-One-Dimensional Cuprates and Multiferroic Materials, 3. One-Dimensional Quantum Magnets with Bond Randomness: μ SR and Neutron Scattering, and 4. Numerical Simulations of Frustrated Correlated Systems. Although all of these targeted projects are in their early stages, they have already yielded important results that are incorporated in the report above. This early success stems from the fact that these projects did not appear out of a vacuum, but are a natural extension to budding collaborative efforts that emerged within Project 6 last year.

MaNEP-related publications

- ▶ [1] P. Bouillot, K. Corinna, A. M. Läuchli, M. Zvonarev, B. Thielemann, C. Rüegg, E. Orignac, R. Citro, M. Horvatić, C. Berthier, M. Klanjšek, , and T. Giamarchi, *Physical Review B* **83**, 054407 (2011).
- ▶ [2] F. Casola, T. Shiroka, S. Wang, K. Conder, E. Pomjakushina, J. Mesot, and H.-R. Ott, *Physical Review Letters* **105**, 067203 (2010).
- ▶ [3] S. Wang, E. Pomjakushina, T. Shiroka, G. Deng, N. Nikseresht, C. Rüegg, H. M. Rønnow, and K. Conder, *Journal of Crystal Growth* **313**, 51 (2010).
- [4] T. Hong, R. Custelcean, B. C. Sales, B. Roesli, D. K. Singh, and A. Zheludev, *Physical Review B* **80**, 132404 (2009).
- [5] B. Náfrádi, T. Keller, H. Manaka, A. Zheludev, and B. Keimer, arXiv:1102.0214 (2011).
- ▶ [6] K.-Y. Yang, K. Huang, W.-Q. Chen, T. M. Rice, and F.-C. Zhang, *Physical Review Letters* **105**, 167004 (2010).
- ▶ [7] T. Coletta, J.-D. Picon, S. Korshunov, and F. Mila, *Physical Review B* **83**, 054402 (2011).
- [8] M. Belesi, I. Rousochatzakis, H. C. Wu, H. Berger, I. V. Shvets, F. Mila, and J. P. Ansermet, *Physical Review B* **82**, 094422 (2010).
- ▶ [9] U. Staub, Y. Bodenthin, C. Piamonteze, S. P. Collins, S. Koohpayeh, D. Fort, and S. W. Lovesey, *Physical Review B* **82**, 104411 (2010).
- [10] U. Staub, Y. Bodenthin, C. Piamonteze, M. García-Fernández, V. Scagnoli, M. Garganourakis, S. Koohpayeh, D. Fort, and S. W. Lovesey, *Physical Review B* **80**, 140410 (2009).
- ▶ [11] T. Shiroka, F. Casola, V. Glazkov, A. Zheludev, K. Prša, H.-R. Ott, and J. Mesot, arXiv:1012.0731 (2011).
- ▶ [12] B. Bauer, P. Corboz, R. Orús, and M. Troyer, *Physical Review B* **83**, 125106 (2011).
- [13] R. N. C. Pfeifer, P. Corboz, O. Buerschaper, M. Aguado, M. Troyer, and G. Vidal, *Physical Review B* **82**, 115126 (2010).
- ▶ [14] B. Bauer, L. D. Carr, A. Feiguin, J. Freire, S. Fuchs, L. Gamper, J. Gukelberger, E. Gull, S. Guertler, A. Hehn, R. Igarashi, S. V. Isakov, D. Koop, P. N. Ma, P. Mates, H. Matsuo, O. Parcollet, G. Pawłowski, J. D. Picon, L. Pollet, E. Santos, V. W. Scarola, U. Schollwöck, C. Silva, B. Surer, S. Todo, S. Trebst, M. Troyer, M. L. Wall, P. Werner, and S. Wessel, arxiv:1101.2646 (2011).

Other references

- [15] T. Hong, Y. H. Kim, C. Hotta, Y. Takano, G. Tremelling, M. M. Turnbull, C. P. Landee, H.-J. Kang, N. B. Christensen, K. Lefmann, K. P. Schmidt, G. S. Uhrig, and C. Broholm, *Physical Review Letters* **105**, 137207 (2010).
- [16] F. Mila, *The European Physical Journal B* **6**, 201 (1998).
- [17] G. Chaboussant, M.-H. Julien, Y. Fagot-Revurat, M. Hanson, L. P. Lévy, C. Berthier, M. Horvatić, and O. Piovesana, *The European Physical Journal B* **6**, 167 (1998).
- [18] A. Zheludev, S. Maslov, I. Tsukada, I. Zaliznyak, L. Regnault, T. Masuda, K. Uchinokura, R. Erwin, and G. Shirane, *Physical Review Letters* **81**, 5410 (1998).
- [19] C. Dasgupta and S.-K. Ma, *Physical Review B* **22**, 1305 (1979).
- [20] D. S. Fisher, *Physical Review B* **50**, 3799 (1994).
- [21] M. B. Stone, C. Broholm, D. H. Reich, P. Schiffer, O. Tchernyshyov, P. Vorderwisch, and N. Harrison, *New Journal of Physics* **9**, 31 (2007).
- [22] V. O. Garlea, A. Zheludev, K. Habicht, M. Meissner, B. Grenier, L.-P. Regnault, and E. Ressouche, *Physical Review B* **79**, 060404(R) (2009).
- [23] J. Jordan, R. Orús, G. Vidal, F. Verstraete, and J. I. Cirac, *Physical Review Letters* **101**, 250602 (2008).

Project **7****Electronic materials with reduced dimensionality**

Project leader: L. Forró (EPFL)

Participating members: Ph. Aebi (UniFR), L. Degiorgi (ETHZ), L. Forró (EPFL), T. Giamarchi (UniGE), M. Grioni (EPFL)

Summary and highlights: The program of the project is to study various electronic instabilities in low-dimensional materials and their competition in stabilizing the ground state of the system. This year the highlight was on dichalcogenides: in $1T$ -TiSe₂ the fingerprints of an excitonic condensate were searched; in $2H$ -NbS₂, the intercalation of a triangular Cobalt lattice drastically changes the electronic structure within the NbS₂ plane and with hydrostatic pressure it changes according to the Doniach phase diagram. Further studies within the project give important contributions to the physics of heavy earth tri-tellurides, to iron-based superconductors, to one-dimensional Vanadium chain conductor and to the orbital currents in ladders.

1 Dramatic effective mass reduction in $1T$ -TiSe₂ (P. Aebi)

1.1 Introduction

In the early 1960s, a new insulating phase was predicted to possibly exist at low temperature in solids having small energy gaps. Jérôme *et al.* [9] published an extended study of this phase developing a BCS-like theory of its ground state. However, at that time, an experimental realization of this phase was missing.

The excitonic insulator phase may occur in a semi-metallic or semiconducting system exhibiting a small (negative, respectively positive) gap. Indeed, for a low carrier density, the Coulomb interaction is weakly screened, allowing therefore bound states of holes and electrons, called excitons, to build up in the system. If the binding energy E_B of such pairs is larger than the gap E_G , the energy to create an exciton becomes negative, so that the ground state of the normal phase becomes unstable with respect to the spontaneous formation of excitons. According to Jérôme *et al.* [9], at low temperature, these excitons may condense into a macroscopic coherent state in a manner similar to Cooper pairs in conventional BCS superconductors. Kohn [10] argued that exciton condensation may lead to the formation of charge density waves (CDW) of purely electronic origin (neglecting any lattice distortion), characterized by an order parameter.

$1T$ -TiSe₂ is a layered transition-metal dichalcogenide exhibiting a commensurate ($2 \times 2 \times 2$) CDW [11] accompanied by a periodic lattice distortion below the transition temperature of $T_c \cong 200$ K. The origin of its CDW phase was controversial for a long time. Different scenar-

ios have been proposed, the best candidates being a band Jahn-Teller effect [12] and the excitonic insulator phase [13, 14]. An angle-resolved photoemission spectroscopy (ARPES) study, evidencing directly the CDW, gave recently much support to the latter by comparison between experiment and theory [1]. Photoemission intensity maps were generated with the spectral function calculated in the framework of the excitonic insulator phase model, which has been adapted to TiSe₂ and renamed the exciton condensate phase model [2].

1.2 Results: temperature dependence and effective mass reduction

Since experiments that would directly prove the existence of an exciton condensate are missing, we pursue the detailed comparison of ARPES experiments with the exciton condensate phase model to verify how far the model agrees with experiment [3]. Fig. 1 shows an unexpected temperature dependence of the Ti $3d$ related elliptically shaped electron pocket, centered at the L point of the Brillouin zone, measured along the long (left panels) and short axis (right panels) [4].

At 288 K, the conduction band follows a clear and wide parabolic dispersion along AL (left panel), with a non-trivial spectral weight distribution that can be understood within the exciton condensate phase model extended to the strong electron-hole fluctuation regime. As the temperature decreases to 141 K, the conduction band gets flatter along AL (left panel). The top of the known, backfolded valence band is also clearly visible below a binding energy

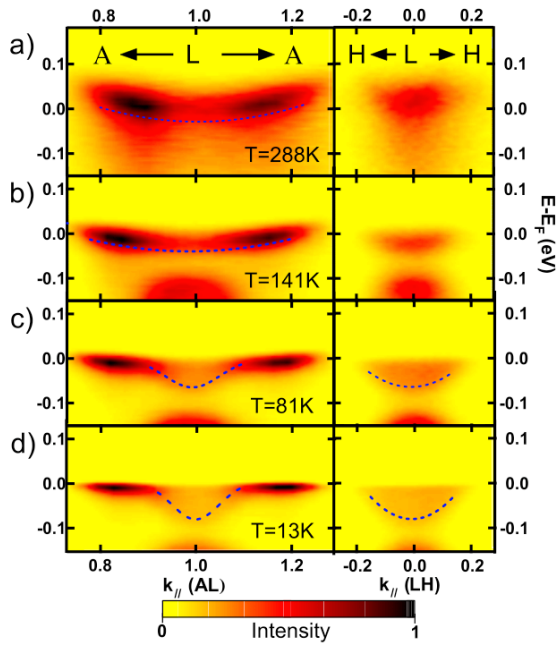


Figure 1: Photoemission intensity maps of the electron pocket around L . (a), (b), (c), (d) Measurements along AL (left panels) and LH (right panels) at 288 K, 141 K, 81 K and 13 K, respectively.

of -0.1 eV. Below 100 K, a dramatic renormalization of the conduction band is visible, as seen in the photoemission intensity maps measured at 81 K and 13 K in Fig. 1c and d. Along AL (left panels), it has no more a simple parabolic shape and divides into different parts. Its branches closer to E_F are getting flatter (heavy part), while it displays a pronounced parabolic dispersion (light part) in the neighborhood of its minimum. The observation of such an effective mass reduction (light part) is surprising for a material with strong interactions.

The origin of the considerable renormalization of the conduction band can be understood in the framework of the exciton condensate phase model. In this model, the electron-hole interaction, responsible for the formation of excitons, couples the three conduction bands to the valence band, so that, in the CDW phase, many backfolded bands appear at L , giving rise to a complicated band structure.

In our calculations, the ratio of the effective masses in the absence of renormalization effects plays an essential role in this mass renormalization at lower temperatures. The larger the anisotropy of the electron pocket, the stronger the renormalization effect and thus the lower the effective mass.

The dramatic renormalization gives an indication towards the understanding of the decrease of resistivity at low temperature: in the frame-

work of the Drude formula, a reduced effective mass leads to a reduced resistivity. However, more complicated calculations using, e.g., the Boltzmann equation in the framework of the exciton condensate phase should be carried out to get a full understanding. Furthermore, the complete geometry of the Fermi surface (with electron pockets having different orientations) must be taken into account.

2 High pressure study of transport properties in $\text{Co}_{1/3}\text{NbS}_2$ (L. Forró)

The interest in layered electronic materials is fueled by their capability to host peculiar electronic phases. Among them, transition metal dichalcogenides (TMD) — of general formula TX_2 , where T = transition element and X = S, Se, Te — are well known as the material where charge density waves, superconductivity, metallic and excitonic phases compete for the ground state [15]. The magnetic ordering, related to ions intercalated in between TMD layers coupled by the van der Waals forces, has also attracted great interest in the past. $M_{1/3}\text{TX}_2$ (M = Co, Fe, Ni, Mn) compounds were of a particular interest because the magnetic ions in their layers form a triangular lattice, which is known to be prone to frustration. Experimentally, several types of magnetic orderings were found in these materials, thought to be driven by competing interactions [16].

The sensitivity of the electronic properties of TMD to pressure in general is well known. We have studied the effect of pressure on transport properties of $\text{Co}_{1/3}\text{NbS}_2$ (Fig. 2), which is known to order magnetically at 26 K at ambient pressure [16].

Our measurements of the temperature and

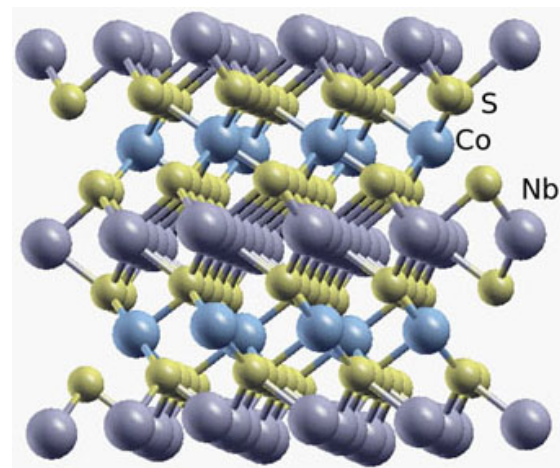


Figure 2: Sketch of the crystal structure of $\text{Co}_{1/3}\text{NbS}_2$.

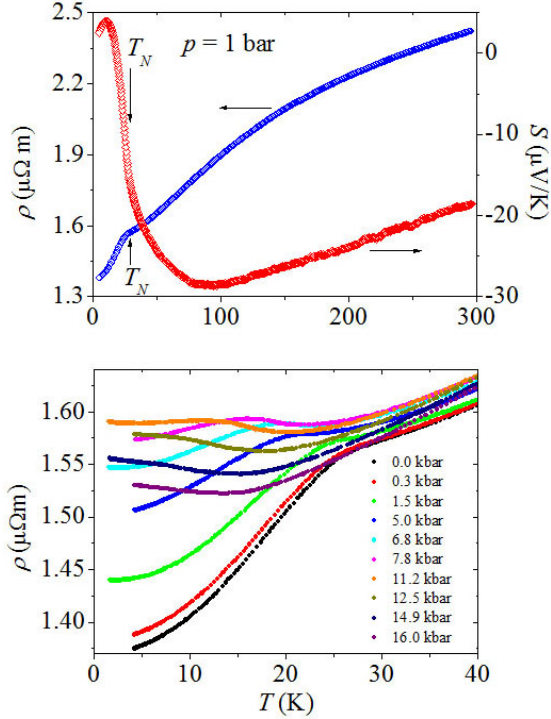


Figure 3: Upper panel: temperature dependence of the ambient pressure dc resistivity, $\rho(T)$, and thermoelectric power, $S(T)$, of $\text{Co}_{1/3}\text{NbS}_2$. The temperature T_N , at which antiferromagnetic ordering sets in, is marked by an arrow. Lower panel: pressure dependence of the low-temperature dc resistivity.

pressure dependence of the transport properties of $\text{Co}_{1/3}\text{NbS}_2$ reveal unexpected effects [5], particularly regarding the behavior of the pressurized system near the magnetic ordering temperature (Fig. 3). The explanation of the observed effects is primarily due to the pressure-induced change of the coupling of Co spin-state to conducting electrons. Our results indicate that the pressure in $x = 1/3$ compound touches the delicate balance between magnetic interaction and spin-states. This motivates further experimental work, to probe more directly the spin- and charge-states in pressurized system. Furthermore, a detailed theoretical work is required to determine the precise band structure which could reveal the role of the possible RKKY interaction. Beyond the dc resistivity the measurements of thermoelectric power helped to establish the $p - T$ phase diagram [5]. From the measurements of the thermal conductivity, it follows that the transition at 26 K is not related to structural ordering of Co. Rather complicated pressure dependences of the dc resistivity and thermoelectric power indicate the presence of competing interactions in the system, while the opposite signs of S and the Hall effect point to a subtle topology of the Fermi

surface consisting of several parts with different dispersions.

3 ARPES of 2D and 1D materials (M. Gri- oni)

3.1 Fe-based chalcogenide superconductors

The recent discovery of superconductivity in some iron-based pnictide and chalcogenide materials at temperatures exceeding the critical temperatures of conventional superconductors has stimulated a flurry of activities [17, 18] only comparable with the aftermath of the two-decade old discovery of the cuprates. Remarkably, the cuprate and Fe-based superconductors indeed display intriguing similarities, besides the large critical temperatures. In both cases, superconductivity is believed to be rooted in weakly coupled two-dimensional layers with square lattice structures, and it emerges from another broken symmetry phase: an antiferromagnetic Mott-insulator in the former, and an antiferromagnetic metal in the latter. The pervasive presence of magnetism has similarly led to speculations that magnetic fluctuations could even provide the glue for the formation of the unconventional superconducting state. The analysis of the similarities and, perhaps more importantly, of the differences in the electronic properties of these two classes of materials could yield new important elements to unravel the mystery of high-temperature superconductivity.

One important difference is the multi-orbital character of the Fe $3d$ states as opposed to the single Cu $3d$ orbital at the origin of the electronic structure of the cuprates. As a consequence, the Fe compounds exhibit a more complex Fermi surface (FS), with multi-sheet hole and electron pockets coexisting in different parts of the Brillouin zone (BZ). A detailed knowledge of the topology and shape of the FS, and of possible nesting conditions that may lead to instabilities like a spin-density wave, is of crucial importance. High-resolution angle-resolved photoelectron spectroscopy (ARPES) can provide this information. The EPFL electron spectroscopy group of Griani has performed ARPES experiments on compounds of the $\text{Fe}_y\text{Se}_x\text{Te}_{1-x}$ family, with high-quality single-crystal samples grown by the MaNEP group of E. Giannini (UniGE). Fig. 4 shows high-resolution data for a superconducting $x = 0.32$, $y = 1.013$ sample ($T_c = 13$ K) measured at 10 K with 50 eV photons, along the ΓM high-symmetry line of the BZ, at the SIS beamline of the Swiss Light Source (with Dr. M. Shi). The ARPES intensity maps of the

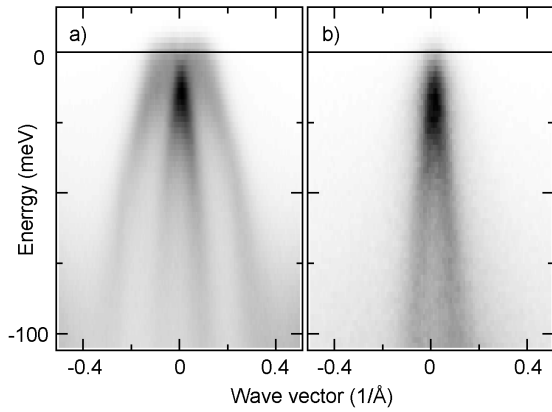


Figure 4: $Fe_{1.013}Se_{0.32}Te_{0.68}$: ARPES intensity maps measured at 10 K and 50 eV, with circularly (a) and π linearly polarized photons (b).

(a) and (b) panels of Fig. 4 have been collected with circularly and, respectively, linearly polarized light in π geometry. They outline the so-called $\alpha 1$ and $\alpha 2$ bands, which form small hole pockets around the Γ point. These bands can be disentangled according to their reflection symmetry exploiting the ARPES selection rules. Namely, only the $\alpha 1$ band, which is even in character, is visible when the even π geometry is used (Fig. 4b). Further measurements at various photon energies show that the Fermi level crossing of these bands, and therefore the size of the hole pockets, varies with the perpendicular wave vector k_z . Such modulation of the FS reveals that the transverse coupling between the square-lattice planes is substantially larger in the Fe chalcogenides than in the case of the cuprates.

3.2 $BaVS_3$, a quasi-one-dimensional conductor

$BaVS_3$ is a rather unique quasi-one-dimensional material, which has been investigated within MaNEP by various complementary techniques to clarify its electronic and magnetic properties. Its structure, based on infinite parallel chains of face-sharing VS_6 octahedra, has a clear 1D character. From a simple picture of the electronic structure, each V^{4+} ions should contribute a single $3d$ electron to a broad, partially filled, 1D $3d_{z^2}$ band dispersing along the chains. On the other hand, the small (~ 4) anisotropy of the electrical resistivity indicates that transverse coupling is certainly relevant, and that other orbitals must be involved, possibly yielding a complex multi-sheet Fermi surface. This is confirmed by recent first-principles calculations of the electronic structure, which also underline the importance of correlations [19]. This complex-

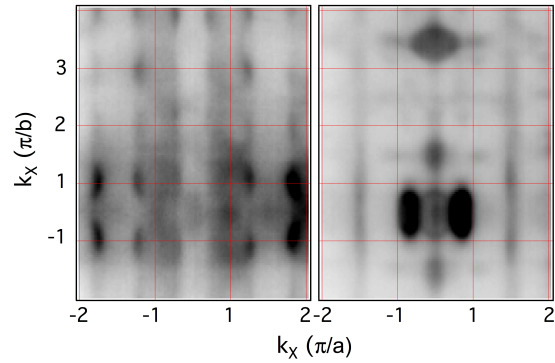


Figure 5: ARPES constant energy cuts of $BaVS_3$ measured at 80 K and 156 eV at the Fermi level (a) and at 1 eV binding energy (b).

ity is reflected in the successive structural and electronic instabilities which bring the system from a bad metal state at room temperature, to a paramagnetic charge density wave insulator at $T_{MI} = 70$ K, and eventually to an incommensurate antiferromagnetic ordered states below 30 K [20].

The group of Grioni has performed a broad ARPES survey of momentum space in $BaVS_3$, in collaboration with L. Moreschini and E. Rotenberg of beamline BL7 of the Advanced Light Source (Berkeley) using high-quality crystals grown by H. Berger (EPFL). Fig. 5 shows two constant energy cuts measured at 80 K, in the metallic phase, on a wide portion of the $k_x - k_y$ cleavage plane containing the V chains; k_x is also the chain direction. The cut at the Fermi energy (Fig. 5a) gives a direct image of the FS of this compound. It shows two symmetric sheets of an *open* FS running along k_y , consistent with the predicted 1D nature of the broad $3d_{z^2}$ (A_{1g}) band. However, these sheets are not straight as in an ideal 1D case, and the strong warping follows the periodicity of the lattice. A fainter, closed structure centered at Γ reveals the partial occupation of the much shallower E_g band built from orbitals directed towards neighboring chains. Hybrid states with a strong S $3p$ component are imaged in a second cut (Fig. 5b) taken 1 eV below the Fermi energy. The closed contours illustrate the 2D/3D nature of these states, which coexist with 1D states at the bottom of the A_{1g} band, appearing as almost straight lines. These results vividly illustrate the complexity of the electronic structure of this material. Temperature-dependent studies across the metal-insulator (MI) transition are currently underway.

4 Temperature dependence of the excitation spectrum in the charge density wave ErTe_3 and HoTe_3 systems (L. Degiorgi)

The attention was focused on HoTe_3 and ErTe_3 , as representative members of the heavy rare earth tri-tellurides (Fig. 6a, inset) with transition temperatures (T_{CDW1} and T_{CDW2}) into the uni- and bidirectional charge density wave (CDW) states both below 300 K (Figs. 6b and d, insets). This allows to have access to the temperature dependence of the relevant energy scales (e.g. the CDW gaps), of which very little was known.

Figs. 6a and c display the reflexivity $R(\omega)$ for both compounds at 300 K (i.e. in the so-called normal state) and at 10 K (i.e. within the CDW states with respect to both transitions at T_{CDW1} and T_{CDW2}). The overall metallic character at any temperatures is well evident by the plasma edge feature at about $2 \cdot 10^4 \text{ cm}^{-1}$ and by $R(\omega \rightarrow 0) \rightarrow 100\%$ (i.e. total reflection). At 10 K one can additionally recognize the depletion in $R(\omega)$ at about 3000 cm^{-1} . These features are very much reminiscent of what has been seen in our previous studies on RTe_3 as a function of chemical and applied pressure. The overall view of the real part $\sigma_1(\omega)$ of the complex optical conductivity at those two selected temperatures, above and well below T_{CDW1} and T_{CDW2} , is shown for both compounds in Figs. 6b and d.

The single-particle energy gap (ω_{SP}) and the fraction (Φ) of the reconstructed FS in the CDW state were extracted. Fig. 7 displays Φ versus ω_{SP} , the temperature being here an implicit

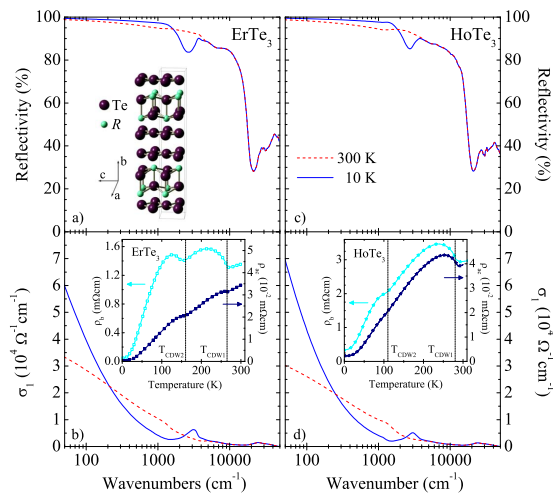


Figure 6: (a-c) Optical reflectivity $R(\omega)$ of ErTe_3 and HoTe_3 at 10 and 300 K. The inset in panel (a) displays the crystal structure. (b-d) Real part $\sigma_1(\omega)$ of the optical conductivity of ErTe_3 and HoTe_3 at 10 and 300 K. The insets in panels (b) and (d) display ρ_{dc} .

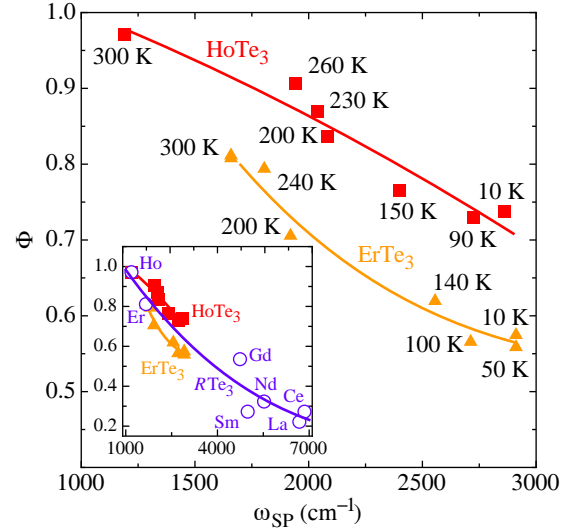


Figure 7: The ratio Φ of the ungapped Fermi surface plotted versus the single-particle excitation ω_{SP} (i.e. CDW gap) for both title compounds. Temperature is here an implicit variable. The inset compares the trend of Φ versus ω_{SP} in temperature (from the main panel) for ErTe_3 and HoTe_3 with the chemical pressure results for selected compounds of the RTe_3 series. The polynomial lines through the data in main panel and inset are meant as guide to the eyes.

variable. Upon increasing the temperature, one observes that the smaller is the CDW gap the larger is the fraction of the ungapped FS. This is totally in accordance with our previous investigation upon compressing the lattice, which reveals the simultaneous closing of the CDW gap with the enhancement of Φ . This is emphasized in the inset of Fig. 7, where the implicit temperature dependence of Φ versus ω_{SP} for the title compounds is in trend with the behavior given by the chemical pressure when going from the lighter to the heavier RTe_3 .

We now turn our attention to the explicit temperature dependence of ω_{SP} , which is shown in Fig. 8. $\omega_{SP}(T)$ for HoTe_3 and ErTe_3 is here normalized by its value deep into the CDW ground state (i.e. $\omega_{SP}(10 \text{ K})$), while the temperature axis is normalized by the respective T_{CDW1} . As expected, ω_{SP} monotonically increases with decreasing temperature below T_{CDW1} . A signature of the gap feature is already present at 300 K, close to but yet above the first high-temperature CDW phase transition at T_{CDW1} (Fig. 8). We remark that this is a rather common situation in prototype CDW materials. The persistence of the gap above the phase transition temperature can be considered as a fingerprint of precursor effects of the CDW formation and has been widely invoked as a manifestation of the fluctuation regime. Therefore, CDW fluctuations seem to play an

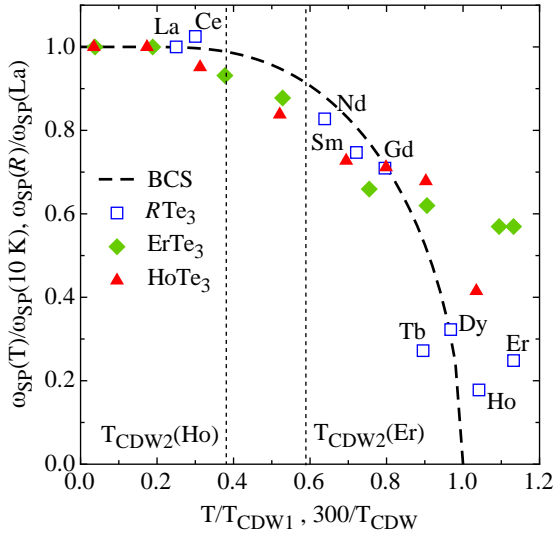


Figure 8: Temperature and chemical pressure dependence of ω_{SP} , normalized by the low-temperature values of $ErTe_3$ and $HoTe_3$ or by the values of $LaTe_3$ in the RTe_3 series. The temperature axis is normalized by the respective critical temperatures (T_{CDW1} for $ErTe_3$ and $HoTe_3$, or T_{CDW} for the RTe_3 series). The vertical thin dotted lines mark the critical temperatures T_{CDW2} for $ErTe_3$ and $HoTe_3$. The BCS predictions for the order parameter is shown for comparison.

important role in RTe_3 as well, despite their two-dimensionality.

It is now instructive to compare the relevant parameter ω_{SP} achieved with our optical experiments when varying the temperature and upon lattice compression. Fig. 8 additionally displays the gap ratio for the chemical series (open squares). We took the ω_{SP} values measured at 300 K, normalized with the gap of $LaTe_3$, assumed to be the largest one for RTe_3 . Instead of the normalized temperature, we consider here the ratio $300\text{ K}/T_{CDW}$ as the effective temperature axis for the chemical series. Within the CDW state, we evince a common trend in the development of the gap for the RTe_3 compounds, when changing R , as well as for $HoTe_3$ and $ErTe_3$, when varying the temperature. As comparison, we reproduce the BCS temperature dependence of the order parameter. The resulting overall decrease of the CDW gap equivalently with increasing temperature or lattice compression roughly agrees with the theoretical predictions, based on the mean-field like BCS theory.

5 Theoretical study of low-dimensional systems (T. Giamarchi)

5.1 Orbital currents in ladders

We pursued our efforts concerning the existence of orbital currents in three band models. In a previous work [6] we had shown that a ladder with a three band structure was able to naturally sustain a phase with orbital currents. We focussed in the present project on the effects of the spin rotational symmetry breaking in two-leg Hubbard ladders [7]. In particular, we investigated the physical consequences of the orbital current patterns (OCP, Fig. 9) in a doped Cu-O Hubbard ladder and looked for measurable signatures of its existence. Using a renormalization group (RG) analysis, we determined the changes that are caused by the $SU(2)$ spin rotational symmetry breaking which occurs when the OCP is present in the ground state phase diagram. We estimated the value

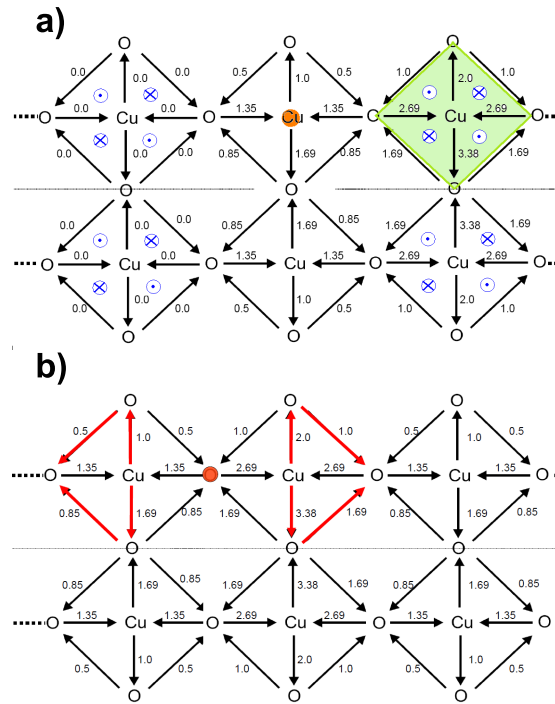


Figure 9: Orbital currents generate a magnetic field that breaks the $SU(2)$ symmetry. The two main contributions to the amplitude of the magnetic field at lattice site x (orange circle) as a result of the o-OCP flow: (a) octupole moments (single octupole = green square) which should be summed up for all elementary unit (squares) along the ladder (except the one which contains the lattice site x) and (b) the quadrupole magnetic moment that is present only if x is one of the on-leg oxygen; the field comes from the asymmetry of OCP amplitudes in two neighboring unit cells (the nonzero contributions are indicated in red); the crosses (dots) correspond to single magnetic dipoles pointing into (out of) the page.

of the new gap, gave an analytic expression for the correlation functions and examined some of the magnetic properties of this new phase which can be revealed in measurements. Further research is being pursued in order to tract the effects of a strong SU(2) symmetry breaking mechanisms like the Rashba coupling.

5.2 Quasi-one-dimensional systems

A review of the properties of quantum phase transitions in quasi-one-dimensional systems (for spin-systems, bosons and fermions — the last situation being relevant for organic superconductors) was given as a chapter of a new book on quantum phase transitions [8].

6 Collaborative efforts

Within the project among the experimentalists there is a focused research on the layered dichalcogenides which manifests in the investigation of the same system by different experimental methods. Furthermore, there is a good collaboration with other MaNEP projects (2, 4, 5) on the study of graphene or other two-dimensional superconductors.

MaNEP-related publications

- [1] H. Cercellier, C. Monney, F. Clerc, C. Battaglia, L. Despont, M. G. Garnier, H. Beck, P. Aebi, L. Patthey, H. Berger, and L. Forró, *Physical Review Letters* **99**, 146403 (2007).
- [2] C. Monney, H. Cercellier, F. Clerc, C. Battaglia, E. F. Schwier, C. Didiot, M. G. Garnier, H. Beck, P. Aebi, H. Berger, L. Forró, and L. Patthey, *Physical Review B* **79**, 045116 (2009).
- ▶ [3] C. Monney, E. F. Schwier, M. G. Garnier, N. Mariotti, C. Didiot, H. Cercellier, J. Marcus, H. Berger, A. N. Titov, H. Beck, and P. Aebi, *New Journal of Physics* **12**, 125019 (2010).

- ▶ [4] C. Monney, E. F. Schwier, M. G. Garnier, C. Battaglia, N. Mariotti, C. Didiot, H. Cercellier, J. Marcus, H. Berger, A. N. Titov, H. Beck, and P. Aebi, *Europhysics Letters* **92**, 47003 (2010).
- [5] N. Barišić, I. Smiljanić, P. Popčević, A. Bilušić, E. Tutiš, A. Smontara, H. Berger, J. Jaćimović, O. Yuli, and L. Forró, *to be published in Physical Review B* (2011), arXiv:1012.2408.
- [6] P. Chudzinski, M. Gabay, and T. Giamarchi, *New Journal of Physics* **11**, 055059 (2009).
- ▶ [7] P. Chudzinski, M. Gabay, and T. Giamarchi, *Physical Review B* **81**, 165402 (2010).
- [8] T. Giamarchi, in *Understanding Quantum Phase Transitions*, L. D. Carr, ed. (CRC Press; Taylor and Francis, 2010).

Other references

- [9] D. Jérôme, T. M. Rice, and W. Kohn, *Physical Review* **158**, 462 (1967).
- [10] W. Kohn, *Physical Review Letters* **19**, 439 (1967).
- [11] F. J. Di Salvo, D. E. Moncton, and J. V. Waszczak, *Physical Review B* **14**, 4321 (1976).
- [12] H. P. Hughes, *Journal of Physics: Condensed Matter* **10**, L319 (1977).
- [13] J. A. Wilson and S. Mahajan, *Communications on Physics* **2**, 23 (1977).
- [14] J. A. Wilson, *Physica Status Solidi (b)* **86**, 11 (1978).
- [15] R. H. Friend and A. D. Yoffe, *Advances In Physics* **36**, 1 (1987).
- [16] S. S. P. Parkin and R. H. Friend, *Philosophical Magazine B* **41**, 65 (1980).
- [17] D. C. Johnston, *Advances In Physics* **59**, 803 (2010).
- [18] J. Paglione and R. L. Greene, *Nature Physics* **6**, 645 (2010).
- [19] F. Lechermann, S. Biermann, and A. Georges, *Physical Review B* **76**, 085101 (2007).
- [20] G. Mihály, I. Kézsmárki, F. Zámorszky, M. Miljak, K. Penc, P. Fazekas, H. Berger, and L. Forró, *Physical Review B* **61**, R7831 (2000).

Project 8

Cold atomic gases as novel quantum simulators for condensed matter

Project leader: T. Giamarchi (UniGE)

Participating members: G. Blatter (ETHZ), T. Esslinger (ETHZ), T. Giamarchi (UniGE), V. Gritsev (UniFR), F. Mila (EPFL), M. Troyer (ETHZ)

Summary and highlights: The project continued to examine the physics of cold atomic gases, in connection with problems of condensed matter. It was mostly centered around three axes. i) The cold atomic systems could be used as quantum simulators, to create model systems. These models were then compared to extremely accurate numerical simulations. It is important to note that the success of such a use of cold atoms was marked as one of the breakthroughs of the year 2010 by the magazine *Science*. ii) In order to study these systems it is important to develop probes and thermometry adapted to such novel systems. This was the goal of the second direction of the project. iii) Finally the cold atomic systems allow to treat unusual situations such as out of equilibrium ones, for which new concepts must be developed. This was the main focus of the third research direction.

1 Models systems

1.1 Bose and Fermi model systems (M. Troyer)

Ultracold atomic gases allow the physical realization of idealized models of strongly interacting electronic materials, such as bosons and fermions with contact interactions, both in the continuum and on a lattice (Hubbard and Bose-Hubbard model). In order to validate the quantum simulators provided by such cold atomic systems, it is necessary to develop quantitatively accurate methods, in particular numerical. This was actively pursued by the Troyer group. In particular they have quantitatively validated experiments on ultracold bosonic gases in optical lattices against quantum Monte Carlo (QMC) simulations [1]. This has been selected by *Science Magazine*, together with several other papers on similar topics, as one of the science breakthroughs of 2010.

For ultracold bosonic gases in optical lattices, the Troyer group has combined diagrammatic techniques and quantum Monte Carlo simulation to test a variant of Beliaev's diagrammatic methods for calculating properties of bosonic gases. They obtain a set of relations that accurately describes the properties of interacting 2D and 3D Bose gases away from the critical region [2]. For fermions [3], they used fits of high-temperature expansions to experiments in order to obtain the temperature in current experiments on ultracold fermionic gases. In another publication [4], they determined the phase diagram of the repulsive interacting Fermi gases, determining the onset of partially and fully polarized ferromag-

netic phases, using variational and fixed node quantum Monte Carlo methods. Finally using a MaNEP-developed continuous time quantum Monte Carlo solver for cluster dynamical mean field theory [5, 6] they have simulated the three-dimensional Hubbard models for interactions up to $U \leq 12t$ and temperatures down to the Néel temperature at all fillings [7] (see also description in Project 5, paragraph 8.2).

1.2 Multicomponent systems (T. Giamarchi, F. Mila)

The cold atoms also allow to realize systems that would be non trivial to obtain in a condensed matter situation. This is in particular the case of multicomponent systems, both bosonic and fermionic.

For the two component Boson system, the Giamarchi group has pursued its efforts to understand the ferromagnetic liquid that was identified in its previous series of works and described in previous activity reports. They have analyzed the problem of a bosonic impurity moving in a bosonic cloud. This situation is relevant for the experimental situation of K impurities moving in a Rb cloud, a situation currently investigated experimentally in M. Inguscio's group in Florence. At the intermediate temperatures and interactions of the experiment, a fruitful approach is to look at the problem as a polaronic problem where the impurity dresses by the density fluctuations of the majority species. They have analyzed the oscillations of the system in this light.

For three-component systems, combining a semiclassical analysis with exact diagonaliza-

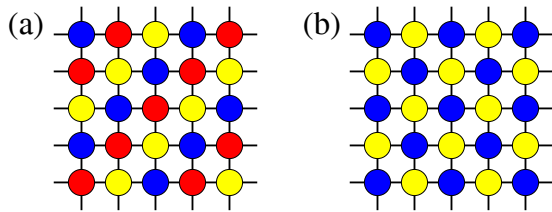


Figure 1: Sketch of the (a) three-sublattice and (b) two-sublattice phases of the $SU(3)$ antiferromagnetic Heisenberg model.

tions [8], the Mila group has shown that the ground state of the $SU(3)$ Heisenberg model on the square lattice develops three-sublattice long-range order (Fig. 1). This surprising pattern for a bipartite lattice with only nearest neighbor interactions has been shown to be the consequence of a subtle quantum order-by-disorder mechanism. By contrast, thermal fluctuations favor two-sublattice configurations via entropic selection. These results are shown to extend to the cubic lattice, with possible realization with the Mott-insulating states of three-flavor fermionic atoms in optical lattices.

1.3 Correlated photons (G. Blatter)

Motivated by the recent success of engineering strong light-matter interaction in various cavity/circuit quantum electrodynamics (QED) architectures, there has been a surge of interest in realizing condensed matter-like systems with optical/photonic setups. So far, the experimental focus has been on the design of the coupling between a single-cavity and a single-qubit and subsequent work demonstrated a great level of control of single-cavity systems. Today, a key challenge for scalability and further progress in the field is the understanding of coupled systems.

Recent theoretical interest in hybrid light-matter systems has been on the superfluid-Mott-insulator (SF-MI) transition of polaritons as described by the Jaynes-Cummings-Hubbard model (JCHM) [33]. In previous work, the Blatter group has calculated the photonic Matsubara Green's function of the JCHM — which is directly accessible in transmission/absorption experiments — using diagrammatic as well as slave-boson techniques in both, the Mott [9] and superfluid phase [10]. From the Green's function they have obtained the phase diagram, elementary excitations, and critical exponents.

Recently, they have proposed that, even in the smallest possible coupled-cavity system of a two-site JCHM (Fig. 2), one can find strong

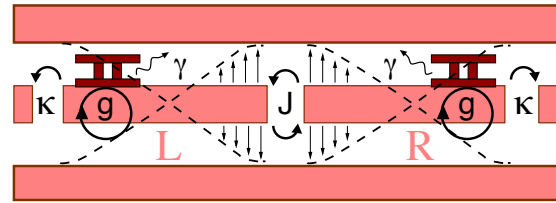


Figure 2: Layout of the two-site JCHM realized with circuit QED technology. Two transmission line microwave resonators (L,R) are coupled in series with a tunneling rate J . Each resonator is strongly coupled (with a rate g) to a superconducting qubit providing a strong non-linearity. Dissipation is accounted for through the photon decay rate κ ; the spontaneous emission rate γ accounts for qubit decoherence.

signatures of the on-site repulsive interaction among photons. They have shown that photons in two tunnel-coupled microwave resonators, each containing a single superconducting qubit, undergo a sharp nonequilibrium delocalization-localization (self-trapping) transition due to strong photon-qubit coupling [11]. Near this self-trapping transition, photons in the two cavities form a many-body entangled state similar to what is known as a N00N state (a Schrödinger cat type Bell state) in quantum metrology. The coupled cavity dimer proposed here is simple enough to be readily realizable with state-of-the-art circuit QED technology. Experiments based on this proposal are currently underway in the research group of A. A. Houck at Princeton.

1.4 Dipolar systems (G. Blatter, M. Troyer)

Although atoms, being neutral, implement naturally systems with contact interactions, there are currently active researches on systems with dipolar molecules, which can potentially open the way to realizing systems with long range forces. In particular, experiments with cold dipolar molecules subject to an optical lattice (of strength V_0) provide a new realization for the physics of competing structures and effects of commensuration. In a two-dimensional confinement [34], the long-range dipolar repulsion between the molecules favors the formation of a triangular lattice which competes with the square lattice structure enforced by the (substrate) potential of an optical lattice. While conventional solid state realizations — e.g. Krypton on graphite or flux quanta in structured superconducting films — could only cover a small parameter window, the high control and tunability of the cold atom setup permits to explore the full variety of different regimes

in the phase diagram, including distorted and rotated phases, commensuration effects and partly/fully locked phases, as well as quantum/classical floating or melting transitions.

The Blatter group looked at the minimal energy states in the absence of (quantum/classical) fluctuations and for particle densities n close to commensurate filling $n = 1/b^2$ (b is the period of the optical lattice). Increasing the ratio v between the substrate potential V_0 and the interparticle interaction D/b^3 (D the dipolar coupling constant), the system goes through various phases.

A perturbative study for weak substrate potentials yields a distorted particle lattice characterized by a non-trivial angle of orientation [35] (interaction-dominated regime). In the opposite limit, the strong substrate potential locks the particles to a square-lattice configuration. As the substrate potential is reduced, an instability of the square lattice towards a shear mode at the Brillouin zone edge manifests itself at v_{c_2} . The resulting lattice with period-doubling along one direction belongs to the symmetry group $p2mg$; the phase line cuts the perturbative line at v_{c_1} . The transition from the interaction-dominated to the substrate-dominated regime has not yet been well-understood. Recent results have provided a better understanding of the system's behavior: within the resonance approximation [36], where only the dominant substrate mode is considered and the particle lattice is viewed as an elastic medium, the problem can be mapped to the one-dimensional (time-independent) Sine-Gordon model. Within this model, the formation of a one-dimensional soliton structure provides a smooth transition at v_c from the period doubled phase to a solitonic phase; the latter then smoothly evolves into the distorted and rotated triangular phase. A further study concerning the effect of the second substrate mode on the soliton solution is in progress; the correction is expected to push v_c beyond v_{c_1} .

On the numerical side, the Troyer group calculated the phase diagram of such dipolar gases on triangular optical lattices and showed the existence of a supersolid phase: a phase with coexisting superfluid and solid order. They could show that, once the temperature of these molecular gases becomes comparable to what can nowadays be achieved for atomic gases, such a supersolid can be realized using dipolar gases in optical lattices [12].

2 Probes and thermometry (G. Blatter, T. Esslinger, T. Giamarchi, M. Troyer)

In order to use efficiently these systems, it is important to have probes allowing to access the rather complex correlations in presence of interactions. Indeed, the response of a quantum many-body system to a weak perturbation can provide fundamental information about its properties. In this regime, the system does not significantly change under probing and basic quantities can be measured, as, for example, charge and spin susceptibilities in electron systems. Due to relatively large sample sizes, weak probing is often naturally achieved in condensed matter physics. Contrariwise, the relatively small number of atoms in quantum gas experiments makes it very challenging to design probes which measure correlation functions through linear or quadratic response. It is also mandatory to have a good control of the temperature (or entropy) of the system, which is non-trivial in such ultracold systems.

For the thermometry, the Troyer group [13] has improved on an idea by T. L. (Jason) Ho on thermometry for trapped atomic gases using the fluctuation-dissipation theorem. Comparing the gradient of the density with (short-ranged in their proposal) density fluctuations one can reliably determine the temperature of a trapped quantum gas with an accuracy of about 10% by recording 10 – 20 density profiles.

The Esslinger group has recently demonstrated a simple method for probing the nearest neighbor correlations of strongly interacting repulsive fermionic gases in optical lattices, inspired by a proposal of the Giamarchi group [14]. This method applies to the Fermi-Hubbard model, as realized with optical lattices [15]. This model is of particular interest, since its phases reflect an intriguing interplay between interactions, kinetic energy and magnetic ordering. Studies of the crossover from a metallic to a Mott-insulating phase have recently provided first aspects of the Fermi-Hubbard physics in optical lattice experiments. A reduction of density fluctuations was observed using a local observable sensitive to the occupation of lattice sites [37][3], and by extracting the compressibility from measured cloud sizes [38]. Yet, crucial aspects of the many-body physics of the Fermi-Hubbard model are closely linked to nearest neighbor correlations. These characterize the spin ordering in an anti-ferromagnetic phase, as well as the presence of holes due to doping or thermal excitations. Therefore probes sensitive to nearest neighbor correlations were required.

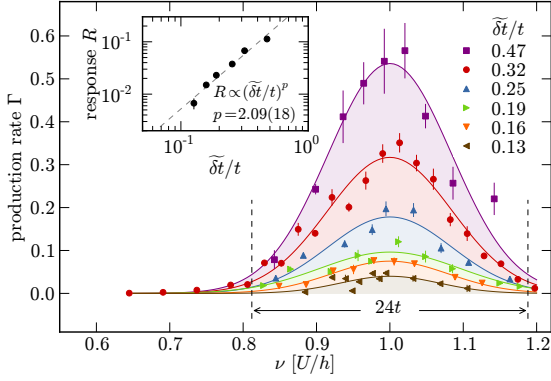


Figure 3: Doublon production rate Γ as a function of the lattice modulation frequency ν , measured for different modulation amplitudes $\delta\tilde{t}/t$. The experiments were performed at $U/6t = 10.6$ and $V = 10E_R$, with U denoting the on-site interaction energy, t the hopping matrix element and E_R the recoil energy. The shaded areas are gaussian fits to the spectra, which are used to extract the frequency integrated response R . The two vertical dashed lines denote twice the three-dimensional bandwidth $4zt$ (with $z = 6$). The inset is a double-logarithmic plot of R for various modulation amplitudes, where the dashed line is a power law fit. Error bars denote the fit errors [17].

The nearest neighbor correlation function for the experimental realization of Hubbard model is given by

$$\mathcal{P}_{i,i+1} = \sum_{\sigma} \langle n_{i,\sigma} n_{i+1,\bar{\sigma}} (1 - n_{i,\bar{\sigma}}) (1 - n_{i+1,\sigma}) \rangle, \quad (2.1)$$

where $\sigma = \{\uparrow, \downarrow\}$, $\bar{\sigma}$ denotes the opposite spin and $i, i+1$ are adjacent sites. This probe determines the probability of finding singly occupied neighboring sites with opposite spins.

The system is excited by a periodic modulation of the lattice depth [39] which leads to tunneling of particles to adjacent sites. If two particles of opposite spin are located on neighboring sites, additional double occupancies (doublons) are created. The resulting doublon production rate is sensitive on the spin correlator $\mathcal{P}_{i,i+1}$. They showed that in the perturbative regime the frequency integrated doublon production rate is given by $\mathcal{P}_{i,i+1}$ [14, 16]. For the experiment they have used a quantum degenerate ^{40}K gas, prepared in a balanced spin mixture of the $m_F = -9/2$ and $-5/2$ magnetic sublevels of the $F = 9/2$ hyperfine manifold. Fig. 3 shows the doublon production rate Γ as a function of the lattice modulation frequency ν . The Esslinger group has further used this technique to measure nearest neighbor correlations as a function of temperature, covering the regime from a paramagnetic Mott-insulator to a strongly interacting metallic state. The re-

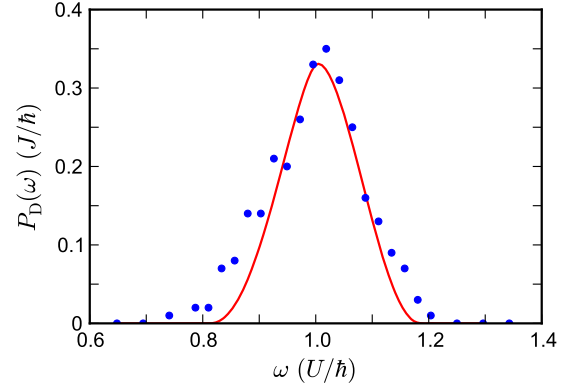


Figure 4: Comparison of the doublon production rate computed by the slave boson theory of the Giamarchi group and the experimental data obtained by the group of T. Esslinger. The agreement is very good. The method is versatile enough to be used in more complicated cases than the two-component boson systems.

sults are in good agreement with the predictions of an *ab initio* theory without any fitting parameters. In connection with this question, the Giamarchi group has developed a slave boson technique allowing to perform the calculation of the effects of the shaking. This technique allows to take into account at the mean-field level the effects of the trap and the finite temperature. The agreement with the experimental results is excellent as shown in Fig. 4.

In addition, the Blatter group has studied [18] the double occupancy at half-filling and found a crossover in the nature of doublon-holon excitations from a Fermi golden rule regime to damped Rabi oscillations. The decay time of excited states diverges at a critical modulation strength, signaling the transition from free doublons and holons to a dynamically bound non-equilibrium state of doublon-holon pairs.

Another type of probe involving modulations of optical lattices, but different from the amplitude modulation (shaking) studied above, was developed in the Giamarchi group. A modified shaking method in which the phase of the optical lattice is modulated was proposed [19]. With this technique, nicknamed sieving, one measures the current-current correlations in the system. This is thus a direct way to probe the equivalent of the optical conductivity of the systems, making it a valuable probe for comparison with condensed matter results or for studying the properties of disordered systems. One can probe such effects either by looking at the energy absorbed in the system, or the doublon production rate just as for the amplitude modulation.

Concerning the probing of cold atoms, a new

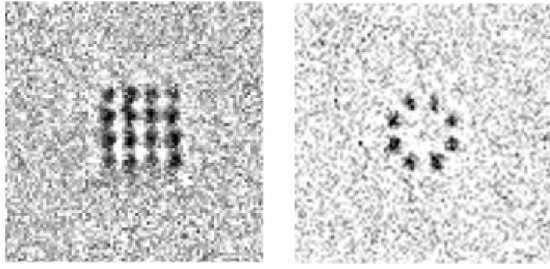


Figure 5: The figure exemplarily shows in situ absorption images of atoms trapped in a 4×4 two-dimensional square lattice with a site separation of $2.5 \mu\text{m}$ (left), and in a ring configuration (right) [20].

experimental apparatus has been set up in the Esslinger group, which allows for local probing and manipulation of an ultracold Fermi gas of Lithium atoms on the length scale of one micrometer, i.e. on the order of the Fermi wavelength. An essential tool of the experimental setup is a pair of identical, high-resolution microscope objectives. One of the microscope objectives allows for local imaging the trapped Fermi gas of ^6Li atoms with a maximum resolution of 660 nm , whereas the other enables the generation of arbitrary optical dipole potentials on the same length scale. Employing a 2D acousto-optical deflector, they have demonstrated the generation of several trapping geometries (Fig 5). The lattice spacing can be adjusted and resolved down to one micrometer. They have loaded and detected a small number of atoms in these trapping potentials. The small site separation of the lattice structures in combination with the low mass of ^6Li will result in sizable tunneling rates of about 1 kHz , thus providing a novel flexible route for the realization of the Hubbard model and beyond [20].

3 Out of equilibrium physics

Cold atomic systems offer an exciting opportunity to simulate quantum non-equilibrium dynamics of many-body systems. Therefore development of theoretical tools and approaches goes closely with experimental efforts. This line of research has been pursued by several groups.

In the Gritsev group, the theoretical activity reported in the previous year is now supported by the first experimental results. Thus, analysis of the density fluctuations in an expanded condensate has been reported by the group of J. Schmiedmayer in Vienna [40]. The analysis of the spectrum of these fluctuations reveals a wealth of information about a system. Non-equilibrium analogue of the full distribu-

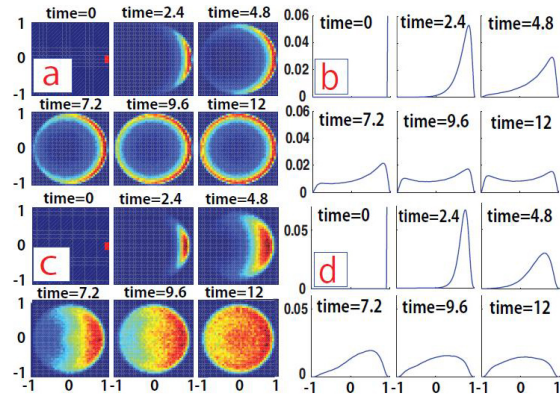


Figure 6: Time evolution of full distribution function for different integration lengths: panels (a) and (b) are for small ratio of the integration length to the spin healing length whereas the panels (c) and (d) are for the corresponding large value. Left column is a 2D plot for the spin distribution function in the x, y -plane and the right column is a projection into the x -axis.

tion function, introduced in [21] (Fig. 6), which provides a tool for deep and systematic analysis of non-equilibrium dynamics of quantum many-body systems, has also been probed in the same group in Vienna. Some experimental results in this direction are reported in [41].

Non-equilibrium effects which were predicted recently by the Gritsev group in dynamically driven many-body spin-systems have been realized now in the group of I. Bloch [42]. In particular, their experiments represent a first steps towards realization of basic quantum gate element with cold atoms in the optical lattices, a so-called SWAP operation. Moreover, these experiments open up a possibility to create strongly-correlated spin-states in controllable fashion, in a way they devised with Peter Barmettler previously in [43].

In addition several new axes were pursued by the Gritsev group

3.1 Slow dynamics and quenches (V. Gritsev)

Problems related to adiabatic dynamics in many body systems have direct relation to quantum annealing and quantum simulation. Many prominent aspects of non-equilibrium dynamics of many-body interacting systems were revealed by the studies of adiabatic (slow) dynamics. In particular they were able to characterize the dynamics near quantum critical points in terms of concepts borrowed from the field of quantum information. These quantities, related to fidelity of the ground state, allow the definition of various susceptibilities to the external drive of parameters and eventu-

ally provide a useful basis for deriving *universal* properties of adiabatic dynamics close to the quantum critical phases [22, 23]. Interestingly, these universalities can be found not only in condensed matter systems but also in cosmology and string theory [24]. Another aspect of slow dynamics is the appearance of geometric effects, characterized by the Berry phase of the curved parameter space of quantum systems. The geometric effects influence non-equilibrium dynamics in a profound way, thus, e.g., allowing the design of a new type of probe for the nature of quantum critical points in many-body systems. They found interesting effects of interplay of dynamics and geometry of the manifold of quantum states which show up in dynamics near quantum critical points. These fundamental issues are of direct experimental significance, as demonstrated for particular models.

They also continued to work on quenches in bosonic and spin-systems [25, 26] where they found several intriguing dynamical phenomena. There are ongoing experiments aiming to observe the unusual dynamical behaviors reported in these papers.

3.2 Novel approach to path integrals with spins (V. Gritsev)

Recently the Gritsev group found a powerful approach for studying dynamics of interacting spin-systems. This approach uses a path integral formulation and a theory of Lie groups. Its main step consists in a disentangling transformation of the time-ordered exponent of expression which is linear in generators of a Lie algebra. This idea leads them to a new technique which suggests various routes of further studies. They have already demonstrated that this method provides a non-trivial exact agreement with dynamics of some exactly solvable systems (e.g. many-body systems which can be solved by the Bethe ansatz). They are going to extend these ideas for many other systems. They strongly hope that it can be a very useful tool for either approximate or numerical treatments of interacting quantum many-body systems, especially what concerns their dynamics. One of the outcome of this approach for current experiments in cold atoms is related to the probe time-dependent correlation functions at high temperatures (which are much larger than the spin exchange coupling constant in current experiments). It follows that in the long time limit their approach predicts non-diffusive exponents for the spin-spin correlation functions. It could be interesting to check these predic-

tions experimentally since this regime would represent a *simulator* of dynamics of quantum system at large temperatures.

3.3 Quantum systems in presence of an out of equilibrium noise (T. Giamarchi)

Another direction for out of equilibrium physics was pursued by the Giamarchi group. They have studied quantum systems, such as a noisy Josephson junction or a chain of ions or dipolar molecules, which are subjected to a $1/f$ noise. The question of quantum systems in presence of an external bath is a very important question relevant for many experimental systems (see, e.g., work in that respect for the MaNEP Projects 2 and 7). In that particular case, the important question to address is whether such systems still retain the criticality that is characteristic of quantum systems at $T = 0$. In other words, is the noise simply acting as a temperature and heating the system, taking it away from the $T = 0$ quantum regime, or can a new regime exist? The answer to this question is that quite surprisingly the $1/f$ noise leaves the system in a new steady state regime which, although intrinsically out of equilibrium, retains critical states and powerlaw decay of correlation functions. Such a state can thus have the equivalent of “quantum phase transitions” between different quantum “phases”. However the system is intrinsically out of equilibrium as can be seen by measuring the response to an external perturbation, such as the one measured in Bragg spectroscopy [27].

4 Collaborative efforts

Several collaborations exist between the different groups in the project and across the MaNEP projects.

Within the project, there were strong collaborations between the Esslinger group and the Troyer group in the comparison/analysis of the experiments in the light of the numerical simulations of the Hubbard model. There were also interactions between the Esslinger group and the Giamarchi group on the question of shaking.

Across the MaNEP projects it is important to notice that many of the concepts that were developed in the framework of this project can be used potentially in the context of the other projects. This is valid for the physics analysis, such as the results of the Mila or the Blatter groups, but also in terms of the methods, both analytic, such as the ones of the Gritsev group that can potentially be used for

other types of out of equilibrium situations, but also on the numerical side. In addition to the above-mentioned research works, several reviews have been written. The first one is a general course on basic interaction effects in quantum systems and on low-dimensional systems [28]. The second and third one are *Review of Modern Physics* on the physics of (quasi-) one dimensional systems [29], and on numerical methods for impurity models [6], respectively. These reviews have bearing both on the cold atoms and condensed matter sides.

On that last point several developments that occurred within the project are potentially useful for other projects. In particular the Troyer group has developed a diagrammatic quantum Monte Carlo (DiagMC) algorithm for the Hubbard model [30]. This algorithm samples connected Feynman diagrams instead of the partition function and works successfully in the correlated Fermi liquid regime of the Hubbard model. They will use it in the future to calculate phase diagrams and equations of state of 2D and 3D fermionic gases (see also report on Project 5, paragraph 8). They have also improved on a proposal by Byczuk and Vollhardt of a bosonic version of dynamical mean field theory (B-DMFT) and developed a quantum Monte Carlo method to solve the B-DMFT equations [31]. The algorithm is very efficient and surprisingly it turns out that the B-DMFT approximation can quantitatively reproduce the phase diagram of a 3D Bose-Hubbard model with errors of less than 2%, making this an extremely good approximative method.

The Troyer group has also developed and published a major new version of the ALPS libraries and applications [32]. These developments are described in more details in Project 5, paragraph 8.1.

There are also collaborations between the Troyer, Mila, and Giamarchi groups in the framework of the MAQUIS project to port the standard numerical tools to massively parallel architectures.

MaNEP-related publications

- ▶ [1] S. Trotzky, L. Pollet, F. Gerbier, U. Schnorrberger, I. Bloch, N. V. Prokof'ev, B. Svistunov, and M. Troyer, *Nature Physics* **6**, 998 (2010).
- [2] B. Capogrosso-Sansone, S. Giorgini, S. Pilati, L. Pollet, N. Prokof'ev, B. Svistunov, and M. Troyer, *New Journal of Physics* **12**, 043010 (2010).
- ▶ [3] R. Jördens, L. Tarruell, D. Greif, T. Uehlinger, N. Strohmaier, H. Moritz, T. Esslinger, L. De Leo, C. Kollath, A. Georges, V. Scarola, L. Pollet, E. Burovski, E. Kozik, and M. Troyer, *Physical Review Letters* **104**, 180401 (2010).
- ▶ [4] S. Pilati, G. Bertaino, S. Giorgini, and M. Troyer, *Physical Review Letters* **105**, 030405 (2010).
- [5] E. Gull, P. Werner, O. Parcollet, and M. Troyer, *Europhysics Letters* **82**, 57003 (2008).
- ▶ [6] E. Gull, A. J. Millis, A. I. Lichtenstein, A. N. Rubtsov, M. Troyer, and P. Werner, *to be published in Reviews of Modern Physics* (2011).
- ▶ [7] S. Fuchs, E. Gull, L. Pollet, E. Burovski, E. Kozik, T. Pruschke, and M. Troyer, *Physical Review Letters* **106**, 030401 (2011).
- ▶ [8] T. A. Tóth, A. M. Läuchli, F. Mila, and K. Penc, *Physical Review Letters* **105**, 265301 (2010).
- [9] S. Schmidt and G. Blatter, *Physical Review Letters* **103**, 086403 (2009).
- ▶ [10] S. Schmidt and G. Blatter, *Physical Review Letters* **104**, 216402 (2010).
- ▶ [11] S. Schmidt, D. Gerace, A. A. Houck, G. Blatter, and H. E. Türeci, *Physical Review B* **82**, 100507(R) (2010).
- ▶ [12] L. Pollet, J. D. Picon, H. P. Büchler, and M. Troyer, *Physical Review Letters* **104**, 125302 (2010).
- [13] P. N. Ma, L. Pollet, and M. Troyer, *Physical Review A* **82**, 033627 (2010).
- [14] C. Kollath, A. Iucci, I. P. McCulloch, and T. Giamarchi, *Physical Review A* **74**, 041604 (2006).
- ▶ [15] T. Esslinger, *Annual Review of Condensed Matter Physics* **1**, 129 (2010).
- [16] S. D. Huber and A. Rüegg, *Physical Review Letters* **102**, 065301 (2009).
- ▶ [17] D. Greif, L. Tarruell, T. Uehlinger, R. Jördens, and T. Esslinger, arXiv:1012.0845 (2010).
- ▶ [18] F. Hassler, A. Rüegg, M. Sigrist, and G. Blatter, *Physical Review Letters* **104**, 220402 (2010).
- ▶ [19] A. Tokuno and T. Giamarchi, arXiv:1101.2469 (2011).
- ▶ [20] B. Zimmermann, T. Müller, J. Meineke, T. Esslinger, and H. Moritz, arXiv:1011.1004 (2010).
- ▶ [21] T. Kitagawa, S. Pielawa, A. Imambekov, J. Schmiedmayer, V. Gritsev, and E. Demler, *Physical Review Letters* **104**, 255302 (2010).
- ▶ [22] C. DeGrandi, V. Gritsev, and A. Polkovnikov, *Physical Review B* **81**, 012303 (2010).
- ▶ [23] C. DeGrandi, V. Gritsev, and A. Polkovnikov, *Physical Review B* **81**, 224301 (2010).
- ▶ [24] A. Polkovnikov and V. Gritsev, in *Understanding Quantum Phase Transitions*, L. D. Carr, ed. (CRC Press, Taylor & Francis Group, Boca Raton, 2011), p. 59.
- ▶ [25] P. Barmettler, M. Punk, V. Gritsev, E. Demler, and E. Altman, *New Journal of Physics* **12**, 055017 (2010).
- ▶ [26] V. Gritsev, T. Rostunov, and E. Demler, *Journal of Statistical Mechanics* p. P05012 (2010).
- ▶ [27] E. G. Dalla Torre, E. Demler, T. Giamarchi, and E. Altman, *Nature Physics* **6**, 806 (2010).
- [28] T. Giamarchi, in *Ultracold Gases and Quantum Information*, C. Miniatura, ed. (Oxford University Press, 2011).
- [29] M. A. Cazalilla, R. Citro, T. Giamarchi, E. Orignac, and M. Rigol, arXiv:1101.5337v1 (2011).
- ▶ [30] E. Kozik, K. Van Houcke, E. Gull, L. Pollet, N. Prokof'ev, B. Svistunov, and M. Troyer, *Europhysics Letters* **90**, 10004 (2010).
- ▶ [31] P. Anders, E. Gull, L. Pollet, M. Troyer, and P. Werner, *Physical Review Letters* **105**, 096402 (2010).

- [32] B. Bauer, L. D. Carr, A. Feiguin, J. Freire, S. Fuchs, L. Gamper, J. Gukelberger, E. Gull, S. Guertler, A. Hehn, R. Igarashi, S. V. Isakov, D. Koop, P. N. Ma, P. Mates, H. Matsuo, O. Parcollet, G. Pawłowski, J. D. Picon, L. Pollet, E. Santos, V. W. Scarola, U. Schollwöck, C. Silva, B. Surer, S. Todo, S. Trebst, M. Troyer, M. L. Wall, P. Werner, and S. Wessel, arxiv:1101.2646 (2011).

Other references

- [33] A. D. Greentree, C. Tahan, J. H. Cole, and L. C. L. Hollenberg, *Nature Physics* **2**, 856 (2006).
- [34] H. P. Büchler, E. Demler, M. Lukin, A. Micheli, N. Prokof'ev, G. Pupillo, and P. Zoller, *Physical Review Letters* **98**, 060404 (2007).
- [35] J. P. McTague and A. D. Novaco, *Physical Review B* **19**, 5299 (1979).
- [36] V. L. Pokrovskii and A. L. Talanov, *Journal of Experimental and Theoretical Physics* **51**, 134 (1980).
- [37] R. Jördens, N. Strohmaier, K. Günter, H. Moritz, and T. Esslinger, *Nature* **455**, 204 (2008).
- [38] U. Schneider, L. Hackermüller, S. Will, T. Best, I. Bloch, T. A. Costi, R. W. Helmes, D. Rasch, and A. Rosch, *Science* **322**, 1520 (2008).
- [39] T. Stöferle, H. Moritz, C. Schori, M. Köhl, and T. Esslinger, *Physical Review Letters* **92**, 130403 (2004).
- [40] S. Manz, R. Bücker, T. Betz, C. Koller, S. Hofferberth, I. E. Mazets, A. Imambekov, E. Demler, A. Perrin, J. Schmiedmayer, and T. Schumm, *Physical Review A* **81**, 031610(R) (2010).
- [41] T. Betz, S. Manz, R. Bücker, T. Berrada, C. Koller, G. Kazakov, I. E. Mazets, H.-P. Stimming, A. Perrin, T. Schumm, and J. Schmiedmayer, *Physical Review Letters* **106**, 020407 (2011).
- [42] S. Trotzky, Y.-A. Chen, U. Schnorrberger, P. Cheinet, and I. Bloch, *Physical Review Letters* **105**, 265303 (2010).
- [43] P. Barmettler, A. M. Rey, E. Demler, M. D. Lukin, I. Bloch, and V. Gritsev, *Physical Review A* **78**, 012330 (2008).



Techniques and know-how

Responsibles: Enrico Giannini (UniGE), Patrycja Paruch (UniGE), Andreas Schilling (UniZH), Ivan Maggio-Aprile (UniGE), Christof Niedermayer (PSI), Philipp Aebi (UniFR), Urs Staub (PSI), Leonardo Degiorgi (ETHZ), Matthias Troyer (ETHZ)

Summary: The nine techniques and know-how topics each represent a watch of techniques important to MaNEP. Financial support for these activities is limited. Thus the proposed actions are mainly carried out in a voluntary basis.

1 Crystal growth and bulk materials processing

Responsible: Enrico Giannini (UniGE)

Following the rush for the Fe-based superconducting materials discovered in 2008, the MaNEP crystal growth community has established itself as a world reference in growing crystals of superconducting pnictides and chalcogenides. In 2010, more than 25 publications from MaNEP members have profited from single-crystalline samples of the various pnictides and chalcogenides grown inside the MaNEP laboratories (ETHZ, PSI and UniGE). Most of these publications are the result of intergroup collaborations among two or more MaNEP institutions, confirming the strong collaborative work in this field of research. Moreover, dozens of publications from international collaborations in general deal with materials grown in MaNEP laboratories. An intense research activity is still demanding crystalline materials to be grown with unique techniques that are an asset of MaNEP laboratories, namely the high-pressure growth (at ETHZ, more than 15 related publications in 2010) and the chemical vapor transport growth (at EPFL, more than 25 related publications in 2010). On the other hand, crystal growth via the traveling solvent floating zone technique has established itself as a highly versatile technique and is nowadays mastered by three groups of three MaNEP institutions (UniGE, PSI and Empa) for growing crystals of an amazing variety of materials: high- T_c cuprates (UniGe and PSI), manganites (Empa and PSI), ferrites and cobaltates (PSI), Fe-chalcogenides (UniGe and PSI), as well as the topological insulators Bi_2Se_3 , Bi_2Te_3 , and $\text{Bi}_{1-x}\text{Sb}_x$ (UniGE). Nanostructured materials for catalysis and gas-sensing have been improved at the UniZH, thanks to the progress achieved in the hydrothermal processing technique. A new superconductor ($\text{Cs}_{0.8}(\text{FeSe}_{0.98})_2$, $T_c = 27$ K) has been discov-

ered at PSI. The complementarity and the variety of the techniques used and the materials processed in the various laboratories allow to meet the demand of the MaNEP community and to promptly react to new discoveries and new inputs.

New facilities

A Czochralski crystal pulling equipment is being installed at UniGE. The home-made furnace is designed to work under oxidizing atmosphere at very high temperature ($> 2200^\circ\text{C}$), and the heating power is provided by a 40 kW Stanelco HF generator. The furnace is equipped with a high-precision commercial pulling system (Cyberstar SA). This new equipment will allow growing crystals of various functional oxides, as well as dedicated perovskite-based substrates for thin film devices. The facilities existing at the UniZH for the microwave-assisted hydrothermal (MW-HT) synthesis of oxide nanomaterials have been updated and further developed. A new mirror furnace (CSI) is operating at Empa and is mostly dedicated to high-temperature thermoelectric materials for environmental technologies.

New materials

The updated list of crystalline materials available within MaNEP can be find at the end of this chapter, p. 120.

New actions

In fall 2010, MaNEP was represented by K. Conder (PSI) at the "European Meeting on Crystal Growth" organized by the Leibniz Institute for Crystal Growth (IKZ) in Berlin. With the aim of strengthening and boosting the European activities and investments on crystal growth, the following decisions were taken. 1) The next European Conference on

Crystal Growth (ECCG-4) will be organized in Glasgow, 17–20 June 2012. The subsequent conferences are planned with periodicity of 3 years (the previous ECCG-3 dated from 1991). 2) A European Network of Crystal Growth (ENCG) will be created as a precursor of a future European Crystal Growth Association. 3) ENCG will promote education in crystal growth (schools, master courses). 4) Collaboration between science and industry should be strengthened. The Swiss community of crystal growers will be ready for these important challenges.

Education on crystal growth techniques will be one of the topics of the satellite tutorial day accompanying the next Swiss Workshop on Materials SWM 2011 (Les Diablerets, June 28, 2011). The course aims primarily at graduate students and will specifically focus on the technical aspects that are usually not detailed in scientific presentations. Emphasis will be placed on processing techniques used for growing the most important materials treated in the SWM 2011.

2 Thin film growth and characterization

Responsible: Patrycja Paruch (UniGE)

During the year 10 reporting period, thin films have continued to play an important role in MaNEP, with ongoing work on bilayers and superlattice structures from many different groups. A new thin film effort in chemical vapor deposition of graphene was also initiated. Although this fascinating material with significant application potential had excited great international research interest, including Nobel Prize recognition for the researchers who first demonstrated and studied single-layer graphene, it was not strongly represented in MaNEP. To allow access to high-quality single-layer graphene to different MaNEP groups, and allow a rapid reaction to continued advances in this field, a one-time MaNEP techniques and know-how post-doctoral fellowship was awarded for 2 years to Dr. Christophe Caillier, who has begun work in December 2010 on optimizing graphene growth on copper crystals, and transfer onto target substrates where its properties can be accessed.

We have also proposed a series of satellite tutorials focused on different themes in techniques and know-how, targeted primarily at graduate students, which will accompany the biennial Swiss Workshop on Materials. The aim of these courses is to present in depth the details of specific experimental techniques useful in modern physics and materials science, includ-

ing applications and advantages, problems or artifacts, and possible routes to troubleshooting, allowing students to understand the technique, rather than focus on a specific set of results obtained with it, as in a standard scientific presentation. The first set of three tutorials on thin film deposition, crystal growth and scanning probe microscopy will be offered on 28 June, 2011 at Les Diablerets in the frame of the next Swiss Workshop on Materials SWM 2011.

4 Scanning local probes techniques

Responsible: Ivan Maggio-Aprile (UniGE)

In condensed matter physics, there is a growing interest in using local probes to investigate, characterize or manipulate materials at the nanometer scale. It is therefore becoming quite common in conferences to hear about measurements obtained with these techniques. However in most cases, the audiences have only a general idea of local probes, and do not possess the required knowledge to catch up what can be really achieved using these techniques. This year, a one-day tutorial on experimental techniques will be provided as a satellite of the Swiss Workshop on Materials SWM 2011, on 28 June, 2011, at Les Diablerets. One of these will focus on local probes, providing a broad overview of the different techniques, focusing on technical aspects, their performances and possible applicability, as well as the problems associated with these sensitive techniques and the possible artifacts encountered in the measurements. This tutorial is dedicated to graduate students.

5 Neutron scattering and muon spin resonance

Responsible: Christof Niedermayer (PSI)

Neutron scattering developments

First successful tests for the development of a neutron reflectometer optimized for measurements of small thin film and multilayer samples with a surface area in the mm² range have been performed. A prototype set-up with a 2 m long elliptically focusing guide element has been realized on the neutron reflectometer AMOR at PSI and resulted in a gain factor of almost 10. This result demonstrates the potential of focusing elements for future neutron scattering instrumentation. The design and test of novel neutron guide concepts can be realized on the newly built flexible test beamline BOA.

Substantial progress has been made in the construction of the thermal triple axis instrument EIGER. The primary spectrometer was completed, including assembly and mechanical testing of the monochromator shielding as well as alignment and installation of the doubly focusing monochromator. After completion of the secondary spectrometer the thermal instrument will significantly extend the available energy range for inelastic neutron scattering experiments.

Muon spin spectroscopy (μ SR) developments

A new spin rotator was designed and constructed for the low-energy μ SR (LEM) beamline. With this new device the time evolution of the muon spin polarization in longitudinal magnetic fields can be determined. Such measurements will have a huge impact for the study of dynamic magnetic processes in thin films and multilayers.

Key components of the new high magnetic field spectrometer have been developed and tested. The superconducting 9.5 T magnet performs according to its specifications (field homogeneity of a few ppm and a field drift of less than 1 ppm/h). A cryogen free horizontal dilution refrigerator extends the temperature range into the mK regime. Avalanche photodiodes directly coupled to a fast plastic scintillator were shown to be competitive to photomultipliers in terms of gain and photon detection efficiency, but are insensitive to magnetic fields.

Novel research areas in condensed matter physics and chemistry will become possible with the commissioning of the high-field μ SR instrument. Examples are high-field studies of the flux line lattice in unconventional superconductors, quantum critical behavior in low-dimensional magnets and interplay of magnetism and superconductivity in high-temperature superconductors, including the pnictides.

6 Electron spectroscopies

Responsible: Philipp Aebi (UniFR)

After the delivery of the endstation for the soft X-ray ARPES experiment at the ADDRESS beamline and extensive commissioning during the last period, very recently now first experiments have been performed with excellent results. It turns out that the beamline delivers 1 to 2 orders of magnitude better flux than other existing soft X-ray beamlines. The photon energy range of this beamline allows for so-called

high-energy ARPES around 1 keV. It is more bulk sensitive and therefore more adequate for the determination of the 3D electronic structure. The first pilot experiments are scheduled and full user operation will follow.

The other planned beamline, the PEARL beamline, has also progressed. PEARL stands for PhotoEmission and Atomic Resolution Laboratory and will be specialized for photoelectron diffraction experiments combined with STM/AFM on nanostructured surfaces of novel materials. Here the frontend at the bending magnet has been installed and the endstation is close to be ordered. The perspective is that first test experiments can start end of 2011. Another positive development is the planned upgrade of the ARPES laboratory at UniFR (P. Aebi). Motivated by the transfer of the lab from Neuchâtel to Fribourg, adequate funds have been granted by the Faculty of Science, the Adolphe Merkle Institute and R'Equip (SNF). The new setup includes Laser ARPES and a sample transfer system which is compatible with the STM and pulsed laser deposition (PLD) system at UniFR and the PEARL endstation.

ARPES experiments are very often interpreted in terms of the one-particle spectral function and the matrix elements are neglected simply because there is no practical manner of evaluating them. Nevertheless, their knowledge may be crucial. Now there is a density functional theory based program package available, the so-called Munich SPR-KKR program package, which allows for one-step calculations (including the matrix elements). Recently there was a hands-on workshop on this, where members of the Fribourg group participated. It is now evaluated how useful/userfriendly this package is, in order to help spread it to other MaNEP groups.

Finally, another edition of the international workshop on ARPES and strong correlations, CORPES11, is being prepared to be held in Berkely this summer. It is organized with the contribution of members of MaNEP and the PSI. As for CORPES09, held at PSI, it brings together world leaders in photoemission and theorists working on correlated electron systems.

7 X-ray elastic and inelastic scattering

Responsible: Urs Staub (PSI)

For the technique of X-ray elastic and inelastic scattering, a one day workshop was organized at the Swiss Light Source (SLS), at PSI, by M. Grioni (EPFL) and U. Staub (PSI). The purpose of the workshop was to gather all interested

groups and persons within MaNEP to discuss resonant X-ray techniques and their possible applications to the understanding of the properties of materials with novel electronic properties. It began with tutorials on X-ray absorption (XAS) (F. Nolting, SLS/PSI), resonant X-ray diffraction (U. Staub) and inelastic resonant X-ray scattering (RIXS) (M. Grioni) aimed at young scientists, PhD students and postdocs. After lunch, Pietro Gambardella (University of Barcelona) gave an invited lecture on magnetic atoms, molecules, and nanostructures investigated by polarized X-ray absorption spectroscopy. This was followed by an overview of the possibilities offered at the Swiss Light Source. In this part, most of the beamlines and experimental options offering resonant X-ray techniques were presented by the representing beamline staff members. This included techniques such as extended X-ray absorption fine structure (EXAFS), microscopic XAS applications as well as several types of resonant soft and hard X-ray scattering techniques. There were then two short contributions by participants on the applications of RIXS and XAS to prototypical cuprates and magnetoelectric PZT/LSMO heterostructures, respectively. The workshop was rounded up by a discussion on needs, questions and wishes. After closing the workshop, a tour to the represented experiments around the SLS were given for those who wanted to see the experiments in real life. This event was a great success, with approximately 30 participants, with active questions and discussions, involving several MaNEP groups from Geneva, Fribourg, Lausanne, Zurich, Empa and the PSI. Most of the participants were postdocs and PhD students (Fig. 1). Due to the success and the mostly young participants, it is foreseen to organize a second small one day workshop in early 2012, with a slightly different focus. The idea is to shift the subject from more absorption based techniques to more scattering techniques. This will include non-resonant diffraction (which was intentionally excluded in the previous workshop to keep a clear focus), which notably can be performed on the newly refurbished materials science beamline at the SLS.

8 Infrared spectroscopy

Responsible: Leonardo Degiorgi (ETHZ)

There is a broad know-how on optics within the Swiss scientific community, particularly as far as the infrared (IR) spectroscopy is concerned. Three research groups at UniGE (D.



Figure 1: Attentive audience of MaNEP Workshop on Resonant X-ray Techniques on November 2, 2010 at PSI

van der Marel), UniFR (Ch. Bernhard) and ETHZ (L. Degiorgi) exploit a wealth of optical techniques, like reflectivity and transmission measurements, broadband ellipsometry, time domain THz and Kerr-effect spectroscopy, as well as IR-microscopy. These methods allow covering a rather broad energy interval from the THz up to the ultraviolet, which is the prerequisite for having access to all energy scales, relevant to the nowadays modern problems in condensed matter. It is also worthwhile to emphasize the combination of those spectroscopies with externally tunable variables like temperature, magnetic and electric field, and also pressure. Several important progresses were recently made in advancing the available setups. Worth mentioning are the following advancements:

- The ETH group successfully installed a new generation spectrometer (Bruker Vertex 80v) and is in the process to adapt the sample holder in order to allow data collection for sample under externally tunable moderate pressures. This latter setup plays an important role for the investigation of pressure-induced single domain (i.e. totally detwinned) iron-pnictide superconductors.
- The Geneva group recently developed two systems for magneto-optics: (i) The first system is based on time-domain THz magneto-optics. This system is equipped with a superconducting magnet providing fields up to 2.5 T at cryogenic temperatures, and can be used routinely for measurement of the Faraday rotation, ellipticity and optical constants of right-handed and left-handed photons in the frequency range from 1 to 100 cm^{-1} . (ii) The sec-

ond one, using Fourier transform infrared spectroscopy and a split-coil magnet, has been equipped for magneto-optical Kerr and Faraday effect in the frequency range of 20 to 600 cm^{-1} , fields up to 7 T, and temperatures between 2.5 and 300 K. Accuracy was demonstrated to be sufficient for detecting the Faraday rotation of monolayer graphene.

There is furthermore an ongoing effort to coordinate and exploit all available synergies and know-how among the three Swiss groups, in order to optimize the employment of this large variety of spectroscopic tools. In this respect, a relevant role is played by the infrared (IR) beamline at the Swiss Light Source (SLS) which is now in operation for more than one year and where important progresses were achieved. The IR microscope allows to perform, with a diffraction limited spot size, spectro-microscopy in transmission and reflection. Moreover, measurements with an ATR objective are possible. This analytical tool opens-up new perspectives in fields like condensed and soft matter physics, chemistry and life science, to name just a few. Spectroscopy experiments at higher pressure using the diamond anvil cell have been conducted successfully. Equipment to perform spectroscopy at lower temperature using the small spot size is also available. The SLS facility attracts scientists from different institutions and boosts the collaboration within (but not only!) the groups of the MaNEP network.

Finally it is worth mentioning that the 9th conference on Low Energy Electrodynamics of Solids (LEES) took place in July 2010 in Switzerland. Experts on optical spectroscopy from all over the world gathered at this meeting. The know-how on optical spectroscopy in Switzerland was involved through MaNEP scientists acting as a conference chair, as local organizers and as program committee members.

9 Theoretical and numerical methods

Responsible: Matthias Troyer (ETHZ)

Software development

Software and algorithm developments are described in the various research projects. For clarity, these are all reported together hereafter.

a) *High Performance and High Productivity Computing (HP2C)* With the start of MAQUIS project (Modern Algorithms for QUantum Interactions Systems) the technology platform

on computational and theoretical methods has been very active in the field of software development for future numerical simulations. This collaboration between three MaNEP groups (T. Giamarchi (UniGE), F. Mila (EPFL) and M. Troyer (ETHZ)) had obtained a grant of 1'200'000 Swiss Francs from the Swiss High Performance and Productivity Computing (HP2C) initiative, to hire software engineers for three years.

This year, all the software developers have been hired and work has started on the development of next-generation high-performance simulation codes for quantum Monte Carlo methods, the density matrix renormalization group (DMRG) method, exact diagonalization, series expansion and new tensor network algorithm. After one year of this collaboration, the codes are approaching production quality. Collaborative scientific projects within MaNEP using these codes are now being planned.

b) *ALPS 2.0* We have developed and published a major new version of the ALPS libraries and applications. ALPS 2.0 contains new applications, such as dynamical mean field theory solvers, and a code for time-dependent DMRG simulations. Other major changes in release 2.0 include the use of HDF5 for binary data, evaluation tools in Python, support for the Windows operating system, the use of CMake as build system and binary installation packages for Mac OS X and Windows, and integration with the VisTrails workflow provenance tool.

Algorithmic developments

Algorithmic developments by MaNEP teams have been discussed in this report already with the individual MaNEP projects. Here we provide a short summary of those developments. We have also written a review article about the recently developed continuous time quantum Monte Carlo algorithms for dynamical mean field theory which are currently being employed for simulating correlated materials and ultracold atomic gases.

c) *Tensor network methods* We have improved new two-dimensional generalizations of the density matrix renormalization group method, especially the infinite system PEPS method. The main achievements of the last year were the implementation of abelian symmetries in these algorithms, and the development of tensor network algorithms for quantum magnets built from non-Abelian anyons instead of standard $SU(2)$ spins.

Another development was new tensor-network algorithms for electronic structure calculations. These are higher-dimensional generalizations of the density matrix renormalization group method and our article is the first development of such a method for the electronic structure of molecules.

d) *Quantum Monte Carlo methods* We have developed a diagrammatic quantum Monte Carlo (DiagMC) algorithm for the Hubbard model. This algorithm samples connected Feynman diagrams instead of the partition function and works successfully in the correlated Fermi liquid regime of the Hubbard model. We will use it in the future to calculate phase diagrams and equations of state of 2D and 3D Hubbard model in the moderately correlated regime.

We have improved on a proposal by Byczuk and Vollhardt of a bosonic version of dynamical mean field theory (B-DMFT) and developed a quantum Monte Carlo method to solve the

B-DMFT equations. The algorithm is very efficient and surprisingly it turns out that the B-DMFT approximation can quantitatively reproduce the phase diagram of a 3D Bose Hubbard model with errors of less than 2%, making this an extremely good approximative method.

Summer school on numerical methods

In the framework of this technology platform we have organized a summer school on numerical methods, held at ETHZ from 13 to 18 September, 2010. Swiss participants were funded by MaNEP and the school was cofinanced by CECAM and the European Science Foundation. Topics covered included Monte Carlo methods, density matrix renormalization group, series expansion, and dynamical mean field theory. The theoretical lectures were complemented by hands-on tutorials using the ALPS software and lectures by experimentalists.

Material	Growth technique	Furnace	Conductor	Insulator	Magnetic	MaNEP Institution	Responsible
Various elemental metals	Bridgman, Zone melting	RF Induction, Electronic bombardment	yes			UniGe	Giannini (022.3796076, enrico.giannini@unige.ch)
Chalcogenides and pnictides							
FeTe(1-x)Sx	self flux, TSFZ	1-zone vertical furnace, Mirror image furnace	yes, superc. Tc<13K			UniGe	Giannini (022.3796076, enrico.giannini@unige.ch)
FeTe(1-x)Sx	self flux	1-zone vertical furnace	yes, superc. Tc<13K			PSI	kazmierz.conder@psi.ch
AFeSe2 (A = K, Cs, Rb)	self flux	1-zone vertical furnace	yes, superc. Tc<30K			PSI	kazmierz.conder@psi.ch
LiFeAsO(1-x)Fx (Li=La, Pr, Nd, Sm, Gd)	flux growth under HP	cubic anvil hot press	Yes superc. Tc = 20 - 55K			ETHZ	Karpinski(044.6332254, karpinski@phys.ethz.ch)
Sr(Fe,Co)AsO(1-x)Fx	flux growth under HP	cubic anvil hot press	Yes superc. Tc = 20 - 55K			ETHZ	Karpinski(044.6332254, karpinski@phys.ethz.ch)
CaFe(2-x)CoAs2	flux growth		Yes superc. Tc = 20K			ETHZ	Karpinski(044.6332254, karpinski@phys.ethz.ch)
EuFe(2-x)CoAs2	flux growth		Yes superc. Tc = 20K			ETHZ	Karpinski(044.6332254, karpinski@phys.ethz.ch)
Ba1-xRbxFeAs2	self flux	1-zone vertical furnace	Yes			UniGe	Giannini (022.3796076, enrico.giannini@unige.ch)
Bi2Se3, Bi2Te3	self flux, TSFZ	1-zone furnace, Mirror image furnace	topological insulator	topological insulator		UniGe	Giannini (022.3796076, enrico.giannini@unige.ch)
CuxBi2Sb3, PbxBi2Te3	Zone melting	Mirror image furnace	yes, superc. Tc = 3 - 5 K	yes (depending on x)	ferromagnetic, Tc = 121K	UniGe	Giannini (022.3796076, enrico.giannini@unige.ch)
CoS2	CVT	2-zone furnace	Yes		ferromagnetic Tc = 86K	EPFL	Berger 021.693.4484, helmuth.berger@epfl.ch
NbSe2	CVT	2-zone furnace	Yes		ferromagnetic Tc = 86K	EPFL	Berger 021.693.4484, helmuth.berger@epfl.ch
NbTe2	CVT	2-zone furnace	Yes		ferromagnetic Tc = 86K	EPFL	Berger 021.693.4484, helmuth.berger@epfl.ch
TaS2	CVT	2-zone furnace	Yes		ferromagnetic Tc = 130K	EPFL	Berger 021.693.4484, helmuth.berger@epfl.ch
TaTe2	CVT	2-zone furnace	Yes		ferromagnetic Tc = 130K	EPFL	Berger 021.693.4484, helmuth.berger@epfl.ch
TiTe2	CVT	2-zone furnace	Yes		ferromagnetic Tc = 130K	EPFL	Berger 021.693.4484, helmuth.berger@epfl.ch
TiSe2	CVT	2-zone furnace	Yes		ferromagnetic Tc = 130K	EPFL	Berger 021.693.4484, helmuth.berger@epfl.ch
ZrS3, ZrSe3, ZrTe3	CVT	2-zone furnace	No	Semiconductor		EPFL	Berger 021.693.4484, helmuth.berger@epfl.ch
HfS3, HfSe3, HfTe3	CVT	2-zone furnace	No	Semiconductor		EPFL	Berger 021.693.4484, helmuth.berger@epfl.ch
GaS, GaSe, GaTe	Bridgman	1-zone furnace with temp.gradient	No	Semiconductor		EPFL	Berger 021.693.4484, helmuth.berger@epfl.ch
BaV3S3	Flux growth	1-zone furnace with temp.gradient	Yes	Insulator		EPFL	Berger 021.693.4484, helmuth.berger@epfl.ch
P03(PS4)2	CVT	2-zone furnace	No	Semiconductor	diamagnetic	EPFL	Berger 021.693.4484, helmuth.berger@epfl.ch
MnPS3	CVT	2-zone furnace	No	Semiconductor	magnetic properties	EPFL	Berger 021.693.4484, helmuth.berger@epfl.ch
MnPSe3	CVT	2-zone furnace	No	Semiconductor	magnetic properties	EPFL	Berger 021.693.4484, helmuth.berger@epfl.ch
NiPS3	CVT	2-zone furnace	No	Semiconductor	magnetic properties	EPFL	Berger 021.693.4484, helmuth.berger@epfl.ch
NiPS63	CVT	2-zone furnace	No	Semiconductor	magnetic properties	EPFL	Berger 021.693.4484, helmuth.berger@epfl.ch
FePS63	CVT	2-zone furnace	No	Semiconductor	magnetic properties	EPFL	Berger 021.693.4484, helmuth.berger@epfl.ch
FePS63	CVT	2-zone furnace	No	Semiconductor	magnetic properties	EPFL	Berger 021.693.4484, helmuth.berger@epfl.ch
CoC2S4	CVT	2-zone furnace	Tc	Semiconductor	ferromagnetic	EPFL	Berger 021.693.4484, helmuth.berger@epfl.ch
CoC2Se4	CVT	2-zone furnace	Yes	Semiconductor	ferromagnetic	EPFL	Berger 021.693.4484, helmuth.berger@epfl.ch
Cuprates							
Sr14Cu24O41	TSFZ	Mirror image furnace	no	yes		UniGe	Giannini (022.3796076, enrico.giannini@unige.ch)
(Sr,M1,M2)14Cu24O41-x (M1, M2 = Ca, Bi, Y, ...)	TSFZ	Mirror image furnace	no	yes		UniGe	Giannini (022.3796076, enrico.giannini@unige.ch)
Sr(14-x)Ca(x)Cu24O41 (x up to 12.2)	high pressure TSFZ	Mirror image furnace				PSI	Kazmierz Conder/Ekaterina Pomjakushina
Bi2-xPbxS2Cu3O10	TSFZ	Mirror image furnace	Yes, superc. Tc=10 K			UniGe	Giannini (022.3796076, enrico.giannini@unige.ch)
Bi2-xPbxS2Cu3O10+d	TSFZ	Mirror image furnace	Yes, superc. Tc=10 K			UniGe	Giannini (022.3796076, enrico.giannini@unige.ch)
Bi2-xPbxS2Cu2O8	TSFZ, self flux	Mirror image furnace	Yes, superc. Tc=91 K			UniGe	Giannini (022.3796076, enrico.giannini@unige.ch)
Bi2-xPbxS2CaCu2O8	TSFZ	Mirror image furnace, 3-zone vertical	Yes, superc. Tc=83 K			UniGe	Giannini (022.3796076, enrico.giannini@unige.ch)
Bi2S2Cu2O8	Flux growth	Mirror image furnace	Yes, superc. Tc=15 K			UniGe	Giannini (022.3796076, enrico.giannini@unige.ch)
Bi1.6Pb0.4S2CaCu2O8 Pr, Y doped	Flux growth	1-zone furnace with temp.gradient	Yes			EPFL	Berger 021.693.4484, helmuth.berger@epfl.ch
Bi1.6Pb0.4S2CaCu2O8	Flux growth	1-zone furnace with temp.gradient	Yes			EPFL	Berger 021.693.4484, helmuth.berger@epfl.ch
Bi2S2CaCu2O8	Flux growth	1-zone furnace with temp.gradient	Yes			EPFL	Berger 021.693.4484, helmuth.berger@epfl.ch
Bi2S2CaCu2O8 Ni, Co doped	Flux growth	1-zone furnace with temp.gradient	Yes			EPFL	Berger 021.693.4484, helmuth.berger@epfl.ch
REBa2Cu3O7	self flux	3-zone furnace, Top seeded growth	Yes, superc. Tc=92 K			UniGe	Giannini (022.3796076, enrico.giannini@unige.ch)
YBa2Cu4O8	HP	high O2 pressure	yes, superc. Tc=80K			ETHZ	Karpinski(044.6332254, karpinski@phys.ethz.ch)
YBa(2-x)SrxCu4O8	solid state synthesis	high O2 pressure	yes, superc. Tc=80K			ETHZ	Karpinski(044.6332254, karpinski@phys.ethz.ch)
YBa2Cu3O(8+x) x=0-1, 1.60-1.80	TSFZ	Mirror image furnace	superconductor			PSI	Kazmierz Conder/Ekaterina Pomjakushina
La(2-x)SrxCuO4	TSFZ	Mirror image furnace	superconductor	AFM		PSI	Kazmierz Conder/Ekaterina Pomjakushina
La2CuO4	solid state synthesis	Mirror image furnace	superconductor			PSI	Kazmierz Conder/Ekaterina Pomjakushina
Ca(2-x)NaxCuO2Cl2	HP	cubic anvil hot press	yes, superc. Tc=13-25K			ETHZ	Karpinski(044.6332254, karpinski@phys.ethz.ch)

Material	Other Transition Metal Oxides	ampoule method	resistive furnace	yes, superc. Tc=9.6K	no	stacked-triangular AF	yes	ETHZ	Karpinski(044.6332254, karpinski@phys.ethz.ch)
NEW!	KO ₂ O6	HP	cubic anvil hot press					ETHZ	Karpinski(044.6332254, karpinski@phys.ethz.ch)
NEW!	Nd ₂ O ₂ O6.5	TSFZ	Mirror image furnace					EMPA	Weidenkaiff(044.8234131, Anke.Weidenkaiff@empa.ch)
	CaMnO3	TSFZ	Mirror image furnace					PSI	Kazmierz Conder/Ekaterina Pomjakushina
	YMnO3	TSFZ	Mirror image furnace					PSI	Kazmierz Conder/Ekaterina Pomjakushina
	DyMnO3	TSFZ	Mirror image furnace					PSI	Kazmierz Conder/Ekaterina Pomjakushina
	LaCoO3	TSFZ	Mirror image furnace					PSI	Kazmierz Conder/Ekaterina Pomjakushina
	La(1-x)SrxCoO3	TSFZ	Mirror image furnace					PSI	Kazmierz Conder/Ekaterina Pomjakushina
	SiCu2(BO3)2	TSFZ	Mirror image furnace					PSI	Kazmierz Conder/Ekaterina Pomjakushina
	LaFeO3	TSFZ	Mirror image furnace					PSI	Kazmierz Conder/Ekaterina Pomjakushina
	La(1-x)SrxFeO3	TSFZ	Mirror image furnace					PSI	Kazmierz Conder/Ekaterina Pomjakushina
	ErFeO3	TSFZ	Mirror image furnace					PSI	Kazmierz Conder/Ekaterina Pomjakushina
	TbBaCo2O(5+x)	TSFZ	Mirror image furnace					PSI	Kazmierz Conder/Ekaterina Pomjakushina
	LuFe2O4	TSFZ	Mirror image furnace					PSI	Kazmierz Conder/Ekaterina Pomjakushina
	NaxCoO2 (x=0.7, 0.75, 1)	TSFZ	Mirror image furnace					PSI	Kazmierz Conder/Ekaterina Pomjakushina
	NdBaCo2O(5+x)	TSFZ	Mirror image furnace					PSI	Kazmierz Conder/Ekaterina Pomjakushina
	Ni1/3Sr2/3FeO3	TSFZ	Mirror image furnace					PSI	Kazmierz Conder/Ekaterina Pomjakushina
	SnBaMn2O6	TSFZ	Mirror image furnace					PSI	Kazmierz Conder/Ekaterina Pomjakushina
	LnBaCo2O5+x, x=0-1, 16O-18O	solid state synthesis	1-zone furnace with temp.gradient	Yes				EPFL	Kazmierz Conder/Ekaterina Pomjakushina
	Nd0.75CoO2	Flux grown	1-zone furnace with temp.gradient					EPFL	Berger 021.693.4484, helmuth.berger@epfl.ch
	Nd0.70CoO2	Flux grown	1-zone furnace with temp.gradient					EPFL	Berger 021.693.4484, helmuth.berger@epfl.ch
	Ca3Co2O6	Flux grown	1-zone furnace with temp.gradient					EPFL	Berger 021.693.4484, helmuth.berger@epfl.ch
	Ca3Co4O9	Flux grown	1-zone furnace with temp.gradient					EPFL	Berger 021.693.4484, helmuth.berger@epfl.ch
	(La(1-x)Prx)1-yCayMnO3, 16O-18O	solid state synthesis	1-zone furnace with temp.gradient					PSI	Kazmierz Conder/Ekaterina Pomjakushina
	CaVO3	TSFZ	Mirror image furnace					PSI	Kazmierz Conder/Ekaterina Pomjakushina
	Fe3O4	CVT	2-zone furnace	Yes	metal below 1K			EPFL	Berger 021.693.4484, helmuth.berger@epfl.ch
	LiCuO2	Flux grown	1-zone furnace with temp.gradient	No				EPFL	Berger 021.693.4484, helmuth.berger@epfl.ch
	alpha TeVO4	CVT	2-zone furnace	No				EPFL	Berger 021.693.4484, helmuth.berger@epfl.ch
	beta TeVO4	CVT	2-zone furnace	No				EPFL	Berger 021.693.4484, helmuth.berger@epfl.ch
	ZnO	CVT	2-zone furnace	No	Yes Tc=1k			EPFL	Berger 021.693.4484, helmuth.berger@epfl.ch
	CoRe2O7	CVT	2-zone furnace	No				EPFL	Berger 021.693.4484, helmuth.berger@epfl.ch
	CuW/O4	Flux grown and CVT	1-zone furnace with temp.gradient	No				EPFL	Berger 021.693.4484, helmuth.berger@epfl.ch
	LiCu2O2	Flux grown	2-zone furnace					EPFL	Berger 021.693.4484, helmuth.berger@epfl.ch
	Mo4O11, MoO3	self-flux	1-zone furnace with temp.gradient					EPFL	Berger 021.693.4484, helmuth.berger@epfl.ch
NEW!	Ca3Co4O9	TSFZ	Mirror image furnace					EMPA	Weidenkaiff(044.8234131, Anke.Weidenkaiff@empa.ch)
NEW!	B2(W,Mo)O6 nanomaterials	MW-HT	hydrothermal autoclave					Unizh	Patzke(044.63.54691, greta.patzke@aci.uzh.ch)
NEW!	B2WO6 nanomaterials	MW-HT	hydrothermal autoclave					Unizh	Patzke(044.63.54691, greta.patzke@aci.uzh.ch)
NEW!	Bi6S2O15 nanowires	MW-HT	hydrothermal autoclave					Unizh	Patzke(044.63.54691, greta.patzke@aci.uzh.ch)
	Berides								
	MgB2	Mg-flux under HP	cubic anvil hot press	yes, superc. Tc=39K				Unige	Giannini (022.3796076, enrico.giannini@unige.ch)
	MgB2	Mg-flux under HP	cubic anvil hot press	yes, superc. Tc=39K				Unige	Karpinski(044.6332254, karpinski@phys.ethz.ch)
	Mg(1-x)AlxB2	Mg-flux under HP	cubic anvil hot press	yes				ETHZ	Karpinski(044.6332254, karpinski@phys.ethz.ch)
	MgB2-xCy	Mg-flux under HP	cubic anvil hot press	yes				ETHZ	Karpinski(044.6332254, karpinski@phys.ethz.ch)
	Mg(1-x)MnxB2	Mg-flux under HP	cubic anvil hot press	yes				ETHZ	Karpinski(044.6332254, karpinski@phys.ethz.ch)
	Mn(1-x)FexB2	Mg-flux under HP	cubic anvil hot press	yes				ETHZ	Karpinski(044.6332254, karpinski@phys.ethz.ch)
	NdNi2B2C	arc melting	cubic anvil hot press	superconductor				PSI	Kazmierz Conder/Ekaterina Pomjakushina
	Chevreil phases								
	SnM6S8	solid state synthesis		Yes superc. Tc = 14K				Unige	Fischer (022.3796270, Oystein.Fischer@unige.ch)
	Sr(1-x)PbMxM6S8	solid state synthesis		Yes superc. Tc = 7-12K				Unige	Fischer (022.3796270, Oystein.Fischer@unige.ch)
	LaM6S8	solid state synthesis		Yes superc. Tc = 7K				Unige	Fischer (022.3796270, Oystein.Fischer@unige.ch)
	Me6Se8	solid state synthesis		Yes superc. Tc = 6K				Unige	Fischer (022.3796270, Oystein.Fischer@unige.ch)
	Me6S8	solid state synthesis		Yes superc. Tc = 1K				Unige	Fischer (022.3796270, Oystein.Fischer@unige.ch)
	Me6S8B2	solid state synthesis		Yes superc. Tc = 13.5K				Unige	Fischer (022.3796270, Oystein.Fischer@unige.ch)
	InM6S8	solid state synthesis		Yes				Unige	Fischer (022.3796270, Oystein.Fischer@unige.ch)
	Tl2M6S6E6	solid state synthesis		Yes superc. Tc = 4.2K				Unige	Fischer (022.3796270, Oystein.Fischer@unige.ch)
	In2M6S6E6	solid state synthesis		Yes superc. Tc = 2.9K				Unige	Fischer (022.3796270, Oystein.Fischer@unige.ch)

Ni ₂ Mo ₆ Se ₆	solid state synthesis	No	Metal-Insulator	UnGe	Fischer (022.3796270, Oystein.Fischer@unige.ch)
K ₂ Mo ₆ Se ₆	solid state synthesis	No	Metal-Insulator	UnGe	Fischer (022.3796270, Oystein.Fischer@unige.ch)
Rb ₂ Mo ₆ Se ₆	solid state synthesis	No	Metal-Insulator	UnGe	Fischer (022.3796270, Oystein.Fischer@unige.ch)
Cs ₂ Mo ₆ Se ₆	solid state synthesis	No	Metal-Insulator	UnGe	Fischer (022.3796270, Oystein.Fischer@unige.ch)
Mo ₆ Se ₆	solid state synthesis	No		UnGe	Fischer (022.3796270, Oystein.Fischer@unige.ch)
Cs ₃ Mo ₁₂ Si ₁₄	solid state synthesis	Yes superc. Tc = 7K		UnGe	Fischer (022.3796270, Oystein.Fischer@unige.ch)
Ba ₂ Mo ₆ S ₉	solid state synthesis	Yes superc. Tc = 5K		UnGe	Fischer (022.3796270, Oystein.Fischer@unige.ch)
Ru ₂ (2n)Mo ₆ (n+9)S ₆ (n+13) (n = 1-4)	solid state synthesis	Yes superc. Tc = 4-10K		UnGe	Fischer (022.3796270, Oystein.Fischer@unige.ch)
Silicides, Germanides, Carbides					
TmSi ₂ (TM=Transition Metal: Co, Fe, Mn, ...)	Czochralski, TSFZ	yes/no		UnGe	Giannini (022.3796076, enrico.giannini@unige.ch)
CeCeGa ₃	flux growth	yes/no		UnGe	Giannini (022.3796076, enrico.giannini@unige.ch)
EuNi ₂ Si ₂ (1-x)Ge _x 2	TSFZ	yes	Insulator	UnGe-PSI	Kazimierz Conder/Ekaterina Pomjakushina
C-60	Sublimation	No	Insulator	EPFL	Berger 021.693.4484, helmuth.berger@epfl.ch
Chalcogenates, Phosphates					
Cu ₃ TeO ₆	CVT and flux grown	No		EPFL	Berger 021.693.4484, helmuth.berger@epfl.ch
Cu ₃ Sb ₂ O ₅	CVT	No		EPFL	Berger 021.693.4484, helmuth.berger@epfl.ch
Ni ₅ (SeO ₃) ₄ Cl ₂	CVT	No		EPFL	Berger 021.693.4484, helmuth.berger@epfl.ch
Ni ₅ (SeO ₃) ₄ Br ₂	CVT	No		EPFL	Berger 021.693.4484, helmuth.berger@epfl.ch
Ni ₅ (SeO ₃) ₄ Br ₂	CVT	No		EPFL	Berger 021.693.4484, helmuth.berger@epfl.ch
Cu ₂ TeO ₅ Cl ₂	CVT	No		EPFL	Berger 021.693.4484, helmuth.berger@epfl.ch
Cu ₂ TeO ₅ Br ₂	CVT	No		EPFL	Berger 021.693.4484, helmuth.berger@epfl.ch
Co ₆ (TeO ₃) ₂ (TeO ₆)Cl ₂	CVT	No		EPFL	Berger 021.693.4484, helmuth.berger@epfl.ch
Co ₆ (TeO ₃) ₂ (TeO ₆)Br ₂	CVT	No		EPFL	Berger 021.693.4484, helmuth.berger@epfl.ch
Co ₂ TeO ₃ Cl ₂	CVT	No		EPFL	Berger 021.693.4484, helmuth.berger@epfl.ch
Co ₂ TeO ₃ Br ₂	CVT	No		EPFL	Berger 021.693.4484, helmuth.berger@epfl.ch
Ni ₅ (TeO ₃) ₄ Cl ₂	CVT	No		EPFL	Berger 021.693.4484, helmuth.berger@epfl.ch
Ni ₅ (TeO ₃) ₄ Br ₂	CVT	No		EPFL	Berger 021.693.4484, helmuth.berger@epfl.ch
Ni ₅ (TeO ₃) ₄ Br ₂ ·xCl _x	CVT	No		EPFL	Berger 021.693.4484, helmuth.berger@epfl.ch
Co ₇ (TeO ₄) ₂ Br ₆	CVT	No		EPFL	Berger 021.693.4484, helmuth.berger@epfl.ch
Cu ₃ Sb ₂ TeO ₃ Cl ₂	CVT	No	Insulator	EPFL	Berger 021.693.4484, helmuth.berger@epfl.ch
Cu ₃ (SeO ₃) ₄ Cl ₂	CVT	No		EPFL	Berger 021.693.4484, helmuth.berger@epfl.ch
Cu ₂ Te ₂ O ₅	CVT	No		EPFL	Berger 021.693.4484, helmuth.berger@epfl.ch
Cu ₂ Te ₂ O ₅ Cl	CVT	No		EPFL	Berger 021.693.4484, helmuth.berger@epfl.ch
Fe ₂ Te ₂ O ₅ Cl	CVT	No	Insulator	EPFL	Berger 021.693.4484, helmuth.berger@epfl.ch
Fe ₂ Te ₂ O ₅ Br	CVT	No	Insulator	EPFL	Berger 021.693.4484, helmuth.berger@epfl.ch
Ni ₅ SeO ₃	CVT	No	Insulator	EPFL	Berger 021.693.4484, helmuth.berger@epfl.ch
TiOBr	CVT	No	Insulator	EPFL	Berger 021.693.4484, helmuth.berger@epfl.ch
Ni ₃ TeO ₆	CVT	No	Insulator	EPFL	Berger 021.693.4484, helmuth.berger@epfl.ch
Co ₃ TeO ₆	CVT	No	Semiconductor	EPFL	Berger 021.693.4484, helmuth.berger@epfl.ch
Cu ₄ CoTeO ₆	Flux grown	No	Semiconductor	EPFL	Berger 021.693.4484, helmuth.berger@epfl.ch
Bi(Cu _{1-x} Zn _x) ₂ PO ₆ (x=0 - 0.05)	TSFZ	No	Semiconductor	PSI	Berger 021.693.4484, helmuth.berger@epfl.ch
Cs ₃ Cu(3-x)Ni _x (PO ₄) ₄	solid state synthesis	No		PSI	Kazimierz Conder/Ekaterina Pomjakushina
Organics					
Pentacene	CVT	No	Insulator	EPFL	Berger 021.693.4484, helmuth.berger@epfl.ch
Rubrene	CVT	No	Insulator	EPFL	Berger 021.693.4484, helmuth.berger@epfl.ch
Coronene	CVT	No	Insulator	EPFL	Berger 021.693.4484, helmuth.berger@epfl.ch
Tetracene	CVT	No	Insulator	EPFL	Berger 021.693.4484, helmuth.berger@epfl.ch
Anthracene	CVT	No	Insulator	EPFL	Berger 021.693.4484, helmuth.berger@epfl.ch
TQNQ	CVT	No	Insulator	EPFL	Berger 021.693.4484, helmuth.berger@epfl.ch
TTF-TCNQ	CVT	No	Organic Conductor	EPFL	Berger 021.693.4484, helmuth.berger@epfl.ch
Perylene	CVT	No	Insulator	EPFL	Berger 021.693.4484, helmuth.berger@epfl.ch
TQNQ-Perylene complex	CVT	No	p-type semiconductor	EPFL	Berger 021.693.4484, helmuth.berger@epfl.ch
Copper Phthalocyanine	CVT	No		EPFL	Berger 021.693.4484, helmuth.berger@epfl.ch
In ₂ V ₀₅	CVT	No		EPFL	Berger 021.693.4484, helmuth.berger@epfl.ch
Co _{1/2} Te _{1/2} O _{1+x} Cl _{1-x}	CVT	No		EPFL	Berger 021.693.4484, helmuth.berger@epfl.ch
Co ₅ (TeO ₃) ₄ X ₂ (X = Cl, Br).	CVT	No	Insulator	EPFL	Berger 021.693.4484, helmuth.berger@epfl.ch
Co ₅ (SeO ₃) ₄ X ₂ (X = Cl, Br).	CVT	No	Insulator	EPFL	Berger 021.693.4484, helmuth.berger@epfl.ch

3 Knowledge and technology transfer

Technology transfer is a process that ensures that scientific and also technological tool developments are accessible to a wider range of users and general public in general. To be effective, the technology transfer process requires a dynamic approach, that should be both proactive and iterative. This is particularly the case with industry, where the concrete exploitation of basic research and technology into new products and applications depends on several factors. The KTT-related MaNEP activities are therefore structured into three main directions which are: continuous contacts and discussions with industry and general public, the establishment of joint projects, and the setting up of internal and external activities for a sustainable technology transfer.

3.1 Contacts with industry

Sécheron

Sécheron is specialized in the design and fabrication of high-voltage switches and current breakers for electric power applications in general. The physics of electric arc interruption is closely related to the electronic and metallurgical properties of alloys used in the electric contacts. The metallurgy laboratory of Dr. Enrico Giannini has been working together with research engineers from Sécheron. This collaborative work has covered the preparation of a CTI proposal (under way), and continuous support and services in sample analysis and characterization in general.

Caran d'Ache SA

Caran d'Ache SA is a renowned Swiss manufacturer of writing instruments and related accessories. New materials and coatings are of particular interest for their products. MaNEP has been invited for visits to their factory in Geneva, and MaNEP activities and laboratory equipment have also been presented to the company. The process of gathering mutual knowledge of skills was completed by selective, successful research support tasks. As a consequence of these preliminary work, several potential projects have been identified. These projects cover both functional applications of thin film technology and micro-metallurgy, as well as decorative applications. A CTI project has been defined, and will be submitted shortly.

LAC Engineering SA

LAC Engineering SA (Laboratory of Advanced Coatings) is a small Swiss company specialized in surface coatings based in Plan-les-Ouates, near Geneva. LAC produces a range of different film types, namely alloys, high-purity metals, nitrides and carbides, amorphous carbon, polymers, oxides, etc. These materials are compatible with a variety of substrates: noble metals, alloys, steels, ceramics, polymers, sapphires, diamonds, etc. In particular, LAC offers physical vapor deposition (PVD) coatings that are suitable for functional and/or decorative applications. The ultra-thin layers are deposited in such a way as to retain the original surface finish, e.g. satin, milled or mirror finish, and to achieve the tolerances required in, for example, microtechnology assemblies. As with Caran d'Ache SA, the potential of collaborative work with MaNEP has successfully been promoted. The established synergy with LAC stems from the fact that the company offers mostly customized solutions, in particular for the watch industry. The changing nature of the industry requirements demands increased flexibility in the design of new coatings. MaNEP has provided access to the analysis of the integrity of the coatings by AFM and SEM and this has opened the door for new applications, and also for new contacts with other industries.

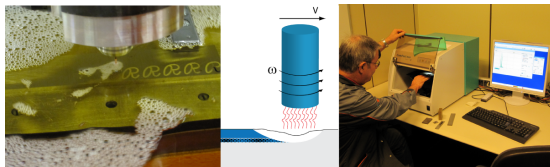


Figure 1: Technology transfer: desktop X-Ray fluorescence analysis was introduced to the tool machine industry.

3.2 Projects

Cut-and-coat project with AgieCharmilles

AgieCharmilles (a company of the +GF+ group) is a worldwide leader in electrical discharge machining (EDM). EDM is a well developed technology that is used to cut and shape a wide variety of conducting materials. The present project, part of the SNF-supported *economic stimulus package* “cut-and-coat process by wire-EDM project”, aims at producing surface and sub-surface alloys by combining EDM machining and new electrode materials. The produced surface alloys should improve mechanical properties such as wear and friction behavior, and also increase the corrosion resistance of the machined parts. The main idea of the project is to combine the possibilities of cutting precise and complicated metal parts by electrical discharge machining, together with the ability to deposit functional coatings on the surface of the machined parts. The research work is focused on the exploration and fine-tuning of new machining parameters, like the peak current, to produce homogeneous surface alloys. An important part of the research plan concerns the chemical analysis of the surface of

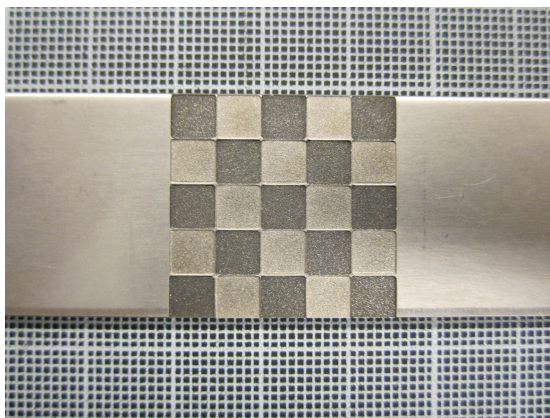


Figure 2: 25 mm × 25 mm “checkerboard” demonstration sample on stainless steel 316L. Dark squares: surface alloy synthesized by the modified EDM process.

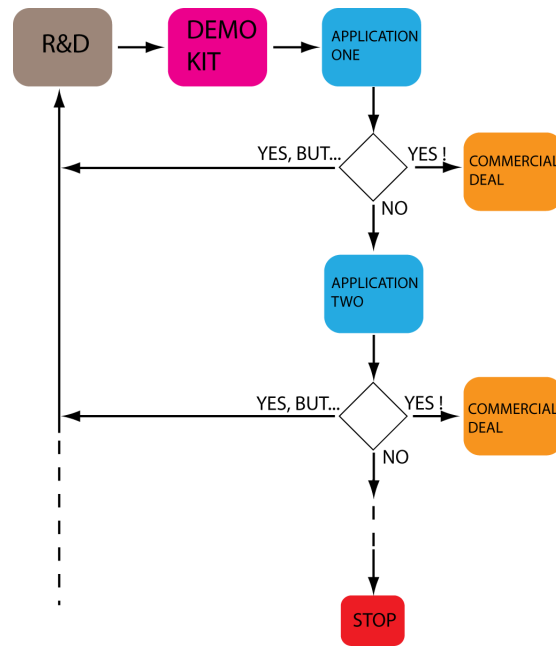


Figure 3: Iterative approach with test samples to create multiplier effects. Several companies are being approached, and the new process will be tested on functional parts, for which the cut-and-coat process can provide a clear commercial/technical advantage.

the machined parts.

In a real situation of technology transfer, this was achieved by extensive use of a Roanalytic ComPact eco X-ray fluorescence desktop analyzer. This instrument was installed close to the laboratory at the AgieCharmilles plant to provide rapid feedback for the iterative tuning of machine settings (Figs. 1 and 2, see also report on Project 3, paragraph 5.2).

Multiplier effects in industry

In this project, test workpieces will be produced and tested under real conditions. The results will be displayed to trigger interest among potential customers of the technology. This process is illustrated in the diagram of Fig. 3.

Asulab

This project is a MaNEP contribution to the “Clean car initiative” launched by the late Nicolas Hayek. The partners are Asulab (the R&D division of the Swatch Group) and the Belenos Holding SA. Belenos is in charge of designing and constructing an hydrogen-powered car, with the support of Asulab. The present project, which is carried out with the support of the CTI, aims at developing tailored

hydrogen sensing devices that are cheaper and more selective than those currently available. This objective is being achieved by using thin film technology and novel materials undergoing H₂-induced metal-insulator transitions. This project benefits from both the experience of Prof. Klaus Yvon's group in the field of materials for hydrogen storage, and the cumulated expertise in thin film growth of Prof. Øystein Fischer's team. Hydrogen fuel cells will certainly play a key role in future energy scenarios. And mass markets such as H₂ powered vehicles and H₂ production units for residential areas require H₂ detectors and sensors on a very large scale.

SwissNeutronics

Inside the SNF-supported *economic stimulus package* "Neutron optical devices for small samples" project, we are working together with SwissNeutronics on the focusing of neutrons for tiny samples (the sample size will be in the range of few mm³). The project covers three main tasks: (1) multichannel focusing guides/lenses; (2) adaptive focusing optics and (3) the new reflectometer concept Selene.

At the beginning of the project we performed extensive Monte Carlo simulations to figure out the optimal design of prototypes for all three main tasks. The proposed prototypes for task (2) and (3) were built and tested successfully in 2010. The simulated prototype for a multichannel neutron lens will be realized in 2011. The expected increase in neutron flux on 5 × 5 mm² sample area is around 10 – 15 (calculated for the BOA beamline at SINQ/PSI). For the new reflectometer concept Selene we have already demonstrated that a gain factor in neutron intensity of almost 10 (in comparison to the existing reflectometer AMOR at SINQ) can be reached.

Now we are working on an improved version where an additional gain factor of 10 is aimed. The adaptive focusing optics — task (2) — is also making good progress. The first prototype was tested in beginning of 2010 and it guided us into a second fully-motorized prototype which came into operation in December 2010. Neutronic tests will be realized soon.

The results of the MC simulations were presented on the neutron optics workshop NOP2010 in Alpe d'Huez (France) and it is planned to present the new results from 2010 on the European Neutron Scattering Conference in Prague (July 2011).

Glass micromachining

This is a new research and technology transfer project launched in October 2010. The main goal of the project is to develop a glass micromachining technology for microfluidics and general engraving applications. A proposal has been submitted to the Interreg authorities of West Switzerland, together with the Claude Bernard University from Lyon (Prof. Didier Léonard), the French company EREO SAS from Saint-Genis-Pouilly, and the genevan watch manufacturer Vacheron Constantin. The proposal has received full support and this two-year project is moving forward at quick pace. Technically, the glass machining method is based on what is known today as spark assisted chemical engraving (SACE). SACE is an unconventional micromachining technology based on electrochemical discharge phenomena on insulating glass. The innovative content of the project lies in the transposition of STM-like axis control of the sparking distance, and the simultaneous use of spectroscopic measurements to characterize and monitor the energy of the sparks (Fig. 4). The project has thus the double objective of achieving improved accuracy and control but also to gather a better understanding of the physical process.

Oxygen sensor with higher resolution

This project aims to develop electrochemical sensors (O₂, H₂, O₃) with higher resolution. It was initiated early in 2010 as part of the SNF-supported *economic stimulus package* "electrochemical sensors with higher resolution project". The initial starting industrial partner of the project, Nirva Industries, has now ceased activities related to electrochemi-

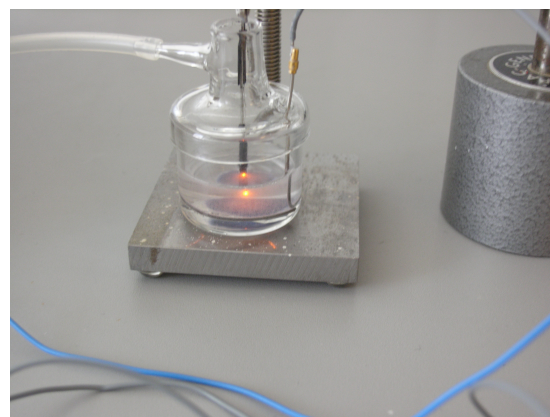


Figure 4: Machining glass at the microscopic scale using STM tools and expertise.

cal sensors. MaNEP is thus in the process of incorporating a new industrial partner into the project. Technically, it has transferred MaNEP STM electronics expertise to design a new amplifier setup for the oxygen sensor. Basically, STM-approved ultra-low leakage current amplifiers (leakage current of 20 – 200 fA) have been used to design a new measuring circuit that is able to measure sensor currents five times smaller than in the commercial electronics. Still in analogy with STM instrumentation, to minimize noise and wiring effects, the amplifier circuit has been miniaturized to be placed in the head of the sensor, very close to the current generation source. Minor mechanical modifications are under way to finish this milestone. A mechanical sampling system is being designed to measure the oxygen content in small packaging units (for example the Nespresso capsules). The system will use a microneedle to extract the gas from the capsule, and the high resolution of the oxygen sensor will help to determine trace levels of air resulting from defective packaging. This sampling system will serve for demonstration purposes (multiplier effects) and collaborative work with industries producing air-free packaged products (food, cosmetics, pharmaceuticals).

Marking technology for watch components

This project is described in detail in chapter 2, on Project 3. It is a particular case in technology transfer. The marking technology developed so far can be used in several industrial applications, of which the high-end watch industry is probably the most demanding in terms of performance and quality of results. The joint project with Vacheron Constantin is structured in such a way to provide a two-way technology transfer, in the sense that watchmaking skills can be “learned” and implemented later on to further develop peripheral devices required for series production, for medical applications for example.

3.3 Sustainability of technology transfer

The applied superconductivity laboratory

Research on applied superconductivity at the University of Geneva plays a key role for the Department of Condensed Matter Physics

(DPMC) and the Applied Physics Group (GAP) at the University of Geneva, as well as for MaNEP. The study and the development of new materials and their applications in superconductivity is a key objective for the DPMC. Until August 2010, research on applied superconductivity has been conducted by Prof. René Flükiger. He has established and developed fruitful collaborative work both with industry (for example Bruker-BioSpin) and international research institutions (CERN). Among the newest results, several “world records” of the superconducting critical current density have to be pointed out. These outstanding results have been achieved with both “conventional” and high- T_c superconductors. The expectations of industry and the general public about superconductivity are very high. It has therefore been decided to further continue research activities in applied superconductivity, after Prof. Flükiger’s retirement, under the responsibility of Prof. Alberto Morpurgo. Dr. Carmine Senatore is taking the operational lead of these activities. He is a young scientist with a very good experience in applied superconductivity. He has already deployed research activities in the group of Prof. René Flükiger. This appointment should ensure a continued research activity in applied superconductivity at the University of Geneva, which is a renowned institution in this field.

The development of high performance MgB_2 wires is one of the main scientific and technological objectives for our collaboration with Bruker-BioSpin. Bruker-BioSpin envisages the use of MgB_2 wires for economical NMR magnets operating at 20 K (low field / low resolution magnets) and also as a partial replacement of the cost intensive Nb_3Sn wires in the high resolution systems operating at 4.2 K. In the frame of the project “Development of MgB_2 wires with high critical current densities for economical NMR magnets at 4.2 and at 20 K”, founded through the *economic stimulus package*, a new processing method for the MgB_2 wires, the cold high pressure densification (CHPD), was developed. Wires submitted to CHPD exhibit a large enhancement of the critical current at temperatures between 4.2 K and 30 K, over the whole range of magnetic fields. Details about the method are presented in chapter 2, on Project 3. This technique opens new way for the industrial processing of MgB_2 and offers new perspectives for a widespread use of this material.

The use of thin films in superconducting fault current limiters has been studied in Øystein Fischers group. This activity is since the begin-

GENEVACREATIVITYCENTER

compétences | sciences | technologies

Figure 5: The Geneva Creativity Center has started activities in 2010 by promoting meetings and creative brainstorming.

ning of the third phase of MaNEP under the responsibility of Michel Decroux. This research is now focusing on the use of coated conductors for this application. Preliminary discussions are presently conducted between Carmine Senatore and Michel Decroux to develop synergies and collaborations between the two groups.

The Geneva Creativity Center

The Geneva Creativity Center (GCC) was initially proposed by MaNEP, who developed the first ideas towards this new structure. GCC is now a collaborative approach between the University of Geneva, the HES-SO in Geneva, the *Office de Promotion de l'Industrie et la Technologie* (OPI) et the *Union Industrielle Genevoise* (UIG) (Fig. 5). This organization is now being implemented with the support of the Geneva authorities. The vision of the GCC is to promote a closer interaction between scientists and engineers from academia and the university of applied sciences (HES-SO), and people from industry, including engineers and managers. The goal is to foster technology transfer by creating the adequate space for preliminary interactions that should help to identify the most promising opportunities. The GCC is also a bridge between the University and the HES-SO, a bridge that should catalyze projects where complementary skills and knowledge can work together in synergy. Under the impulsion of Dr. Carmine Senatore (appointed by the University of Geneva) and Nicola Giandomenico (appointed by HES-SO), the first activities of the GCC have started. Meetings and brainstorming sessions have been already carried out with a first round of industries, and a programme of activities has been prepared for 2011.

The MaNEP Development Lab

The sustainability of technology transfer requires developments and facilities that encompass basic research activities. For example, a key vector for a successful technology transfer is the availability of working prototypes and demonstrators (Fig. 6). In technology transfer, prototypes play the same role as scientific articles in basic and fundamental research.

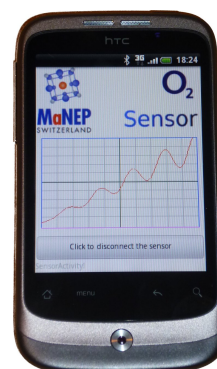


Figure 6: Example: Bluetooth technology has been implemented for measurements on electrochemical sensors using a commercial mobile phone.

By displaying a new technology in a concrete way, prototypes and demonstration devices create the necessary awareness to awake interest among potential industrial partners. However, this requires the availability of supplementary laboratory space specifically dedicated to industry-related work. In order to facilitate the design and construction of prototype devices, a dedicated laboratory space has been created: the MaNEP Development Lab. These new MaNEP laboratories are located in the *Centre de Technologies Nouvelles* in a modern building of the industrial zone of Plan-les-Ouates, near Geneva (Fig. 7). These new facilities have started operations by elaborating the required electronics and software in the framework of the SNF-supported *economic stimulus package* (cut-and-Coat and electrochemical sensors). With an easy access from the highway, and the availability of meeting rooms, this modern space constitutes a new asset for MaNEP activities related to technology transfer.



Figure 7: The "Centre des Technologies Nouvelles" building, where the MaNEP Development Lab has been set up in 2010.

4 Education, training and advancement of women

4.1 Education and training

4.1.1 Doctoral School

PhD students: statistics for 2010

In 2010, the number of MaNEP Geneva PhD students has increased slightly to 22, due to five arrivals — three women and two men — and only three departures. The majority of this staff is constituted by international students, as only 6 of the 22 have graduated from the University of Geneva. Interestingly, the full group of PhD students presents an outstanding 32% of women.

Teaching activities

The two first semesters of the course *Applications of the Many-Body Formalism in Condensed-Matter Physics* took place as announced in spring and autumn 2010, and will be followed by a last semester in spring 2011. The latter will focus on experimental techniques, starting with a presentation of angle-resolved photoemission by Dr Claude Monney from PSI. The course is attended regularly by 11 PhD students.

Conférence Universitaire de Suisse Occidentale (CUSO) doctoral program in physics

The *Doctoral Program in Physics*, which is an evolution of the *3^{ème} Cycle de la Physique en Suisse Romande*, was launched in January 2011 (see <http://physics.cuso.ch>). All MaNEP-Geneva PhD students are registered to this program, and gain access to a variety of activities. These include the usual series of high-quality lectures that the *3^{ème} Cycle* has been organizing since many years, as well as new courses devoted to generic skills such as project or career management, scientific writing, etc. (see the program at <http://competences.cuso.ch/en/activities>). The teaching of the MaNEP doctoral program also becomes part of

the offer and is available to all students registered to the CUSO program.

4.1.2 PhysiScope Genève

Summary

The Physiscope has been running for a third successful year. Attendance is still increasing. Since its inauguration in 2008, over 5000 visitors, school children and VIPs alike, enjoyed a performance on physics. The PhysiScope has participated in several events over the past twelve months, such as the Science week with nine shows presented at CERN's Globe of Science and Innovation and the Nuit de la Science.

A third successful year

The PhysiScope is a public science-theatre and laboratory operated jointly by MaNEP and the Physics Section since 2008 at the University of Geneva. This endeavor strives to motivate the younger generations to embrace a scientific career and introduce the general public to some of the current scientific challenges in physics. To do so, the PhysiScope offers a close and personal encounter with physics through interactive and entertaining shows.

Maintaining high standards and ensuring a constant renewal of its presentations are paramount to the long term durability of the PhysiScope. Hence, special attention is devoted to developing new content to convey the fascination of science in an attractive manner. Two new shows dealing with colors, and with waves and light have been prepared. A new show about the scientific method has also been added this year.

The PhysiScope relies on a team of 10 assistants who develop the content and take turns presenting the shows as part of their teaching duties. With attendance peaking at four shows



Figure 1: Screen shot of the new webpage. Graphic design: J. Behar; web design: L. Prodon and N. Wolf.

per day during several weeks, this makes for a busy schedule. As part of the consolidation effort of MaNEP by the University of Geneva, the Physiscope obtained a new position for a full time technician. His tasks include the safe and effective operation of the Physiscope, as well as the development and construction of new demonstrations in collaboration with scientists.

The Physiscope activities were featured in a number of newspaper articles and several publications, including the bulletin of the Swiss Physical Society (*SPG Mitteilungen/Communications de la SSP*) and the *Clés de l'Ecole*, a magazine of the Geneva Department for Public Education. In an effort to improve our communication and visitor information, the Physiscope webpage (Fig. 1) and the on-line reservation tool have been completely redesigned (www.physiscope.ch).

Collaborations and outreach

Over the past twelve months, the Physiscope has taken part in a number of public outreach events and developed new collaborations. In summer 2010, the Physiscope, MaNEP and the Physics Section contributed to the *Nuit de la Science* in Geneva. A range of new experiments were presented to the public on a 100 m² display, some broadcasted by the *Télévision Suisse Romande* in the main evening news (<http://www.tsr.ch/video/info/journal-19h30/2259448-geneve-la-nuit-de-la-science-a-eu-lieu-ce-week-end.html>).

During the summer holidays, the Physiscope has opened its doors for the first time to the *Passeport Vacances*, with four groups of 25 children (10 – 13 and 13 – 15 years old) spending an afternoon playing with physics. The Physiscope has also participated in an open day for young children organized by the University of Geneva in the frame of *Futur en tous genres*.

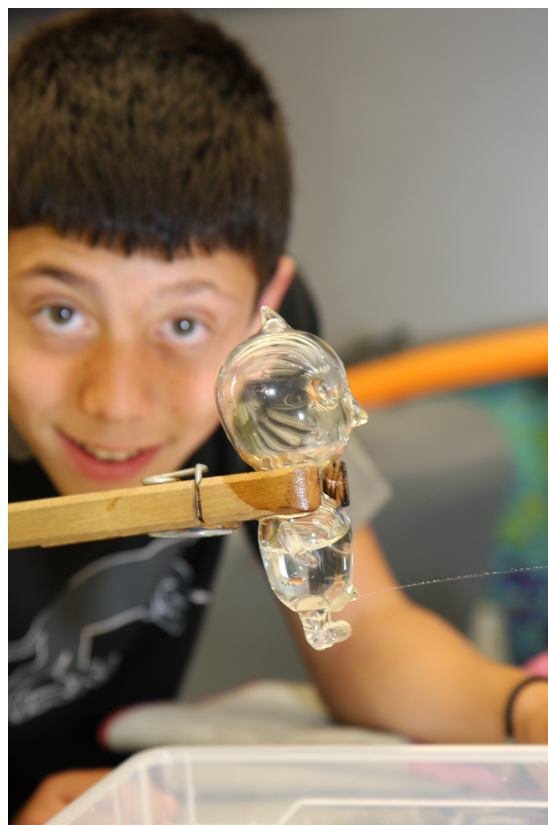


Figure 2: Young visitor experimenting the state of matter.

In October 2010, the Physiscope performed nine shows in CERN's *Globe of Science and Innovation* during the Science week for primary, secondary, high school students and the general public. These were the first performances of the Physiscope team outside the Physics Section, with a record attendance of 180 people for a single show.

From February to May 2011, the Physiscope and the CERN communication office co-organized an educational project called *Dans la peau d'un chercheur*. Its aim is to introduce primary school children to the scientific procedure at tackling a problem. It is a follow up to last year's *Dessine-moi un physicien* lead by CERN which was a great success reported by several local French and Swiss newspapers.

ChimiScope offspring and special guests

The Physiscope has again been a very popular stage for numerous VIP visits to the University of Geneva and the Faculty of Science. We are proud to report the Wilsdorf Foundation and a delegation of the Geneva Rotary Club among this year's visitors. The whole of the *Rectorat* of the University of Geneva and the CERN press office did both celebrate their Christmas party

with a show at the PhysiScope. Finally, the PhysiScope hosted a school from Denmark and a specialized class for children with high potential from Geneva.

The PhysiScope has inspired a first offspring within the Science Faculty of the University of Geneva. 2011 is “Year of Chemistry”, and on that occasion the chemistry department in collaboration with local industrial partners, has initiated the setup of a ChimiScope. The PhysiScope team is sharing its experiences and provides advice for this endeavor whose opening is expected for June 2011.

Acknowledgments

The PhysiScope thanks the foundations H. Dudley Wright, Mark Birkigt and E. Boninchi for their continued support. We further acknowledge support from the University of Geneva, the Faculty of Science and the Geneva department of public education.

The PhysiScope team 2010/2011

Executive committee: Ch. Renner (president), Ø. Fischer, M. Pohl, J.-G. Bosch, O. Gaumer, A. Bonito Aleman. **Model maker:** C. Corthay. **Assistants and students:** U. Cannella, N. Curtz, A. Erie, L. Favre-Quattropani, A. Fête, S. Gariglio, F. Glass, S. Henin, D. Kambly, C. Lichtensteiger, D. van Mechelen, M. Rinaldi, P. Sekatski. **Teachers:** R. Achimescu, A. Bardiot, D. Boehm and B. Gisin.

4.1.3 Swiss Physical Society (SPS) meeting

The general meeting of the Swiss Physical Society (SPS) was held on June 21–22, 2010 at the University of Basel. As on previous recent occasions, different NCCRs — including the three NCCR in physics — were invited to participate to the event. The NCCR MaNEP contributed with a parallel session extending through the entire duration of the meeting. A total of 138 scientists, including 59 PhD students, participated to this session, which consisted in 22 oral presentations (6 invited and 16 selected among the submitted abstracts) and in 100 poster presentations (thereby representing the largest among all parallel sessions that have taken place at the meeting). In addition, Professor Molenkamp from Wurzburg University — who recently received the EuroPhysics prize for his work on topological insulators — was invited to give a plenary talk, which was attended by a large audience.

4.1.4 LEES 2010 — conference on Low Energy Electrodynamics in Solids

From July 5 to 10, 2010 more than hundred experts on low energy spectroscopies of solids came from all corners of the world to les Diablerets for the biannual conference on Low Energy Electrodynamics in Solids (LEES).

Some 50 talks and 50 posters were presented on the properties of graphene, superconductors, heavy fermions, metal-insulator transitions and topological insulators. The meeting took place with the precision of a Swiss watch due to the fact that everyone showed up as announced. The posters and talks were extremely well prepared, well attended, truly interesting, and provoking many scientific discussions, which were conducted outside on the lawns of Les Diablerets thanks to the excellent weather.

One of the highlights was the attribution of the Ludwig Genzel Prize to Alfred Leitenstorfer for pushing the limits of ultrafast optical spectroscopy and applying it to fundamental problems in condensed matter physics.

LEES 2010 has benefited from financial support by MaNEP, the Department of Condensed Matter Physics and the Sciences Faculty from UniGE, The Swiss National Science Foundation, Bruker, LOT, the Paul Scherrer Institute, Andor, Quantum Design and Teraview.

4.1.5 Swiss Swedish Workshop

A workshop on the topic of “Quantum Materials and Quantum Circuits” between Swedish and Swiss took place on January 7 to 9, 2011, at Les Diablerets, Switzerland. The meeting was organized by Øystein Fischer, MaNEP and Dag Winkler, Chalmers, Sweden. 20 researchers from each country were present and the meeting focused on several topics of common scientific interests to researchers from the two countries. The organization was largely carried out by MaNEP and among the 20 Swiss participants a majority was members of MaNEP. Representatives from the SNSF and VR in Sweden were present and informed the participants about possibilities for support for common projects.

4.1.6 MaNEP Winter School 2011

From 9 to 14 January 2011, the fourth MaNEP school, the second in the winter after the successful one in 2009, was organized in Saas-Fee. The program of this school was set under the



Figure 3: Participants to the fourth MaNEP Winter School in Saas-Fee.

guidance of Professor B. Batlogg together with Professors C. Bernhard, T. Giamarchi, L. Forró, A. Morpurgo, M. Sigrist and A. Zheludev. 66 students, postdocs or professors attended this school (Fig. 3).

The scope of this school was focused on the physics of new peculiar states of electronic phases. This is a very large scope, which covers almost all the scientific activities within MaNEP. From the survey realized in 2009, the participants emphasized that this event has to

be a school, not a conference. For this edition we have carefully renewed the spirit of the 2009 edition where, for the first time, we have proposed a program build around three basic subjects. This edition was therefore organized around three basic courses, each course having three lectures of two hours. That made possible to develop in detail the basic concepts required to have a better understanding of the four dedicated lectures. These three basics courses were perfectly given by Professors C. Bernhard, A. Georges and A. Zheludev. The three dedicated lectures, which have the aim to present the state of the art in this domain, were given by M. Norman, P. Paruch and I. Iwasa (Fig. 4). Unfortunately, A. Vishwanath was not able to attend this school and his lecture was canceled.

Finally the fourth dedicated lecture, dealing with the centennial of the discovery of superconductivity in 1911, was magisterially given by Prof. H.-R. Ott. This lecture was followed by a special dinner (superconducting *fondue* or *raclette*).

The survey realized at the end of this school confirmed that all the participants had greatly appreciated this school. Minors objections were made about organization, accommodation, but a large majority found this winter school fantastic.

The success of this edition is coming essentially from the high level of the lectures given during the week. Therefore we would like once again to thank warmly all the lecturers for the quality of the courses they presented.

In addition we would like to warmly thank G. Cravotto and G. Manfrini for the work they did by taking care of all the inherent problems related to the organization of this event (material aspect, printing, badges and coffee breaks). M. Bagnoud at the beginning and P. Cugny for the end of the school overtake the responsibility of the administrative organization of this school and also share part of the work done by G. Cravotto and G. Manfrini. Finally a special thank to A. Bonito Aleman and C. Berthod for their great help to set up the web site and for disseminating the information all over the MaNEP community.

4th MaNEP Winter School
9–14 January 2011 in Saas-Fee

Emergent States of Electronic Matter

This winter school will introduce modern themes related to emergent states of electronic matter.

A broad introduction will be given in three basic courses, covering the topics of electronic properties and basic phenomena, experimental studies of spin and charge responses and quantum magnetism. More specialized courses will cover topological insulators, molecular semiconductors, pnictide superconductors, multiferroics, and a century of superconductivity.

The school is for doctoral and young post-doctoral associates. A background in general solid-state physics is sufficient to participate. The courses will be taught in English.

Program Committee
Bertram Batlogg (Chair), Christian Bernhard, Laszlo Forró, Thierry Giamarchi, Alberto Morpurgo, Manfred Sigrist, and Andrey Zheludev.

Organization
Michel Decroux, Adriana Aleman, Marie Bagnoud, Christophe Berthod, Gregory Manfrini.

Applications should be made via the MaNEP web site (<http://www.manep.ch/en/events/saasfee11>) where further information can be obtained.
Closing date for applications is October 31, 2010.




Program

Basic lectures

Charge and spin response
Christian Bernhard
University of Fribourg

Electronic properties
Antoine Georges
CPHT, Ecole Polytechnique Paris

Quantum magnets
Andrey Zheludev
ETHZ

Specialized lectures

100 year of superconductivity
Hans-Rudolf Ott
ETHZ

Topological insulators
Ashvin Vishwanath
University of California, Berkeley

Pnictides
Mike Norman
Argonne National Laboratory

Ferroelectrics and multiferroics
Patrycja Paruch
University of Geneva

Molecular semiconductors
Yoshi Iwasa
Tohoku University

Figure 4: Poster announcing the fourth MaNEP Winter School in Saas-Fee.

4.2 Advancement of women

4.2.1 Summer internships

For the seventh year, the MaNEP internship program was organized for all the female students working within the MaNEP network. In 2010, MaNEP supported ten candidates: 5 at EPFL, 2 at UniFR, 1 at ETHZ, 1 at PSI and 1 at UniGE. All these internships were very successful. For several female students, the internship has convinced both parties to continue their collaboration at the PhD level. In addition to that, two exchange programs were launch for men students.

As it has been pointed out in the previous report, we do not restrict these internships to candidate interested to continue in domains related to MaNEP activities, but we offer this opportunity to all the female students whatever is their interest for the future of their carer. By this way, MaNEP is an important structure to give a chance to a female student to be confronted with the reality of research.

At the end of their internship, the candidates were asked to write down a short text describing their personal experience during this stay, about their ability to manage research, how they improve their self-confidence and if this internship modify their career strategy. We give hereafter parts of these texts.

- [...] I had chosen to work with Prof. Sigrist on superconductivity before I entered the MaNEP program. However, the scope provided by the internship as opposed to a simple semester research project has significantly influenced my experience. Being employed, for the duration of the project, I had a seat in one of the offices and was thus able to get to know the group members through lunch, seminar and other activities in a way I had never experienced in previous research projects that were part of the curriculum. I benefited from this close contact in many ways: I was able to discuss direct aspects of my project as well as general questions on programming calculations, I gained insight into the projects of the others and also learnt how a PhD at ETH works.

This experience did not change my career strategy but rather confirmed my plans and encouraged me to carry on this way. It is nice to know that what you think you like to do is actually working out.

- My internship took place at EPFL (short for École Polytechnique Fédérale de Lausanne) in July and August. During that period, my job was to examine the thermal conductivity properties of CNT (Carbon nanotube) samples prepared by a PhD student at the institute. I did a lot of laboratory work, which helped to improve my practical skills a lot. [...] I can safely say that I have become very familiar with the laboratory in a few days thanks to my supervisors, Richárd Gaál and Laszló Forró and the PhD students working there. I managed to improve my English, mostly in the use of laboratory terminology. I really got to experience the life of an experimental physicist, which helps me decide how to go on with my studies. I personally think that this internship was a great step towards a successful career in Physics. Last, but not least, I have made a lot of relations and met people who remained my dear friends even up until now. I would recommend it to anyone who is hard working ambitious.

- [...] Ich denke, dass ich in dem Monat des Praktikums sehr viel gelernt habe. Vor allem im selbstständigen Experimentieren und im Umgang mit den Messinstrumenten habe ich viel praktisches Wissen gesammelt und Selbstvertrauen gewonnen. Da ich - was vielleicht ein wenig typisch für Frauen ist - in meiner Kindheit und Jugend nicht sehr viel Kontakt mit Technik hatte, habe ich hier noch einen gewissen Nachholbedarf. Ich würde sagen, dass mir das Praktikum ein paar Berührungängste mit Technik genommen hat. [...]

Allgemein kann ich sagen, dass mein "physikalisches Selbstvertrauen" durch das Praktikum gewachsen ist. Ich hatte vorher oft daran gezweifelt, ob ich selbstständig eine Forschungsarbeit durchführen könne, und hatte eine gewisse Hemmung, einfach mal an Geräten herumzuprobieren. Diese Zweifel sind natürlich nicht komplett verschwunden, denn ich habe während des Praktikums ja auch gemerkt, dass die Arbeit anspruchsvoll ist, dass es viele Möglichkeiten gibt, Fehler zu machen und dass man viel Wissen und Erfahrung

braucht, um zu experimentieren. Im Großen und Ganzen jedoch habe ich während des Praktikums gelernt, mir mehr zuzutrauen, bei Problemen einfach zu fragen und auch, dass jeder einmal Fehler macht. [...]

Finally, all the female students who have participated to the internship 2010 received the new *Agenda 2011 des femmes/der Frauen* to remind them during 2011 that MaNEP did something specially dedicated for the women

4.2.2 New developments

As announced in the last report, together with the Equality Office of the University of Geneva, we prepared a survey that we sent at the beginning of the summer 2010 to all the

women researchers in MaNEP. In this survey, we prepared questions to evaluate the current work and to see how to promote new activities devoted to the advancement of women (AOW). We considered three important points for the AOW program to follow and oriented the questions of the survey consequently. 1. We should encourage more young women to choose science, particularly physics. 2. We should encourage women physics students to continue their careers in research. 3. We should consider the situation of women researchers (PhD students and post-docs, in particular) and help them combine professional and family life.

19 questionnaire out of a total of 31 were returned. These are in the process of being treated and the results will be dealt with before the end of year 10.

5 Communication

The main event of 2011 will be the celebration the 100th anniversary of the discovery of that fascinating physics phenomenon — superconductivity. Certainly the preparation for the festivities marked the year 2010. The development of a program, collaboration with partners, scientific validation and experiments preparation, etc., the Communication staff is coordinating every aspect of this event. The creation of special events for this centennial will certainly reinforce our links among MaNEP members as well as with our academic and industrial partners and is a golden opportunity to reach out to a wide audience of decision makers and the general public. Moreover, in 2010, MaNEP had regular contact with the media thanks to graphene, as the scientists who discovered it received the Nobel Prize for Physics. It was a great opportunity to highlight MaNEP’s research in this area. Other important events were the Wright Colloquium on “Quantum Revolution” with brilliant speakers, the *Nuit de la Science* in Geneva, as well as a special visit by a group of Swedish Scientists.

5.1 The superconductivity centennial



Figure 1: Logo (french and english versions) proposed for the superconductivity centennial to all Swiss partners.

In 2011, the centennial of the discovery of superconductivity will be celebrated around the world. MaNEP is launching a large programme of collaboration with many different partners and is playing a coordinating role in Switzerland (Fig. 1). In 2010, a great deal of time and effort was put into organizing these festivities.

Vital collaboration is being carried out with the University of Geneva (UniGE) and the PhysScope, the Paul Scherrer Institute (PSI), the Swiss Physical Society, CERN, Europhysics-Fun (a cooperative project between European physics shows, which work towards forming a community of science shows), the Museum of the History of Sciences in Geneva, the well known Bâtie Festival in Geneva, as well as the University of Paris XI. Moreover, MaNEP is also working closely with Bruker Biospin AG for one particular project. Collaboration is at all

levels including exchange of services, equipment loans, common organization and technical support.

MaNEP and the PSI plan to celebrate the centennial of superconductivity for the Institute’s open house day. Events for the general public will be organized with an attractive and comprehensive programme that will be approved soon.

In Geneva, MaNEP, the University of Geneva and the PhysScope are planning on organizing several special events in April as well as in the autumn of 2011. They will be meant for the general public (families), schools, decision makers and the media. The actual day of the discovery of superconductivity is the 8th of April and MaNEP will be active in April with open days at the PhysScope. A daily one hour show on superconductivity will be offered to the general public for a week. Moreover, a joint press conference with CERN will be organized for the media. This will be an excellent opportunity to promote research in our labs and highlight many important results.

In September and October, Science and Art will work hand in hand to highlight the “magic” of superconductivity. This include an exhibition about superconductivity with a work of art on display by the artist Etienne Krähenbühl who will illustrate the phenomenon. In 2010, collaboration between the artist, scientists and technicians strongly evolved, always under the watchful eye of the filmmaker (Fig. 2). More-



Figure 2: *Filming and discussion between scientists, technicians and the artist in the Art-Science project. A work of art incorporating the superconductivity will be inaugurated in autumn 2011.*

over an artistic performance by the company Exos where the phenomenon of levitation will be shown will be proposed. A family day with experiments, demonstrations, laboratory visits, shows, and a grand conference for the general public are also planned. Full details will be announced in April. We would like to emphasize the fact that we have launched a fund raising campaign and the achievement of these projects depends on whether we receive these funds. A communication coordinator was hired to support the communication officer with the organization of these events.

5.2 The secrets of graphene

The 2010 Nobel Prize for Physics was awarded to Profs. Andre Geim and Konstantin Novoselov of the University of Manchester (UK) for their discovery of graphene. Graphene is a new material, consisting of a regular lattice of Carbon atoms, only one atom thick. With less than 6 years passed from the discovery, the unique properties of graphene are at the focus of worldwide research in disciplines as diverse as biology, chemistry and engineering, with great potential for future applications. MaNEP scientists are involved in research in graphene. Some MaNEP groups were amongst the first to start working in this direction after the original discovery of graphene, and are actively collaborating with the two Nobel Laureates. Indeed, this Nobel Prize was a terrific opportunity for MaNEP to communicate to the media about its activities. Thus, in October 2010, there were reports on MaNEP's research in both the newspaper *Le Temps* and the *Télévision Suisse Romande*. There was also a broadcast on *Euronews* showing

films of MaNEP's labs. This Nobel Prize gave some of our scientists an excellent opportunity to publicize their research with the Swiss media and be personally introduced to media. Graphene never ceases to surprise us. Thus, in the autumn of 2010 physicists from UniGE discovered a new optical effect at the heart of the world's thinnest material. This result was published in the journal *Nature Physics* in January 2011 and covered by a press release. Against all odds, MaNEP researchers observed the rotation of light of very large amplitude at the heart of graphene, a rotation that makes the material usable in new optical applications. More details can be found in chapter 2, on Project 2. This discovery was echoed in the media, namely *Frankfurter Allgemeine Zeitung*, *la Tribune de Genève*, *Horizons/Horizonte*, as well as on www.physicworld.com, www.myscience.ch, www.futura-sciences.com, www.2physics.com, www.etudiant.ch or www.enviescope.com web sites.

5.3 UniGE staff evening event

MaNEP continues its partnership with the company Exos. In 2009, the troupe gave an extract of their work to a limited audience at the ITU World Telecom and then to scientists of the School of Physics at UniGE. On May 20, 2010, no fewer than 2000 employees of the UniGE strongly applauded part of their show during the staff evening event (Fig. 3). Being closely linked with the show, MaNEP was very visible during this event. Many people discovered MaNEP and its research through the show "La supraconductivité mise en scène", but also through various communications created for the occasion, such as invitations, posters advertising the show (Fig. 4) and posters promoting MaNEP and its activities. This partnership continues and an artistic creation will be



Figure 3: *Exos show on superconductivity in partnership with MaNEP presented on May 20, 2010.*



Figure 4: Poster for the Exos show on superconductivity, in partnership with MaNEP, on May 20, 2010.

shown for the first time to the general public as part of the superconductivity centennial in partnership with the Bâtie Festival in Geneva. The Exos Show may then go on tour to MaNEP’s academic partners and theaters.

5.4 The sky was the limit for physics during the Nuit de la Science

The *Nuit de la Science* took place on 11 and 12 July in Geneva (Fig. 5) in which MaNEP, the



Figure 5: Exchanges, discoveries and discussions were held during all the *Nuit de la Science*.



Figure 6: Young people discovering unusual devices especially created for the *Nuit de la Science*. Top: how to be weight on a string board? Center: how do crystals grow? Bottom: how do interfaces move and propagate?

PhysiScope and the Physics section of UniGE joined forces to create the booth of all records (in term of size). It was a great success and the public came out in force. Unusual devices were provided for this event: sitting on a 5 meter spring board and bouncing up and down to find out your weight in order to understand how to weigh very light elements (Fig. 6, top); seeing crystals grow (Fig. 6, center); discovering the laws of physics of interface by dipping your drawing into colored water (Fig. 6, bottom); making square soap bubbles; observing

atoms with a scanning tunneling microscope; and many other experiments that drew fascinated crowds.

The media came out in force to report on our activities, the *Tribune de Genève* had three articles on 2, 8, and 12 July 2010, *Radio Suisse Romande* on 9 July 2010, and on the evening news of 11 July 2010 on the *Télévision Suisse Romande*.

5.5 2010 Wright Colloquium “Quantum revolution”

MaNEP was actively involved in the organization and promotion of the 2010 Wright Colloquium which was entitled “Quantum revolution” and took place from November 15 to 19 at the University of Geneva (Fig. 7). The scientific director of this event was Thierry Giamarchi, a MaNEP professor. It was an opportunity for the general public to explore, in the company of five internationally renowned specialists — Jochen Mannhart, Wolfgang Ketterle, Alain Aspect, Rainer Blatt and David Gross, two of whom were Nobel Prize Laureates — some of the fascinating aspects of quantum mechanics, which are also part of MaNEP’s research. The Wright Colloquium welcomed over than 800 people every night. After each lecture, members of the audience were able to participate at round table discussions by asking questions. Unfortunately many questions from the public were unable to be answered at these sessions through lack of time. However the public were able to write down their questions which were then transferred to our scien-

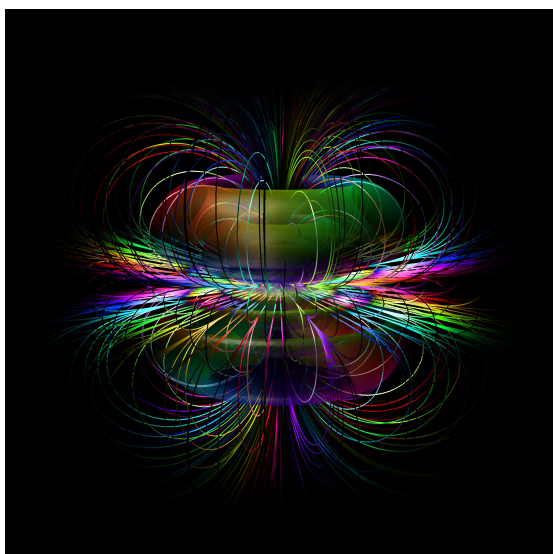


Figure 7: Hydrogen eigenstate with spin. Illustration: B. Thaller and Etienne & Etienne used for the Wright Colloquium poster.



Figure 8: Members of the Physics Class of the Swedish Royal Academy of Sciences visiting labs last November.

tists, answered and published on the web site www.questionsur.ch from *TSR Découverte*.

5.6 Visit of the physics class of the Swedish Royal Academy of Sciences

MaNEP and the Physics section of UniGE welcomed the physics class of the Swedish Royal Academy of Sciences, on 11 November 2010. About fifty guests attended presentations by professors from MaNEP and the physics section, and visit labs (Fig. 8) and the PhysiScope. Among them were members of the Physics Nobel Prize Committee. The visit, led by the Director of MaNEP, was not only a unique opportunity to hold discussions and exchanges between scientists, but also a chance for internal communication.

5.7 MaNEP in the media

MaNEP and superconductivity were in the spotlight of the magazine *ISO Focus+* in November, as MaNEP director, Øystein Fischer, was invited to give an interview. The magazine generally interviews personalities from around the world such as the Director General of the ILO or of the WTO, or the CEO of Royce Rolls, and is aimed at decision makers in governments and international organizations. A great way to raise MaNEP’s and superconductivity’s visibility with this important audience! An excellent opportunity to

demonstrate the importance of MaNEP's research is its regular presence in high profile scientific magazines, as the Nature publications or Physical Review Letters. For example, in January 2011, *Nature Physics* featured three MaNEP/UniGE articles.

5.8 Several other outreach activities in year 10

MaNEP experts were invited to give talks for the general public, like Prof. Christoph Renner with "Atomes à portée de main, synthèse et maîtrise de la matière à l'échelle atomique", *Culture&Rencontres, Collège de Saussure*, Geneva, in January 2011 and "La matière à l'ère des nanotechnologies", *Collège Rousseau*, Geneva, in February 2011. Anke Weidenkaff delivered a conference at the *Berner Chemische Gesellschaft* entitled "Was kann die Festkörperchemie für die Energi-

etechnik tun?", in November 2010.

Moreover, this year, we have made an attractive new poster for high-school students, which illustrates the University of Geneva's Department of Condensed Matter Physics and MaNEP. It showcases the work of researchers in this area with opportunities in industry. This poster is displayed in physics classrooms of secondary schools in Geneva and is thought-provoking for teachers. It will also be used in training courses for teachers. Moreover, MaNEP is actively collaborating with communications officers from the Sciences Faculty of UniGE, via a special "cell". This not only enables us to share information and coordinate activities vis-à-vis the media, but also to discover new communication tools. We have also created MaNEP notepads that are given to participants at our conferences. The usual channels of communication work well. In 2010, three issues of the e-newsletter were published and the website has evolved dynamically according to news and events.

6 Structural aspects

Whereas during the last 10 years we have considered MaNEP largely as one homogeneous research team, the approach of the end of MaNEP and the question of a stabilization of its activities beyond 2013 has increasingly led the director and his team to follow two very different paths: the stabilization of MaNEP Geneva which largely depends on the local authorities and the Geneva *Grand Conseil*, on the one hand, and the stabilization of the network which can only depend on institutions at a national level and for which at present no possible approach is offered to the NCCRs by the SNSF or the federal authorities, on the other hand.

6.1 Stabilization of MaNEP Geneva

Following the strategic goals of the NCCR program, the University of Geneva has since the beginning of MaNEP started to reinforce the research field represented by MaNEP. These efforts have been reported yearly in the MaNEP progress reports.

The approach to stabilization of MaNEP Geneva has three distinct aspects: a) the financial one, providing an increased budget, b) the human resources one, reorienting positions in the scientific orientation of MaNEP, and c) the institutional one, giving MaNEP the status of a legal unit in the Geneva University system.

Financial aspects

Within the first years of MaNEP, MaNEP Geneva received an important budget increase through the University development plan. This reinforcement of the budget was continued by the transfer of personnel and funds for consumable. In 2009, the MaNEP director took over the responsibility of the crystallography laboratory and the budget was transferred to the MaNEP budget. The present sum of these transfers amounts to a budget of 1'980'000 CHF. Within the University *Convention d'objectifs* (COB) with the Geneva Government (*Conseil d'Etat*) 2009 – 2011, an allocation of a budget of 1'500'000 CHF was decided. This is in the final phase of realization. Finally, the new COB 2012 – 2015, not yet finalized, foresees an additional budget increase of 500'000 CHF.

Human resources, professor positions

Since the beginning of MaNEP, 5 new professors have been appointed in the topic of MaNEP, of which 2 were reorientations and one new position was established. Furthermore, the open professor position for crystallography has been reoriented in the direction of MaNEP. As a part of this policy, Prof. Antoine George (*Collège de France*) is about to be appointed part time (20%) professor in Geneva.

Institutional stabilization of MaNEP

The present goal is to establish a new institute at the University of Geneva which shall take over the activities of MaNEP Geneva. The fact that this will make a very strong and large condensed matter physics activity at the faculty of sciences in Geneva, and the fact that within Physics, Mathematics and Astronomy there are other very strong scientific activities as well, has led the MaNEP director and the *Rectorat*, as well as the Physics section, the Mathematics section, the department of Astronomy and the Faculty of Science to consider the stabilization of MaNEP as the nucleus of a much larger project. This project plans to rethink the scientific projects of the various partners, to stimulate synergies between them and to regroup all these activities in a new center, meaning a new building.

We started to work on this larger project in 2007. The present situation is that we are working on elaborating a detailed project in which we are working closely with architects, mandated to elaborate this project by a large Foun-

dition in Geneva. The present elaboration is based on a convention between, in particular, the Canton of Geneva, the Foundation, and the University. The preproject is planned to be ready by August 2011.

6.2 The MaNEP network

Another strategic goal strongly encouraged by the SNSF has been to build networks between researchers at different institutions in order to reinforce the impact of Swiss research on a world wide scale. We consider it as a major success of MaNEP that a broad national network has been established and that abroad the name MaNEP is largely associated with this success. MaNEP has practically become a Swiss trademark.

Whereas the idea that the University of Geneva takes over the high level of activity installed, thanks to the NCCR, at the leading house can be well planned, the responsibility for the longer term structural efforts concerning the network can only be decided at the national level and the responsibility for this strategic goal is clearly with the Swiss National Science Foundation and with the State Secretariat of Education and Research (SBF).

The question of the continuation of the MaNEP network after 2013 was discussed during the last year in the scientific committee and in the MaNEP Forum. A first white paper was elaborated by Thierry Giamarchi and other members of the scientific committee and discussed at the last Forum in January 2011.

Following this, the director took the initiative to contact the director of one of the other NCCRs, Thomas Stocker of the NCCR Climate. In fact, only some NCCRs have a broad national network and therefore have the problem we face in MaNEP. The NCCR Climate is one that has a similar network situation.

Our plan is to discuss with all the partners in this project the organizational structure during the coming year and to establish formally the new institute containing the continuation of MaNEP during year 12 of MaNEP.

On March 5, 2011 the NCCRs MaNEP and Climate sent in a common white paper to the Swiss National Science Foundation to propose that a new instrument be funded to support the most successful national networks. The executive summary of this white paper reads:

The Swiss National Science Foundation's program of National Centres of Competence in Research (NCCR) has established highly successful science networks in Switzerland. They have demonstrated long-term excellence in research. The foreseen closure of two NCCRs working in areas of strategic national priority puts these highly efficient networks at serious risk, and hence the competitiveness of Swiss research in these topics at the international level is at stake. In response, this White Paper proposes the establishment of a new instrument, the Swiss Networks of Excellence in Research and Teaching (NEXT). This new initiative would prevent the fragmentation of research in Switzerland, which would be caused by the closure of NCCRs in science topics of strategic significance whose international competitiveness fundamentally depends on inter-institutional cooperation. It is proposed that NEXT will be established by the State Secretariat of Education and Research (SBF) by 2013, and will guarantee the next step in the development of Swiss research and training networks in areas of strategic national priority with a budget of 3 to 5 Mio CHF per year and network.

At the moment of writing this report a roundtable discussion on this proposal is being planned by the SNSF.

7 Management

7.1 Activities

The MaNEP management has been active in all the aspects of running MaNEP in year 10 on the one hand, and has been increasingly involved in the efforts to prepare the future of MaNEP after 2013, on the other hand.

MaNEP in 2010

There were several new arrivals to the staff of MaNEP this year. Marie Viry Obataya was hired from March to July 2010 as a temporary secretary to help with the Progress Report and to provide assistance in the secretariat in anticipation of the accounting report year 9. During the summer, Edward Coutureau joined the NCCR as the new administrative assistant to closely assist the Director with the preparation of MaNEP's future projects after 2013. In December, Christophe Schwarz was hired as the successor of Marie Viry Obataya to complete the secretariat team. During this same period, Daria Lopez Alegria and Julien Pitton joined MaNEP as consultants to the director bringing with them their know-how in strategic development as well as the realization of multi-partner projects. David Parietti was hired as a temporary communication coordinator to support our communication officer, Adriana Bonito Aleman, with the preparation of the Superconductivity Centennial. Last but not least we are currently looking for hiring a KTT officer to replace Matthias Kuhn who left MaNEP at the end of October 2009.

During the year, the MaNEP administrative manager, Marie Bagnoud, has been increasingly involved in the effort we are carrying out to stabilize MaNEP Geneva after to 2013. The fact that the MaNEP secretariat has taken over the secretarial assistance of the laboratory for crystallography has this year also led to an increased work load of the management team.

As a result, Pascal Cugni and Elizabeth Guénat have taking more responsibility in

the financial aspects and the human resources management respectively. In order to meet the temporary increased work load the employment of Christophe Schwarz has been increased from 50% to 80%. And the activity rate of Pascal Cugni has been increased from 60% to 80%.

On the administrative side, this year has been characterized by an effort to complete the information contained in NIRA 2.0 concerning the personnel and the finances, and especially the relations between the two, requested by the FNS data base system. The new scientific structure of MaNEP in Phase III has requested an important effort of the management to adapt the administrative and accounting structures to this situation. This new administrative structure is now in a steady state.

Implications of the management in the effort to stabilize MaNEP after 2013

Following the recommendations of the Review Panel members to continue MaNEP beyond Phase III, the management has been increasingly involved in MaNEP efforts to find ways to maintain the NCCR activities after 2013.

On the financial side, the University of Geneva is increasing the budget for MaNEP through their *Convention d'objectifs* with the Canton of Geneva. These funds are managed in a different process from the usual budget and this leads to an increased complexity and work load for the administration especially since the control of these funds are not directly in the hands of MaNEP. This situation also introduces new complexity in this process. However we would like to stress here that the collaboration with the UniGE *Rectorat* is excellent and this temporary difficulty will disappear in future years. In any case the result of this process is

a strong increase in the funds available for the research in MaNEP making this extra administrative work load well worth the effort.

As it is explained in the structural aspects in chapter 6, the structural stabilization of MaNEP will take place within a more global restructuring of the physical and mathematical sciences at the University of Geneva. This more global improvement is a result of the establishment of MaNEP, and the NCCR has the lead in this reorganization. MaNEP's director has been charged by the *Rectorat* of the University to conduct this effort and to elaborate specific plans for the realization of a new center. This mission also concerns MaNEP's management through the direct involvement of MaNEP's administrator, Marie Bagnoud, and the employment of Edward Coutureau as a secretary for the director. The finance and administration of these developments are carried out by MaNEP's management team. We stress here that the financial effort for this part is compensated by the University.

Presently, MaNEP has also taken the initiative to propose a constructive way of how the MaNEP network may continue after 2013. The MaNEP network is a key achievement and has clearly an important national value. The MaNEP management is deeply involved in this part which also implies its will to stimulate and organize meetings of the network during the year. We anticipate that, as this initiative evolves, the MaNEP management will be increasingly occupied in contributing to creating a dynamic continuation of the network.

Events organized by MaNEP management

The **Scientific Committee** met in Geneva on April 14, 2010. The committee is composed of the director, two deputy directors, the project leaders plus two additional members appointed by the director. The composition is as follows: Prof. Leonardo Degiorgi (ETHZ), Prof. Øystein Fischer (UniGE), Director, Prof. László Forró (EPFL), Prof. Thierry Giamarchi (UniGE), Prof. Dirk van der Marel (UniGE), Deputy Director, Prof. Frédéric Mila (EPFL), Prof. Alberto Morpurgo (UniGE), Prof. Christoph Renner (UniGE), Deputy Director, Prof. Manfred Sigrist (ETHZ), Prof. Jean-Marc Triscone (UniGE), Dr. Urs Staub (PSI), Prof. Andrey Zheludev (ETHZ).

The meeting discussed the recommendations by the Review Panel regarding the future MaNEP network. Several options were proposed to continue MaNEP and create a new

network beyond 2013.

It was decided to elaborate a white paper on the necessity of a continued activity and financing of the MaNEP network. This white paper was written by Thierry Giamarchi and subsequently discussed among the members of the scientific committee and the MaNEP forum. This document was the scientific basis for the proposal NEXT, described in chapter 6, now in the hands of the SNSF Research Council.

The **MaNEP Forum** met in Neuchâtel on January 17, 2011, with the participation of a large number of MaNEP Forum members. In particular, the question of MaNEP's future took a good part of the meeting. Thierry Giamarchi presented the white paper and several options were discussed. A general consensus was that it is of great importance to continue the MaNEP network and that it is essential that this is financed with sufficient funds in order to stimulate future activities within the network.

The **MaNEP Internal Workshops** took place in Neuchâtel during the week on January 17-21, 2011. The eight MaNEP scientific projects were discussed among the main participants of each project. This resulted in vivid and stimulating discussions over the whole week. These meetings are the basis for the elaboration of the scientific report and for each MaNEP member the deadline for the report was one week after the meeting.

The **fourth MaNEP Winter School 2011** took place in Saas-Fee on 9-14 January, 2011. This school is for doctoral and young post-doctoral students and introduces them to modern themes related to emergent states of electronic matter.

The **MaNEP Management Committee** meets regularly once a month to discuss and monitor the evolution of MaNEP's daily activities: events, meetings, newsletters, accounting, KTT, education, doctoral school, advancement of women, communication, etc. These meetings are essential to keep the different parts of the large MaNEP organization mutually informed and to coordinate these activities.

Events and meetings co-organized by MaNEP management

The **Swiss Physical Society (SPS) annual meeting** took place on June 21-22, 2010 in the University of Basel. This year MaNEP was present, as it is every second year, with a special session and its own invited speakers. Also this year MaNEP was present with the large number of participants and posters. During this meeting, Erik van Heumen was pre-

sented with a SPS Award for Condensed Matter Physics, sponsored by IBM for his research on superconductivity. He gained his PhD thesis in the NCCR MaNEP and in the Department of Condensed Matter Physics at the University of Geneva. More good news for MaNEP, of the five new persons appointed as honorary members of the Swiss Physical Society four are from MaNEP, Professors Hans Beck, Øystein Fischer, T. Maurice Rice and Louis Schlapbach. The **LEES 2010 conference** organized by the University of Geneva and the support of MaNEP management team was held from July 5 to 10, 2010 in Les Diablerets. This is the 9th conference in this biannual series of international conferences on low-energy electrodynamics in solids. The chairman of the 2010 edition was Dirk van der Marel, MaNEP deputy director.

The *Nuit de la Science* took place in Geneva on 10-11 June, 2010. The event, organised by the entire School of Physics, was a great success with the public who came out in force.

MaNEP, the Section of Physics and the PhysicoScope joined forces to develop this event and enhance physics in Geneva.

The **2010 Wright Colloquium** entitled "Quantum revolution" took place in the University of Geneva on 15-19 November, 2010. MaNEP was actively involved in its organization and promotion, supervised by Prof. Thierry Giamarchi.

The **visit of the physics class of the Swedish Royal Academy of Sciences** took place in the Physics section of UniGE and MaNEP on November 11, 2010. The visit was led by Prof. Øystein Fischer, Director of MaNEP and the local organization was held by the MaNEP management.

We are now preparing for the next **Review Panel Meeting** which will take place in Geneva on 30-31 May, 2011. The meeting will be organized by the Swiss National Science Foundation in collaboration with the management team of MaNEP.

7.2 Experiences, recommendations to the SNSF

As already noted last year, NIRA 2.0 is a wonderfully complex and exciting tool for those who are not concerned with keeping administration costs low. By creating links between the different inputs and calculating everything in a manner that cannot be easily controlled by the user it represents a fabulous administrative labyrinth with no real exit between the progress report and the financial report. Therefore we had to reinforce our administrative

staff. Specifically Elizabeth Gueniat and Pascal Cugni have been trained in order to join our NIRA 2.0 team. And we employed a new secretary, Christophe Schwarz.

In addition to this general statement, we have encountered difficulties in using NIRA 2.0 because it is very slow to react and to register or upload information which is hampering the efficiency of our administrative staff.

8 Reactions to the recommendations of the Review Panel

There was no meeting of the Review Panel last year.

9.3 Publications over the last period

The following lists cover the period from April 1st, 2010 to March 31st, 2011:

1. Scientific articles in journals with peer review
2. Scientific articles in journals without peer review
3. Publications from lists 1 and 2 involving several groups

The first two lists are sorted by the name of the group leaders. The most important publications are outlined by a red mark.

9.3.1 Scientific articles in journals with peer review

Group of Ph. Aebi

- ▶ C. MONNEY, E. F. SCHWIER, M. G. GARNIER, N. MARIOTTI, C. DIDOT, H. CERCELLIER, J. MARCUS, H. BERGER, A. N. TITOV, H. BECK, AND P. AEBI

Probing the exciton condensate phase in 1T - TiSe₂ with photoemission

New Journal of Physics **12**, 125019 (2010).

Group(s): Aebi, Forró / Project(s): 7

- ▶ C. MONNEY, E. F. SCHWIER, M. G. GARNIER, C. BATTAGLIA, N. MARIOTTI, C. DIDOT, H. CERCELLIER, J. MARCUS, H. BERGER, A. N. TITOV, H. BECK, AND P. AEBI

Dramatic effective mass reduction driven by a strong potential of competing periodicity

Europhysics Letters **92**, 47003 (2010).

Group(s): Aebi, Forró / Project(s): 7

C. BATTAGLIA, C. MONNEY, C. DIDOT, E. F. SCHWIER, N. MARIOTTI, M. G. GARNIER, AND P. AEBI

Atomically precise Si(331)-(12x1) surfaces

AIP Conference Proceedings **1199**, 5 (2010).

Group(s): Aebi / Project(s): 7

C. MONNEY, E. F. SCHWIER, M. G. GARNIER, N. MARIOTTI, C. DIDOT, H. BECK, P. AEBI, H. CERCELLIER, J. MARCUS, C. BATTAGLIA, H. BERGER, AND A. N. TITOV

Temperature-dependent photoemission on 1T-TiSe₂: Interpretation within the exciton condensate phase model

Physical Review B **81**, 155104 (2010).

Group(s): Aebi, Forró / Project(s): 7

Group of D. Baeriswyl

D. BAERISWYL

Superconductivity in the repulsive Hubbard model

Journal of Superconductivity and Novel Magnetism **24**, 1157 (2011).

Group(s): Baeriswyl / Project(s): 4

Group of B. Batlogg

- ▶ P. J. W. MOLL, R. PUZNIAK, F. BALAKIREV, K. ROGACKI, J. KARPINSKI, N. D. ZHIGADLO, AND B. BATLOGG

High magnetic-field scales and critical currents in SmFeAs(O, F) crystals

Nature Materials **9**, 628 (2010).

Group(s): Batlogg, Karpinski / Project(s): 4

- ▶ N. D. ZHIGADLO, S. KATRYCH, S. WEYENETH, R. PUZNIAK, P. J. W. MOLL, Z. BUKOWSKI, J. KARPINSKI, H. KELLER, AND B. BATLOGG

- Th-substituted SmFeAsO: Structural details and superconductivity with T_c above 50 K*
Physical Review B **82**, 064517 (2010).
Group(s): Batlogg, Karpinski, Keller / Project(s): 4
- W. L. KALB, S. HAAS, C. KRELLNER, T. MATHIS, AND B. BATLOGG
Trap density of states in small-molecule organic semiconductors: A quantitative comparison of thin-film transistors with single crystals
Physical Review B **81**, 155315 (2010).
Group(s): Batlogg / Project(s): 4
- W. L. KALB AND B. BATLOGG
Calculating the trap density of states in organic field-effect transistors from experiment: A comparison of different methods
Physical Review B **81**, 035327 (2010).
Group(s): Batlogg / Project(s): 4
- N. D. ZHIGADLO, S. KATRYCH, J. KARPINSKI, B. BATLOGG, F. BERNARDINI, S. MASSIDDA, AND R. PUZNIAK
Influence of Mg deficiency on crystal structure and superconducting properties in MgB₂ single crystals
Physical Review B **81**, 054520 (2010).
Group(s): Batlogg, Karpinski / Project(s): 4
- A. BELOUSOV, J. KARPINSKI, AND B. BATLOGG
Thermodynamics of the Al-Ga-N₂ system
Journal of Crystal Growth **312**, 2579 (2010).
Group(s): Batlogg, Karpinski / Project(s): 4
- A. BELOUSOV, S. KATRYCH, K. HAMETNER, D. GÜNTHER, J. KARPINSKI, AND B. BATLOGG
Al_xGa_{1-x}N bulk crystal growth: Crystallographic properties and $p - T$ phase diagram
Journal of Crystal Growth **312**, 2585 (2010).
Group(s): Batlogg, Karpinski / Project(s): 4
- S. WEYENETH, P. J. W. MOLL, R. PUZNIAK, K. NINIOS, F. F. BALAKIREV, R. D. McDONALD, H. B. CHAN, N. D. ZHIGADLO, S. KATRYCH, Z. BUKOWSKI, J. KARPINSKI, H. KELLER, B. BATLOGG, AND L. BALICAS
Rearrangement of the antiferromagnetic ordering at high magnetic fields in SmFeAsO and SmFeAsO_{0.9}F_{0.1} single crystals
to be published in Physical Review B (2011).
Group(s): Batlogg, Karpinski, Keller / Project(s): 4
- Z. SHERMADINI, J. KANTER, C. BAINES, M. BENDELE, Z. BUKOWSKI, R. KHASANOV, H.-H. KLAUSS, H. LUETKENS, H. MAETER, G. PASCUA, B. BATLOGG, AND A. AMATO
Microscopic study of the superconducting state of the iron pnictide RbFe₂As₂ via muon spin rotation
Physical Review B **82**, 144527 (2010).
Group(s): Batlogg, Karpinski, Keller / Project(s): 4
- Group of Ch. Bernhard**
- ▶ J. HOPPLER, H. FRITZSCHE, V. K. MALIK, J. STAHN, G. CRISTIANI, H. U. HABERMEIER, M. RÖSSLE, J. HONOLKA, A. ENDERS, AND C. BERNHARD
Polarized neutron reflectometry study of the magnetization reversal process in YBa₂Cu₃O₇/La_{2/3}Ca_{1/3}MnO₃ superlattices grown on SrTiO₃ substrates
Physical Review B **82**, 174439 (2010).
Group(s): Bernhard / Project(s): 1
- ▶ A. DUBROKA, M. RÖSSLE, K. W. KIM, V. K. MALIK, D. MUNZAR, D. N. BASOV, A. A. SCHAFGANS, S. J. MOON, C. T. LIN, D. HAUG, V. HINKOV, B. KEIMER, T. WOLF, J. G. STOREY, J. L. TALLON, AND C. BERNHARD
Evidence of a Precursor Superconducting Phase at Temperatures as High as 180 K in RBa₂Cu₃O_{7- δ} (R = Y; Gd; Eu) Superconducting Crystals from Infrared Spectroscopy
Physical Review Letters **106**, 047006 (2011).
Group(s): Bernhard / Project(s): 1
- ▶ A. DUBROKA, M. RÖSSLE, K. W. KIM, V. K. MALIK, L. SCHULTZ, S. THIEL, C. W. SCHNEIDER, J. MANNHART, G. HERRANZ, C. O., M. BIBES, A. BARTHELEMY, AND C. BERNHARD
Dynamical Response and Confinement of the Electrons at the LaAlO₃/SrTiO₃ Interface
Physical Review Letters **104**, 156807 (2010).
Group(s): Bernhard / Project(s): 1
- ▶ A. PASHKIN, M. PORER, M. BEYER, K. W. KIM, A. DUBROKA, C. BERNHARD, X. YAO, Y. DAGAN, R. HACKL, A. ERB, J. DEMSAR, R. HUBER, AND A. LEITENSTORFER
Femtosecond Response of Quasiparticles and Phonons in Superconducting YBa₂Cu₃O_{7- δ} Studied by Wideband Terahertz Spectroscopy
Physical Review Letters **105**, 067001 (2010).
Group(s): Bernhard / Project(s): 1
- ▶ L. SCHULZ, L. NUCCIO, M. WILLIS, P. DESAI, P. SHAKYA, T. KREOUZIS, V. K. MALIK, C. BERNHARD, F. L. PRATT, N. A. MORLEY, A. SUTER, G. J. NIEUWENHUIS, T. PROKSCHA, E. MORENZONI, W. P. GILLIN, AND A. J. DREW
Engineering spin propagation across a hybrid organic/inorganic interface using a polar layer
Nature Materials **10**, 39 (2011).
Group(s): Bernhard, Morenzoni / Project(s): 1

- P. MARSIK, K. W. KIM, A. DUBROKA, M. RÖSSLE, V. K. MALIK, L. SCHULZ, C. N. WANG, C. NIEDERMAYER, A. J. DREW, M. WILLIS, T. WOLF, AND C. BERNHARD
Coexistence and Competition of Magnetism and Superconductivity on the Nanometer Scale in Underdoped $BaFe_{1.89}Co_{0.11}As_2$
Physical Review Letters **105**, 057001 (2010).
Group(s): Bernhard, Niedermayer / Project(s): 1, 4
- A. DUBROKA, L. YU, D. MUNZAR, K. W. KIM, M. RÖSSLE, V. K. MALIK, C. T. LIN, B. KEIMER, T. WOLF, AND C. BERNHARD
Pseudogap and precursor superconductivity in underdoped cuprate high temperature superconductors: A far-infrared ellipsometry study
The European Physical Journal – Special Topics **188**, 73 (2010).
Group(s): Bernhard / Project(s): 1
- K. W. KIM, M. RÖSSLE, A. DUBROKA, V. K. MALIK, T. WOLF, AND C. BERNHARD
Evidence for multiple superconducting gaps in optimally doped $BaFe_{1.87}Co_{0.13}As_2$ from infrared spectroscopy
Physical Review B **81**, 214508 (2010).
Group(s): Bernhard / Project(s): 1
- Group of G. Blatter**
- V. S. DOTSENKO, V. B. GESHKENBEIN, D. A. GOROKHOV, AND G. BLATTER
Free-energy distribution functions for the randomly forced directed polymer
Physical Review B **82**, 174201 (2010).
Group(s): Blatter / Project(s): 5
- S. SCHMIDT AND G. BLATTER
Excitations of Strongly Correlated Lattice Polaritons
Physical Review Letters **104**, 216402 (2010).
Group(s): Blatter / Project(s): 8
- S. SCHMIDT, D. GERACE, A. A. HOUCK, G. BLATTER, AND H. E. TÜRECI
Nonequilibrium delocalization-localization transition of photons in circuit quantum electrodynamics
Physical Review B **82**, 100507(R) (2010).
Group(s): Blatter / Project(s): 8
- F. HASSLER, A. RÜEGG, M. SIGRIST, AND G. BLATTER
Dynamical Unbinding Transition in a Periodically Driven Mott Insulator
Physical Review Letters **104**, 220402 (2010).
Group(s): Blatter, Sigrist / Project(s): 8
- A. V. LEBEDEV, G. B. LESOVIK, AND G. BLATTER
Statistics of radiation emitted from a quantum point contact
Physical Review B **81**, 155421 (2010).
Group(s): Blatter / Project(s): 2
- G. B. LESOVIK, M. V. SUSLOV, AND G. BLATTER
Quantum counting algorithm and its application in mesoscopic physics
Physical Review A **82**, 012316 (2010).
Group(s): Blatter / Project(s): 2
- B. SURER, A. GLATZ, H. G. KATZGRABER, G. T. ZIMANYI, B. A. ALLGOOD, AND G. BLATTER
Surer et al. Reply:
Physical Review Letters **105**, 039702 (2010).
Group(s): Blatter / Project(s): 5
- Group of M. Büttiker**
- J. LI, I. MARTIN, M. BÜTTIKER, AND A. F. MORPURGO
Topological origin of subgap conductance in insulating bilayer graphene
Nature Physics **7**, 38 (2011).
Group(s): Büttiker, Morpurgo / Project(s): 2
- J. LI, A. F. MORPURGO, M. BÜTTIKER, AND I. MARTIN
Marginality of bulk-edge correspondence for single-valley Hamiltonians
Physical Review B **82**, 245404 (2010).
Group(s): Büttiker, Morpurgo / Project(s): 2
- Group of M. Decroux**
- L. ANTOGNAZZA, M. DECROUX, M. THERASSE, AND M. ABPLANALP
Heat Propagation Velocities in Coated Conductors for Fault Current Limiter Applications
IEEE Transactions on Applied Superconductivity (2011), doi:10.1109/TASC.2010.2100351.
Group(s): Abplanalp, Decroux / Project(s): 3
- A. P. PETROVIĆ, R. LORTZ, G. SANTI, C. BERTHOD, C. DUBOIS, M. DECROUX, A. DEMUER, A. B. ANTUNES, A. PARÉ, D. SALLOUM, P. GOUGEON, M. POTEL, AND Ø. FISCHER
Multi-band Superconductivity in the Chevrel Phases $SnMo_6S_8$ and $PbMo_6S_8$
Physical Review Letters **106**, 017003 (2011).
Group(s): Decroux, Fischer, Giamarchi / Project(s): 4

N. CURTZ, E. KOLLER, H. ZBINDEN, M. DECROUX, L. ANTOGNAZZA, Ø. FISCHER, AND N. GISIN

Patterning of ultrathin YBCO nanowires using a new focused-ion-beam process

Superconductor Science & Technology **23**, 45015 (2010).

Group(s): Decroux, Fischer / Project(s): 3

Group of L. Degiorgi

- ▶ F. PFUNER, P. LERCH, J.-H. CHU, H.-H. KUO, I. R. FISHER, AND L. DEGIORGI

Temperature dependence of the excitation spectrum in the charge-density-wave $ErTe_3$ and $HoTe_3$ systems

Physical Review B **81**, 195110 (2010).

Group(s): Degiorgi / Project(s): 7

- ▶ A. LUCARELLI, A. DUSZA, F. PFUNER, P. LERCH, J. G. ANALYTIS, J.-H. CHU, I. R. FISHER, AND L. DEGIORGI

Charge dynamics of Co-doped $BaFe_2As_2$

New Journal of Physics **12**, 073036 (2010).

Group(s): Degiorgi / Project(s): 4

M. LAVAGNINI, H.-M. EITER, L. TASSINI, B. MUSCHLER, R. HACKL, R. MONNIER, J.-H. CHU, I. R. FISHER, AND L. DEGIORGI

Raman scattering evidence for a cascade evolution of the charge-density-wave collective amplitude mode

Physical Review B **81**, 081101(R) (2010).

Group(s): Degiorgi / Project(s): 7

A. SANNA, F. BERNARDINI, G. PROFETA, S. SHARMA, J. K. DEWHURST, A. LUCARELLI, L. DEGIORGI, E. K. U. GROSS, AND S. MASSIDDA

Theoretical investigation of optical conductivity in $Ba(Fe_{1-x}Co_x)_2As_2$

Physical Review B **83**, 054502 (2011).

Group(s): Degiorgi / Project(s): 4

Group of T. Esslinger

- ▶ R. JÖRDENS, L. TARRUELL, D. GREIF, T. UEHLINGER, N. STROHMAIER, H. MORITZ, T. ESSLINGER, L. DE LEO, C. KOLLATH, A. GEORGES, V. SCAROLA, L. POLLET, E. BUROVSKI, E. KOZIK, AND M. TROYER

Quantitative Determination of Temperature in the Approach to Magnetic Order of Ultracold Fermions in an Optical Lattice

Physical Review Letters **104**, 180401 (2010).

Group(s): Esslinger, Troyer / Project(s): 8

Group of Ø. Fischer

- ▶ A. PIRIOU, N. JENKINS, C. BERTHOD, I. MAGGIO-APRILE, AND Ø. FISCHER

First direct observation of the Van Hove singularity in the tunneling spectra of cuprates

Nature Communications **2**, 221 (2011).

Group(s): Fischer, Giamarchi / Project(s): 4

- ▶ A. P. PETROVIĆ, R. LORTZ, G. SANTI, C. BERTHOD, C. DUBOIS, M. DECROUX, A. DEMUER, A. B. ANTUNES, A. PARÉ, D. SALLOUM, P. GOUGEON, M. POTEL, AND Ø. FISCHER

Multi-band Superconductivity in the Chevrel Phases $SnMo_6S_8$ and $PbMo_6S_8$

Physical Review Letters **106**, 017003 (2011).

Group(s): Decroux, Fischer, Giamarchi / Project(s): 4

- ▶ Y. FASANO, I. MAGGIO-APRILE, N. D. ZHIGADLO, S. KATRYCH, J. KARPINSKI, AND Ø. FISCHER

Local Quasiparticle Density of States of Superconducting $SmFeAsO_{1-x}F_x$ Single Crystals: Evidence for Spin-Mediated Pairing

Physical Review Letters **105**, 167005 (2010).

Group(s): Fischer, Karpinski / Project(s): 4

- ▶ C. M. SCHLEPÜTZ, M. BJÖRCK, E. KOLLER, S. A. PAULI, D. MARTOCCIA, Ø. FISCHER, AND P. R. WILLMOTT

Structure of ultrathin heteroepitaxial superconducting $YBa_2Cu_3O_{7-x}$ films

Physical Review B **81**, 174520 (2010).

Group(s): Fischer, Willmott / Project(s): 1

N. CURTZ, E. KOLLER, H. ZBINDEN, M. DECROUX, L. ANTOGNAZZA, Ø. FISCHER, AND N. GISIN

Patterning of ultrathin YBCO nanowires using a new focused-ion-beam process

Superconductor Science & Technology **23**, 45015 (2010).

Group(s): Decroux, Fischer / Project(s): 3

C. BERTHOD

Tunneling spectra of strongly coupled superconductors: Role of dimensionality

Physical Review B **82**, 024504 (2010).

Group(s): Fischer, Giamarchi / Project(s): 4

A. PIRIOU, E. GIANNINI, Y. FASANO, C. SENATORE, AND Ø. FISCHER

Vortex phase diagram and temperature-dependent second-peak effect in overdoped $Bi_2Sr_2CuO_{6+\delta}$ crystals

Physical Review B **81**, 144517 (2010).

Group(s): Fischer, Flükiger, Giannini / Project(s): 4

G. LEVY DE CASTRO, C. BERTHOD, A. PIRIOU,

E. GIANNINI, AND Ø. FISCHER

Reply to Comment on "Preeminent Role of the Van Hove Singularity in the Strong-Coupling Analysis of Scanning Tunneling Spectroscopy for Two-Dimensional Cuprate Superconductors"

Physical Review Letters **105**, 099702 (2010).

Group(s): Fischer, Giamarchi, Giannini / Project(s): 4

Group of R. Flükiger

- ▶ B. SEEBER, A. FERREIRA, G. MONDONICO, F. BUTA, C. SENATORE, R. FLÜKIGER, AND T. TAKEUCHI

Critical current of a rapid-quenched Nb₃Al conductor under transverse compressive and axial tensile stress

Superconductor Science & Technology **24**, 035011 (2011).

Group(s): Flükiger / Project(s): 3

- ▶ R. FLÜKIGER, M. S. A. HOSSAIN, C. SENATORE, F. BUTA, AND M. RINDFLEISCH

A new generation of in situ MgB₂ wires with improved J_c and B_{irr} values obtained by Cold Densification (CHPD)

to be published in IEEE Transactions on Applied Superconductivity (2011).

Group(s): Flükiger / Project(s): 3

- ▶ C. SENATORE, M. S. A. HOSSAIN, AND R. FLÜKIGER

Enhanced Connectivity and Percolation in Binary and Doped in situ MgB₂ Wires after Cold High Pressure Densification

to be published in IEEE Transactions on Applied Superconductivity (2011).

Group(s): Flükiger / Project(s): 3

G. MONDONICO, B. SEEBER, C. SENATORE, R. FLÜKIGER, V. CORATO, G. DE MARZI, AND L. MUZZI

Improvement of electromechanical properties of an ITER internal tin Nb₃Sn wire

Journal of Applied Physics **108**, 093906 (2010).

Group(s): Flükiger / Project(s): 3

C. SCHEUERLEIN, I. PONG, C. SENATORE, M. DI MICHIEL, L. THILLY, A. GERARDIN, B. REHMER, L. OBERLI, G. WILLERING, AND L. BOTTURA

Temperature induced degradation of Nb-Ti/Cu composite superconductors

Journal of Physics: Conference Series **234**, 022031 (2010).

Group(s): Flükiger / Project(s): 3

C. SCHEUERLEIN, M. DI MICHIEL, L. THILLY, F. BUTA, X. PENG, E. GREGORY, J. A. PAR-

RELL, I. PONG, B. BORDINI, AND M. CANTONI
Phase transformations during the reaction heat treatment of Nb₃Sn superconductors

Journal of Physics: Conference Series **234**, 022032 (2010).

Group(s): Flükiger / Project(s): 3

I. PONG, C. SCHEUERLEIN, C. SENATORE, L. THILLY, M. DI MICHIEL, A. GERARDIN, S. C. HOPKINS, L.-R. OBERLI, G. GEANDIER, B. A. GLOWACKI, AND L. BOTTURA

Cu-Ti Formation in Nb-Ti/Cu Superconducting Strand Monitored by in situ Techniques

Defect and Diffusion Forum **297-301**, 695 (2010).

Group(s): Flükiger / Project(s): 3

A. UBALDINI, E. GIANNINI, C. SENATORE, AND D. VAN DER MAREL

BiOCuS: A new superconducting compound with oxypnictide-related structure

Physica C **470**, S356 (2010).

Group(s): Flükiger, Giannini, van der Marel / Project(s): 4

B. SEEBER, A. FERREIRA, G. MONDONICO, F. BUTA, C. SENATORE, R. FLÜKIGER, AND T. TAKEUCHI

Low critical current sensitivity of RHQT Nb₃Al wires under transverse compressive stress up to 300 MPa

to be published in IEEE Transactions on Applied Superconductivity (2011).

Group(s): Flükiger / Project(s): 3

B. BORDINI, D. BESSETTE, L. BOTTURA, A. DEVRED, M. JEWELL, D. RICHTER, AND C. SENATORE

Magnetization and Inter-Filament Contact in HEP and ITER Bronze-Route Nb₃Sn Wires

to be published in IEEE Transactions on Applied Superconductivity (2011).

Group(s): Flükiger / Project(s): 3

C. SCHEUERLEIN, M. DI MICHIEL, G. ARNAU, R. FLÜKIGER, F. BUTA, I. PONG, L. OBERLI, AND L. BOTTURA

Coarse Nb₃Sn grain formation and phase evolution during the reaction of a high Sn content Internal Sn strand

to be published in IEEE Transactions on Applied Superconductivity (2011).

Group(s): Flükiger / Project(s): 3

M. BONURA, A. A. GALLITTO, M. LI VIGNI, AND M. M.

Fluxon dynamics in Li-Al codoped MgB₂ by microwave surface resistance measurements

Physica C **470**, 907 (2010).

Group(s): Flükiger / Project(s): 3

P.-E. LE RENARD, R. LORTZ, C. SENATORE, J.-P. RAPIN, F. BUCHEGGER, A. PETRI-FINK, H. HOFMANN, E. DOELKER, AND J. OLIVIER

Magnetic and in vitro heating properties of implants formed in situ from injectable formulations and containing superparamagnetic iron oxide nanoparticles (SPIONs) embedded in silica microparticles for magnetically induced local hyperthermia

Journal of Magnetism and Magnetic Materials **323**, 1054 (2011).

Group(s): Flükiger / Project(s): 3

A. PIRIOU, E. GIANNINI, Y. FASANO, C. SENATORE, AND Ø. FISCHER

Vortex phase diagram and temperature-dependent second-peak effect in overdoped $\text{Bi}_2\text{Sr}_2\text{CuO}_{6+\delta}$ crystals

Physical Review B **81**, 144517 (2010).

Group(s): Fischer, Flükiger, Giannini / Project(s): 4

Group of L. Forró

- ▶ C. MONNEY, E. F. SCHWIER, M. G. GARNIER, N. MARIOTTI, C. DIDOT, H. CERCELLIER, J. MARCUS, H. BERGER, A. N. TITOV, H. BECK, AND P. AEBI

Probing the exciton condensate phase in 1T - TiSe_2 with photoemission

New Journal of Physics **12**, 125019 (2010).

Group(s): Aebi, Forró / Project(s): 7

- ▶ C. MONNEY, E. F. SCHWIER, M. G. GARNIER, C. BATTAGLIA, N. MARIOTTI, C. DIDOT, H. CERCELLIER, J. MARCUS, H. BERGER, A. N. TITOV, H. BECK, AND P. AEBI

Dramatic effective mass reduction driven by a strong potential of competing periodicity

Europhysics Letters **92**, 47003 (2010).

Group(s): Aebi, Forró / Project(s): 7

- ▶ L. ĆIRIĆ, A. SIENKIEWICZ, D. M. DJOKIĆ, R. SMAJDA, A. MAGREZ, T. KASPAR, R. NESPER, AND L. FORRÓ

Size dependence of the magnetic response of graphite oxide and graphene flakes — an electron spin resonance study

Physica Status Solidi (b) **247**, 2958 (2010).

Group(s): Forró / Project(s): 2

- ▶ M. GUARISE, B. DALLA PIAZZA, M. MORETTI SALA, G. GHIRINGHELLI, L. BRAICOVICH, H. BERGER, J. N. HANCOCK, D. VAN DER MAREL, T. SCHMITT, V. N. STROCOV, L. J. P. AMENT, J. VAN DEN BRINK, P.-H. LIN, P. XU, H. M. RØNNOW, AND M. GRIONI

Measurement of Magnetic Excitations in the Two-Dimensional Antiferromagnetic $\text{Sr}_2\text{CuO}_2\text{Cl}_2$ Insulator Using Resonant X-Ray Scattering: Evidence for Extended Interactions

Physical Review Letters **105**, 157006 (2010).

Group(s): Forró, Grioni, Rønnow, van der Marel / Project(s): 6, 7

- ▶ P. XU, J. O. PIATEK, P.-H. LIN, B. SIPOS, H. BERGER, L. FORRÓ, H. M. RØNNOW, AND M. GRIONI

Superconducting phase in the layered dichalcogenide 1T-TaS_2 upon inhibition of the metal-insulator transition

Physical Review B **81**, 172503 (2010).

Group(s): Forró, Grioni, Rønnow / Project(s): 7

- ▶ N. P. ARMITAGE, R. TEDIOSI, F. LÉVY, E. GIANNINI, L. FORRÓ, AND D. VAN DER MAREL

Infrared Conductivity of Elemental Bismuth under Pressure: Evidence for an Avoided Lifshitz-Type Semimetal-Semiconductor Transition

Physical Review Letters **104**, 237401 (2010).

Group(s): Forró, Giannini, van der Marel / Project(s): 4

C. MONNEY, E. F. SCHWIER, M. G. GARNIER, N. MARIOTTI, C. DIDOT, H. BECK, P. AEBI, H. CERCELLIER, J. MARCUS, C. BATTAGLIA, H. BERGER, AND A. N. TITOV

Temperature-dependent photoemission on 1T- TiSe_2 : Interpretation within the exciton condensate phase model

Physical Review B **81**, 155104 (2010).

Group(s): Aebi, Forró / Project(s): 7

B. NÁFRÁDI, A. OLARIU, L. FORRÓ, C. MÉZIÈRE, P. BATAIL, AND A. JÁNOSSY

Spin dynamics in the $S = 1/2$ antiferromagnetic chain compounds $\delta\text{-(EDT-TTF-CONMe}_2)_2\text{X}$ ($\text{X}=\text{AsF}_6, \text{Br}$): A multifrequency electron spin resonance study

Physical Review B **81**, 224438 (2010).

Group(s): Forró / Project(s): 7

Y. LAKHDAR, C. MÉZIÈRE, L. ZORINA, M. GIFFARD, P. BATAIL, E. CANADELL, P. AUBAN-SENZIER, C. PASQUIER, D. JÉROME, B. NÁFRÁDI, AND L. FÓRRÓ

Dual [proton]/[hole] mixed valence in a molecular metal: balancing chemical activity in the solid state by tapping into a molecular hole reservoir

Journal of Materials Chemistry **21**, 1516 (2011).

Group(s): Forró / Project(s): 7

Á. ANTAL, T. FEHÉR, B. NÁFRÁDI, R. GAÁL, L. FORRÓ, AND A. JÁNOSSY

- Measurement of interlayer spin diffusion in the organic conductor κ -(BEDT-TTF)₂Cu[N(CN)₂]X, X=Cl, Br*
 Physica B **405**, S168 (2010).
 Group(s): Forró / Project(s): 7
- A. AKRAP, M. ANGST, P. KHALIFAH, D. MANDRUS, B. C. SALES, AND L. FORRÓ
Electrical transport in charge-ordered Fe₂OBO₃: Resistive switching and pressure effects
 Physical Review B **82**, 165106 (2010).
 Group(s): Forró / Project(s): 7
- Á. ANTAL, A. JÁNOSSY, L. FORRÓ, E. J. M. VERTELMAN, P. J. VAN KONINGSBRUGGEN, AND P. H. M. VAN LOOSDRECHT
Origin of the ESR spectrum in the Prussian blue analog RbMn[Fe(CN)₆]·H₂O
 Physical Review B **82**, 014422 (2010).
 Group(s): Forró / Project(s): 7
- Y. LAKHDAR, C. MÉZIÈRE, L. ZORINA, M. GIFFARD, P. BATAIL, E. CANADELL, P. AUBAN-SENZIER, C. PASQUIER, D. JÉROME, B. NÁFRÁDI, AND L. FORRÓ
Dual [proton]/[hole] mixed valence in a molecular metal: balancing chemical activity in the solid state by tapping into a molecular hole reservoir
 Journal of Materials Chemistry **21**, 1516 (2011).
 Group(s): Forró / Project(s): 7
- A. EL-GHAYOURY, C. MÉZIÈRE, S. SIMONOV, L. ZORINA, M. COBIÁN, E. CANADELL, C. ROVIRA, B. NÁFRÁDI, B. SIPOS, L. FORRÓ, AND P. BATAIL
A Neutral Zwitterionic Molecular Solid
 Chemistry–A European Journal **16**, 14051 (2010).
 Group(s): Forró / Project(s): 7
- N. BARIŠIĆ, I. SMILJANIĆ, P. POPČEVIĆ, A. BILUŠIĆ, E. TUTIŠ, A. SMONTARA, H. BERGER, J. JAĆIMOVIĆ, O. YULI, AND L. FORRÓ
High pressure study of transport properties in Co_{1/3}NbS₂
to be published in Physical Review B (2011), arXiv:1012.2408.
 Group(s): Forró / Project(s): 7
- M. BELESI, I. ROUSOCHATZAKIS, H. C. WU, H. BERGER, I. V. SHVETS, F. MILA, AND J. P. ANSERMET
Ferrimagnetism of the magnetoelectric compound Cu₂OSeO₃ probed by ⁷⁷Se NMR
 Physical Review B **82**, 094422 (2010).
 Group(s): Forró, Mila / Project(s): 6
- Group of T. Giamarchi**
- ▶ A. PIRIOU, N. JENKINS, C. BERTHOD, I. MAGGIO-APRILE, AND Ø. FISCHER
First direct observation of the Van Hove singularity in the tunneling spectra of cuprates
 Nature Communications **2**, 221 (2011).
 Group(s): Fischer, Giamarchi / Project(s): 4
- ▶ E. AGORITSAS, V. LECOMTE, AND T. GIAMARCHI
Temperature-induced crossovers in the static roughness of a one-dimensional interface
 Physical Review B **82**, 184207 (2010).
 Group(s): Giamarchi / Project(s): 1
- ▶ S. BUSTINGORRY, A. B. KOLTON, AND T. GIAMARCHI
Random-manifold to random-periodic depinning of an elastic interface
 Physical Review B **82**, 094202 (2010).
 Group(s): Giamarchi / Project(s): 1
- ▶ A. M. LOBOS AND T. GIAMARCHI
Dissipative phase fluctuations in superconducting wires capacitively coupled to diffusive metals
 Physical Review B **82**, 104517 (2010).
 Group(s): Giamarchi / Project(s): 2
- ▶ A. P. PETROVIĆ, R. LORTZ, G. SANTI, C. BERTHOD, C. DUBOIS, M. DECROUX, A. DEMUER, A. B. ANTUNES, A. PARÉ, D. SALLOUM, P. GOUGEON, M. POTEI, AND Ø. FISCHER
Multi-band Superconductivity in the Chevrel Phases SnMo₆S₈ and PbMo₆S₈
 Physical Review Letters **106**, 017003 (2011).
 Group(s): Decroux, Fischer, Giamarchi / Project(s): 4
- ▶ T. JARLBORG
A model of the T-dependent pseudogap and its competition with superconductivity in copper oxides
 Solid State Communications **151**, 639 (2011).
 Group(s): Giamarchi / Project(s): 4
- ▶ P. BOUILLOT, K. CORINNA, A. M. LÄUCHLI, M. ZVONAREV, B. THIELEMANN, C. RÜEGG, E. ORIGNAC, R. CITRO, M. HORVATIĆ, C. BERTHIER, M. KLANJŠEK, , AND T. GIAMARCHI
Statics and dynamics of weakly coupled antiferromagnetic spin-1/2 ladders in a magnetic field
 Physical Review B **83**, 054407 (2011).
 Group(s): Giamarchi / Project(s): 6
- ▶ P. CHUDZINSKI, M. GABAY, AND T. GIAMARCHI
Spin rotational symmetry breaking by orbital current patterns in two-leg ladders

Physical Review B **81**, 165402 (2010).

Group(s): Giamarchi / Project(s): 7

- ▶ E. G. DALLA TORRE, E. DEMLER, T. GIAMARCHI, AND E. ALTMAN

Quantum critical states and phase transitions in the presence of non-equilibrium noise

Nature Physics **6**, 806 (2010).

Group(s): Giamarchi / Project(s): 8

C. BERTHOD

Tunneling spectra of strongly coupled superconductors: Role of dimensionality

Physical Review B **82**, 024504 (2010).

Group(s): Fischer, Giamarchi / Project(s): 4

G. LEVY DE CASTRO, C. BERTHOD, A. PIRIOU, E. GIANNINI, AND Ø. FISCHER

Reply to Comment on "Preeminent Role of the Van Hove Singularity in the Strong-Coupling Analysis of Scanning Tunneling Spectroscopy for Two-Dimensional Cuprate Superconductors"

Physical Review Letters **105**, 099702 (2010).

Group(s): Fischer, Giamarchi, Giannini / Project(s): 4

Group of E. Giannini

- ▶ J. TEYSSIER, E. GIANNINI, V. GURITANU, R. VIENNOIS, D. VAN DER MAREL, A. AMATO, AND S. N. GVASALIYA

Spin-glass ground state in $Mn_{1-x}Co_xSi$

Physical Review B **82**, 064417 (2010).

Group(s): Giannini, van der Marel / Project(s): 5

- ▶ J. N. HANCOCK, S. I. MIRZAEI, J. GILLET, S. E. SEBASTIAN, J. TEYSSIER, R. VIENNOIS, E. GIANNINI, AND D. VAN DER MAREL

Strong coupling to magnetic fluctuations in the charge dynamics of iron-based superconductors

Physical Review B **82**, 014523 (2010).

Group(s): van der Marel, Giannini / Project(s): 4

- ▶ N. P. ARMITAGE, R. TEDIOSI, F. LÉVY, E. GIANNINI, L. FORRÓ, AND D. VAN DER MAREL

Infrared Conductivity of Elemental Bismuth under Pressure: Evidence for an Avoided Lifshitz-Type Semimetal-Semiconductor Transition

Physical Review Letters **104**, 237401 (2010).

Group(s): Forró, Giannini, van der Marel / Project(s): 4

A. UBALDINI, E. GIANNINI, C. SENATORE, AND D. VAN DER MAREL

BiOCuS: A new superconducting compound with oxypnictide-related structure

Physica C **470**, S356 (2010).

Group(s): Flükiger, Giannini, van der Marel / Project(s): 4

M. WEIGAND, M. EISTERER, E. GIANNINI, AND H. W. WEBER

Mixed state properties of $Bi_2Sr_2Ca_2Cu_3O_{10+\delta}$ single crystals before and after neutron irradiation

Physical Review B **81**, 014516 (2010).

Group(s): Giannini / Project(s): 4

A. PIRIOU, E. GIANNINI, Y. FASANO, C. SENATORE, AND Ø. FISCHER

Vortex phase diagram and temperature-dependent second-peak effect in overdoped $Bi_2Sr_2CuO_{6+\delta}$ crystals

Physical Review B **81**, 144517 (2010).

Group(s): Fischer, Flükiger, Giannini / Project(s): 4

R. VIENNOIS, E. GIANNINI, D. VAN DER MAREL, AND R. ČERNÝ

Effect of Fe excess on structural, magnetic and superconducting properties of single-crystalline $Fe_{1+x}Te_{1-y}Se_y$

Journal of Solid State Chemistry **183**, 769 (2010).

Group(s): Giannini, van der Marel / Project(s): 4

R. VIENNOIS, E. GIANNINI, D. VAN DER MAREL, AND R. ČERNÝ

Phase diagram of single-crystalline tetragonal iron chalcogenides

Physica C **470**, S370 (2010).

Group(s): Giannini, van der Marel / Project(s): 4

O. ZAREMBA, O. SHCHERBAN, L. AKSELRUD, R. GLADYSHEVSKII, F. BANFI, AND E. GIANNINI

The 5:7 Member of the Spin-Ladder Series in the Bi-Sr-Ca-Cu-O System

Acta Physica Polonica A **117**, 42 (2010).

Group(s): Giannini / Project(s): 4

G. LEVY DE CASTRO, C. BERTHOD, A. PIRIOU, E. GIANNINI, AND Ø. FISCHER

Reply to Comment on "Preeminent Role of the Van Hove Singularity in the Strong-Coupling Analysis of Scanning Tunneling Spectroscopy for Two-Dimensional Cuprate Superconductors"

Physical Review Letters **105**, 099702 (2010).

Group(s): Fischer, Giamarchi, Giannini / Project(s): 4

Group of M. Grioni

- ▶ E. FRANTZESKAKIS, S. PONS, AND M. GRIONI
- Band structure scenario for the giant spin-orbit splitting observed at the Bi/Si(111) interface*

Physical Review B **82**, 085440 (2010).

Group(s): Grioni / Project(s): 7

- M. GUARISE, B. DALLA PIAZZA, M. MORETTI SALA, G. GHIRINGHELLI, L. BRAICOVICH, H. BERGER, J. N. HANCOCK, D. VAN DER MAREL, T. SCHMITT, V. N. STROCOV, L. J. P. AMENT, J. VAN DEN BRINK, P.-H. LIN, P. XU, H. M. RØNNOW, AND M. GRIONI
Measurement of Magnetic Excitations in the Two-Dimensional Antiferromagnetic Sr₂CuO₂Cl₂ Insulator Using Resonant X-Ray Scattering: Evidence for Extended Interactions
Physical Review Letters **105**, 157006 (2010).
Group(s): Forró, Grioni, Rønnow, van der Marel / Project(s): 6, 7
- P. XU, J. O. PIATEK, P.-H. LIN, B. SIPOS, H. BERGER, L. FORRÓ, H. M. RØNNOW, AND M. GRIONI
Superconducting phase in the layered dichalcogenide 1T-TaS₂ upon inhibition of the metal-insulator transition
Physical Review B **81**, 172503 (2010).
Group(s): Forró, Grioni, Rønnow / Project(s): 7
- J. N. HANCOCK, R. VIENNOIS, D. VAN DER MAREL, H. M. RØNNOW, M. GUARISE, P.-H. LIN, M. GRIONI, M. MORETTI SALA, G. GHIRINGHELLI, V. N. STROCOV, J. SCHLAPPA, AND T. SCHMITT
Evidence for core-hole-mediated inelastic x-ray scattering from metallic Fe_{1.087}Te
Physical Review B **82**, 020513(R) (2010).
Group(s): Grioni, Rønnow, van der Marel / Project(s): 4, 6
- E. FRANTZESKAKIS, A. CREPALDI, S. PONS, K. KERN, AND M. GRIONI
Tuning the giant Rashba effect on a BiAg₂ surface alloy: Two different approaches
Journal of Electron Spectroscopy and Related Phenomena **181**, 88 (2010).
Group(s): Grioni / Project(s): 7
- Group of V. Gritsev**
- T. KITAGAWA, S. PIELAWA, A. IMAMBEKOV, J. SCHMIEDMAYER, V. GRITSEV, AND E. DEMLER
Ramsey Interference in One-Dimensional Systems: The Full Distribution Function of Fringe Contrast as a Probe of Many-Body Dynamics
Physical Review Letters **104**, 255302 (2010).
Group(s): Gritsev / Project(s): 8
- C. DEGRANDI, V. GRITSEV, AND A. POLKOVNIKOV
Quench dynamics near a quantum critical point: Application to the sine-Gordon model
Physical Review B **81**, 224301 (2010).
Group(s): Gritsev / Project(s): 8
- C. DEGRANDI, V. GRITSEV, AND A. POLKOVNIKOV
Quench dynamics near a quantum critical point
Physical Review B **81**, 012303 (2010).
Group(s): Gritsev / Project(s): 8
- P. BARMETTLER, M. PUNK, V. GRITSEV, E. DEMLER, AND E. ALTMAN
Quantum quenches in the anisotropic spin- $\frac{1}{2}$ Heisenberg chain: different approaches to many-body dynamics far from equilibrium
New Journal of Physics **12**, 055017 (2010).
Group(s): Gritsev / Project(s): 8
- V. GRITSEV, T. ROSTUNOV, AND E. DEMLER
Exact methods in the analysis of the non-equilibrium dynamics of integrable models: application to the study of correlation functions for non-equilibrium 1D Bose gas
Journal of Statistical Mechanics p. P05012 (2010).
Group(s): Gritsev / Project(s): 8
- V. GRITSEV, P. BARMETTLER, AND E. DEMLER
Scaling approach to quantum non-equilibrium dynamics of many-body systems
New Journal of Physics **12**, 113005 (2010).
Group(s): Gritsev / Project(s): 8
- Group of D. Jaccard**
- A.-S. RÜETSCHI, K. SENGUPTA, G. SEYFARTH, AND D. JACCARD
Nernst effect in CeCu₂Si₂
Journal of Physics: Conference Series **273**, 012052 (2011).
Group(s): Jaccard / Project(s): 5
- K. SENGUPTA AND D. JACCARD
Multiprobe experiments under high pressure: Resistivity, magnetic susceptibility, heat capacity, and thermopower measurements around 5 GPa
Review of Scientific Instruments **81**, 043908 (2010).
Group(s): Jaccard / Project(s): 5
- Group of J. Karpinski**
- P. J. W. MOLL, R. PUZNIAK, F. BALAKIREV, K. ROGACKI, J. KARPINSKI, N. D. ZHIGADLO, AND B. BATLOGG
High magnetic-field scales and critical currents in SmFeAs(O, F) crystals
Nature Materials **9**, 628 (2010).
Group(s): Batlogg, Karpinski / Project(s): 4

- Y. FASANO, I. MAGGIO-APRILE, N. D. ZHIGADLO, S. KATRYCH, J. KARPINSKI, AND Ø. FISCHER
Local Quasiparticle Density of States of Superconducting $\text{SmFeAsO}_{1-x}\text{F}_x$ Single Crystals: Evidence for Spin-Mediated Pairing
Physical Review Letters **105**, 167005 (2010).
Group(s): Fischer, Karpinski / Project(s): 4
- S. WEYENETH, M. BENDELE, R. PUZNIAK, F. MURÁNYI, A. BUSSMANN-HOLDER, N. D. ZHIGADLO, S. KATRYCH, Z. BUKOWSKI, J. KARPINSKI, A. SHENGE-LAYA, R. KHASANOV, AND H. KELLER
Field-dependent superfluid density in the optimally doped $\text{SmFeAsO}_{1-x}\text{F}_y$ superconductor
Europhysics Letters **91**, 47005 (2010).
Group(s): Karpinski, Keller / Project(s): 4
- N. D. ZHIGADLO, S. KATRYCH, S. WEYENETH, R. PUZNIAK, P. J. W. MOLL, Z. BUKOWSKI, J. KARPINSKI, H. KELLER, AND B. BATLOGG
Th-substituted SmFeAsO : Structural details and superconductivity with T_c above 50 K
Physical Review B **82**, 064517 (2010).
Group(s): Batlogg, Karpinski, Keller / Project(s): 4
- T. KONDO, R. KHASANOV, J. KARPINSKI, S. KAZAKOV, N. ZHIGADLO, Z. BUKOWSKI, M. SHI, A. BENDOUNAN, Y. SASSA, J. CHANG, S. PAILHÉS, J. MESOT, J. SCHMALIAN, H. KELLER, AND A. KAMINSKI
Anomalies in the Fermi Surface and Band Dispersion of Quasi-One-Dimensional CuO Chains in the High-Temperature Superconductor $\text{YBa}_2\text{Cu}_4\text{O}_8$
Physical Review Letters **105**, 267003 (2010).
Group(s): Karpinski, Keller / Project(s): 4
- M. BENDELE, S. WEYENETH, R. PUZNIAK, A. MAISURADZE, E. POMJAKUSHINA, K. CONDER, V. POMJAKUSHIN, H. LUETKENS, S. KATRYCH, A. WISNIEWSKI, R. KHASANOV, AND H. KELLER
Anisotropic superconducting properties of single-crystalline $\text{FeSe}_{0.5}\text{Te}_{0.5}$
Physical Review B **81**, 224520 (2010).
Group(s): Karpinski, Keller, Kenzelmann / Project(s): 4
- M. BENDELE, P. BABKEVICH, S. KATRYCH, S. N. GVASALIYA, E. POMJAKUSHINA, K. CONDER, B. ROESSLI, A. T. BOOTHROYD, R. KHASANOV, AND H. KELLER
Tuning the superconducting and magnetic properties of $\text{Fe}_y\text{Se}_{0.25}\text{Te}_{0.75}$ by varying the iron content
Physical Review B **82**, 212504 (2010).
Group(s): Karpinski, Keller, Kenzelmann / Project(s): 4
- T. MERTELJ, P. KUSAR, V. V. KABANOV, L. STOJCHEVSKA, N. D. ZHIGADLO, S. KATRYCH, Z. BUKOWSKI, J. KARPINSKI, S. WEYENETH, AND D. MIHAJLOVIC
Quasiparticle relaxation dynamics in spin-density-wave and superconducting $\text{SmFeAsO}_{1-x}\text{F}_x$ single crystals
Physical Review B **81**, 224504 (2010).
Group(s): Karpinski / Project(s): 4
- M. MATUSIAK, Z. BUKOWSKI, AND J. KARPINSKI
Nernst effect in single crystals of the pnictide superconductor $\text{CaFe}_{1.92}\text{Co}_{0.08}\text{As}_2$ and parent compound CaFe_2As_2
Physical Review B **81**, 020510(R) (2010).
Group(s): Karpinski / Project(s): 4
- N. D. ZHIGADLO, S. KATRYCH, J. KARPINSKI, B. BATLOGG, F. BERNARDINI, S. MASSIDDA, AND R. PUZNIAK
Influence of Mg deficiency on crystal structure and superconducting properties in MgB_2 single crystals
Physical Review B **81**, 054520 (2010).
Group(s): Batlogg, Karpinski / Project(s): 4
- A. BELOUSOV, J. KARPINSKI, AND B. BATLOGG
Thermodynamics of the Al-Ga-N_2 system
Journal of Crystal Growth **312**, 2579 (2010).
Group(s): Batlogg, Karpinski / Project(s): 4
- A. BELOUSOV, S. KATRYCH, K. HAMETNER, D. GÜNTHER, J. KARPINSKI, AND B. BATLOGG
 $\text{Al}_x\text{Ga}_{1-x}\text{N}$ bulk crystal growth: Crystallographic properties and $p - T$ phase diagram
Journal of Crystal Growth **312**, 2585 (2010).
Group(s): Batlogg, Karpinski / Project(s): 4
- M. MATUSIAK, K. ROGACKI, N. D. ZHIGADLO, AND J. KARPINSKI
Influence of carbon on intraband scattering in $\text{Mg}(\text{B}_{1-x}\text{C}_x)_2$
Europhysics Letters **90**, 27009 (2010).
Group(s): Karpinski / Project(s): 4
- S. WEYENETH, P. J. W. MOLL, R. PUZNIAK, K. NINIOS, F. F. BALAKIREV, R. D. McDONALD, H. B. CHAN, N. D. ZHIGADLO, S. KATRYCH, Z. BUKOWSKI, J. KARPINSKI, H. KELLER, B. BATLOGG, AND L. BALICAS
Rearrangement of the antiferromagnetic ordering at high magnetic fields in SmFeAsO and $\text{SmFeAsO}_{0.9}\text{F}_{0.1}$ single crystals
to be published in Physical Review B (2011).
Group(s): Batlogg, Karpinski, Keller / Project(s): 4
- T. MERTELJ, P. KUSAR, L. STOJCHEVSKA, V. V.

KABANOV, N. D. ZHIGADLO, S. KATRYCH,
J. KARPINSKI, AND D. MIHAILOVIC

*Doping Dependent Quasiparticle Relaxation
Dynamics in SmFeAsO_{1-x}F_x Single Crystals:
Comparison of Spin-Density Wave and Super-
conducting States*

Journal of Superconductivity and Novel Mag-
netism (2010).

Group(s): Karpinski / Project(s): 4

T. NISHIO, R. B. G. KRAMER, V. H. DAO, L. F.
CHIBOTARU, N. D. ZHIGADLO, J. KARPINSKI,
K. KADOWAKI, AND V. V. MOSHCHALOV

*Inhomogeneity of initial flux penetration in
MgB₂ single crystals*

Physica C **470**, S932 (2010).

Group(s): Karpinski / Project(s): 4

A. RICCI, N. POCCIA, B. JOSEPH, L. BARBA,
G. ARRIGHETTI, G. CIASCA, J.-Q. YAN, R. W.
MCCALLUM, T. A. LOGRASSO, N. D. ZHI-
GADLO, J. KARPINSKI, AND A. BIANCONI

*Structural phase transition and superlattice
misfit strain of RFeAsO (R=La, Pr, Nd, Sm)*

Physical Review B **82**, 144507 (2010).

Group(s): Karpinski / Project(s): 4

M. EISTERER, M. ZEHETMAYER, H. W. WE-
BER, J. JIANG, J. D. WEISS, A. YAMAMOTO,
E. E. HELLSTROM, D. C. LARBALESTIER, N. D.
ZHIGADLO, AND J. KARPINSKI

*Disorder effects and current percolation in
FeAs-based superconductors*

Superconductor Science & Technology **23**,
054006 (2010).

Group(s): Karpinski / Project(s): 4

M. LE TACON, T. R. FORREST, C. RÜEGG,
A. BOSAK, J. NOFFSINGER, A. C. WALTERS,
P. TOULEMONDE, A. PALENZONA, N. D. ZHI-
GADLO, J. KARPINSKI, J. P. HILL, M. KRISCH,
AND D. F. MCMORROW

*Inelastic X-ray scattering investigations of lat-
tice dynamics in SmFeAsO_{1-x}F_y superconduc-
tors*

Journal of the Physics and Chemistry of Solids
(2010), doi:10.1016/j.jpics.2010.10.006.

Group(s): Karpinski / Project(s): 4

M. WÄLLE, J. KOCH, D. TABERSKY,
K. HAMETNER, N. D. ZHIGADLO, S. KA-
TRYCH, J. KARPINSKI, AND D. GÜNTHER

*Analyses of lithium-doped and pure magnesium
diboride using ultraviolet nano- and femtosec-
ond laser ablation inductively coupled plasma
mass spectrometry*

Journal of Analytical Atomic Spectrometry **25**,
193 (2010).

Group(s): Karpinski / Project(s): 4

Z. BUKOWSKI, S. WEYENETH, R. PUZNIAK,
J. KARPINSKI, AND B. BATLOGG

*Bulk Superconductivity at 2.6 K in undoped
RbFe₂As₂*

Physica C **470**, S328 (2010).

Group(s): Karpinski / Project(s): 4

M. CISZEK, K. ROGACKI, K. OGANISIAN,
N. D. ZHIGADLO, AND J. KARPINSKI

*Influence of the carbon substitution on the criti-
cal current density and AC losses in MgB₂ sin-
gle crystals*

The European Physical Journal B **78**, 359
(2010).

Group(s): Karpinski / Project(s): 4

Z. SHERMADINI, J. KANTER, C. BAINES,
M. BENDELE, Z. BUKOWSKI, R. KHASANOV,
H.-H. KLAUSS, H. LUETKENS, H. MAETER,
G. PASCUA, B. BATLOGG, AND A. AMATO

*Microscopic study of the superconducting state
of the iron pnictide RbFe₂As₂ via muon spin ro-
tation*

Physical Review B **82**, 144527 (2010).

Group(s): Batlogg, Karpinski, Keller / Project(s): 4

A. ALFONSOV, F. MURÁNYI, V. KATAEV,
G. LANG, N. LEPS, L. WANG, R. KLINGELER,
A. KONDRAT, C. HESS, S. WURMEHL,
A. KÖHLER, G. BEHR, S. HAMPPEL,
M. DEUTSCHMANN, S. KATRYCH, N. D.
ZHIGADLO, Z. BUKOWSKI, J. KARPINSKI,
AND B. BÜCHNER

*High-field electron spin resonance spectroscopy
study of GdFeAsO_{1-x}F_x superconductors*

Physical Review B **83**, 094526 (2011).

Group(s): Karpinski / Project(s): 4

Group of H. Keller

► N. D. ZHIGADLO, S. KATRYCH,
S. WEYENETH, R. PUZNIAK, P. J. W. MOLL,
Z. BUKOWSKI, J. KARPINSKI, H. KELLER, AND
B. BATLOGG

*Th-substituted SmFeAsO: Structural details
and superconductivity with T_c above 50 K*

Physical Review B **82**, 064517 (2010).

Group(s): Batlogg, Karpinski, Keller / Project(s): 4

S. WEYENETH, P. J. W. MOLL, R. PUZNIAK,
K. NINIOS, F. F. BALAKIREV, R. D. MC-
DONALD, H. B. CHAN, N. D. ZHIGADLO,
S. KATRYCH, Z. BUKOWSKI, J. KARPINSKI,
H. KELLER, B. BATLOGG, AND L. BALICAS

*Rearrangement of the antiferromagnetic order-
ing at high magnetic fields in SmFeAsO and
SmFeAsO_{0.9}F_{0.1} single crystals*

to be published in Physical Review B (2011).

Group(s): Batlogg, Karpinski, Keller / Project(s): 4

Z. SHERMADINI, J. KANTER, C. BAINES, M. BENDELE, Z. BUKOWSKI, R. KHASANOV, H.-H. KLAUSS, H. LUETKENS, H. MAETER, G. PASCUA, B. BATLOGG, AND A. AMATO

Microscopic study of the superconducting state of the iron pnictide $RbFe_2As_2$ via muon spin rotation

Physical Review B **82**, 144527 (2010).

Group(s): Batlogg, Karpinski, Keller / Project(s): 4

- ▶ S. WEYENETH, M. BENDELE, R. PUZNIAK, F. MURÁNYI, A. BUSSMANN-HOLDER, N. D. ZHIGADLO, S. KATRYCH, Z. BUKOWSKI, J. KARPINSKI, A. SHENGE-LAYA, R. KHASANOV, AND H. KELLER

Field-dependent superfluid density in the optimally doped $SmFeAsO_{1-x}F_y$ superconductor

Europhysics Letters **91**, 47005 (2010).

Group(s): Karpinski, Keller / Project(s): 4

- ▶ T. KONDO, R. KHASANOV, J. KARPINSKI, S. KAZAKOV, N. ZHIGADLO, Z. BUKOWSKI, M. SHI, A. BENDOUNAN, Y. SASSA, J. CHANG, S. PAILHÉS, J. MESOT, J. SCHMALIAN, H. KELLER, AND A. KAMINSKI

Anomalies in the Fermi Surface and Band Dispersion of Quasi-One-Dimensional CuO Chains in the High-Temperature Superconductor $YBa_2Cu_4O_8$

Physical Review Letters **105**, 267003 (2010).

Group(s): Karpinski, Keller / Project(s): 4

- ▶ M. BENDELE, S. WEYENETH, R. PUZNIAK, A. MAISURADZE, E. POMJAKUSHINA, K. CONDER, V. POMJAKUSHIN, H. LUETKENS, S. KATRYCH, A. WISNIEWSKI, R. KHASANOV, AND H. KELLER

Anisotropic superconducting properties of single-crystalline $FeSe_{0.5}Te_{0.5}$

Physical Review B **81**, 224520 (2010).

Group(s): Karpinski, Keller, Kenzelmann / Project(s): 4

- ▶ M. BENDELE, P. BABKEVICH, S. KATRYCH, S. N. GVASALIYA, E. POMJAKUSHINA, K. CONDER, B. ROESSLI, A. T. BOOTHROYD, R. KHASANOV, AND H. KELLER

Tuning the superconducting and magnetic properties of $Fe_ySe_{0.25}Te_{0.75}$ by varying the iron content

Physical Review B **82**, 212504 (2010).

Group(s): Karpinski, Keller, Kenzelmann / Project(s): 4

- ▶ R. KHASANOV, M. BENDELE, K. CONDER, H. KELLER, E. POMJAKUSHINA, AND V. POMJAKUSHIN

Iron isotope effect on the superconducting transition temperature and the crystal structure of $FeSe_{1-x}$

New Journal of Physics **12**, 073024 (2010).

Group(s): Keller / Project(s): 4

- ▶ R. KHASANOV, M. BENDELE, A. AMATO, K. CONDER, H. KELLER, H.-H. KLAUSS, H. LUETKENS, AND E. POMJAKUSHINA

Evolution of Two-Gap Behavior of the Superconductor $FeSe_{1-x}$

Physical Review Letters **104**, 087004 (2010).

Group(s): Keller / Project(s): 4

- ▶ R. KHASANOV, M. BENDELE, A. BUSSMANN-HOLDER, AND H. KELLER

Intrinsic and structural isotope effects in iron-based superconductors

Physical Review B **82**, 212505 (2010).

Group(s): Keller / Project(s): 4

- ▶ A. BUSSMANN-HOLDER, A. SIMON, H. KELLER, AND A. R. BISHOP

Identifying the Pairing Mechanism in Fe-As Based Superconductors: Gaps and Isotope Effects

Journal of Superconductivity and Novel Magnetism (2010), doi:10.1007/s10948-010-0864-z.

Group(s): Keller / Project(s): 4

- ▶ A. BUSSMANN-HOLDER, H. KELLER, J. MUSTRE DE LEON, A. SIMON, A. BISHOP, AND K. A. MÜLLER

Testing Polaron Coherence and the Pairing Symmetry in Cuprate Superconductors by Local Probe Methods

Journal of Superconductivity and Novel Magnetism **23**, 295 (2010).

Group(s): Keller / Project(s): 4

P. BABKEVICH, M. BENDELE, A. T. BOOTHROYD, K. CONDER, S. N. GVASALIYA, R. KHASANOV, E. POMJAKUSHINA, AND B. ROESSLI

Magnetic excitations of $Fe_{1+y}Se_xTe_{1-x}$ in magnetic and superconductive phases

Journal of Physics: Condensed Matter **22**, 142202 (2010).

Group(s): Keller / Project(s): 4

R. KHASANOV, T. KONDO, M. BENDELE, Y. HAMAYA, A. KAMINSKI, S. L. LEE, S. J. RAY, AND T. TAKEUCHI

Suppression of the antinodal coherence of superconducting $(Bi,Pb)_2(Sr,La)_2CuO_{6+\delta}$ as revealed by muon spin rotation and angle-resolved photoemission

Physical Review B **82**, 020511(R) (2010).

Group(s): Keller / Project(s): 4

R. KHASANOV, A. SHENGE-LAYA, I. SAVIĆ, C. BAINES, AND H. KELLER

Comment on "Muon-spin-rotation study of the superconducting properties of Mo_3Sb_7 "

Physical Review B **82**, 016501 (2010).

Group(s): Keller / Project(s): 4

A. BUSSMANN-HOLDER AND H. KELLER
Comment on "Isotope Effect in Multi-Band and Multi-Channel Attractive Systems and Inverse Isotope Effect in Iron-Based Superconductors"

Journal of the Physical Society of Japan **79**, 126001 (2010).

Group(s): Keller / Project(s): 4

H. KELLER AND A. BUSSMANN-HOLDER
Local Electron-Lattice Interactions in High-Temperature Cuprate Superconductors

Advances in Condensed Matter Physics **2010**, 393526 (2010).

Group(s): Keller / Project(s): 4

- ▶ M. BENDELE, A. AMATO, K. CONDER, M. ELENDE, H. KELLER, H.-H. KLAUSS, H. LUETKENS, E. POMJAKUSHINA, A. RASELLI, AND R. KHASANOV
Pressure Induced Static Magnetic Order in Superconducting $FeSe_{1-x}$

Physical Review Letters **104**, 087003 (2010).

Group(s): Keller, Kenzelmann / Project(s): 4

Group of M. Kenzelmann

- ▶ M. BENDELE, A. AMATO, K. CONDER, M. ELENDE, H. KELLER, H.-H. KLAUSS, H. LUETKENS, E. POMJAKUSHINA, A. RASELLI, AND R. KHASANOV
Pressure Induced Static Magnetic Order in Superconducting $FeSe_{1-x}$

Physical Review Letters **104**, 087003 (2010).

Group(s): Keller, Kenzelmann / Project(s): 4

- ▶ M. BENDELE, S. WEYENETH, R. PUZNIAK, A. MAISURADZE, E. POMJAKUSHINA, K. CONDER, V. POMJAKUSHIN, H. LUETKENS, S. KATRYCH, A. WISNIEWSKI, R. KHASANOV, AND H. KELLER
Anisotropic superconducting properties of single-crystalline $FeSe_{0.5}Te_{0.5}$

Physical Review B **81**, 224520 (2010).

Group(s): Karpinski, Keller, Kenzelmann / Project(s): 4

- ▶ M. BENDELE, P. BABKEVICH, S. KATRYCH, S. N. GVASALIYA, E. POMJAKUSHINA, K. CONDER, B. ROESSLI, A. T. BOOTHROYD, R. KHASANOV, AND H. KELLER
Tuning the superconducting and magnetic properties of $Fe_ySe_{0.25}Te_{0.75}$ by varying the iron content

Physical Review B **82**, 212504 (2010).

Group(s): Karpinski, Keller, Kenzelmann / Project(s): 4

- ▶ A. KRZTON-MAZIOPA, Z. SHERMADINI, E. POMJAKUSHINA, V. POMJAKUSHIN, M. BENDELE, A. AMATO, R. KHASANOV, H. LUETKENS, AND K. CONDER
Synthesis and crystal growth of $Cs_{0.8}(FeSe_{0.98})_2$: a new iron-based superconductor with $T_c = 27$ K

Journal of Physics: Condensed Matter **23**, 052203 (2011).

Group(s): Kenzelmann / Project(s): 4, 5

- ▶ F. CASOLA, T. SHIROKA, S. WANG, K. CONDER, E. POMJAKUSHINA, J. MESOT, AND H.-R. OTT
Direct Observation of Impurity-Induced Magnetism in a Spin- $\frac{1}{2}$ Antiferromagnetic Heisenberg Two-Leg Spin Ladder

Physical Review Letters **105**, 067203 (2010).

Group(s): Kenzelmann, Mesot, Ott, Rønnow / Project(s): 6

- ▶ M. KENZELMANN, S. GERBER, N. EGETENMEYER, J. L. GAVILANO, T. STRÄSSLE, A. D. BIANCHI, E. RESSOUCHE, R. MOVSHOVICH, E. D. BAUER, J. L. SARRAO, AND J. D. THOMPSON
Evidence for a Magnetically Driven Superconducting Q Phase of $CeCoIn_5$

Physical Review Letters **104**, 127001 (2010).

Group(s): Kenzelmann / Project(s): 5

- P. BABKEVICH, M. BENDELE, A. T. BOOTHROYD, K. CONDER, S. N. GVASALIYA, R. KHASANOV, E. POMJAKUSHINA, AND B. ROESSLI
Magnetic excitations of $Fe_{1+y}Se_xTe_{1-x}$ in magnetic and superconductive phases

Journal of Physics: Condensed Matter **22**, 142202 (2010).

Group(s): Kenzelmann / Project(s): 5

- N. TSYRULIN, F. XIAO, A. SCHNEIDEWIND, P. LINK, H. M. RØNNOW, J. GAVILANO, C. P. LANDEE, M. M. TURNBULL, AND M. KENZELMANN
Two-dimensional square-lattice $S = \frac{1}{2}$ antiferromagnet $Cu(pz)_2(ClO_4)_2$

Physical Review B **81**, 134409 (2010).

Group(s): Kenzelmann, Rønnow / Project(s): 6

Group of D. van de Marel

- ▶ M. GUARISE, B. DALLA PIAZZA, M. MORETTI SALA, G. GHIRINGHELLI, L. BRAICOVICH, H. BERGER, J. N. HANCOCK, D. VAN DER MAREL, T. SCHMITT, V. N. STROCOV, L. J. P. AMENT, J. VAN DEN BRINK, P.-H. LIN, P. XU, H. M. RØNNOW, AND M. GRIONI

Measurement of Magnetic Excitations in the Two-Dimensional Antiferromagnetic Sr₂CuO₂Cl₂ Insulator Using Resonant X-Ray Scattering: Evidence for Extended Interactions

Physical Review Letters **105**, 157006 (2010).

Group(s): Forró, Grioni, Rønnow, van der Marel / Project(s): 6, 7

- ▶ I. CRASSEE, J. LEVALLOIS, A. L. WALTER, M. OSTLER, A. BOSTWICK, E. ROTENBERG, T. SEYLLER, D. VAN DER MAREL, AND A. B. KUZMENKO

Giant Faraday rotation in single- and multi-layer graphene

Nature Physics **7**, 48 (2011).

Group(s): van der Marel / Project(s): 2, 5

- ▶ D. N. BASOV, R. D. AVERITT, D. VAN DER MAREL, M. DRESSEL, AND K. HAULE

Electrodynamics of Correlated Electron Materials

to be published in Reviews of Modern Physics (2011).

Group(s): van der Marel / Project(s): 2, 4, 5

- ▶ J. TEYSSIER, E. GIANNINI, V. GURITANU, R. VIENNOIS, D. VAN DER MAREL, A. AMATO, AND S. N. GVASALIYA

Spin-glass ground state in Mn_{1-x}Co_xSi

Physical Review B **82**, 064417 (2010).

Group(s): Giannini, van der Marel / Project(s): 5

- ▶ J. N. HANCOCK, S. I. MIRZAEI, J. GILLET, S. E. SEBASTIAN, J. TEYSSIER, R. VIENNOIS, E. GIANNINI, AND D. VAN DER MAREL

Strong coupling to magnetic fluctuations in the charge dynamics of iron-based superconductors

Physical Review B **82**, 014523 (2010).

Group(s): van der Marel, Giannini / Project(s): 4

- ▶ N. P. ARMITAGE, R. TEDIOSI, F. LÉVY, E. GIANNINI, L. FORRÓ, AND D. VAN DER MAREL

Infrared Conductivity of Elemental Bismuth under Pressure: Evidence for an Avoided Lifshitz-Type Semimetal-Semiconductor Transition

Physical Review Letters **104**, 237401 (2010).

Group(s): Forró, Giannini, van der Marel / Project(s): 4

- ▶ J. N. HANCOCK, R. VIENNOIS, D. VAN DER MAREL, H. M. RØNNOW, M. GUARISE, P.-H. LIN, M. GRIONI, M. MORETTI SALA, G. GHIRINGHELLI, V. N. STROCOV, J. SCHLAPPA, AND T. SCHMITT

Evidence for core-hole-mediated inelastic x-ray scattering from metallic Fe_{1.087}Te

Physical Review B **82**, 020513(R) (2010).

Group(s): Grioni, Rønnow, van der Marel / Project(s): 4, 6

- ▶ E. VAN HEUMEN, Y. HUANG, S. DE JONG,

A. B. KUZMENKO, M. S. GOLDEN, AND D. VAN DER MAREL

Optical properties of BaFe_{2-x}Co_xAs₂

Europhysics Letters **90**, 37005 (2010).

Group(s): van der Marel / Project(s): 4

A. UBALDINI, E. GIANNINI, C. SENATORE, AND D. VAN DER MAREL

BiOCuS: A new superconducting compound with oxypnictide-related structure

Physica C **470**, S356 (2010).

Group(s): Flükiger, Giannini, van der Marel / Project(s): 4

R. VIENNOIS, E. GIANNINI, D. VAN DER MAREL, AND R. ČERNÝ

Effect of Fe excess on structural, magnetic and superconducting properties of single-crystalline Fe_{1+x}Te_{1-y}Se_y

Journal of Solid State Chemistry **183**, 769 (2010).

Group(s): Giannini, van der Marel / Project(s): 4

R. VIENNOIS, E. GIANNINI, D. VAN DER MAREL, AND R. ČERNÝ

Phase diagram of single-crystalline tetragonal iron chalcogenides

Physica C **470**, S370 (2010).

Group(s): Giannini, van der Marel / Project(s): 4

J. T. DEVREESE, S. N. KLIMIN, J. L. M. VAN MECHELEN, AND D. VAN DER MAREL

Many-body large polaron optical conductivity in SrTi_{1-x}Nb_xO₃

Physical Review B **81**, 125119 (2010).

Group(s): van der Marel / Project(s): 4, 5

Group of J. Mesot

- ▶ F. CASOLA, T. SHIROKA, S. WANG, K. CONDER, E. POMJAKUSHINA, J. MESOT, AND H.-R. OTT

Direct Observation of Impurity-Induced Magnetism in a Spin- $\frac{1}{2}$ Antiferromagnetic Heisenberg Two-Leg Spin Ladder

Physical Review Letters **105**, 067203 (2010).

Group(s): Kenzelmann, Mesot, Ott, Rønnow / Project(s): 6

- ▶ S. WANG, E. POMJAKUSHINA, T. SHIROKA, G. DENG, N. NIKSERESHT, C. RÜEGG, H. M. RØNNOW, AND K. CONDER

Crystal growth and characterization of the dilutable frustrated spin-ladder compound Bi(Cu_{1-x}Zn_x)₂PO₆

Journal of Crystal Growth **313**, 51 (2010).

Group(s): Mesot, Ott, Rønnow / Project(s): 6

Group of F. Mila

- ▶ B. GEORGEOT AND F. MILA
Chirality of Triangular Antiferromagnetic Clusters as a Qubit
Physical Review Letters **104**, 200502 (2010).
Group(s): Mila / Project(s): 6
 - ▶ T. A. TÓTH, A. M. LÄUCHLI, F. MILA, AND K. PENC
Three-Sublattice Ordering of the SU(3) Heisenberg Model of Three-Flavor Fermions on the Square and Cubic Lattices
Physical Review Letters **105**, 265301 (2010).
Group(s): Mila / Project(s): 6, 8
 - ▶ H.-Y. YANG, A. M. LÄUCHLI, F. MILA, AND K. P. SCHMIDT
Effective Spin Model for the Spin-Liquid Phase of the Hubbard Model on the Triangular Lattice
Physical Review Letters **105**, 267204 (2010).
Group(s): Mila / Project(s): 6
 - ▶ T. COLETTA, J.-D. PICON, S. KORSHUNOV, AND F. MILA
Phase diagram of the fully frustrated transverse-field Ising model on the honeycomb lattice
Physical Review B **83**, 054402 (2011).
Group(s): Mila / Project(s): 6
 - M. BELESI, I. ROUSOCHATZAKIS, H. C. WU, H. BERGER, I. V. SHVETS, F. MILA, AND J. P. ANSERMET
Ferrimagnetism of the magnetoelectric compound Cu_2OSeO_3 probed by ^{77}Se NMR
Physical Review B **82**, 094422 (2010).
Group(s): Forró, Mila / Project(s): 6
 - S. A. ZVYAGIN, E. ČIŽMAR, M. OZEROV, J. WOSNITZA, R. FEYERHERM, S. MANMANA, AND F. MILA
Field-Induced Gap in a Quantum Spin- $\frac{1}{2}$ Chain in a Strong Magnetic Field
Physical Review B **83**, 060409(R) (2011).
Group(s): Mila / Project(s): 6
 - C. LACROIX, P. MENDELS, AND F. MILA
Introduction to Frustrated Magnetism, vol. 164 of *Springer Series in Solid-State Sciences* (Springer, Berlin, 2011).
Group(s): Mila / Project(s): 6
- Group of E. Morenzoni**
- ▶ L. SCHULZ, L. NUCCIO, M. WILLIS, P. DESAI, P. SHAKYA, T. KREOUZIS, V. K. MALIK, C. BERNHARD, F. L. PRATT, N. A. MORLEY, A. SUTER, G. J. NIEUWENHUYS,

T. PROKSCHA, E. MORENZONI, W. P. GILLIN, AND A. J. DREW

Engineering spin propagation across a hybrid organic/inorganic interface using a polar layer

Nature Materials **10**, 39 (2011).

Group(s): Bernhard, Morenzoni / Project(s): 1

- ▶ S. R. DUNSIGER, J. P. CARLO, T. GOKO, G. NIEUWENHUYS, T. PROKSCHA, A. SUTER, E. MORENZONI, D. CHIBA, Y. NISHITANI, T. TANIKAWA, F. MATSUKURA, H. OHNO, J. OHE, S. MAEKAWA, AND Y. J. UEMURA

Spatially homogeneous ferromagnetism of (Ga,Mn)As

Nature Materials **9**, 299 (2010).

Group(s): Morenzoni / Project(s): 1

R. F. KIEFL, M. D. HOSSAIN, B. M. WOJEK, S. R. DUNSIGER, G. D. MORRIS, T. PROKSCHA, Z. SALMAN, J. BAGLO, D. A. BONN, R. LIANG, W. N. HARDY, A. SUTER, AND E. MORENZONI

Direct measurement of the London penetration depth in $\text{YBa}_2\text{Cu}_3\text{O}_{6.92}$ using low-energy μSR

Physical Review B **81**, 180502(R) (2010).

Group(s): Morenzoni / Project(s): 4

V. G. STORCHAK, D. G. ESHCHENKO, E. MORENZONI, N. INGLE, W. HEISS, T. SCHWARZL, G. SPRINGHOLZ, R. L. KALLAHER, AND S. VON MOLNÁR

Magnetic polarons in Eu-based films of magnetic semiconductors

Physical Review B **81**, 153201 (2010).

Group(s): Morenzoni / Project(s): 5

Group of A. Morpurgo

- ▶ J. LI, I. MARTIN, M. BÜTTIKER, AND A. F. MORPURGO
Topological origin of subgap conductance in insulating bilayer graphene
Nature Physics **7**, 38 (2011).
Group(s): Büttiker, Morpurgo / Project(s): 2
- ▶ J. LI, A. F. MORPURGO, M. BÜTTIKER, AND I. MARTIN
Marginality of bulk-edge correspondence for single-valley Hamiltonians
Physical Review B **82**, 245404 (2010).
Group(s): Büttiker, Morpurgo / Project(s): 2
- ▶ R. DANNEAU, F. WU, M. Y. TOMI, J. B. OOSTINGA, A. F. MORPURGO, AND P. J. HAKONEN
Shot noise suppression and hopping conduction in graphene nanoribbons
Physical Review B **82**, 161405(R) (2010).
Group(s): Morpurgo / Project(s): 2

- ▶ S. ONO, N. MINDER, Z. CHEN, A. FACCHETTI, AND A. F. MORPURGO
High-performance n-type organic field-effect transistors with ionic liquid gates
Applied Physics Letters **97**, 143307 (2010).
Group(s): Morpurgo / Project(s): 2
- ▶ M. NAKANO, H. ALVES, A. S. MOLINARI, S. ONO, N. MINDER, AND A. F. MORPURGO
Small gap semiconducting organic charge-transfer interfaces
Applied Physics Letters **96**, 232102 (2010).
Group(s): Morpurgo / Project(s): 1
- ▶ J. B. OOSTINGA, B. SACÉPÉ, M. F. CRACIUN, AND A. F. MORPURGO
Magnetotransport through graphene nanoribbons
Physical Review B **81**, 193408 (2010).
Group(s): Morpurgo / Project(s): 2
- ▶ A. D. CAVIGLIA, S. GARIGLIO, C. CANCELLIERI, B. SACÉPÉ, A. FÊTE, N. REYREN, M. GABAY, A. F. MORPURGO, AND J.-M. TRISCONE
Two-Dimensional Quantum Oscillations of the Conductance at LaAlO₃/SrTiO₃ Interfaces
Physical Review Letters **105**, 236802 (2010).
Group(s): Morpurgo, Triscone / Project(s): 1, 2
- I. HELLER, S. CHATOOR, J. MÄNNIK, M. A. G. ZEVENBERGEN, J. B. OOSTINGA, A. F. MORPURGO, C. DEKKER, AND S. G. LEMAY
Charge Noise in Graphene Transistors
Nano Letters **10**, 1563 (2010).
Group(s): Morpurgo / Project(s): 2
- S. RUSSO, M. F. CRACIUN, M. YAMAMOTO, A. F. MORPURGO, AND S. TARUCHA
Contact resistance in graphene-based devices
Physica E **42**, 677 (2010).
Group(s): Morpurgo / Project(s): 2
- R. SCHERWITZL, P. ZUBKO, I. GUTIERREZ LEZAMA, S. ONO, A. F. MORPURGO, G. CATALAN, AND J.-M. TRISCONE
Electric-Field Control of the Metal-Insulator Transition in Ultrathin NdNiO₃ Films
Advanced Materials **22**, 5517 (2010).
Group(s): Morpurgo, Triscone (JM) / Project(s): 1, 2
- Group of Ch. Niedermayer**
- ▶ P. MARSIK, K. W. KIM, A. DUBROKA, M. RÖSSLE, V. K. MALIK, L. SCHULZ, C. N. WANG, C. NIEDERMAYER, A. J. DREW, M. WILLIS, T. WOLF, AND C. BERNHARD
Coexistence and Competition of Magnetism and Superconductivity on the Nanometer Scale in Underdoped BaFe_{1.89}Co_{0.11}As₂
Physical Review Letters **105**, 057001 (2010).
Group(s): Bernhard, Niedermayer / Project(s): 1, 4
- ▶ E. BLACKBURN, P. DAS, M. R. ESKILDSEN, E. M. FORGAN, M. LAVER, C. NIEDERMAYER, C. PETROVIC, AND J. S. WHITE
Exploring the Fragile Antiferromagnetic Superconducting Phase in CeCoIn₅
Physical Review Letters **105**, 187001 (2010).
Group(s): Niedermayer / Project(s): 4
- ▶ C. W. SCHNEIDER, M. ESPOSITO, I. MAROZAU, K. CONDER, M. DOEBELI, Y. HU, M. MALLEPELL, A. WOKAUN, AND T. LIPPERT
The origin of oxygen in oxide thin films: Role of the substrate
Applied Physics Letters **97**, 192107 (2010).
Group(s): Niedermayer / Project(s): 1
- Group of H.-R. Ott**
- ▶ F. CASOLA, T. SHIROKA, S. WANG, K. CONDER, E. POMJAKUSHINA, J. MESOT, AND H.-R. OTT
Direct Observation of Impurity-Induced Magnetism in a Spin- $\frac{1}{2}$ Antiferromagnetic Heisenberg Two-Leg Spin Ladder
Physical Review Letters **105**, 067203 (2010).
Group(s): Kenzelmann, Mesot, Ott, Rønnow / Project(s): 6
- ▶ S. WANG, E. POMJAKUSHINA, T. SHIROKA, G. DENG, N. NIKSERESHT, C. RÜEGG, H. M. RØNNOW, AND K. CONDER
Crystal growth and characterization of the dilutable frustrated spin-ladder compound Bi(Cu_{1-x}Zn_x)₂PO₆
Journal of Crystal Growth **313**, 51 (2010).
Group(s): Mesot, Ott, Rønnow / Project(s): 6
- Group of P. Paruch**
- ▶ J. GUYONNET, H. BÉA, AND P. PARUCH
Lateral piezoelectric response across ferroelectric domain walls in thin films
Journal of Applied Physics **108**, 042002 (2010).
Group(s): Paruch / Project(s): 1
- H. BÉA, B. ZIEGLER, M. BIBES, A. BARTHÉLÉMY, AND P. PARUCH
Nanoscale polarization switching mechanisms in multiferroic BiFeO₃ thin films
Journal of Physics: Condensed Matter **23**, 142201 (2011).
Group(s): Paruch / Project(s): 1

Group of G. Patzke

- Y. ZHOU, K. ZHENG, J.-D. GRUNWALDT, T. FOX, L. GU, X. MO, G. CHEN, AND G. R. PATZKE

W/Mo-Oxide Nanomaterials: Structure-Property Relationships and Ammonia-Sensing Studies

The Journal of Physical Chemistry C **115**, 1134 (2011).

Group(s): Patzke / Project(s): 3

- F. CONRAD, Y. ZHOU, M. YULIKOV, K. HAMETNER, S. WEYENETH, G. JESCHKE, D. GÜNTHER, J.-D. GRUNWALDT, AND G. R. PATZKE

Microwave-Hydrothermal Synthesis of Nanostructured Zinc-Copper Gallates

European Journal of Inorganic Chemistry **2010**, 2036 (2010).

Group(s): Patzke / Project(s): 3

- Y. ZHOU, F. KRUMEICH, A. HEEL, AND G. R. PATZKE

One-step hydrothermal coating approach to photocatalytically active oxide composites

Dalton Transactions **39**, 6043 (2010).

Group(s): Patzke / Project(s): 3

- Y. ZHOU, J.-D. GRUNWALDT, F. KRUMEICH, K. ZHENG, G. CHEN, J. STÖTZEL, R. FRAHM, AND G. R. PATZKE

Hydrothermal Synthesis of Bi₆S₂O₁₅ Nanowires: Structural, in situ EXAFS and Humidity-Sensing Studies

Small **6**, 1173 (2010).

Group(s): Patzke / Project(s): 3

- K. ZHENG, Y. ZHOU, L. GU, X. MO, G. R. PATZKE, AND G. CHEN

Humidity sensors based on Aurivillius type Bi₂MO₆ (M = W, Mo) oxide films

Sensors and Actuators B: Chemical **148**, 240 (2010).

Group(s): Patzke / Project(s): 3

- Y. ZHOU, E. ANTONOVA, W. BENSCH, AND G. R. PATZKE

In situ X-ray diffraction study of the hydrothermal crystallization of hierarchical Bi₂WO₆ nanostructures

Nanoscale **2**, 2412 (2010).

Group(s): Patzke / Project(s): 3

- L. GU, K. ZHENG, Y. ZHOU, J. LI, X. MO, G. R. PATZKE, AND G. CHEN

Humidity sensors based on ZnO/TiO₂ core/shell nanorod arrays with enhanced sensitivity

Sensors and Actuators B: Chemical (2011),

doi:10.1016/j.snb.2010.12.024.

Group(s): Patzke / Project(s): 3

Group of Ch. Renner

- B. BRYANT, C. RENNER, Y. TOKUNAGA, Y. TOKURA, AND G. AEPPLI

Imaging oxygen defects and their motion at a manganite surface

Nature Communications **2**, 212 (2011).

Group(s): Renner / Project(s): 6

- J. S. MILNE, A. C. H. ROWE, S. ARSCOTT, AND C. RENNER

Giant Piezoresistance Effects in Silicon Nanowires and Microwires

Physical Review Letters **105**, 226802 (2010).

Group(s): Renner / Project(s): 3

- J. H. G. OWEN, F. BIANCO, S. A. KÖSTER, D. MAZUR, D. R. BOWLER, AND C. RENNER

One-dimensional Si-in-Si(001) template for single-atom wire growth

Applied Physics Letters **97**, 093102 (2010).

Group(s): Renner / Project(s): 7

- J. JAVORSKÝ, J. H. G. OWEN, M. SETVÍN, AND K. MIKI

Electronic structure of Bi lines on clean and H-passivated Si(100)

Journal of Physics: Condensed Matter **22**, 175006 (2010).

Group(s): Renner / Project(s): 7

Group of T. M. Rice

- R. M. KONIK, T. M. RICE, AND A. M. TSVELIK
- Superconductivity generated by coupling to a cooperon in a two-dimensional array of four-leg Hubbard ladders*

Physical Review B **82**, 054501 (2010).

Group(s): Rice, Sigrist / Project(s): 4

- K.-Y. YANG, K. HUANG, W.-Q. CHEN, T. M. RICE, AND F.-C. ZHANG

Andreev and Single-Particle Tunneling Spectra of Underdoped Cuprate Superconductors

Physical Review Letters **105**, 167004 (2010).

Group(s): Rice, Sigrist / Project(s): 4

Group of N. de Rooij

- D. ISARAKORN, A. SAMBRI, P. JANPHUANG, D. BRIAND, S. GARIGLIO, J.-M. TRISCONNE, F. GUY, J. W. REINER, C. H. AHN, AND N. F. DE ROOIJ

Epitaxial piezoelectric MEMS on silicon

Journal of Micromechanics and Microengineering **20**, 055008 (2010).

Group(s): de Rooij, Triscone (JM) / Project(s): 3

D. ISARAKORN, D. BRIAND, A. SAMBRI, S. GARIGLIO, J.-M. TRISCONI, F. GUY, J. W. REINER, C. H. AHN, AND N. F. DE ROOIJ

Finite element analysis and experiments on a silicon membrane actuated by an epitaxial PZT thin film for localized-mass sensing applications

Sensors and Actuators B: Chemical **153**, 54 (2010).

Group(s): de Rooij, Triscone (JM) / Project(s): 3

D. ISARAKORN, D. BRIAND, P. JANPHUANG, A. SAMBRI, S. GARIGLIO, J.-M. TRISCONI, F. GUY, J. W. REINER, C. H. AHN, AND N. F. DE ROOIJ

The realization and performance of vibration energy harvesting MEMS devices based on an epitaxial piezoelectric thin film

Smart Materials and Structures **20**, 025015 (2011).

Group(s): de Rooij, Triscone (JM) / Project(s): 3

D. ISARAKORN, M. LINDER, D. BRIAND, AND N. F. DE ROOIJ

Evaluation of static measurement in piezoelectric cantilever sensors using a charge integration technique for chemical and biological detection

Measurement Science & Technology **21**, 075801 (2010).

Group(s): de Rooij / Project(s): 3

Group of H. M. Rønnow

- ▶ F. CASOLA, T. SHIROKA, S. WANG, K. CONDER, E. POMJAKUSHINA, J. MESOT, AND H.-R. OTT

Direct Observation of Impurity-Induced Magnetism in a Spin- $\frac{1}{2}$ Antiferromagnetic Heisenberg Two-Leg Spin Ladder

Physical Review Letters **105**, 067203 (2010).

Group(s): Kenzelmann, Mesot, Ott, Rønnow / Project(s): 6

- ▶ S. WANG, E. POMJAKUSHINA, T. SHIROKA, G. DENG, N. NIKSERESHT, C. RÜEGG, H. M. RØNNOW, AND K. CONDER

Crystal growth and characterization of the dilutable frustrated spin-ladder compound $\text{Bi}(\text{Cu}_{1-x}\text{Zn}_x)_2\text{PO}_6$

Journal of Crystal Growth **313**, 51 (2010).

Group(s): Mesot, Ott, Rønnow / Project(s): 6

- ▶ M. GUARISE, B. DALLA PIAZZA, M. MORETTI SALA, G. GHIRINGHELLI, L. BRAICOVICH, H. BERGER, J. N. HANCOCK,

D. VAN DER MAREL, T. SCHMITT, V. N. STROCOV, L. J. P. AMENT, J. VAN DEN BRINK, P.-H. LIN, P. XU, H. M. RØNNOW, AND M. GRIONI

Measurement of Magnetic Excitations in the Two-Dimensional Antiferromagnetic $\text{Sr}_2\text{CuO}_2\text{Cl}_2$ Insulator Using Resonant X-Ray Scattering: Evidence for Extended Interactions

Physical Review Letters **105**, 157006 (2010).

Group(s): Forró, Grioni, Rønnow, van der Marel / Project(s): 6, 7

- ▶ P. XU, J. O. PIATEK, P.-H. LIN, B. SIPOS, H. BERGER, L. FORRÓ, H. M. RØNNOW, AND M. GRIONI

Superconducting phase in the layered dichalcogenide 1T-TaS_2 upon inhibition of the metal-insulator transition

Physical Review B **81**, 172503 (2010).

Group(s): Forró, Grioni, Rønnow / Project(s): 7

- ▶ J. N. HANCOCK, R. VIENNOIS, D. VAN DER MAREL, H. M. RØNNOW, M. GUARISE, P.-H. LIN, M. GRIONI, M. MORETTI SALA, G. GHIRINGHELLI, V. N. STROCOV, J. SCHLAPPA, AND T. SCHMITT

Evidence for core-hole-mediated inelastic x-ray scattering from metallic $\text{Fe}_{1.087}\text{Te}$

Physical Review B **82**, 020513(R) (2010).

Group(s): Grioni, Rønnow, van der Marel / Project(s): 4, 6

N. TSYRULIN, F. XIAO, A. SCHNEIDEWIND, P. LINK, H. M. RØNNOW, J. GAVILANO, C. P. LANDEE, M. M. TURNBULL, AND M. KENZELMANN

Two-dimensional square-lattice $S = \frac{1}{2}$ antiferromagnet $\text{Cu}(\text{pz})_2(\text{ClO}_4)_2$

Physical Review B **81**, 134409 (2010).

Group(s): Kenzelmann, Rønnow / Project(s): 6

M. MOURIGAL, M. ENDERLE, R. K. KREMER, J. M. LAW, AND B. FAK

Ferroelectricity from spin supercurrents in LiCuVO_4

to be published in Physical Review B (2011).

Group(s): Rønnow / Project(s): 6

Group of M. Sigrist

- ▶ P. M. R. BRYDON, C. INIOTAKIS, D. MANSKE, AND M. SIGRIST

Functional Superconductor Interfaces from Broken Time-Reversal Symmetry

Physical Review Letters **104**, 197001 (2010).

Group(s): Sigrist / Project(s): 4

- ▶ F. HASSLER, A. RÜEGG, M. SIGRIST, AND G. BLATTER

Dynamical Unbinding Transition in a Periodically Driven Mott Insulator

- Physical Review Letters **104**, 220402 (2010).
Group(s): Blatter, Sigrist / Project(s): 8
- H. KANEYASU, N. HAYASHI, B. GUT, K. MAKOSHI, AND M. SIGRIST
Phase Transition in the 3-Kelvin Phase of Eutectic Sr_2RuO_4 -Ru
Journal of the Physical Society of Japan **79**, 104705 (2010).
Group(s): Sigrist / Project(s): 4
- R. M. KONIK, T. M. RICE, AND A. M. TSVELIK
Superconductivity generated by coupling to a cooperon in a two-dimensional array of four-leg Hubbard ladders
Physical Review B **82**, 054501 (2010).
Group(s): Rice, Sigrist / Project(s): 4
- K.-Y. YANG, K. HUANG, W.-Q. CHEN, T. M. RICE, AND F.-C. ZHANG
Andreev and Single-Particle Tunneling Spectra of Underdoped Cuprate Superconductors
Physical Review Letters **105**, 167004 (2010).
Group(s): Rice, Sigrist / Project(s): 4
- C. F. MICLEA, A. C. MOTA, M. NICKLAS, R. CARDOSO, F. STEGLICH, M. SIGRIST, A. PROKOFIEV, AND E. BAUER
Extreme vortex pinning in the noncentrosymmetric superconductor $CePt_3Si$
Physical Review B **81**, 014527 (2010).
Group(s): Sigrist / Project(s): 5
- A. BOUHON AND M. SIGRIST
Influence of the domain walls on the Josephson effect in Sr_2RuO_4
New Journal of Physics **12**, 043031 (2010).
Group(s): Sigrist / Project(s): 4
- M. H. FISCHER AND M. SIGRIST
Effect of a staggered spin-orbit coupling on the occurrence of a nematic phase in $Sr_3Ru_2O_7$
Physical Review B **81**, 064435 (2010).
Group(s): Sigrist / Project(s): 5
- A. RÜEGG, S. D. HUBER, AND M. SIGRIST
 Z_2 -slave-spin theory for strongly correlated fermions
Physical Review B **81**, 155118 (2010).
Group(s): Sigrist / Project(s): 5
- H. KANEYASU AND M. SIGRIST
Nucleation of Vortex State in Ru-Inclusion in Eutectic Ruthenium Oxide Sr_2RuO_4 -Ru
Journal of the Physical Society of Japan **79**, 053706 (2010).
Group(s): Sigrist / Project(s): 4
- M. H. FISCHER AND M. SIGRIST
Slave-boson mean-field study of the dimensional crossover in Sr_2RuO_4
Journal of Physics: Conference Series **200**, 012034 (2010).
Group(s): Sigrist / Project(s): 4
- K. WAKABAYASHI, Y. TAKANE, AND M. SIGRIST
Electronic transport properties and perfectly conducting channel of the disordered graphene nanoribbons
AIP Conference Proceedings **1199**, 539 (2010).
Group(s): Sigrist / Project(s): 2
- M. H. FISCHER AND M. SIGRIST
Effects of spin-orbit coupling on the metamagnetic transition in $Sr_3Ru_2O_7$
AIP Conference Proceedings **1297**, 412 (2010).
Group(s): Sigrist / Project(s): 5
- Y. YANASE AND M. SIGRIST
Magnetic structure of the antiferromagnetic Fulde-Ferrell-Larkin-Ovchinnikov state
Journal of Physics: Condensed Matter **23**, 094219 (2011).
Group(s): Sigrist / Project(s): 5
- Group of U. Staub**
- M. GARCÍA-FERNÁNDEZ, U. STAUB, Y. BODENTHIN, V. POMJAKUSHIN, A. MIRONE, J. FERNÁNDEZ-RODRÍGUEZ, V. SCAGNOLI, A. M. MULDEERS, S. M. LAWRENCE, AND E. POMJAKUSHINA
Doping and temperature dependence of Mn 3d states in A-site ordered manganites
Physical Review B **82**, 235108 (2010).
Group(s): Staub / Project(s): 6
- U. STAUB, Y. BODENTHIN, C. PIAMONTEZE, S. P. COLLINS, S. KOOHPAYEH, D. FORT, AND S. W. LOVESEY
Magnetoelectric effects studied by resonant x-ray diffraction in ferrimagnetic $GaFeO_3$
Physical Review B **82**, 104411 (2010).
Group(s): Staub / Project(s): 6
- Group of J.-M. Triscone**
- A. D. CAVIGLIA, S. GARIGLIO, C. CANCELLIERI, B. SACÉPÉ, A. FÊTE, N. REYREN, M. GABAY, A. F. MORPURGO, AND J.-M. TRISCONI
Two-Dimensional Quantum Oscillations of the Conductance at $LaAlO_3/SrTiO_3$ Interfaces
Physical Review Letters **105**, 236802 (2010).
Group(s): Morpurgo, Triscone (JM) / Project(s): 1, 2

- ▶ A. D. CAVIGLIA, M. GABAY, S. GARIGLIO, N. REYREN, C. CANCELLIERI, AND J.-M. TRISCONE
Tunable Rashba spin-orbit interaction at oxide interfaces
Physical Review Letters **104**, 126803 (2010).
Group(s): Triscone (JM) / Project(s): 1
- ▶ A. SAMBRI, S. GARIGLIO, A. TORRES PARDO, J.-M. TRISCONE, O. STÉPHAN, J. W. REINER, AND C. H. AHN
Enhanced critical temperature in epitaxial ferroelectric $Pb(Zr_{0.2}Ti_{0.8})O_3$ thin films on silicon
Applied Physics Letters **98**, 012903 (2011).
Group(s): Triscone (JM) / Project(s): 3
- ▶ P. ZUBKO, N. STUCKI, C. LICHTENSTEIGER, AND J.-M. TRISCONE
X-Ray Diffraction Studies of 180° Ferroelectric Domains in $PbTiO_3/SrTiO_3$ Superlattices under an Applied Electric Field
Physical Review Letters **104**, 187601 (2010).
Group(s): Triscone (JM) / Project(s): 1
- R. SCHERWITZL, P. ZUBKO, C. LICHTENSTEIGER, AND J.-M. TRISCONE
Electric-field tuning of the metal-insulator transition in ultrathin films of $LaNiO_3$
Applied Physics Letters **95**, 222114 (2009).
Group(s): Triscone (JM) / Project(s): 1
- J. GUYONNET, H. BÉA, F. GUY, S. GARIGLIO, S. FUSIL, K. BOUZEHOANE, J.-M. TRISCONE, AND P. PARUCH
Shear effects in lateral piezoresponse force microscopy at 180° ferroelectric domain walls
Applied Physics Letters **95**, 132902 (2009).
Group(s): Paruch, Triscone (JM) / Project(s): 1
- C. CANCELLIERI, N. REYREN, S. GARIGLIO, A. D. CAVIGLIA, A. FÊTE, AND J.-M. TRISCONE
Influence of the growth conditions on the $LaAlO_3/SrTiO_3$ interface electronic properties
Europhysics Letters **91**, 17004 (2010).
Group(s): Triscone (JM) / Project(s): 1
- D. ISARAKORN, A. SAMBRI, P. JANPHUANG, D. BRIAND, S. GARIGLIO, J.-M. TRISCONE, F. GUY, J. W. REINER, C. H. AHN, AND N. F. DE ROOIJ
Epitaxial piezoelectric MEMS on silicon
Journal of Micromechanics and Microengineering **20**, 055008 (2010).
Group(s): De Rooij, Triscone (JM) / Project(s): 3
- D. ISARAKORN, D. BRIAND, A. SAMBRI, S. GARIGLIO, J.-M. TRISCONE, F. GUY, J. W. REINER, C. H. AHN, AND N. F. DE ROOIJ
Finite element analysis and experiments on a silicon membrane actuated by an epitaxial PZT thin film for localized-mass sensing applications
Sensors and Actuators B: Chemical **153**, 54 (2010).
Group(s): De Rooij, Triscone (JM) / Project(s): 3
- D. ISARAKORN, D. BRIAND, P. JANPHUANG, A. SAMBRI, S. GARIGLIO, J.-M. TRISCONE, F. GUY, J. W. REINER, C. H. AHN, AND N. F. DE ROOIJ
The realization and performance of vibration energy harvesting MEMS devices based on an epitaxial piezoelectric thin film
Smart Materials and Structures **20**, 025015 (2011).
Group(s): De Rooij, Triscone (JM) / Project(s): 3
- Ø. NORDSETH, C. C. YOU, E. FOLVEN, S. GARIGLIO, A. SAMBRI, J.-M. TRISCONE, J. W. REINER, C. H. AHN, T. TYBELL, AND J. K. GREPSTAD
Growth and characterization of $(Pb,La)(Zr,Ti)O_3$ thin film epilayers on $SrTiO_3$ -buffered $Si(001)$
Thin Solid Films **518**, 5471 (2010).
Group(s): Triscone (JM) / Project(s): 3
- I. PALLECCHI, M. CODDA, E. GALLEANI D'AGLIANO, D. MARRÉ, A. D. CAVIGLIA, N. REYREN, S. GARIGLIO, AND J.-M. TRISCONE
Seebeck effect in the conducting $LaAlO_3/SrTiO_3$ interface
Physical Review B **81**, 085414 (2010).
Group(s): Triscone (JM) / Project(s): 1
- R. SCHERWITZL, P. ZUBKO, I. GUTIERREZ LEZAMA, S. ONO, A. F. MORPURGO, G. CATALAN, AND J.-M. TRISCONE
Electric-Field Control of the Metal-Insulator Transition in Ultrathin $NdNiO_3$ Films
Advanced Materials **22**, 5517 (2010).
Group(s): Morpurgo, Triscone (JM) / Project(s): 1, 2
- Group of M. Troyer**
- ▶ S. FUCHS, E. GULL, L. POLLET, E. BUROVSKI, E. KOZIK, T. PRUSCHKE, AND M. TROYER
Thermodynamics of the 3D Hubbard Model on Approaching the Néel Transition
Physical Review Letters **106**, 030401 (2011).
Group(s): Troyer / Project(s): 5, 8
- ▶ P. ANDERS, E. GULL, L. POLLET, M. TROYER, AND P. WERNER
Dynamical Mean Field Solution of the Bose-Hubbard Model

- Physical Review Letters **105**, 096402 (2010).
Group(s): Troyer / Project(s): 8
- ▶ S. PILATI, G. BERTAINA, S. GIORGINI, AND M. TROYER
Itinerant Ferromagnetism of a Repulsive Atomic Fermi Gas: A Quantum Monte Carlo Study
Physical Review Letters **105**, 030405 (2010).
Group(s): Troyer / Project(s): 8
 - ▶ L. POLLET, J. D. PICON, H. P. BÜCHLER, AND M. TROYER
Supersolid Phase with Cold Polar Molecules on a Triangular Lattice
Physical Review Letters **104**, 125302 (2010).
Group(s): Troyer / Project(s): 8
 - ▶ R. JÖRDENS, L. TARRUELL, D. GREIF, T. UEHLINGER, N. STROHMAIER, H. MORITZ, T. ESSLINGER, L. DE LEO, C. KOLLATH, A. GEORGES, V. SCAROLA, L. POLLET, E. BUROVSKI, E. KOZIK, AND M. TROYER
Quantitative Determination of Temperature in the Approach to Magnetic Order of Ultracold Fermions in an Optical Lattice
Physical Review Letters **104**, 180401 (2010).
Group(s): Esslinger, Troyer / Project(s): 8
 - ▶ E. KOZIK, K. VAN HOUCKE, E. GULL, L. POLLET, N. PROKOF'EV, B. SVISTUNOV, AND M. TROYER
Diagrammatic Monte Carlo for correlated fermions
Europhysics Letters **90**, 10004 (2010).
Group(s): Troyer / Project(s): 5,8
 - ▶ E. GULL, A. J. MILLIS, A. I. LICHTENSTEIN, A. N. RUBTSOV, M. TROYER, AND P. WERNER
Continuous-time Monte Carlo methods for quantum impurity models
to be published in *Reviews of Modern Physics* (2011).
Group(s): Troyer / Project(s): 5
 - ▶ B. BAUER, P. CORBOZ, R. ORÚS, AND M. TROYER
Implementing global Abelian symmetries in projected entangled-pair state algorithms
Physical Review B **83**, 125106 (2011).
Group(s): Troyer / Project(s): 6
 - ▶ S. TROTZKY, L. POLLET, F. GERBIER, U. SCHNORRBERGER, I. BLOCH, N. V. PROKOF'EV, B. SVISTUNOV, AND M. TROYER
Suppression of the critical temperature for superfluidity near the Mott transition
Nature Physics **6**, 998 (2010).
Group(s): Troyer / Project(s): 8
 - E. ARDONNE, J. GUKELBERGER, A. W. W. LUDWIG, S. TREBST, AND M. TROYER
Microscopic models of interacting Yang-Lee anyons
to be published in *New Journal of Physics* (2011).
Group(s): Troyer / Project(s): 5
 - S. PILATI, S. GIORGINI, M. MODUGNO, AND N. PROKOF'EV
Dilute Bose gas with correlated disorder: a path integral Monte Carlo study
New Journal of Physics **12**, 073003 (2010).
Group(s): Troyer / Project(s): 8
 - B. CAPOGROSSO-SANSONE, S. GIORGINI, S. PILATI, L. POLLET, N. PROKOF'EV, B. SVISTUNOV, AND M. TROYER
The Beliaev technique for a weakly interacting Bose gas
New Journal of Physics **12**, 043010 (2010).
Group(s): Troyer / Project(s): 8
 - P. N. MA, L. POLLET, AND M. TROYER
Measuring the equation of state of trapped ultracold bosonic systems in an optical lattice with in situ density imaging
Physical Review A **82**, 033627 (2010).
Group(s): Troyer / Project(s): 8
 - R. N. C. PFEIFER, P. CORBOZ, O. BUERSCHAPER, M. AGUADO, M. TROYER, AND G. VIDAL
Simulation of anyons with tensor network algorithms
Physical Review B **82**, 115126 (2010).
Group(s): Troyer / Project(s): 5
 - K. H. MARTI, B. BAUER, M. REIHER, M. TROYER, AND F. VERSTRAETE
Complete-graph tensor network states: a new fermionic wave function ansatz for molecules
New Journal of Physics **12**, 103008 (2010).
Group(s): Troyer / Project(s): 5
 - E. GULL, P. WERNER, S. FUCHS, B. SURER, T. PRUSCHKE, AND M. TROYER
Continuous-time quantum Monte Carlo impurity solvers
Computer Physics Communications **182**, 1078 (2011).
Group(s): Troyer / Project(s): 5, 8

Group of A. Weidenkaff

M. H. AGUIRRE, A. SHKABKO, AND A. WEIDENKAFF

- Microwave Plasma Nitridation of SrTiO₃: A Quantitative EELS, TEM, and STEM-HAADF Analysis of the SrTiO_{3-x}N_y Growth and the Structural Evolution*
Crystal Growth and Design **10**, 3562 (2010).
Group(s): Weidenkaff / Project(s): 3
- J. BARTH, G. H. FECHER, B. BALKE, S. OUARDI, T. GRAF, C. FELSER, A. SHKABKO, A. WEIDENKAFF, P. KLAER, H. J. ELMERS, H. YOSHIKAWA, S. UEDA, AND K. KOBAYASHI
Itinerant half-metallic ferromagnets Co₂TiZ (Z = Si, Ge, Sn): Ab initio calculations and measurement of the electronic structure and transport properties
Physical Review B **81**, 064404 (2010).
Group(s): Weidenkaff / Project(s): 3
- T. GRAF, J. BARTH, B. BALKE, S. POPULOH, A. WEIDENKAFF, AND C. FELSER
Tuning the carrier concentration for thermoelectrical application in the quaternary Heusler compound Co₂TiAl_(1-x)Si_x
Scripta Materialia **63**, 925 (2010).
Group(s): Weidenkaff / Project(s): 3
- D. LOGVINOVICH, A. ARAKCHEEVA, P. PATTON, S. ELISEEVA, P. TOMEŠ, I. MAROZAU, AND G. CHAPUIS
Crystal Structure and Optical and Magnetic Properties of Pr₂(MoO₄)₃
Inorganic Chemistry **49**, 1587 (2010).
Group(s): Weidenkaff / Project(s): 3
- D. LOGVINOVICH, S. G. EBBINGHAUS, A. RELLER, I. MAROZAU, D. FERRI, AND A. WEIDENKAFF
Synthesis, Crystal Structure and Optical Properties of LaNbON₂
Zeitschrift für Anorganische und Allgemeine Chemie **636**, 905 (2010).
Group(s): Weidenkaff / Project(s): 3
- R. ROBERT, D. LOGVINOVICH, M. H. AGUIRRE, S. G. EBBINGHAUS, L. BOCHER, P. TOMEŠ, AND A. WEIDENKAFF
Crystal structure, morphology and physical properties of LaCo_{1-x}Ti_xO_{3±δ} perovskites prepared by a citric acid assisted soft chemistry synthesis
Acta Materialia **58**, 680 (2010).
Group(s): Weidenkaff / Project(s): 3
- C. SUTER, P. TOMEŠ, A. WEIDENKAFF, AND A. STEINFELD
Heat Transfer and Geometrical Analysis of Thermoelectric Converters Driven by Concentrated Solar Radiation
Materials **3**, 2735 (2010).
Group(s): Weidenkaff / Project(s): 3
- P. TOMEŠ, K. KNÍŽEK, A. WEIDENKAFF, AND J. HEJTMÁNEK
On the physical properties of Sr_{1-x}Na_xRuO₃ (x = 0 – 0.19)
Solid State Sciences **12**, 1112 (2010).
Group(s): Weidenkaff / Project(s): 3
- P. TOMEŠ, R. ROBERT, M. TROTTMANN, L. BOCHER, M. AGUIRRE, A. BITSCHI, J. HEJTMÁNEK, AND A. WEIDENKAFF
Synthesis and Characterization of New Ceramic Thermoelectrics Implemented in a Thermoelectric Oxide Module
Journal of Electronic Materials **39**, 1696 (2010).
Group(s): Weidenkaff / Project(s): 3
- P. TOMEŠ, M. TROTTMANN, C. SUTER, M. H. AGUIRRE, A. STEINFELD, P. HAUETER, AND A. WEIDENKAFF
Thermoelectric Oxide Modules (TOMs) for the Direct Conversion of Simulated Solar Radiation into Electrical Energy
Materials **3**, 2801 (2010).
Group(s): Weidenkaff / Project(s): 3
- A. WEIDENKAFF, M. H. AGUIRRE, L. BOCHER, M. TROTTMANN, P. TOMEŠ, AND R. ROBERT
Development of perovskite-type cobaltates and manganates for thermoelectric oxide modules
Journal of the Korean Ceramic Society **47**, 47 (2010).
Group(s): Weidenkaff / Project(s): 3
- Group of Ph. Willmott**
- ▶ C. M. SCHLEPÜTZ, M. BJÖRCK, E. KOLLER, S. A. PAULI, D. MARTOCCIA, Ø. FISCHER, AND P. R. WILLMOTT
Structure of ultrathin heteroepitaxial superconducting YBa₂Cu₃O_{7-x} films
Physical Review B **81**, 174520 (2010).
Group(s): Fischer, Willmott / Project(s): 1
- ▶ S. A. PAULI, S. J. LEAKE, B. DELLEY, M. BJÖRCK, C. W. SCHNEIDER, C. M. SCHLEPÜTZ, D. MARTOCCIA, S. PAETEL, J. MANNHART, AND P. R. WILLMOTT
Evolution of the Interfacial Structure of LaAlO₃ on SrTiO₃
Physical Review Letters **106**, 036101 (2011).
Group(s): Willmott / Project(s): 1
- D. MARTOCCIA, M. BJÖRCK, C. M. SCHLEPÜTZ, T. BRUGGER, S. A. PAULI, B. D. PATTERSON, T. GREBER, AND P. R.

WILLMOTT

*Graphene on Ru(0001): a corrugated and chiral structure*New Journal of Physics **12**, 043028 (2010).

Group(s): Willmott / Project(s): 1

D. MARTOCCIA, S. A. PAULI, T. BRUGGER, T. GREBER, B. D. PATTERSON, AND P. R. WILLMOTT

*h-BN on Rh(111): Persistence of a commensurate 13-on-12 superstructure up to high temperatures*Surface Science **604**, L9 (2010).

Group(s): Willmott / Project(s): 1

D. MARTOCCIA, T. BRUGGER, M. BJÖRCK, C. M. SCHLEPÜTZ, S. A. PAULI, T. GREBER, B. D. PATTERSON, AND P. R. WILLMOTT

*h-BN/Ru(0001) nanomesh: A 14-on-13 superstructure with 3.5 nm periodicity*Surface Science **604**, L16 (2010).

Group(s): Willmott / Project(s): 1

Group of A. Zheludev

- ▶ V. N. GLAZKOV, G. DHALENNE, A. REVCOLEVSCHI, AND A. ZHELUDEV

*Multiple spin-flop phase diagram of BaCu₂Si₂O₇*Journal of Physics: Condensed Matter **23**, 086003 (2011).

Group(s): Zheludev / Project(s): 6

- ▶ V. N. GLAZKOV, A. I. SMIRNOV, A. ZHELUDEV, AND B. SALES

*Modes of magnetic resonance of the S=1 dimer chain compound NTENP*Physical Review B **82**, 184406 (2010).

Group(s): Zheludev / Project(s): 6

- ▶ T. HONG, S. N. GVASALIYA, S. HERRINGER, M. M. TURNBULL, C. P. LANDEE, L.-P. REGNAULT, M. BOEHM, AND A. ZHELUDEV

*Dynamics of the two-dimensional S=1/2 dimer system (C₅H₆N₂F)₂CuCl₄*Physical Review B **83**, 052401 (2011).

Group(s): Zheludev / Project(s): 6

- ▶ T. HONG, A. ZHELUDEV, H. MANAKA, AND L.-P. REGNAULT

*Evidence for a magnetic Bose glass in (CH₃)₂CHNH₃Cu(Cl_{0.95}Br_{0.05})₃ from neutron diffraction*Physical Review B **81**, 060410(R) (2010).

Group(s): Zheludev / Project(s): 6

9.3.2 Scientific articles in journals without peer review

Group of B. Batlogg

S. WEYENETH, P. J. W. MOLL, R. PUZNIAK, K. NINIOS, F. F. BALAKIREV, R. D. McDONALD, H. B. CHAN, N. D. ZHIGADLO, S. KATRYCH, Z. BUKOWSKI, J. KARPINSKI, H. KELLER, B. BATLOGG, AND L. BALICAS
Rearrangement of the antiferromagnetic ordering at high magnetic fields in SmFeAsO and SmFeAsO_{0.9}F_{0.1} single crystals
arXiv:1102.3312v1 (2011).

Group(s): Batlogg, Karpinski, Keller / Project(s): 4

Group of T. Esslinger

- ▶ D. GREIF, L. TARRUELL, T. UEHLINGER, R. JÖRDENS, AND T. ESSLINGER
Probing nearest-neighbor correlations of ultracold fermions in an optical lattice
arXiv:1012.0845 (2010).

Group(s): Esslinger / Project(s): 8

- ▶ T. ESSLINGER
Fermi-Hubbard Physics with Atoms in an Optical Lattice
Annual Review of Condensed Matter Physics 1, 129 (2010).

Group(s): Esslinger / Project(s): 8

- ▶ B. ZIMMERMANN, T. MÜLLER, J. MEINEKE, T. ESSLINGER, AND H. MORITZ
High-resolution imaging and manipulation of ultracold fermions
arXiv:1011.1004 (2010).

Group(s): Esslinger / Project(s): 8

Group of Ø. Fischer

- ▶ I. MAGGIO-APRILE, C. BERTHOD, N. JENKINS, Y. FASANO, A. PIRIOU, AND Ø. FISCHER
Scanning Tunneling Spectroscopy of High T_c Cuprates
in *Nanoscience and Engineering in Superconductivity*, V. MOSHCHALOV, R. WOERDENWEBER, AND W. LANG, eds. (Springer-Verlag, Berlin, 2010), Springer Series in Nanoscience and Technology, chap. 9, p. 231.

Group(s): Fischer, Giamarchi / Project(s): 4

Group of T. Giamarchi

T. GIAMARCHI
Quantum Phase Transitions in quasi-one dimensional systems

in *Understanding Quantum Phase Transitions*, L. D. CARR, ed. (CRC Press; Taylor and Francis, 2010).

Group(s): Giamarchi / Project(s): 7

- ▶ A. TOKUNO AND T. GIAMARCHI
Spectroscopy for cold atom gases in periodically phase-modulating optical lattices
arXiv:1101.2469 (2011).

Group(s): Giamarchi / Project(s): 8

T. GIAMARCHI
Interactions in Quantum Fluids
in *Ultracold Gases and Quantum Information*, C. MINIATURA, ed. (Oxford University Press, 2011).

Group(s): Giamarchi / Project(s): 8

M. A. CAZALILLA, R. CITRO, T. GIAMARCHI, E. ORIGNAC, AND M. RIGOL
One dimensional Bosons: From Condensed Matter Systems to Ultracold Gases
arXiv:1101.5337v1 (2011).

Group(s): Giamarchi / Project(s): 8

- ▶ I. MAGGIO-APRILE, C. BERTHOD, N. JENKINS, Y. FASANO, A. PIRIOU, AND Ø. FISCHER
Scanning Tunneling Spectroscopy of High T_c Cuprates
in *Nanoscience and Engineering in Superconductivity*, V. MOSHCHALOV, R. WOERDENWEBER, AND W. LANG, eds. (Springer-Verlag, Berlin, 2010), Springer Series in Nanoscience and Technology, chap. 9, p. 231.

Group(s): Fischer, Giamarchi / Project(s): 4

Group of E. Giannini

B. SACÉPÉ, J. B. OOSTINGA, J. LI, A. UBALDINI, N. J. G. COUTO, E. GIANNINI, AND A. F. MORPURGO
Gate-tuned normal and superconducting transport at the surface of a topological insulator
arXiv:1101.2352 (2011).

Group(s): Giannini, Morpurgo / Project(s): 2

Group of V. Gritsev

- ▶ A. POLKOVNIKOV AND V. GRITSEV
Universal Dynamics Near Quantum Critical Points
in *Understanding Quantum Phase Transitions*, L. D. CARR, ed. (CRC Press, Taylor & Francis Group, Boca Raton, 2011), p. 59.

Group(s): Gritsev / Project(s): 8

Group of J. Karpinski

Z. GUGUCHIA, J. ROOS, A. SHENGELAYA, S. KATRYCH, Z. BUKOWSKI, S. WEYENETH, F. MURÁNYI, S. STRÄSSLE, A. MAISURADZE, J. KARPINSKI, AND H. KELLER

Magnetic and structural properties of Co-substituted single crystal $\text{EuFe}_{1.9}\text{Co}_{0.1}\text{As}_2$

arXiv:1010.5948 (2010).

Group(s): Karpinski, Keller / Project(s): 4

S. WEYENETH, P. J. W. MOLL, R. PUZNIAK, K. NINIOS, F. F. BALAKIREV, R. D. MCDONALD, H. B. CHAN, N. D. ZHIGADLO, S. KATRYCH, Z. BUKOWSKI, J. KARPINSKI, H. KELLER, B. BATLOGG, AND L. BALICAS

Rearrangement of the antiferromagnetic ordering at high magnetic fields in SmFeAsO and $\text{SmFeAsO}_{0.9}\text{F}_{0.1}$ single crystals

arXiv:1102.3312v1 (2011).

Group(s): Batlogg, Karpinski, Keller / Project(s): 4

Group of H. Keller

Z. GUGUCHIA, J. ROOS, A. SHENGELAYA, S. KATRYCH, Z. BUKOWSKI, S. WEYENETH, F. MURÁNYI, S. STRÄSSLE, A. MAISURADZE, J. KARPINSKI, AND H. KELLER

Magnetic and structural properties of Co-substituted single crystal $\text{EuFe}_{1.9}\text{Co}_{0.1}\text{As}_2$

arXiv:1010.5948 (2010).

Group(s): Karpinski, Keller / Project(s): 4

S. WEYENETH, P. J. W. MOLL, R. PUZNIAK, K. NINIOS, F. F. BALAKIREV, R. D. MCDONALD, H. B. CHAN, N. D. ZHIGADLO, S. KATRYCH, Z. BUKOWSKI, J. KARPINSKI, H. KELLER, B. BATLOGG, AND L. BALICAS

Rearrangement of the antiferromagnetic ordering at high magnetic fields in SmFeAsO and $\text{SmFeAsO}_{0.9}\text{F}_{0.1}$ single crystals

arXiv:1102.3312v1 (2011).

Group(s): Batlogg, Karpinski, Keller / Project(s): 4

Group of D. van der Marel

D. VAN DER MAREL

Superconductivity: Beware of the pseudogap

Nature Physics 7, 10 (2011).

Group(s): van der Marel / Project(s): 4

Group of J. Mesot

- ▶ T. SHIROKA, F. CASOLA, V. GLAZKOV, A. ZHELUDEV, K. PRŠA, H.-R. OTT, AND J. MESOT

Distribution of NMR relaxations in a random Heisenberg chain

arXiv:1012.0731 (2011).

Group(s): Mesot, Ott, Zheludev / Project(s): 6

Group of A. Morpurgo

B. SACÉPÉ, J. B. OOSTINGA, J. LI, A. UBALDINI, N. J. G. COUTO, E. GIANNINI, AND A. F. MORPURGO

Gate-tuned normal and superconducting transport at the surface of a topological insulator

arXiv:1101.2352 (2011).

Group(s): Giannini, Morpurgo / Project(s): 2

Group of H.-R. Ott

- ▶ T. SHIROKA, F. CASOLA, V. GLAZKOV, A. ZHELUDEV, K. PRŠA, H.-R. OTT, AND J. MESOT

Distribution of NMR relaxations in a random Heisenberg chain

arXiv:1012.0731 (2011).

Group(s): Mesot, Ott, Zheludev / Project(s): 6

Group of T. M. Rice

M. KHODAS, H. B. YANG, J. RAMEAU, P. D. JOHNSON, A. M. TSVELIK, AND T. M. RICE

Analysis of the Quasiparticle Spectral Function in the Underdoped Cuprates

arXiv:1007.4837 (2010).

Group(s): Rice, Sigrist / Project(s): 4

K.-Y. YANG, Y. YAMASHITA, A. M. LÄUCHLI, M. SIGRIST, AND T. M. RICE

Microscopic model for the semiconductor-to-ferromagnetic-metal transition in $\text{FeSi}_{1-x}\text{Ge}_x$ Alloys

arXiv:1102.1190 (2011).

Group(s): Rice, Sigrist / Project(s): 5

Group of M. Sigrist

M. KHODAS, H. B. YANG, J. RAMEAU, P. D. JOHNSON, A. M. TSVELIK, AND T. M. RICE

Analysis of the Quasiparticle Spectral Function in the Underdoped Cuprates

arXiv:1007.4837 (2010).

Group(s): Rice, Sigrist / Project(s): 4

K.-Y. YANG, Y. YAMASHITA, A. M. LÄUCHLI, M. SIGRIST, AND T. M. RICE

Microscopic model for the semiconductor-to-ferromagnetic-metal transition in $\text{FeSi}_{1-x}\text{Ge}_x$ Alloys

arXiv:1102.1190 (2011).

Group(s): Rice, Sigrist / Project(s): 5

Group of J.-M. Triscone

S. GARIGLIO, M. GABAY, AND J.-M. TRISCONÉ
Oxide Materials: Superconductivity on the other side

Nature Nanotechnology **5**, 13 (2010).

Group(s): Triscone (JM) / Project(s): 1

Group of M. Troyer

- ▶ B. BAUER, L. D. CARR, A. FEIGUIN, J. FREIRE, S. FUCHS, L. GAMPER, J. GUKELBERGER, E. GULL, S. GUERTLER, A. HEHN, R. IGARASHI, S. V. ISAKOV, D. KOOP, P. N. MA, P. MATES, H. MATSUO, O. PARCOLLET, G. PAWLOWSKI, J. D. PICON, L. POLLET, E. SANTOS, V. W. SCAROLA, U. SCHOLLWÖCK, C. SILVA, B. SURER, S. TODO, S. TREBST, M. TROYER, M. L. WALL, P. WERNER, AND S. WESSEL

The ALPS project release 2.0: Open source software for strongly correlated systems

arxiv:1101.2646 (2011).

Group(s): Troyer / Project(s): 5, 6, 8

Group of A. Weidenkaff

N. SCHAEUBLE AND Y. ROMANYUK
Aluminium-substituted Zinc Oxide thin films: thermoelectric properties and characterization
in *8th European Conference on Thermoelectrics* (Como, Italy, 2010).

Group(s): Weidenkaff / Project(s): 3

M. AGUIRRE, P. TOMĚS, AND R. ROBERT
Transport properties and crystal structure of $\text{PrCo}_{1-x}\text{Ni}_x\text{O}_3$ mixed valence oxides.

in *8th European Conference on Thermoelectrics* (Italy, Como, 2010).

Group(s): Weidenkaff / Project(s): 3

P. TOMES AND A. WEIDENKAFF
Construction and modelling of a thermoelectric oxide module (TOM) as a demonstrator: Schlussbericht. BFE-Vertrags- und Projektnummer 152820 / 101356, 2010, 26 pp.

Tech. rep. (2010).

Group(s): Weidenkaff / Project(s): 3

Group of A. Zheludev

B. NÁFRÁDI, T. KELLER, H. MANAKA, A. ZHELUDEV, AND B. KEIMER
Low Temperature Dynamics of Magnons in a Spin-1/2 Ladder Compound

arXiv:1102.0214 (2011).

Group(s): Zheludev / Project(s): 6

- ▶ T. SHIROKA, F. CASOLA, V. GLAZKOV, A. ZHELUDEV, K. PRŠA, H.-R. OTT, AND J. MESOT

Distribution of NMR relaxations in a random Heisenberg chain

arXiv:1012.0731 (2011).

Group(s): Mesot, Ott, Zheludev / Project(s): 6

9.3.3 Publications involving several groups

- ▶ C. MONNEY, E. F. SCHWIER, M. G. GARNIER, N. MARIOTTI, C. DIDOT, H. CERCELLIER, J. MARCUS, H. BERGER, A. N. TITOV, H. BECK, AND P. AEBI
Probing the exciton condensate phase in 1T - TiSe₂ with photoemission
New Journal of Physics **12**, 125019 (2010).
Group(s): Aebi, Forró / Project(s): 7
- ▶ C. MONNEY, E. F. SCHWIER, M. G. GARNIER, C. BATTAGLIA, N. MARIOTTI, C. DIDOT, H. CERCELLIER, J. MARCUS, H. BERGER, A. N. TITOV, H. BECK, AND P. AEBI
Dramatic effective mass reduction driven by a strong potential of competing periodicity
Europhysics Letters **92**, 47003 (2010).
Group(s): Aebi, Forró / Project(s): 7
- ▶ L. ANTOGNAZZA, M. DECROUX, M. THERASSE, AND M. ABPLANALP
Heat Propagation Velocities in Coated Conductors for Fault Current Limiter Applications
IEEE Transactions on Applied Superconductivity (2011), doi:10.1109/TASC.2010.2100351.
Group(s): Abplanalp, Decroux / Project(s): 3
- ▶ A. PIRIOU, N. JENKINS, C. BERTHOD, I. MAGGIO-APRILE, AND Ø. FISCHER
First direct observation of the Van Hove singularity in the tunneling spectra of cuprates
Nature Communications **2**, 221 (2011).
Group(s): Fischer, Giamarchi / Project(s): 4
- ▶ A. P. PETROVIĆ, R. LORTZ, G. SANTI, C. BERTHOD, C. DUBOIS, M. DECROUX, A. DEMUER, A. B. ANTUNES, A. PARÉ, D. SALLOUM, P. GOUGEON, M. POTEL, AND Ø. FISCHER
Multi-band Superconductivity in the Chevrel Phases SnMo₆S₈ and PbMo₆S₈
Physical Review Letters **106**, 017003 (2011).
Group(s): Decroux, Fischer, Giamarchi / Project(s): 4
- ▶ P. J. W. MOLL, R. PUZNIAK, F. BALAKIREV, K. ROGACKI, J. KARPINSKI, N. D. ZHIGADLO, AND B. BATLOGG
High magnetic-field scales and critical currents in SmFeAs(O, F) crystals
Nature Materials **9**, 628 (2010).
Group(s): Batlogg, Karpinski / Project(s): 4
- ▶ Y. FASANO, I. MAGGIO-APRILE, N. D. ZHIGADLO, S. KATRYCH, J. KARPINSKI, AND Ø. FISCHER
Local Quasiparticle Density of States of Superconducting SmFeAsO_{1-x}F_x Single Crystals: Evidence for Spin-Mediated Pairing
Physical Review Letters **105**, 167005 (2010).
Group(s): Fischer, Karpinski / Project(s): 4
- ▶ S. WEYENETH, M. BENDELE, R. PUZNIAK, F. MURÁNYI, A. BUSSMANN-HOLDER, N. D. ZHIGADLO, S. KATRYCH, Z. BUKOWSKI, J. KARPINSKI, A. SHENGE-LAYA, R. KHASANOV, AND H. KELLER
Field-dependent superfluid density in the optimally doped SmFeAsO_{1-x}F_y superconductor
Europhysics Letters **91**, 47005 (2010).
Group(s): Karpinski, Keller / Project(s): 4
- ▶ N. D. ZHIGADLO, S. KATRYCH, S. WEYENETH, R. PUZNIAK, P. J. W. MOLL, Z. BUKOWSKI, J. KARPINSKI, H. KELLER, AND B. BATLOGG
Th-substituted SmFeAsO: Structural details and superconductivity with T_c above 50 K
Physical Review B **82**, 064517 (2010).
Group(s): Batlogg, Karpinski, Keller / Project(s): 4
- ▶ T. KONDO, R. KHASANOV, J. KARPINSKI, S. KAZAKOV, N. ZHIGADLO, Z. BUKOWSKI, M. SHI, A. BENDOUNAN, Y. SASSA, J. CHANG, S. PAILHÉS, J. MESOT, J. SCHMALIAN, H. KELLER, AND A. KAMINSKI
Anomalies in the Fermi Surface and Band Dispersion of Quasi-One-Dimensional CuO Chains in the High-Temperature Superconductor YBa₂Cu₄O₈
Physical Review Letters **105**, 267003 (2010).
Group(s): Karpinski, Keller / Project(s): 4
- ▶ M. BENDELE, A. AMATO, K. CONDER, M. ELENDER, H. KELLER, H.-H. KLAUSS, H. LUETKENS, E. POMJAKUSHINA, A. RASELLI, AND R. KHASANOV
Pressure Induced Static Magnetic Order in Superconducting FeSe_{1-x}
Physical Review Letters **104**, 087003 (2010).
Group(s): Keller, Kenzelmann / Project(s): 4
- ▶ M. BENDELE, S. WEYENETH, R. PUZNIAK, A. MAISURADZE, E. POMJAKUSHINA, K. CONDER, V. POMJAKUSHIN, H. LUETKENS, S. KATRYCH, A. WISNIEWSKI, R. KHASANOV, AND H. KELLER
Anisotropic superconducting properties of single-crystalline FeSe_{0.5}Te_{0.5}
Physical Review B **81**, 224520 (2010).
Group(s): Karpinski, Keller, Kenzelmann / Project(s): 4

- M. BENDELE, P. BABKEVICH, S. KATRYCH, S. N. GVASALIYA, E. POMJAKUSHINA, K. CONDER, B. ROESSLI, A. T. BOOTHROYD, R. KHASANOV, AND H. KELLER
Tuning the superconducting and magnetic properties of $Fe_ySe_{0.25}Te_{0.75}$ by varying the iron content
Physical Review B **82**, 212504 (2010).
Group(s): Karpinski, Keller, Kenzelmann / Project(s): 4
- L. SCHULZ, L. NUCCIO, M. WILLIS, P. DE-SAI, P. SHAKYA, T. KREOUZIS, V. K. MALIK, C. BERNHARD, F. L. PRATT, N. A. MORLEY, A. SUTER, G. J. NIEUWENHUYS, T. PROKSCHA, E. MORENZONI, W. P. GILLIN, AND A. J. DREW
Engineering spin propagation across a hybrid organic/inorganic interface using a polar layer
Nature Materials **10**, 39 (2011).
Group(s): Bernhard, Morenzoni / Project(s): 1
- J. LI, I. MARTIN, M. BÜTTIKER, AND A. F. MORPURGO
Topological origin of subgap conductance in insulating bilayer graphene
Nature Physics **7**, 38 (2011).
Group(s): Büttiker, Morpurgo / Project(s): 2
- J. LI, A. F. MORPURGO, M. BÜTTIKER, AND I. MARTIN
Marginality of bulk-edge correspondence for single-valley Hamiltonians
Physical Review B **82**, 245404 (2010).
Group(s): Büttiker, Morpurgo / Project(s): 2
- P. MARSIK, K. W. KIM, A. DUBROKA, M. RÖSSLE, V. K. MALIK, L. SCHULZ, C. N. WANG, C. NIEDERMAYER, A. J. DREW, M. WILLIS, T. WOLF, AND C. BERNHARD
Coexistence and Competition of Magnetism and Superconductivity on the Nanometer Scale in Underdoped $BaFe_{1.89}Co_{0.11}As_2$
Physical Review Letters **105**, 057001 (2010).
Group(s): Bernhard, Niedermayer / Project(s): 1, 4
- F. CASOLA, T. SHIROKA, S. WANG, K. CONDER, E. POMJAKUSHINA, J. MESOT, AND H.-R. OTT
Direct Observation of Impurity-Induced Magnetism in a Spin- $\frac{1}{2}$ Antiferromagnetic Heisenberg Two-Leg Spin Ladder
Physical Review Letters **105**, 067203 (2010).
Group(s): Kenzelmann, Mesot, Ott, Rønnow / Project(s): 6
- S. WANG, E. POMJAKUSHINA, T. SHIROKA, G. DENG, N. NIKSERESHT, C. RÜEGG, H. M. RØNNOW, AND K. CONDER
Crystal growth and characterization of the dilutable frustrated spin-ladder compound $Bi(Cu_{1-x}Zn_x)_2PO_6$
Journal of Crystal Growth **313**, 51 (2010).
Group(s): Mesot, Ott, Rønnow / Project(s): 6
- M. GUARISE, B. DALLA PIAZZA, M. MORETTI SALA, G. GHIRINGHELLI, L. BRAICOVICH, H. BERGER, J. N. HANCOCK, D. VAN DER MAREL, T. SCHMITT, V. N. STROCOV, L. J. P. AMENT, J. VAN DEN BRINK, P.-H. LIN, P. XU, H. M. RØNNOW, AND M. GRIONI
Measurement of Magnetic Excitations in the Two-Dimensional Antiferromagnetic $Sr_2CuO_2Cl_2$ Insulator Using Resonant X-Ray Scattering: Evidence for Extended Interactions
Physical Review Letters **105**, 157006 (2010).
Group(s): Forró, Grioni, Rønnow, van der Marel / Project(s): 6, 7
- P. XU, J. O. PIATEK, P.-H. LIN, B. SIPOS, H. BERGER, L. FORRÓ, H. M. RØNNOW, AND M. GRIONI
Superconducting phase in the layered dichalcogenide $1T-TaS_2$ upon inhibition of the metal-insulator transition
Physical Review B **81**, 172503 (2010).
Group(s): Forró, Grioni, Rønnow / Project(s): 7
- F. HASSLER, A. RÜEGG, M. SIGRIST, AND G. BLATTER
Dynamical Unbinding Transition in a Periodically Driven Mott Insulator
Physical Review Letters **104**, 220402 (2010).
Group(s): Blatter, Sigrist / Project(s): 8
- R. M. KONIK, T. M. RICE, AND A. M. TSVELIK
Superconductivity generated by coupling to a cooperon in a two-dimensional array of four-leg Hubbard ladders
Physical Review B **82**, 054501 (2010).
Group(s): Rice, Sigrist / Project(s): 4
- K.-Y. YANG, K. HUANG, W.-Q. CHEN, T. M. RICE, AND F.-C. ZHANG
Andreev and Single-Particle Tunneling Spectra of Underdoped Cuprate Superconductors
Physical Review Letters **105**, 167004 (2010).
Group(s): Rice, Sigrist / Project(s): 4
- A. D. CAVIGLIA, S. GARIGLIO, C. CANCELLIERI, B. SACÉPÉ, A. FÊTE, N. REYREN, M. GABAY, A. F. MORPURGO, AND J.-M. TRISCONE
Two-Dimensional Quantum Oscillations of the Conductance at $LaAlO_3/SrTiO_3$ Interfaces
Physical Review Letters **105**, 236802 (2010).
Group(s): Morpurgo, Triscone (JM) / Project(s): 1, 2
- R. JÖRDENS, L. TARRUELL, D. GREIF, T. UEHLINGER, N. STROHMAIER, H. MORITZ, T. ESSLINGER, L. DE LEO, C. KOLLATH, A. GEORGES, V. SCAROLA, L. POLLET,

- E. BUROVSKI, E. KOZIK, AND M. TROYER
Quantitative Determination of Temperature in the Approach to Magnetic Order of Ultracold Fermions in an Optical Lattice
Physical Review Letters **104**, 180401 (2010).
Group(s): Esslinger, Troyer / Project(s): 8
- ▶ J. TEYSSIER, E. GIANNINI, V. GURITANU, R. VIENNOIS, D. VAN DER MAREL, A. AMATO, AND S. N. GVASALIYA
Spin-glass ground state in $Mn_{1-x}Co_xSi$
Physical Review B **82**, 064417 (2010).
Group(s): Giannini, van der Marel / Project(s): 5
- ▶ J. N. HANCOCK, S. I. MIRZAEI, J. GILLET, S. E. SEBASTIAN, J. TEYSSIER, R. VIENNOIS, E. GIANNINI, AND D. VAN DER MAREL
Strong coupling to magnetic fluctuations in the charge dynamics of iron-based superconductors
Physical Review B **82**, 014523 (2010).
Group(s): van der Marel, Giannini / Project(s): 4
- ▶ N. P. ARMITAGE, R. TEDIOSI, F. LÉVY, E. GIANNINI, L. FORRÓ, AND D. VAN DER MAREL
Infrared Conductivity of Elemental Bismuth under Pressure: Evidence for an Avoided Lifshitz-Type Semimetal-Semiconductor Transition
Physical Review Letters **104**, 237401 (2010).
Group(s): Forró, Giannini, van der Marel / Project(s): 4
- ▶ J. N. HANCOCK, R. VIENNOIS, D. VAN DER MAREL, H. M. RØNNOW, M. GUARISE, P.-H. LIN, M. GRIONI, M. MORETTI SALA, G. GHIRINGHELLI, V. N. STROCOV, J. SCHLAPPA, AND T. SCHMITT
Evidence for core-hole-mediated inelastic x-ray scattering from metallic $Fe_{1.087}Te$
Physical Review B **82**, 020513(R) (2010).
Group(s): Grioni, Rønnow, van der Marel / Project(s): 4, 6
- ▶ C. M. SCHLEPÜTZ, M. BJÖRCK, E. KOLLER, S. A. PAULI, D. MARTOCCIA, Ø. FISCHER, AND P. R. WILLMOTT
Structure of ultrathin heteroepitaxial superconducting $YBa_2Cu_3O_{7-x}$ films
Physical Review B **81**, 174520 (2010).
Group(s): Fischer, Willmott / Project(s): 1
- C. MONNEY, E. F. SCHWIER, M. G. GARNIER, N. MARIOTTI, C. DIDOT, H. BECK, P. AEBI, H. CERCELLIER, J. MARCUS, C. BATTAGLIA, H. BERGER, AND A. N. TITOV
Temperature-dependent photoemission on $1T-TiSe_2$: Interpretation within the exciton condensate phase model
Physical Review B **81**, 155104 (2010).
Group(s): Aebi, Forró / Project(s): 7
- N. CURTZ, E. KOLLER, H. ZBINDEN, M. DECROUX, L. ANTOGNAZZA, Ø. FISCHER, AND N. GISIN
Patterning of ultrathin YBCO nanowires using a new focused-ion-beam process
Superconductor Science & Technology **23**, 45015 (2010).
Group(s): Decroux, Fischer / Project(s): 3
- A. UBALDINI, E. GIANNINI, C. SENATORE, AND D. VAN DER MAREL
 $BiOCuS$: A new superconducting compound with oxypnictide-related structure
Physica C **470**, S356 (2010).
Group(s): Flükiger, Giannini, van der Marel / Project(s): 4
- C. BERTHOD
Tunneling spectra of strongly coupled superconductors: Role of dimensionality
Physical Review B **82**, 024504 (2010).
Group(s): Fischer, Giamarchi / Project(s): 4
- N. D. ZHIGADLO, S. KATRYCH, J. KARPINSKI, B. BATLOGG, F. BERNARDINI, S. MASSIDDA, AND R. PUZNIAK
Influence of Mg deficiency on crystal structure and superconducting properties in MgB_2 single crystals
Physical Review B **81**, 054520 (2010).
Group(s): Batlogg, Karpinski / Project(s): 4
- A. BELOUSOV, J. KARPINSKI, AND B. BATLOGG
Thermodynamics of the $Al-Ga-N_2$ system
Journal of Crystal Growth **312**, 2579 (2010).
Group(s): Batlogg, Karpinski / Project(s): 4
- A. BELOUSOV, S. KATRYCH, K. HAMETNER, D. GÜNTHER, J. KARPINSKI, AND B. BATLOGG
 $Al_xGa_{1-x}N$ bulk crystal growth: Crystallographic properties and $p - T$ phase diagram
Journal of Crystal Growth **312**, 2585 (2010).
Group(s): Batlogg, Karpinski / Project(s): 4
- S. WEYENETH, P. J. W. MOLL, R. PUZNIAK, K. NINIOS, F. F. BALAKIREV, R. D. McDONALD, H. B. CHAN, N. D. ZHIGADLO, S. KATRYCH, Z. BUKOWSKI, J. KARPINSKI, H. KELLER, B. BATLOGG, AND L. BALICAS
Rearrangement of the antiferromagnetic ordering at high magnetic fields in $SmFeAsO$ and $SmFeAsO_{0.9}F_{0.1}$ single crystals
to be published in Physical Review B (2011).
Group(s): Batlogg, Karpinski, Keller / Project(s): 4
- Z. SHERMADINI, J. KANTER, C. BAINES, M. BENDELE, Z. BUKOWSKI, R. KHASANOV, H.-H. KLAUSS, H. LUETKENS, H. MAETER, G. PASCUA, B. BATLOGG, AND A. AMATO

- Microscopic study of the superconducting state of the iron pnictide RbFe_2As_2 via muon spin rotation*
Physical Review B **82**, 144527 (2010).
Group(s): Batlogg, Karpinski, Keller / Project(s): 4
- M. BELESI, I. ROUSOCHATZAKIS, H. C. WU, H. BERGER, I. V. SHVETS, F. MILA, AND J. P. ANSERMET
Ferrimagnetism of the magnetoelectric compound Cu_2OSeO_3 probed by ^{77}Se NMR
Physical Review B **82**, 094422 (2010).
Group(s): Forró, Mila / Project(s): 6
- N. TSYRULIN, F. XIAO, A. SCHNEIDEWIND, P. LINK, H. M. RÖNNOW, J. GAVILANO, C. P. LANDEE, M. M. TURNBULL, AND M. KENZELMANN
Two-dimensional square-lattice $S = \frac{1}{2}$ antiferromagnet $\text{Cu}(\text{pz})_2(\text{ClO}_4)_2$
Physical Review B **81**, 134409 (2010).
Group(s): Kenzelmann, Rønnow / Project(s): 6
- D. ISARAKORN, A. SAMBRI, P. JANPHUANG, D. BRIAND, S. GARIGLIO, J.-M. TRISCONE, F. GUY, J. W. REINER, C. H. AHN, AND N. F. DE ROOIJ
Epitaxial piezoelectric MEMS on silicon
Journal of Micromechanics and Microengineering **20**, 055008 (2010).
Group(s): de Rooij, Triscone (JM) / Project(s): 3
- D. ISARAKORN, D. BRIAND, A. SAMBRI, S. GARIGLIO, J.-M. TRISCONE, F. GUY, J. W. REINER, C. H. AHN, AND N. F. DE ROOIJ
Finite element analysis and experiments on a silicon membrane actuated by an epitaxial PZT thin film for localized-mass sensing applications
Sensors and Actuators B: Chemical **153**, 54 (2010).
Group(s): de Rooij, Triscone (JM) / Project(s): 3
- D. ISARAKORN, D. BRIAND, P. JANPHUANG, A. SAMBRI, S. GARIGLIO, J.-M. TRISCONE, F. GUY, J. W. REINER, C. H. AHN, AND N. F. DE ROOIJ
The realization and performance of vibration energy harvesting MEMS devices based on an epitaxial piezoelectric thin film
Smart Materials and Structures **20**, 025015 (2011).
Group(s): de Rooij, Triscone (JM) / Project(s): 3
- R. SCHERWITZL, P. ZUBKO, I. GUTIERREZ LEZAMA, S. ONO, A. F. MORPURGO, G. CATALAN, AND J.-M. TRISCONE
Electric-Field Control of the Metal-Insulator Transition in Ultrathin NdNiO_3 Films
Advanced Materials **22**, 5517 (2010).
Group(s): Morpurgo, Triscone (JM) / Project(s): 1, 2
- A. PIRIOU, E. GIANNINI, Y. FASANO, C. SENATORE, AND Ø. FISCHER
Vortex phase diagram and temperature-dependent second-peak effect in overdoped $\text{Bi}_2\text{Sr}_2\text{CuO}_{6+\delta}$ crystals
Physical Review B **81**, 144517 (2010).
Group(s): Fischer, Flükiger, Giannini / Project(s): 4
- R. VIENNOIS, E. GIANNINI, D. VAN DER MAREL, AND R. ČERNÝ
Effect of Fe excess on structural, magnetic and superconducting properties of single-crystalline $\text{Fe}_{1+x}\text{Te}_{1-y}\text{Se}_y$
Journal of Solid State Chemistry **183**, 769 (2010).
Group(s): Giannini, van der Marel / Project(s): 4
- R. VIENNOIS, E. GIANNINI, D. VAN DER MAREL, AND R. ČERNÝ
Phase diagram of single-crystalline tetragonal iron chalcogenides
Physica C **470**, S370 (2010).
Group(s): Giannini, van der Marel / Project(s): 4
- G. LEVY DE CASTRO, C. BERTHOD, A. PIRIOU, E. GIANNINI, AND Ø. FISCHER
Reply to Comment on "Preeminent Role of the Van Hove Singularity in the Strong-Coupling Analysis of Scanning Tunneling Spectroscopy for Two-Dimensional Cuprate Superconductors"
Physical Review Letters **105**, 099702 (2010).
Group(s): Fischer, Giamarchi, Giannini / Project(s): 4
- B. SACÉPÉ, J. B. OOSTINGA, J. LI, A. UBALDINI, N. J. G. COUTO, E. GIANNINI, AND A. F. MORPURGO
Gate-tuned normal and superconducting transport at the surface of a topological insulator
arXiv:1101.2352 (2011).
Group(s): Morpurgo, Giannini / Project(s): 2

11 Finance

Contents

11.1 Finance NCCR Overview	180
11.2 Funding sources	182
11.3 Allocation to projects	183
11.4 Expenditures	186
11.5 Comments on finances	189

NCCR: MaNEP
 Director: Fischer Oystein
 Home: Université de Genève - GE
 Start Date: 01.07.2001

Report: Year 10 Intermediate Report
 Period: 01.07.2009 - 30.06.2013
 Year: 9 - 12
 Status: in preparation

Criteria:

Finance NCCR Overview

Project leader	Institution	Project title	Group leader	Start of project	Duration	Total SNSF-funding	Total other funding	Total
Management								
Bagnoud Marie		Office		01.07.2001	156	1'897'704	4'304'124	6'201'827
Decroux Michel	Université de Genève	Education / Women		01.07.2001	156	927'260	1'416'811	2'344'071
Bonito Aleman Adriana		Knowledge and Technology Transfer		01.07.2001	156	361'896	952'149	1'314'045
Bonito Aleman Adriana		Communication		01.07.2001	156	373'741	822'321	1'196'062
						234'807	1'112'843	1'347'649
Reserve						3'676'534	0	3'676'534
			Fischer Øystein			3'676'534	0	3'676'534
Project(s) without workpackage								
Fischer Øystein	Université de Genève	Balance Phase II		01.07.2009	48	145'902	15'000	160'902
Fischer Øystein	Université de Genève	Fischer Oystein, Ph3, GCC		01.07.2010	36	0	72'254	72'254
Triscone Jean-Marc	Université de Genève	Project 1 - Novel phenomena at interfaces and in superlattices		01.07.2009	48	425'553	5'838'063	6'263'617
Morpurgo Alberto	Université de Genève	Project 2 - Materials for future electronics		01.07.2009	48	353'397	6'869'943	7'223'340
Fischer Øystein	Université de Genève	Project 3 - Electronic materials for energy systems and other applications		01.07.2009	48	1'292'044	13'186'373	14'478'417

Signature of NCCR Director:.....

Project leader	Institution	Project title	Group leader	Start of project	Duration	Total SNSF-funding	Total other funding	Total
Van der Marel Dirk	Université de Genève	Project 4 - Electronic properties of oxide superconductors and related materials		01.07.2009	48	1'213'153	10'421'287	11'634'441
Sigrist Manfred	ETH Zürich	Project 5 - Novel electronic phases in strongly correlated electron systems		01.07.2009	48	475'852	4'647'976	5'123'828
Mila Frederic	EPF Lausanne	Project 6 - Magnetism and competing interactions in bulk materials		01.07.2009	48	679'431	5'727'908	6'407'339
Forro Laszlo	EPF Lausanne	Project 7 - Electronic materials with reduced dimensionality		01.07.2009	48	697'921	5'875'811	6'573'732
Giamarchi Thierry	Université de Genève	Project 8 - Cold atomic gases as novel quantum simulators for condensed matter		01.07.2009	48	468'633	5'347'511	5'816'144
Cors Jorge	Université de Genève	Economic stimulus package - Cut-and-coat process by wire-EDM		01.11.2009	24	434'263	53'021	487'285
Flükiger Rene	Université de Genève	Economic stimulus package - Development of MgB2 wires		01.10.2009	24	191'119	62'191	253'310
Cors Jorge	Université de Genève	Economic stimulus package - Electrochemical sensors with higher resolution		01.10.2009	24	145'843	57'555	203'397
Kenzelmann Michel	PSI	Economic stimulus package - Neutron optical devices for small samples		01.10.2009	24	225'736	152'500	378'236
Fischer Øystein	Université de Genève	Equipment Geneva		01.07.2001	144	244'192	1'065'000	1'309'192
Fischer Øystein	Université de Genève	Collaborations		01.02.2010	28	375'495	123'319	498'815
Fischer Øystein	Université de Genève	Techniques Know-How		01.07.2009	48	65'175	3'044'221	3'109'396
Total:						13'007'949	66'864'058	79'872'006

NCCR: MaNEP **Year 10 Intermediate Report**
Director: Fischer Oystein **Report:** 01.07.2009 - 30.06.2013
Home: Université de Genève - GE **Year:** 9 - 12
Start Date: 01.07.2001 **Status:** in preparation

Criteria:

Funding sources

Funding source	Year 9	Year 10	Year 11	Year 12	Total Cash Total in Kind	% %	Reserve	Total	%
SNSF-funding	Cash in Kind 2'770'798 0	3'302'589 0	2'546'580 0	7'114'48	9'331'415 0	33.3 0.0	3'676'534	13'007'949	16.3
Self-funding from Home Institution	Cash in Kind 2'883'030 0	2'737'214 0	4'462'624 0	5'889'072	15'971'939 0	57.0 0.0	0	15'971'939	20.0
Self-funding from groups	Cash in Kind 14'302'737	11'718'013	10'092'350	8'799'350	44'912'450	93.3	0	44'912'450	56.2
Self-funding other	Cash in Kind 849'091	812'494	496'200	121'200	617'400 1'661'584	2.2 3.5	0	2'278'984	2.9
3rd party-funding	Cash in Kind 1'198'607	385'667	1'058'205	1'058'205	2'116'410 1'584'274	7.5 3.3	0	3'700'684	4.6
Total:	Cash in Kind 5'653'828 16'350'434	6'039'802 12'916'174	8'563'609 10'092'350	7'779'925 8'799'350	28'037'164 48'158'308		3'676'534	79'872'006	100.0

Signature of NCCR Director:.....

NCCR: MaNEP **Report:** Year 10 Intermediate Report
Director: Fischer Oystein **Period:** 01.07.2009 - 30.06.2013
Home: Université de Genève - GE **Year:** 9 - 12
Start Date: 01.07.2001 **Status:** in preparation

Criteria:

Allocation to projects

Project leader	Project title	Relation % P.J.- WP	Year 9	Year 10	Year 11	Year 12	SNSF Funded	Total Funded	Total Not SNSF Funded	Total	%
Management											
Bagnoud Marie	Office	100	1'456'601	1'341'063	1'689'790	1'714'373	1'897'704	4'304'124	6'201'827	7.8	
			577'817	617'357	471'930	466'967	927'260	1'206'811	2'344'071	2.9	
			105'000	105'000	0	0	0	2'10'000			
Decroux Michel	Education / Women	100	170'726	157'259	443'030	443'030	36'1896	852'149	1'314'045	1.6	
			50'000	50'000	0	0	0	100'000			
Bonito Aleman Adriana	Knowledge and Technology Transfer	100	280'077	149'320	361'568	361'568	373'741	778'792	1'196'062	1.5	
			43'529	0	0	0	0	43'529			
Bonito Aleman Adriana	Communication	100	194'453	262'127	413'262	442'808	234'807	1'077'843	1'347'649	1.7	
			35'000	0	0	0	0	35'000			
Reserve											
Fischer Øystein	Cash						3'676'534	0	3'676'534	4.6	
Project(s) without workpackage											
Fischer Øystein	Balance Phase II	100	20'547'661	17'614'913	16'966'169	14'864'902	7'433'711	62'559'934	69'993'645	87.6	
			133'302	12'600	0	0	145'902	0	160'902	0.2	
			7'500	7'500	0	0	0	15'000			
Fischer Øystein	Fischer Oystein, Ph3, GCC	100	0	64'754	0	0	0	64'754	72'254	0.1	
			0	7'500	0	0	0	7'500			

Signature of NCCR Director:.....

Project leader	Project title	Relation % PJ- WP	Year					Year 12		Total SNSF Funded	Total Not SNSF Funded	Total	%
			Year 9	Year 10	Year 11	Year 12	SNSF Funded	Total Funded					
Triscone Jean-Marc	Project 1 - Novel phenomena at	100 Cash in Kind	320'711 1'591'373	443'921 1'347'930	581'333 810'600	410'149 757'600	425'553 0	1'330'560 4'507'503	6'263'617	7.8			
Morpurgo Alberto	Project 2 - Materials for future electronics	100 Cash in Kind	142'575 1'915'756	44'132 1'432'500	475'408 1'302'700	607'569 1'302'700	353'397 0	916'287 5'953'656	7'223'340	9.0			
Fischer Øystein	Project 3 - Electronic materials for energy	100 Cash in Kind	1'179'815 3'141'045	1'144'625 2'352'607	2'295'932 1'196'175	2'071'043 1'097'175	1'292'044 0	5'399'371 7'787'002	14'478'417	18.1			
Van der Marel Dirk	Project 4 - Electronic properties of oxide	100 Cash in Kind	636'026 3'358'247	930'207 1'876'102	858'738 1'786'750	692'621 1'495'750	1'213'153 0	1'904'439 8'516'849	11'634'441	14.6			
Sigrist Manfred	Project 5 - Novel electronic phases in	100 Cash in Kind	258'810 1'580'600	86'306 1'454'834	233'278 797'400	30'000 682'600	475'852 0	132'542 4'515'434	5'123'828	6.4			
Milla Frederic	Project 6 - Magnetism and competing	100 Cash in Kind	118'775 1'630'207	236'795 1'751'701	375'561 1'304'600	73'300 916'400	679'431 0	125'000 5'602'908	6'407'339	8.0			
Förro Laszlo	Project 7 - Electronic materials with	100 Cash in Kind	267'851 1'268'472	200'508 940'500	258'700 1'769'500	98'700 1'769'500	697'921 0	127'839 5'747'972	6'573'732	8.2			
Giamarchi Thierry	Project 8 - Cold atomic gases as novel	100 Cash in Kind	286'637 1'459'353	251'573 1'381'000	330'588 1'124'625	204'743 777'625	468'633 0	604'907 4'742'603	58'16'144	7.3			
Cors Jorge	Economic stimulus package -	100 Cash in Kind	165'743 0	297'541 24'000	0 0	0 0	434'263 0	29'021 24'000	487'285	0.6			
Fliükiger Rene	Economic stimulus package -	100 Cash in Kind	62'184 7'500	176'125 7'500	0 0	0 0	191'119 0	47'191 15'000	253'310	0.3			

Project leader	Project title	Relation % PJ- WP	Year 9	Year 10	Year 11	Year 12	SNSF Funded	Total Funded	Not SNSF Funded	Total	%
Cors Jorge	Economic stimulus package -	100 Cash in Kind	56'656 28'533	118'208 0	0 0	0 0	145'843 0	145'843	29'021 28'533	203'397	0.3
Kenzelmann Michel	Economic stimulus package - Neutron	100 Cash in Kind	79'122 72'500	146'614 80'000	0 0	0 0	225'736 0	225'736	0 152'500	378'236	0.5
Fischer Øystein	Equipment Geneva	100 Cash in Kind	323'238 7'500	20'955 7'500	400'000 0	550'000 0	244'192 0	244'192	1'050'000 15'000	1'309'192	1.6
Fischer Øystein	Collaborations	100 Cash in Kind	36'271 40'819	339'224 82'500	0 0	0 0	375'495 0	375'495	0 123'319	498'815	0.6
Fischer Øystein	Techniques Know-How	100 Cash in Kind	363'038 7'500	339'651 7'500	1'064'281 0	1'327'427 0	65'175 0	65'175	3'029'221 15'000	3'109'396	3.9
Total			22'004'262.25	18'955'976.33	18'655'959.00	16'579'275.00	13'007'949	13'007'949	66'864'058	79'872'006	100.0

Criteria:

Expenditures

Project	Project leader	Gross salaries	Social charges	Equipment	Consumables	Travel	Miscellaneous	Credit	Total Cash Total in Kind	Total
Management		3'971'927.62	725'511.22	46'965.54	474'986.06	131'822.30	850'614.62	0.00		6'201'827.36
Office	Bagnoud Marie	Cash 1'310'822.00 in Kind 210'000.00	266'541.64 0.00	0.00 0.00	127'150.80 0.00	25'543.50 0.00	404'013.18 0.00	0.00	2'134'071.12 210'000.00	2'344'071.12
Education / Women	Decroux Michel	Cash 719'645.12 in Kind 100'000.00	142'085.34 0.00	0.00 0.00	54'856.82 0.00	54'974.80 0.00	242'482.80 0.00	0.00	1'214'044.88 100'000.00	1'314'044.88
Knowledge and Technology Transfer	Bonito Aleman Adriana	Cash 798'639.15 in Kind 0.00	158'852.98 0.00	23'445.52 0.00	123'546.44 0.00	2'070.60 0.00	45'978.61 43'528.63	0.00	1'152'533.30 43'528.63	1'196'061.93
Communication	Bonito Aleman Adriana	Cash 797'821.35 in Kind 35'000.00	158'031.26 0.00	23'520.02 0.00	169'432.00 0.00	49'233.40 0.00	114'611.40 0.00	0.00	1'312'649.43 35'000.00	1'347'649.43
Reserve										3'676'533.81
	Fischer Øystein	Cash								3'676'533.81
Project(s) without workpackage		58'096'116.00	2'432'206.15	3'094'773.39	2'377'607.04	795'001.87	3'205'343.72	-7'402.95		69'993'645.22
Balance Phase II	Fischer Øystein	Cash 49'730.05 in Kind 15'000.00	10'046.55 0.00	62'505.70 0.00	62.75 0.00	7'382.50 0.00	23'577.60 0.00	-7'402.95	145'902.20 15'000.00	160'902.20
Fischer Oystein, Ph3, GCC	Fischer Øystein	Cash 53'962.00 in Kind 7'500.00	10'792.40 0.00	0.00 0.00	0.00 0.00	0.00 0.00	0.00 0.00	0.00	64'754.40 7'500.00	72'254.40

Signature of NCCR Director:.....

Project	Project leader	Gross salaries	Social charges	Equipment	Consumables	Travel	Miscellaneous	Credit	Total Cash Total in Kind	Total
Project 1 - Novel phenomena at interfaces and in superlattices	Triscone Jean-Marc	Cash 1'261'191.25 in Kind 4'213'403.15	234'713.85 0.00	730.60 94'000.00	73'035.80 79'000.00	29'192.03 39'100.00	157'250.00 82'000.00	0.00	1756'113.53 4'507'503.15	6'263'616.68
Project 2 - Materials for future electronics	Morpurgo Alberto	Cash 802'025.45 in Kind 5'474'655.67	162'898.65 0.00	23'481.41 137'000.00	209'020.64 256'000.00	26'805.30 71'000.00	45'452.60 15'000.00	0.00	1'269'684.05 5'953'655.67	7'223'339.72
Project 3 - Electronic materials for energy systems and other applications	Fischer Øystein	Cash 4'449'036.74 in Kind 6'765'036.93	654'150.98 0.00	57'335.45 55'000.00	304'706.02 203'000.00	43'640.92 42'000.00	1'182'545.54 721'964.80	0.00	6'691'415.65 7'787'001.73	14'478'417.38
Project 4 - Electronic properties of oxide superconductors and related materials	Van der Marel Dirk	Cash 2'292'477.89 in Kind 7'997'281.73	428'448.11 0.00	16'097.70 99'000.00	140'424.91 226'000.00	36'341.64 95'540.80	203'802.00 99'026.00	0.00	3'117'592.25 8'516'848.53	11'634'440.78
Project 5 - Novel electronic phases in strongly correlated electron systems	Sigrist Manfred	Cash 364'025.54 in Kind 4'336'833.89	49'520.58 0.00	119'072.00 89'000.00	27'607.69 50'400.00	29'163.81 39'200.00	19'004.18 0.00	0.00	608'393.80 4'515'433.89	5'123'827.69
Project 6 - Magnetism and competing interactions in bulk materials	Mila Frederic	Cash 604'572.49 in Kind 5'205'818.18	78'134.25 0.00	0.00 45'000.00	15'455.00 123'000.00	14'569.30 108'000.00	91'700.00 121'090.20	0.00	804'431.04 5'602'908.38	6'407'339.42
Project 7 - Electronic materials with reduced dimensionality	Forro Laszlo	Cash 532'799.75 in Kind 4'784'372.34	83'335.78 0.00	20'428.66 590'000.00	119'338.07 291'000.00	15'253.80 77'600.00	54'603.40 5'000.00	0.00	825'759.46 5'747'972.34	6'573'731.80
Project 8 - Cold atomic gases as novel quantum simulators for condensed matter	Giamarchi Thierry	Cash 786'812.85 in Kind 4'562'603.34	131'230.11 0.00	23'172.52 60'000.00	77'206.11 40'000.00	30'047.14 80'000.00	25'072.00 0.00	0.00	1'073'540.73 4'742'603.34	5'816'144.07
Economic stimulus package - Cut-and-coat process by wire-EDM	Cors Jorge	Cash 265'755.40 in Kind 24'000.00	47'154.43 0.00	120'992.49 0.00	28'195.55 0.00	1'186.63 0.00	0.00 0.00	0.00	463'284.50 24'000.00	487'284.50

Project	Project leader	Gross salaries	Social charges	Equipment	Consumables	Travel	Miscellaneous	Credit	Total Cash Total in Kind	Total
Economic stimulus package - Development of MgB2 wires	Flükiger Rene	Cash 111'281.16 15'000.00	22'386.22 0.00	82'190.45 0.00	13'902.85 0.00	8'549.00 0.00	0.00 0.00	0.00	238'309.68 15'000.00	253'309.68
Economic stimulus package - Neutron optical devices for small samples	Kenzelmann Michel	Cash 174'247.85 152'500.00	24'874.25 0.00	17'004.00 0.00	9'610.35 0.00	0.00 0.00	0.00 0.00	0.00	225'736.45 152'500.00	378'236.45
Economic stimulus package - Electrochemical sensors with higher resolution	Cors Jorge	Cash 106'140.45 28'533.33	15'699.68 0.00	39'988.60 0.00	13'035.15 0.00	0.00 0.00	0.00 0.00	0.00	174'863.88 28'533.33	203'397.21
Equipment Geneva	Fischer Øystein	Cash 0.00 15'000.00	0.00 0.00	1'294'192.31 0.00	0.00 0.00	0.00 0.00	0.00 0.00	0.00	1'294'192.31 15'000.00	1'309'192.31
Collaborations	Fischer Øystein	Cash 265'318.00 123'319.35	43'560.55 0.00	48'581.50 0.00	17'606.15 0.00	429.00 0.00	0.00 0.00	0.00	375'495.20 123'319.35	498'814.55
Techniques Know-How	Fischer Øystein	Cash 2'240'881.22 15'000.00	435'259.76 0.00	0.00 0.00	60'000.00 0.00	0.00 0.00	358'255.40 0.00	0.00	3'094'396.38 15'000.00	3'109'396.38
Total		62'068'043.62	3'157'717.37	3'141'738.93	2'852'593.10	926'824.17	4'055'958.34	-7'402.95		79'872'006.39

11.5 Comments on finances

Referring to our comments last year, we have been able to catch up on the use of NIRA 2.0, thanks to an intense effort by our management team. We confirm that NIRA 2.0 has increased the workload for our management. With respect to third party funding, the amounts introduced for the moment in NIRA 2.0 correspond only to persons working at the university and paid by the industry. The rest of the third party funding will be introduced in the accounting report due in September. The same comment is true for some of the home institution self-funding, especially the equipment.

Explanations to the reserve

The “reserve” which appears in the NIRA summary is CHF 3'676'534. This is composed of two parts: about CHF 2'975'000 which is not a real reserve but is composed of funds which have been allocated differently to the initial allocation at the beginning of Phase III; and about CHF 700'000 which we consider as a reserve which has not yet been allocated but for which we have definitive plans.

Allocated expenses which appear as an apparent, but not real, reserve

In the financial plan for the 8 large MaNEP research projects, we allowed the groups to plan their expenses concentrated on the three first years in the Phase III. The reason for this was that this would allow each group to employ the equivalent of one doctoral student for the three first years, but with no funding for the fourth year. The reality, which was expected, is that most groups took a delay in starting using these funds, so that some of the funding is shifted *de facto* to the fourth year and this shall allow the groups to have some funds also for the fourth year. Thus there is a shift in the planned financing of up to one year. This may in the end correspond to the funding of one doctoral student per group for the fourth year. This would amount to approximately CHF 2'100'000, an amount which will appear in year 10 and year 11 as an apparent reserve in NIRA. On March 31, 2011 there remains about CHF 1'600'000 for the 8 main projects. We expect that about CHF 1'200'000 will be transferred to year 11 in the sense as explained above. This will appear as an apparent reserve in NIRA and is equivalent to covering

about half a doctoral student per group during year 12.

We allocated, as announced, CHF 715'000 to new collaborative projects after the beginning of Phase III. These funds were taken from the “Balance Phase II”. These projects will run for another one and a half to two years and the funds put aside to cover the corresponding expenses appear as a part of the apparent “reserve”. This amounts to about CHF 500'000.

The *economic stimulus packages* were an excellent initiative to boost the applied part of our activity. The still to be used funds in the next six months of approximately CHF 375'000 appears also as a part of the apparent reserve.

The total funds allotted for equipment in Geneva (funds from the University and the SNSF) during the two first years of Phase III amount to CHF 1'094'754. We have so far spent about CHF 666'000 and equipments for several CHF 100'000 have been ordered and will be paid during 2011–2012. To cover these expenses, we have at present put aside CHF 400'000. This amount, which appears as an apparent reserve, is planned to be paid during 2011 and 2012.

For the techniques and know-how activity, we planned to use CHF 100'000 in year 9 and CHF 100'000 in year 10. We have now employed a researcher for two years, which will use this amount. This expense is however delayed compared to the initial budget and thus about CHF 150'000 will appear as an apparent reserve in NIRA.

In education and advancement of women, we have set aside funds for employing an expert to boost the advancement of women. This is now planned for the two last years and accounts for about CHF 150'000 of the apparent reserve.

We have this year an ambitious program in communication with the events for the centennial of the discovery of superconductivity. This implies several activities of open house with the elaboration of new demonstration equipment, two projects of art and science, an exhibition on superconductivity and other activities. The total amount for this program is about CHF 700'000. The University of Geneva will participate with an important amount, directly or through the Physics Section and the Department of Condensed Matter Physics. We are at present searching for sponsors to cover another large part of this amount. To this end, we have received CHF 350'000 from the Wright Foun-

dation. We have put aside CHF 200'000 in the apparent reserve to cover additional expenses for these events and other activities for the remaining two and a half years of Phase III.

Reserves not yet firmly allocated

Our knowledge and technology transfer activities have been developing during the last year and we have, in agreement with the request of the review panel, put aside funds from the "Balance Phase II" to support these activities in the last part of MaNEP Phase III.




Two new senior scientists have started their activities in the field of MaNEP in Switzerland recently. We plan to use some of our reserve to support these groups during the two last years of MaNEP.

Following the same reasoning, as exposed above for the fourth year, we expect that some groups will have financial difficulties to cover a full activity during year 12, thus we plan to use part of the real reserve to contribute towards maintaining a full activity until the end of MaNEP.





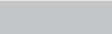



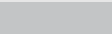



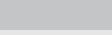



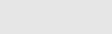



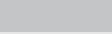



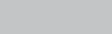
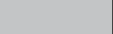
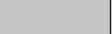
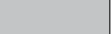
12 Appendix: milestones of the MaNEP projects

The tables of milestones allow one to follow the time evolution of MaNEP scientific activities. The tables below are drawn from the situation at the end of the previous reporting period (year 9) and displays the changes for year 10.

Color code

Milestones unchanged since the Proposal	
Milestones added this year	
Milestones suppressed this year	

Project 1: Novel phenomena at interfaces and in superlattices

	Milestones	Year 9	Year 10	Year 11	Year 12
1.	Conducting interfaces				
	Growth and characterization of oxide interfaces (LaAlO ₃ /SrTiO ₃) [Triscone, Willmott, Niedermayer]				
	Study of the electronic properties of conducting oxide interface systems (transport properties) [Jaccard, Triscone, van der Marel]				
	Structure of LAO/STO interface [Aebi, Willmott]				
	Control of interface mobility using field effect [Triscone, Willmott]				
	Fabrication of novel 2D electron gases not based on SrTiO ₃ [Triscone, Willmott]				
	Structural studies using SXR on the SC interface between under- and overdoped LSCO [Willmott]				
	Optical probes of metallic interface states in oxide heterostructures [Bernhard, van der Marel]				

	Milestones (Project 1, continued)	Year 9	Year 10	Year 11	Year 12
	<p>Oxygen diffusion studies in thin films [Niedermayer]</p> <p>Electronic properties of ¹⁸O exchanged interfaces [Niedermayer]</p> <p>Resistivity and Hall effect of the LAO/STO interface in pressurized liquid [Jaccard, Triscone]</p> <p>Multi-probe investigation of the LAO/STO interface in various pressure media [Jaccard, Triscone]</p> <p>Aspects of mechanisms [Sigrist]</p> <p>Aspects of non-centrosymmetry [Sigrist]</p> <p>Investigate the atomic environment at surfaces and interfaces close to the surface [Aebi, Triscone]</p> <p>PES/ARPES of oxide films and oxide interfaces [Aebi, Triscone]</p> <p>RIX of interfaces and superlattices [Triscone]</p> <p>Spectroscopic studies (Raman, optical studies) [Niedermayer]</p> <p>Magneto-transmission in the THz range [van der Marel, Triscone]</p>			<p>■</p>	
2.	Coupling of instabilities at insulating interfaces				
	<p>Growth and characterization of oxide interfaces (PbTiO₃/SrTiO₃ and novel systems) [Aebi, Paruch Triscone]</p> <p>Structural studies using SXRD of improper FE lattices [Triscone, Willmott]</p> <p>XPD measurement of tetragonality in ultra-thin PTO films as a function of temperature [Aebi, Triscone]</p> <p>Investigate the atomic environment at surfaces and interfaces close to the surface [Aebi, Triscone]</p> <p>Study of the electronic properties of insulating oxide systems (dielectric, ferroelectric, multiferroic) [Paruch, Triscone]</p>				

	Milestones (Project 1, continued)	Year 9	Year 10	Year 11	Year 12
3.	Magnetic/superconducting interfaces				
	μ SR and optical experiments on Y123/Pr123 [Fischer, Morenzoni, Bernhard, Keller]				
	μ SR experiments in 214 superlattices (Interface superconductivity and magnetism) [Morenzoni, Keller, Bernhard]				
	Experiments on LSCO tri- and bilayers (study of proximity effects in UD and OD layers) [Morenzoni, Keller, Bernhard]				
	Magnetic interface states in oxide heterostructures from paramagnetic materials [Bernhard]				
	Spectroscopic studies (Raman, optical studies) [Niedermayer, Bernhard]				
	Study electronic properties at magnetic/superconducting interfaces close to the surface [Aebi, Bernhard]				
	Superconductivity induced changes in magnetic states of high- T_c -manganite multilayers [Bernhard, Niedermayer]				
4.	Electronic properties of organic charge transfer interfaces				
	Identification of new materials for charge-transfer interfaces [Morpurgo]				
	Magneto-transmission in the THz range [Morpurgo, van der Marel]				
	Low-temperature transport through metallic charge transfer interfaces [Morpurgo]				
5.	Domain walls in ferroelectrics/multiferroics: a model interface system				
	Domains with internal degrees of freedom [Giamarchi, Paruch]				
	Response to oscillatory fields [Giamarchi, Paruch]				
	AFM studies of magnetoelectric coupling in nanocomposite multiferroic materials [Paruch, Triscone]				
	Nanoscale variable temperature studies of ferroelectric domain walls in $\text{PbZr}_{0.2}\text{Ti}_{0.8}\text{O}_3$ [Paruch, Triscone]				

	Milestones (Project 1, continued)	Year 9	Year 10	Year 11	Year 12
	Nanoscale variable temperature studies of ferroelectric domain walls in BiFeO ₃ [Paruch]				
	Effects of atmosphere and surface chemical modification on ferroelectric polarization [Aebi, Paruch]				
6.	Crystal growth of new substrates with tuned structural and physical properties				
	Preliminary growth experiments of SrTiO ₃ crystals with the existing equipment [Giannini]				
	Growth of various oxide substrates with the improved Czocharlski technique [Giannini]				
	Development of new substrates with tuned structural and electronic properties [Giannini]				

Project 2: Materials for future electronics

	Milestones	Year 9	Year 10	Year 11	Year 12
1.	Oxide heterostructures				
	Nano-patterned top gates on LaAlO ₃ /SrTiO ₃ heterostructures [Triscone, Morpurgo]				
	Electrostatically controlled Josephson junctions [Triscone, Morpurgo]				
	Interplay of superconductivity and confinement in LaAlO ₃ /SrTiO ₃ heterostructures [Triscone, Morpurgo]				
	Nanostructures for the investigation of spin-orbit interaction [Triscone, Morpurgo]				
	Atomic force microscopy writing of nanostructures at the LaAlO ₃ /SrTiO ₃ interface [Paruch, Triscone]				
	Atomic force microscopy reading (conducting AFM and capacitive) of nanostructures at the LaAlO ₃ /SrTiO ₃ interface [Paruch, Triscone]				

	Milestones (Project 2, continued)	Year 9	Year 10	Year 11	Year 12
	<p>Transport properties of AFM written nanostructures at the $\text{LaAlO}_3/\text{SrTiO}_3$ interface at room temperature [Paruch, Triscone]</p> <p>Low temperature investigations of AFM written nanostructures at the $\text{LaAlO}_3/\text{SrTiO}_3$ interface [Paruch, Triscone]</p>				
2.	Carbon based materials				
2.1	Graphene				
	Optimization of sample preparation and atomic scale imaging of single layer and bilayer graphene [Renner]				
	Implementation of combined AFM/STM imaging/spectroscopy on graphene [Renner]				
	Structural and spectroscopic characterisation of few-layer graphene [Renner]				
	Spectroscopy on doped/intercalated few-layer graphene devices [Renner]				
	Edge-state tunneling spectroscopy of single layer graphene [Renner]				
	Spin dependent tunneling spectroscopy of graphene [Renner]				
	Nature of transport gap in graphene nano-ribbons [Morpurgo]				
	Magnetoresistance of graphene nano-ribbons [Morpurgo]				
	Comparison of transport in few-layer graphene of different thickness [Morpurgo]				
	Transport through suspended graphene [Morpurgo]				
	Magnetotransport in high-mobility graphene [Morpurgo]				
	Transport through graphene on high-k dielectrics or ferroelectric substrates [Paruch, Morpurgo, Triscone]				
	Gate-dependent spectroscopy of bi-layer graphene [van der Marel]				

	Milestones (Project 2, continued)	Year 9	Year 10	Year 11	Year 12
	<p>Spectroscopy of few-layer graphene in different dielectric environments [van der Marel]</p> <p>Magneto-optical spectroscopy of epitaxial graphene [van der Marel]</p> <p>ESR on exfoliated graphene [Forró]</p>				
2.2	<p>Carbon Nanotubes</p> <p>Ferroelectric field-effect modulation of carbon nanotube resistivity [Paruch]</p> <p>Controlled manipulation of carbon nanotubes on ferroelectric substrates [Paruch]</p> <p>Non-destructive AFM measurements of polarization around carbon nanotubes [Paruch]</p> <p>Mechanism of domain switching and growth using carbon nanotubes [Paruch]</p>				
2.3	<p>Organic semiconductors</p> <p>New molecular materials for the study of intrinsic transport [Morpurgo]</p> <p>Mechanisms of threshold voltage shift and drift [Morpurgo]</p> <p>Low-temperature transport measurements [Morpurgo]</p> <p>Comparison of intrinsic transport properties in different organic semiconductors [Morpurgo]</p> <p>Infrared spectroscopy of organic semiconductor interfaces [van der Marel]</p>				
3.	<p>Theory</p>				
	<p>Aharonov-Bohm effect in topological insulators [Büttiker]</p> <p>Edge conductance in gapped bilayer graphene [Büttiker]</p> <p>Topological properties of gapped bilayer graphene [Büttiker]</p>				

	Milestones (Project 2, continued)	Year 9	Year 10	Year 11	Year 12
	Shot-noise and pre-formed pairs: High- T_c -normal junction [Büttiker]				
	Shot-noise and pre-formed pairs: Analysis of shot noise [Büttiker]				
	Effect of electron-phonon coupling on transport through graphene nano-ribbons [Sigrist]				
	Ordered phases in heterostructures of correlated electrons [Sigrist]				
	Transport properties of heterostructures of correlated electrons [Sigrist]				
	Exploring new directions in heterostructures of correlated electrons [Sigrist]				
	Luttinger liquids with an external bath [Giamarchi]				

Project 3: Electronic materials for energy systems and other applications

	Milestones	Year 9	Year 10	Year 11	Year 12
1.	Applied superconductivity				
	Development of a new method to fabricate MgB ₂ wires with higher critical current [Flükiger]				
	Development of long lengths of MgB ₂ wires [Flükiger]				
	Investigation of relaxation in inhomogenous YBCO [Flükiger]				
	Study of contact resistance between coated conductors and other superconductors [Flükiger, Bruker]				
	Development and calibration of an experimental setup for the measurement of thermal conductivity of coated conductors [Decroux]				
	Study of the influence of the substrate thickness on the thermal behavior of coated conductors [Decroux]				

	Milestones (Project 3, continued)	Year 9	Year 10	Year 11	Year 12
	<p>Thermal conductance of interfaces in coated conductors [Decroux]</p> <p>Measurement of propagation velocities on coated conductors [Decroux]</p>				
2.	Oxides for energy harvesting				
	<p>Optimization and full characterization of ultra-thin SrTiO₃ epitaxial buffer layers on silicon [J.-M. Triscone, G. Triscone]</p> <p>Growth of epitaxial Pb(Zr,Ti)O₃, 50/50, with high piezoelectric coefficient on silicon with metallic oxide electrodes [J.-M. Triscone, G. Triscone]</p> <p>Growth of epitaxial PMN-PT on silicon with giant piezoelectric response [J.-M. Triscone, G. Triscone]</p> <p>Realization and mechanical and electrical characterization of membranes based on fully epitaxial oxide materials [J.-M. Triscone, de Rooij]</p> <p>Realization and characterization of nano-beams based on fully epitaxial oxide materials [J.-M. Triscone, de Rooij]</p> <p>Realization of an energy harvesting demonstrator based on piezoelectric materials [J.-M. Triscone, de Rooij]</p> <p>Investigation of the thermoelectric properties of the 2-DEG electron gas at the LaAlO₃/SrTiO₃ interface [J.-M. Triscone]</p> <p>Investigation of the thermoelectric properties of LaAlO₃/SrTiO₃ superlattices [J.-M. Triscone]</p> <p>Investigation of the thermoelectric properties of thin doped SrTiO₃ layers on silicon [J.-M. Triscone, Weidenkaff]</p> <p>Identification of new promising thermoelectric oxides and synthesis of performing polycrystalline thermoelectric materials of a new generation [Weidenkaff]</p> <p>Modeling of energy conversion based on data from the material specification [Weidenkaff]</p> <p>Synthesis of single crystalline materials [Weidenkaff]</p>				

	Milestones (Project 3, continued)	Year 9	Year 10	Year 11	Year 12
	<p>Evaluation of candidate materials and decision about which to use for the p and n type legs of a ceramic converter [Weidenkaff]</p> <p>Assembling of a first generation oxide thermoelectric converter based on the news materials [Weidenkaff]</p> <p>Second generation thermoelectric convertor as demonstrator [Weidenkaff]</p>				
3.	Application of artificial superlattices				
	<p>Investigation of the growth process of Ni/Ti layers to achieve lower roughness as well as an improved homogeneity of the layers [Kenzelmann]</p> <p>Systematic characterization of various substrate materials in order to find a tool for selecting substrates experiencing the required surface quality [Kenzelmann]</p> <p>Developing polishing processes to manufacture metal substrates with a very low roughness [Kenzelmann]</p> <p>Improvement of polarizing supermirrors, i.e. extending the critical angle of reflection [Kenzelmann]</p> <p>Develop Co-free, remanent magnetic layers for polarizing supermirrors [Kenzelmann]</p> <p>Development of adaptive neutron optics [Kenzelmann]</p>				
4.	Hydrogen detectors and other sensors				
	<p>Setup of experimental tools for conductance measurements in H₂ atmosphere [Yvon, Fischer/Cors]</p> <p>Identification of hydrogen sensitive intermetallic compounds, fabrication of thin films [Yvon, Fischer/Cors]</p> <p>Performance validation [Asulab, Yvon, Fischer/Cors]</p> <p>Design of the resistive detector electronics layout and fabrication of first prototype devices [Asulab, Yvon, Fischer/Cors]</p>				

Milestones (Project 3, continued)	Year 9	Year 10	Year 11	Year 12
Benchmarking against the performance of commercial devices [Asulab, Yvon, Fischer/Cors]	█	█	█	
Fine tuning of device design [Asulab]			█	
Fabrication of a large number of devices and testing/homologisation at sensor performance facility (NL) [Asulab, Yvon, Fischer/Cors]			█	
Study and optimization of cantilever surface passivation for optimal piezo-resistive effect. Functional cantilever using piezo-resistive deflection readout for AFM [Renner]	█	█		
Deflection and torsion mode AFM cantilever using non-optical readout [Renner]	█		█	█
Development and optimization of one-step hydrothermal approaches to functionalized oxidic nanorods and nanowires for sensor applications: W/Mo-oxide nanorods and Bi ₂ O ₃ /SnO ₂ composite nanowires as major preparative targets [Patzke]	█	█	█	
Setup of gas sensor construction [Patzke, Phasis, Fischer/Cors]	█			
Preparative exploration of advanced ternary and higher oxide systems with sensor activity, e.g. ZnGa ₂ O ₄ -based spinel nanorods and targeted modification of MoO ₃ nanowires [Patzke, Phasis, Fischer/Cors]		█	█	
Fabrication of portable gas-sensors based on oxidic nanomaterials for KTI applications [Patzke, Phasis, Fischer/Cors]		█	█	
Development of market-ready gas phase sensors with special emphasis on new portable devices for environmental applications and industrial process control [Patzke, Phasis, Fischer/Cors]	█	█	█	█
Industrial implementation and marketing optimization of the gas sensor devices [Patzke, Phasis, Fischer/Cors]			█	█

	Milestones (Project 3, continued)	Year 9	Year 10	Year 11	Year 12
5.	New surface treatments for microcomponents				
	Experimental investigation of compounds suitable for chemical marking on stainless steel, brass, gold and platinum [Fischer/Cors, Phasis, Vacheron Constantin]				
	Definition of the identification tools for reliable identification of the microscopic marks [Fischer/Cors, Phasis, Vacheron Constantin]				
	Design and construction of an automatic marking prototype [Fischer/Cors, Phasis, Vacheron Constantin]				
	Experimental validation of the ability to mark 20'000 parts/year [Fischer/Cors, Phasis, Vacheron Constantin]				
	Research of visually attractive surface effects using the marking technology at a macroscopic scale [Fischer/Cors, Phasis]				
	Selective coating of watch cases and other parts with transition metal carbides and nitrides. [Fischer/Cors, Phasis]				
	Implementation and measurement of tribological nanomaterial-based coatings on selected substrates [Fischer/Cors, Phasis]				

Project 4: Electronic properties of oxide superconductors and related materials

	Milestones	Year 9	Year 10	Year 11	Year 12
1.	Optical conductivity, ARPES, RIXS, STM, muons, neutrons studies of cuprate superconductors				
1.1	What is the nature of the pseudo-gap?				
	ARPES studies of SC and pseudo-gaps in $(\text{La,Nd})_{2-x}\text{Sr}_x\text{CuO}_4$ [Mesot]				
	Muon spectroscopy and influence of isotope substitution on the gap in cuprate high- T_c [Keller]				

	Milestones (Project 4, continued)	Year 9	Year 10	Year 11	Year 12
1.2	<p>How does the spectrum of collective spin excitations evolve from anti-ferromagnetic state to the high-T_c phase?</p> <p>STM studies of strongly overdoped Bi2201 [Fischer]</p> <p>STM studies of strongly overdoped Bi2212 and Bi2223 [Fischer]</p> <p>STM studies of tunneling asymmetry in $Y_{1-x}Pr_xBa_2Cu_3O_7$ [Fischer]</p> <p>Resonant inelastic soft X-ray scattering (RIXS) at the SLS [Grioni]</p>				
1.3	<p>What is the mechanism of superconductivity pairing in the cuprates: is there a pairing glue?</p> <p>Calculation of spin susceptibility from ARPES spectral function [Mesot]</p> <p>The interplay between superconductivity and magnetism [Mesot]</p> <p>Electron-boson scattering in optical- and single particle spectral functions [van der Marel]</p>				
2.	New materials and crystal growth				
2.1	<p>Iron pnictide high-T_c superconductors</p> <p>STM studies of iron-pnictides [Fischer]</p> <p>Processing and crystal growth of Sb-based ternary and quaternary pnictides [Giannini]</p> <p>Crystal growth of superconducting Fe-chalcogenides and related materials [Giannini]</p> <p>Processing and growth of new binary pnictides with a tetrahedral structure [Giannini]</p> <p>Crystal growth of $LnFeAsO$ and $A(Me)As_2Fe_2$ [Karpinski]</p> <p>Substitutions in $LnFeAsO$ and $A(Me)As_2Fe_2$ [Karpinski]</p>				

	Milestones (Project 4, continued)	Year 9	Year 10	Year 11	Year 12
	<p>Muon spectroscopy of the multiple-gap behavior in pnictide superconductors [Morenzoni, Keller]</p> <p>Optical investigations of pnictides [van der Marel]</p> <p>Study of the coexistence and competition of antiferromagnetism and superconductivity in $\text{Ba}(\text{Fe}_{1-x}\text{Co}_x)_2\text{As}_2$ [Niedermayer]</p>				
2.2	<p>Other non-cuprate high-T_c superconductors</p> <p>Development of hydrothermal growth technique and application to the Sr_2VO_4 system [Giannini]</p> <p>Searching for new superconductors [Karpinski]</p> <p>Optical investigations of Sr_2VO_4 [van der Marel]</p>				
2.3	<p>Cuprate high-T_c superconductors</p> <p>Growth of Tl-based cuprates [Giannini]</p> <p>Cuprates with reduced lattice parameter [Jaccard]</p> <p>investigations on the 122 FeAs compounds [Degiorgi]</p> <p>Interaction of localized f electrons with superconductivity [Morenzoni]</p>				
3.	Microscopic theories for cuprate superconductivity and novel superconductors				
3.1	<p>Variational many-body wavefunctions</p> <p>Coexistence of hot spots and superconductivity [Baeriswyl]</p> <p>Superconductivity and ferromagnetism (multilayers), superfluid density [Baeriswyl]</p> <p>Broken symmetry and long-range order [Baeriswyl]</p>				

	Milestones (Project 4, continued)	Year 9	Year 10	Year 11	Year 12
3.2	The chiral p-wave (spin triplet) state of Sr_2RuO_4				
	study of the 3K phase in Sr_2RuO_4 [Sigrist]				
	study of Josephson effect in Sr_2RuO_4 [Sigrist]				
	study of Sr_2RuO_4 in magnetic field [Sigrist]				
	study of exotic vortices in Sr_2RuO_4 [Sigrist]				

Project 5: Novel electronic phases in strongly correlated electron systems

	Milestones	Year 9	Year 10	Year 11	Year 12
1.	Unconventional superconductivity in heavy fermion metals				
1.1	Superconductivity and magnetism				
	Study of influence of FFLO phase of $CeCoIn_5$ on flux lattice of fields along c -axis [Kenzelmann]				
	Symmetry of flux lattice in $CeCoIn_5$ for fields in basal plane (in Q-phase) [Kenzelmann]				
	Form factor of flux lattice in $CeCoIn_5$ for fields in the basal plane [Kenzelmann]				
	Microscopic measurements of magnetism in superconducting phase [Kenzelmann]				
	Temperature dependence of the flux lattice in $CeCoIn_5$ for fields in the basal plane [Kenzelmann]				
	Theoretical discussion of Q-phase of $CeCoIn_5$ [Sigrist]				
	Investigation of $CeRhIn_5$ [Jaccard, Morenzoni]				
1.2	Superconductivity and valence fluctuations				
	Hall and Nernst effect in $CeCu_2Si_2$ [Jaccard]				
	Investigation of $CeNi_2Ge_2$ [Jaccard]				

	Milestones (Project 5, continued)	Year 9	Year 10	Year 11	Year 12
1.3	Non-centrosymmetric superconductors Phenomenology and microscopic theory [Sigrist] Processing of polycrystal and crystal growth of CeCo(Ge,Si) ₃ [Giannini]				
1.4	Vortex matter in superconductors Study of pinning-depinning transition [Blatter] Geometric barriers in superconductors with complex shape [Blatter]				
2.	Novel quantum phases and phase transitions in 4f- and 5f-electron systems				
	NMR under pressure and at low temperatures on Ce intermetallics [Ott] Optical studies of (Eu,Ba)Si [Degiorgi] Optical studies on the hidden phase of URu ₂ Si ₂ [van der Marel]				
3.	Magnetic, optical and transport properties in TM Si/Ge and Bi				
	Optical studies of Co-doped FeSb ₂ [Degiorgi] Growth of 3d- and 4d-TM silicides [Giannini] High-pressure synthesis of TM germanides [Giannini] Optical and transport studies of TM silicides [van der Marel] Optical studies of TM germanides [van der Marel] Theoretical discussion of transition metal sili- cides/germanides [Sigrist] Sb-tuning in Bi _{1-x} Sb _x crystals and related materials [Giannini] Optical studies of topological band-edge insulators [van der Marel]				

	Milestones (Project 5, continued)	Year 9	Year 10	Year 11	Year 12
4.	Theoretical and computational developments for strongly correlated electrons				
	Characterization of crossover phenomena [Baeriswyl]				
	Competition between (positional) disorder and (electron-electron) interaction [Baeriswyl]				
	Development of new QMC algorithms [Troyer]				

Project 6: Magnetism and competing interactions in bulk materials

	Milestones	Year 9	Year 10	Year 11	Year 12
1.	Spin chains and ladders				
	Excitations experimental [Rønnow, Mesot, Ott, Zheludev]				
	NMR/NQR on low-dimensional systems [Mesot, Ott]				
	Theoretical [Giamarchi, Troyer]				
	Quenched disorder [Zheludev]				
	μ SR [Morenzoni, Zheludev]				
	1D spin chains (KTi(SO ₄)H ₂ O, NaV ₂ O ₄) [Degiorgi, Rønnow]				
2.	Spin-dimer physics				
	Exotic phases in Shastry-Sutherland model [Mila, Troyer]				
	High-pressure studies of SrCu ₂ (BO ₃) ₂ [Rønnow]				
	Frustration effects in Han Purple [Mila, Rønnow]				
3.	Spin-liquids				
	Quadrupolar order in NiGaS ₄ [Mila]				
	Kagome spin-1/2 theory [Mila]				

	Milestones (Project 6, continued)	Year 9	Year 10	Year 11	Year 12
	Kagome spin-1/2 experimental realizations [Rønnow]				
4.	Multiferroics and helimagnets				
	Resonant X-ray diffraction [Staub]				
	Magnetic structures in multiferroic and magneto-electric model materials [Kenzelmann, Staub, Zheludev]				
	Topological phases in helimagnets [Zheludev]				
5.	Magneto-resistive materials				
	STM on perovskite manganites [Fischer]				
	Spin-polarized STM on bi-layer manganites [Renner]				
6.	Resonant inelastic X-ray scattering				
	Theory of light scattering in frustrated magnets [Mila]				
	Experiments on collective excitations [Rønnow, Schmitt]				

Project 7: Electronic materials with reduced dimensionality

	Milestones	Year 9	Year 10	Year 11	Year 12
1.	Investigation of the electronic properties of TiSe₂ and related dichalcogenides				
	T dependence of ARPES in TiSe ₂ [Aebi]				
	ARPES study of intercalated TiSe ₂ [Aebi]				
	High pressure study of TiSe ₂ and related compounds [Forró]				

	Milestones (Project 7, continued)	Year 9	Year 10	Year 11	Year 12
2.	Spectroscopic and structural investigation of $R\text{Te}_3$				
	Optical spectroscopy of $R\text{Te}_3$ [<i>Degiorgi</i>]				
	X-ray and neutron scattering measurements of rare-earth tritellurides [<i>Rønnow</i>]				
3.	ESR, ARPES and transport study of organic charge transfer salts				
	ESR and transport study of ET-based salts [<i>Forró, Giamarchi, Grioni, Mila</i>]				
4.	Study of quasi-1D vanadates				
	ARPES and RIXS of BaVS_3 [<i>Grioni</i>]				
	Magnetic measurements of BaVS_3 [<i>Forró, Ott</i>]				
5.	Study of other low-dimensional materials				
	ESR study of quasi 1-D organic conductors [<i>Forró, Giamarchi</i>]				
	Transport and STM study of Chevrel phases [<i>Fischer</i>]				
	Spin and charge degrees of freedom in $\text{Sr}_{14}\text{Cu}_{24}\text{O}_{41}$ [<i>Rønnow, Mila, Giannini, Degiorgi, Conder</i>]				

Project 8: Cold atomic gases as novel quantum simulators for condensed matter

	Milestones	Year 9	Year 10	Year 11	Year 12
1.	Model Systems and novel phases				
	Strongly correlated quantum states of cold atoms and light [<i>Gritsev</i>]				
	Phase diagram of two-dimensional dipolar gases on a square- lattice substrate potential [<i>Blatter</i>]				
	Observation of anti-ferromagnetic order in an optical lattice [<i>Esslinger</i>]				

	Milestones (Project 8, continued)	Year 9	Year 10	Year 11	Year 12
	Quantitative comparison between experiment and theory on spin ordering [Esslinger]				
	Study of the two-dimensional Hubbard model in the low entropy regime [Esslinger]				
	Numerical simulations of cold atomic systems [Troyer]				
	Equation of state of 3D Fermi gases [Troyer]				
	Equation of state of 2D Fermi gases [Troyer]				
	Density functional theory for cold gases [Troyer]				
	Mott transition and antiferromagnetism in cold atomic gases [Giamarchi]				
	Bose mixture [Giamarchi]				
2.	Probe and Thermometry				
	Validation of cold atomic systems [Troyer, Esslinger]				
	Spectroscopy [Giamarchi]				
3.	Dynamics and novel Phases				
	Nonequilibrium dynamics [Gritsev]				
	Dynamics and strong correlation of condensates for precision measurements [Gritsev]				
	Quantum phase transition and non-equilibrium dynamics of polaritons in an array of coupled QED cavities [Blatter]				
	Non-equilibrium physics in the Mott-insulating phase [Esslinger]				
	Disordered Bosonic and Fermionic systems [Giamarchi]				